INVESTIGATION INTO PRESSURE SIGNAL FLUCTUATIONS DURING FLUIDIZED DENSE-PHASE PNEUMATIC CONVEYING OF POWDERS

A thesis submitted in fulfillment

of the requirement for the award of the degree of

DOCTOR OF PHILOSOPHY

Submitted by

ANU MITTAL

Registration No.: 951208003

DEPARTMENT OF MECHANICAL ENGINEERING

THAPAR UNIVERSITY, PATIALA-147004,

PUNJAB, INDIA

February2016

This thesis is dedicated to my parents,

Chander Shashi and Sukhdev Lal, husband Amit Goyal and sonPranavfor their love, support and patience

THESIS CERTIFICATION

I, Anu Mittal, declare that the work presented in this thesis report entitled, **"Investigation into Pressure Signal Fluctuations During Fluidized Dense-Phase Pneumatic Conveying of Powders"** submitted in fulfillment of requirement for the award of degree of Doctor of Philosophy in Department of Mechanical Engineering, Thapar University Patiala, is an authentic record of my own work carried out under the supervision of Dr. S.S. Mallick (Associate Professor, Department of Mechanical Engineering, Thapar University, Patiala) from July 2012 to January 2016. The matter presented in this thesis has not been submitted either in part or full to any other University or Institute for the award of any other degree.

Anu Mittal — Date: February 25, 2016

Registration No.: 951208003

It is certified that the above statement made by the student is correct to the best of my knowledge and belief.

Dr. S.S. Mallick, PhD Supervisor — Date: February 25, 2016

Associate Professor,

Department of Mechanical Engineering, Thapar University, Patiala

ACKNOWLEDGEMENTS

At first, I would like to express sincere thanks to my supervisor Dr. S.S.Mallick, Associate Professor at Thapar University, Patiala. Without Dr. Mallick's encouragement, valuable advice and supervision, this work would not have been successfully completed. In addition, I am also grateful for the amount of concern and attention that he has devoted as a supervisor during the entire research period. It has been an honor for me to be a student of Dr. Mallick.

I am thankful to Prof. Dr. Peter Wypych for arranging the large amount of raw data from conveying trails conducted at University of Wollongong and for his valuable guidance at times and support.

I also express my gratitude to my Master degree supervisor, Dr. Rajiv Verma (Assistant professor, NIT Kurukshetra) for inspiring me to go for Doctorate research. He has always been source of great motivation for me. In addition, I would like to thank him for educating me on computer programming skills.

I express my sincere gratitude to my colleagues Mr. Atul Sharma and Mr. Gautam Setia, Lecturer, Mechanical Engineering Department, Thapar University, Patiala; who helped me a number of times especially during my initial period of time at the University.

I acknowledge my heartiest gratitude to my younger sister Shikha and her husband Mr. Virender Deepak Goyal for their moral support in my difficult times and helping me in providing resources related to electronics engineering background. In particular, Mr. Virender

Deepak Goyal for clarifying the discussions on some of the early signal processing techniques, tools and approaches.

I will always remain thankful to my family and friends for their good wishes and prayers, especially my parents for their never ending love, sisters for their support, my son and husband for their patience when I was not able to spend time with them. I am also grateful to my loving younger brother, Harsh and his wife who used to come and pick me up during my late evening stays at the University.

I am highly indebted to Department of Science and Technology (DST), Science and Engineering Research Board, Ministry of Science and Technology, Government of India (Young Scientific Scheme No: SR/FTP/ETA-15/2011; PI: Dr. S.S. Mallick), and Council for Scientific and Industrial Research (CSIR) Government of India, (Scheme no: 22(0614)/12/EMR-II; PI: Dr. S.S. Mallick), for the financial support to pursue research work.

Finally, I thank, Thapar University, Patiala, for providing me such a great atmosphere to learn and perform my research. I also extend my thanks to the mechanical engineering laboratory staff and the library staff of Thapar University, Patiala.

ABSTRACT

This thesis aims to provide a new method based on signal analysis for flow mode investigation in dense phase pneumatic conveying. In spite of numerous benefits offered by dense-phase pneumatic conveying of powders (which include minimum gas flows and power consumption; improved product quality and increased workplace safety etc) only limited progress has been achieved so far in understanding the fundamental transport mechanisms due to the highly concentrated and turbulent mode of the solids-gas flow. As a result, for the accurate design of dense phase pneumatic conveying systems, further research should be carried out.

For carrying out analysis work, extensive amount of test data made available from University of Wollongong, Australia has been considered, whichincluded two types of materials conveyed in different flow regimes varying from fluidized dense- to dilute phase including fly ash (median particle diameter 30 μm; particle density 2300 kg m^{-3}; loose-poured bulk density 700 kg m^{-3}) conveyed through a 69 mm I.D. × 168 m long pipeline and white powder (median particle diameter 55 μm; particle density 1600 kg m^{-3}; loose-poured bulk density 620 kg m^{-3}) conveyed through a 69 mm I.D. × 148 m long test rig. Analysis work also included data analysis from the pressure signals obtained during pneumatic conveying experiments conducted at the test setup of Thapar University, Patiala by conveying Indian fly ash (median particle diameter 19 μm; particle density 1950 kg m^{-3}; loose-poured bulk density 950 kg m^{-3}) through two different test set ups i.e. 54 mm I.D. × 70 m long and 54 mm I.D. × 24 m long.

Various methods of analysis involve different techniques, which could be grouped into two categories. First group of techniques (i.e., Hurst exponent, phase space diagram and Shannon entropy) aim to provide information on the qualitative nature of entire time-series as a whole, i.e. content of information (Shannon entropy) in the signal, degree of co-correlation between different parts of the signal (Hurst exponent) and amount of chaos (attractor analysis).These techniques mainly focus on searching for the hidden information in the time series signal and using these techniques, emphasis is made on the extraction and selection of key features that distinguish different pressure time signals to represent different flow mechanisms. Results show that with increasing conveying distance (i.e. with an increase in conveying velocity in the direction of flow), there is an overall decrease in the values of Hurst exponent, an increase in the area covered by the phase-space diagram and an increase in the Shannon entropy values, indicating an increase in the degree of complexity of flow mechanism (or turbulence) along the length of the conveying pipeline. All the three methods have revealed that the closely coupled bends reverse the trend of change of Hurst exponent, phase-space diagram area and Shannon entropy values. This is due to the slowing down of particles caused by the friction of particles along the bend wall resulting in dampened particle turbulence (particle roping effect).

Second group of techniques includesanalysis based on frequency domain or both frequency and time domain need to be performed so as to obtain information on the frequency content of the pressure signals. These include power spectral density (PSD), Wavelet transformation and Hilbert-Huang transformation (HHT).Power spectra obtained from PSD analysis, energy distribution of intrinsic mode functions (IMF) obtained from HHT transformation and wavelet scalogram show unique features related to the changing flow mechanism along the length of

the pipeline. Results indicate variation from low frequency to higher frequency components in the signal, along the flow direction. Higher frequency components and wide range of frequencies in the signal obtained at pipeline exit might have resulted from the increased level of interactions amongstthe solid particles, carrier gas and pipe wall as compared to the power spectra with single dominant frequency (which corresponds to probable periodic dune formation) at the pipeline entry region.

The Present work also aims to represent minimum transport boundary by analyzing the pressure signals obtained from pneumatic conveying trials, which were conducted for low conveying velocity and high solid flow rates. Results show that various signal parameters could be used for the online prediction of blockage boundary. Present work attempts to test the applicability of pressure fluctuations to be used for dune velocity estimation. It was found that the degree of cross-correlation between two signals from adjacent transducers was not sufficient to correlate the dunes (as the signal characteristics were modified while moving from one location to the other).

TABLE OF CONTENTS

		Page
THESIS CERTIFICATION		i
ACKNOWLEDGEMENTS		ii
ABSTRACT		iv
TABLE OF CONTENTS		vii
LIST OF FIGURES		x
LIST OF TABLES		xx
LIST OF SYMBOLS AND ABBREVIATIONS		xxi
CHAPTER 1		
Introduction and Objectives		1
1.1	Introduction	2
1.2	Objectives	9
1.3	Thesis Outline	10
CHAPTER 2		
Literature Review		12
CHAPTER 3		
Test Facilities and Experimental Procedures		27
3.1	Introduction	28
3.2	Experimental setup	28

3.3 Product Characterization 37

3.3.1 Particle size distribution 37

3.3.2 Particle density 38

3.3.3 Bulk density 39

3.3.4 Particle shape 39

3.4 Calibration procedure 41

3.5 Pneumaticconveyingtestingprocedure 44

CHAPTER 4

Investigation into Pressure Signal Fluctuations 52

4.1 Introduction 53

4.2 HurstExponent 62

4.3 Phasespacediagrams 65

4.4 Shannonentropy 66

4.5 Powerspectraldensity(PSD) 68

4.6 Wavelet Transformation 71

4.7 HilbertHuangTransform(HHT) 73

4.8 Cross-correlation 77

CHAPTER 5

Results and Discussion 80

5.1 HurstExponent 81

5.2 Phasespacediagram 88

5.3 Shannonentropy 94

5.4 Powerspectraldensity(PSD) 99

5.5 HilbertHuangTransform(HHT) 103

5.6 WaveletTransformation 110

5.7 MinimumTransportBoundary 115

5.8 Dunevelocityestimation 138

CHAPTER 6

Conclusions and Future Scope of Work 145

6.1 Conclusions 146

6.2 Future scope of work 148

REFERENCES 149

APPENDIX A 163

APPENDIXB 169

LIST OF PUBLICATIONS DURING COURSE OF PhD 185

LIST OF FIGURES

Page

CHAPTER 3

Figure 3.1 Schematic for 69 mm I.D. and 168 m long test rig for fly ash indicating locations of pressure tapping points, blow tank, receiver bin arrangement 29

Figure 3.2 Schematic for 69 mm I.D. and 148 m long test rig for white powder 31

Figure 3.3 Schematic of the pneumatic conveying test facility developed at Thapar University, Patiala 33

Figure 3.4 Piping and instrumentation diagram for compressed air at test set of Thapar University, Patiala 34

Figure 3.5 Particle size distribution of fly ash 38

Figure 3.6 Microscope image of fly ash sample (median particle size 21 μm) 40

Figure 3.7 Calibration curve for pressure transducer P4 43

Figure 3.8 Calibration curve for pressure transducer P7 43

Figure 3.9 Variation of mass flow rate of conveying air during complete conveying cycle, (m_f); (test setup of Thapar University, Figure 3.3); m_f =0.05 kg/s, m_s = 1.21 kg/s 47

Figure 3.10 Variation of solid mass in blow tank and receiver bin during complete conveying cycle, m_s; (test setup of Thapar University, Figure 3.3); m_f =0.05 kg/s, m_s = 1.21 kg/s 48

Figure 3.11 Typical Pressure signal obtained during the conveying cycle; (test setup of Thapar University, Figure 3.3); m_f =0.05 kg/s, m_s = 1.21 kg/s 49

obtained during conveying cycle of fly ash conveyed at Thapar University, India

Figure 3.12 Pressure fluctuations at different transducer location during a typical pneumatic conveying trial (first run); m_f =0.07 kg/s, m_s = 2.71 kg/s 50

Figure 3.13 Pressure fluctuations at different transducer location during a typical pneumatic conveying trial (repeat test); m_f =0.07 kg/s, m_s = 2.71 kg/s 50

Figure 3.14 Error analysis for the data recorded by different transducers during a typical pneumatic conveying trial; m_f = 0.07 kg/s, m_s = 2.71 kg/s 51

CHAPTER 4

Figure 4.1.1 Power spectral density plot from pneumatic conveying of white powder at University of Wollongong 55

Figure 4.1.2 Pressure versus time plot for fly ash at low solids loading ratio; (m_f= 0.107 kg/s; m_s = 2.35 kg/s; m^* = 21.96) 56

Figure 4.1.3 Pressure versus time plot for fly ash at high solids loading ratio; (m_f = 0.07 kg/s; m_s = 4.41 kg/s; m^* = 63) 57

Figure 4.1.4 Pressure versus time plot for white powder for low solids loading ratio; (m_f = 0.085 kg/s; m_s = 2.29 kg/s; m^* = 26.89) 57

Figure 4.1.5 Pressure versus time plot for white powder for high solids loading ratio; (m_f = 0.05 kg/s; m_s = 2.34 kg/s; m^* = 46.8) 58

Figure 4.1.6 Power spectral density plot from pneumatic conveying of Fly ash (Thapar University, Patiala) 61

Figure 4.2.1 Illustration of the procedure used for calculation of Hurst exponent 64

CHAPTER5

Figure 5.1.1	Hurst Exponent calculation; Exp-37 (Flyash; m_f = 0.03 kg/s; m_s = 5.83 kg/s; m^* = 182.37)	83
Figure 5.1.2	Variation of Hurst Exponent along the length of pipeline for fly ash	84
Figure 5.1.3	Variation of Hurst Exponent along length of pipeline for white powder	85
Figure 5.2.1	Variation of mutual information versus time lag Exp-24; White powder; (at P2)	89
Figure 5.2.2	Variation of false nearest neighbors percentage embedding dimension Exp-24; White powder; (at P2)	90
Figure 5.2.3	Variation of phase space attractor along length of pipeline for fly ash: m_f = 0.11 kg/s ; m_s= 2.36 kg/s; m^*= 21.45; V_f = 12.28 m/s (at P2) - 16.6 m/s (at P5)	91
Figure 5.2.4	Variation of Phase space attractor along length of pipeline for fly ash: m_f = 0.07 kg/s; m_s= 3.98 kg/s; m^* = 56.85; V_f = 7.11 m/s (at P2) - 10.6 m/s (at P5)	91
Figure 5.2.5	Variation of phase space attractor along length of pipeline for white powder: m_f=0.20 kg/s; m_s=1.83 kg/s; m^* = 9.15; V_f = 20.86 m/s (at P2) - 31.28 m/s (at P5)	92
Figure 5.2.6	Variation of phase space attractor along length of pipeline for white powder: m_f = 0.05 kg/s; m_s= 2.19 kg/s; m^*= 43.8; V_f = 4.18 m/s (at P2) - 9.09 m/s (at P5)	92
Figure 5.3.1	Variation of Shannon entropy along length of pipeline for fly ash	95
Figure 5.3.2	Variation of Shannon entropy along length of pipeline for white	96

powder flow condition

Figure 5.4.1 Variation of power spectral density along pipeline length for fly ash; (m_f = 0.107 kg/s; m_s = 2.35 kg/s; m^* = 21.96) 99

Figure 5.4.2 Variation of power spectral density along pipeline length for fly ash; (m_f = 0.07 kg/s; m_s = 4.41 kg/s; m^* = 63) 100

Figure 5.4.3 Variation of power spectral density along pipeline length for white powder; (m_f = 0.085 kg/s; m_s =2.29 kg/s; m^* = 26.89) 100

Figure 5.4.4 Variation of power spectral density along pipeline length for white powder; m_f = 0.05 kg/s; m_s = 2.34 kg/s; m^* = 46.8) 101

Figure 5.5.1 Upper and lower envelopes of mean adjusted series at 1st step (applied to typical pressure signal) 104

Figure 5.5.2 Upper and lower envelopes of mean adjusted series at 2nd step (applied to typical pressure signal) 105

Figure 5.5.3 Intrinsic mode function extracted from a signal 105

Figure 5.5.4 Variation of energy distribution index (by Hilbert Transformation) along pipeline length: fly ash (m_f = 0.107 kg/s; m_s = 2.35 kg/s; m^* = 21.96) 106

Figure 5.5.5 Variation of energy distribution index (Hilbert Transformation) along pipeline length: fly ash (m_f = 0.07 kg/s; m_s = 4.41 kg/s; m^* = 63) 107

Figure 5.5.6 Variation of energy distribution index (Hilbert Transformation) along the pipeline length: white powder (m_f = 0.085 kg/s; m_s =2.29 kg/s; m^* = 26.89) 107

Figure 5.5.7 Variation of energy distribution index (Hilbert Transformation) along 108

pipeline length: white powder (m_f = 0.05 kg/s; m_s = 2.34 kg/s; m^* = 46.8)

Figure 5.6.1 Variationof wavelet scalogramalong the length of pipeline: fly ash (m_f = 0.107 kg/s; m_s = 2.35 kg/s; m^* = 21.96) 112

Figure 5.6.2 Variationof wavelet scalogram along the length of pipeline:fly ash (m_f = 0.07 kg/s; m_s = 4.41 kg/s; m^* = 63) 112

Figure 5.6.3 Variationof wavelet scalogram along the length of pipeline: white powder (m_f = 0.085 kg/s; m_s =2.29 kg/s; m^* = 26.89) 113

Figure 5.6.4 Variationof wavelet scalogramthe length of pipeline:White powder (m_f = 0.05 kg/s; m_s = 2.34 kg/s; m^* = 46.8) 113

Figure 5.7.1 Pressure signals for Flyash; Exp-35; m_f = 0.04 m/s; m_s = 5.98 m/s; m^* = 150.6; V_f = 4 m/s (at P1) - 7 m/s (at P5) 116

Figure 5.7.2 Pressure signals for Flyash; Exp-37; m_f = 0.03 m/s; m_s = 5.84 m/s; m^* = 182.3; V_f = 2 m/s (at P1) - 5 m/s (at P5) 117

Figure 5.7.3 Pressure signals for White powder; Exp-23; m_f = 0.04 m/s; m_s = 2.05 m/s; m^* = 50.8; V_f = 3 m/s (at P1) - 7 m/s (at P6) 118

Figure 5.7.4 Pressure signals for White powder; Exp-20; m_f = 0.01 m/s; m_s = 2.53 m/s; m^* = 253; V_f = 1 m/s (at P1) - 2 m/s (at P6) 118

Figure 5.7.5 Variation of power spectral density along the length of pipeline:Flyash; Exp-36 (m_f = 0.03kg/s; m_s = 4.38 kg/s; m^* = 136; V_f = 4-6 m/s) 121

Figure 5.7.6 Variation of power spectral density along the length of pipeline:Flyash; Exp-35 (m_f = 0.04 kg/s; m_s = 5.98 kg/s; m^* = 150; V_f 121

= 4.5-7.5 m/s)

Figure 5.7.7 Variation of power spectral density along the length of pipeline:Flyash; Exp-37 (m_f = 0.032 kg/s; m_s = 5.84 kg/s; m^* = 182.5; V_f = 2 - 5 m/s) 122

Figure 5.7.8 Variation of power spectral density along the length of pipeline:White powder; Exp-20 (m_f = 0.01kg/s; m_s = 2.53kg/s; m^* = 253; V_f = 1-2 m/s) 122

Figure 5.7.9 Variation of power spectral density along the length of pipeline:White powder; Exp-21 (m_f = 0.01kg/s; m_s = 2.64kg/s; m^* = 264; V_f = 1-2 m/s) 123

Figure 5.7.10 Variation of power spectral density along the length of pipeline:White powder; Exp-24 (m_f = 0.04kg/s; m_s = 1.93 kg/s; m^* = 47.28; V_f = 3-7 m/s) 123

Figure 5.7.11 Variation of wavelet scalogram along the length of pipeline:Flyash; Exp-36 (m_f = 0.03kg/s; m_s = 4.38 kg/s; m^* = 136; V_f = 4-6 m/s) 124

Figure 5.7.12 Variation of wavelet scalogram along the length of pipeline:Flyash; Exp-35 (m_f = 0.04 kg/s; m_s = 5.98 kg/s; m^* = 150; V_f = 4.5-7.5 m/s) 124

Figure 5.7.13 Variation of wavelet scalogram along the length of pipeline:Flyash; Exp-37 (m_f = 0.032 kg/s; m_s = 5.84 kg/s; m^* = 182.5; V_f = 2 - 5 m/s) 125

Figure 5.7.14 Variation of wavelet scalogram along the length of pipeline:White powder; Exp-20 (m_f = 0.01kg/s; m_s = 2.53kg/s; m^* = 253; V_f = 1-2 m/s) 125

Figure 5.7.15 Variation of wavelet scalogram along the length of pipeline: White 126

powder; Exp-21 (m_f = 0.01kg/s; m_s = 2.64kg/s; m^* = 264; V_f = 1-2 m/s)

Figure 5.7.16 Variation of wavelet scalogram along the length of pipeline: White powder; Exp-24 (m_f = 0.04kg/s; m_s = 1.93 kg/s; m^* = 47.28; V_f = 3-7 m/s) 126

Figure 5.7.17 Attractor variation along the length of pipeline:Flyash; Exp-36 (m_f = 0.03kg/s; m_s = 4.38 kg/s; m^* = 136; V_f = 4-6 m/s) 127

Figure 5.7.18 Attractor variation along the length of pipeline:Flyash; Exp-35 (m_f = 0.04 kg/s; m_s = 5.98 kg/s; m^* = 150; V_f = 4.5-7.5 m/s) 127

Figure 5.7.19 Attractor variation along the length of pipeline:Flyash; Exp-37 (m_f = 0.032 kg/s; m_s = 5.84 kg/s; m^* = 182.5; V_f = 2 - 5 m/s) 128

Figure 5.7.20 Attractor variation along the length of pipeline:White powder; Exp-20 (m_f = 0.01kg/s; m_s = 2.53kg/s; m^* = 253; V_f = 1-2 m/s) 128

Figure 5.7.21 Attractor variation along the length of pipeline: White powder; Exp-21 (m_f = 0.01kg/s; m_s = 2.64kg/s; m^* = 264; V_f = 1-2 m/s) 129

Figure 5.7.22 Attractor variation along the length of pipeline:White powder; Exp-24 (m_f = 0.04kg/s; m_s = 1.93 kg/s; m^* = 47.28; V_f = 3-7 m/s) 129

Figure 5.7.23 Variation of energy distribution among various IMF's along the length of pipeline: Flyash; Exp-36 (m_f = 0.03 kg/s ; m_s = 4.38 kg/s ; m^* = 146; V_f = 4-6 m/s) 130

Figure 5.7.24 Variation of energy distribution among various IMF's along the length of pipeline: Flyash; Exp-35 (m_f = 0.04 kg/s; m_s = 5.98 kg/s; m^* = 150; V_f = 4.5-7.5 m/s) 130

Figure 5.7.25 Variation of energy distribution among various IMF's along the length of pipeline: Flyash; Exp-37 (m_f = 0.032 kg/s; m_s = 5.84 kg/s; m^* = 182.5; V_f = 2 - 5 m/s) 131

Figure 5.7.26 Variation of energy distribution among various IMF's along the length of pipeline: White powder; Exp-20 (m_f = 0.01kg/s; m_s = 2.53kg/s; m^* = 253; V_f = 1-2 m/s) 131

Figure 5.7.27 Variation of energy distribution among various IMF's along the length of pipeline: White powder; Exp-21 (m_f = 0.01kg/s; m_s = 2.64kg/s; m^* = 264; V_f = 1-2 m/s) 132

Figure 5.7.28 Variation of energy distribution among various IMF's along the length of pipeline: White powder; Exp-24 (m_f = 0.04kg/s; m_s = 1.93 kg/s; m^* = 47.28; V_f = 3-7 m/s) 132

Figure 5.7.29 Variation of Shannon entropy along pipeline length; Flyash 133

Figure 5.7.30 Variation of Shannon entropy along pipeline length; White powder 134

Figure 5.7.31 Variation of Hurst exponent along pipeline length; Flyash 135

Figure 5.7.32 Variation of Hurst exponent along pipeline length; White powder 136

Figure 5.8.1 Output signals from two pressure transducers when distance between them in 19.9 m (Exp-14; White powder; m_f = 0.15 m/s; m_s = 1.38 m/s; m^* = 9.49 m/s; V_f = 23.5 m/s at P5 to 27.2 m/s at P6) 141

Figure 5.8.2 Detailed examination of pressure signals at transducer locations P5 and P6 (19.9 m apart) (Exp-14; White powder; m_f = 0.15 m/s; m_s = 1.38 m/s; m^* = 9.49 m/s; V_f = 23.5 m/s at P5 to 27.2 m/s at P6) 142

Figure 5.8.3 Typical cross-correlation between two signals when distance between 143

transducers is 19.9 m (Exp-14; white powder)

Figure 5.8.4 Typical cross-correlation between two signals when distance between transducers is 19.9 m (Exp-71; white powder) 143

Figure B1 Shannon entropy variation along pipeline length (54 mm I.D. × 70 m long pipe) 171

Figure B2 Shannon entropy variation along pipeline length (54 mm I.D. × 24 m long pipe) 172

Figure B3 Power spectral density at different locations along pipeline length (54 mm I.D. × 70 m long pipe; m_f = 0.031 kg/s; m_s = 1.21 kg/s; m^* = 39.03) 174

Figure B4 Power spectral density at different locations along pipeline length (54 mm I.D. × 70 m long pipe; m_f = 0.029 kg/s; m_s = 0.5 kg/s; m^* = 17.3) 174

Figure B5 Power spectral density at different locations along pipeline length (Exp.1: m_f = 0.049 kg/s; m_s = 3.47 kg/s; m^* = 70.8; 54 mm I.D. × 24 m long pipe) 175

Figure B6 Variation of mutual information versus time lag Exp-1; Fly ash; (at P2) 176

Figure B7 Variation of false nearest neighbors percentage embedding dimension Exp-1; Fly ash; (at P2) 177

Figure B8 Phase space diagram at different locations along pipeline length (54 mm I.D. × 70 m long pipe; m_f = 0.031 kg/s; m_s = 1.21 kg/s; m^* = 39.03) 178

Figure B9 Phase space diagram at different locations along pipeline length (54 178

mm I.D. × 70 m long pipe; m_f = 0.029 kg/s; m_s = 0.5 kg/s; m^* = 17.3)

Figure B10 Phase space diagram at different locations along pipeline length (Exp.1: m_f = 0.049 kg/s; m_s = 3.47 kg/s; m^* = 70.8; 54 mm I.D. × 24 m long pipe) 179

Figure B11 Wavelet scalogram at different locations along pipeline length (54 mm I.D. × 70 m long pipe; m_f = 0.031 kg/s; m_s = 1.21 kg/s; m^* = 39.03) 180

Figure B12 Wavelet scalogram at different locations along pipeline length (54 mm I.D. × 70 m long pipe; m_f = 0.029 kg/s; m_s = 0.5 kg/s; m^* = 17.3) 181

Figure B13 Wavelet scalogram at different locations along pipeline length (54 mm I.D. × 70 m long pipe; m_f = 0.029 kg/s; m_s = 0.5 kg/s; m^* = 17.3) 182

Figure B14 Power spectral density at different locations along pipeline length (54 mm I.D. × 70 m long pipe; m_f = 0.031 kg/s; m_s = 1.21 kg/s; m^* = 39.03) 183

Figure B15 Power spectral density at different locations along pipeline length (54 mm I.D. × 70 m long pipe; m_f = 0.029 kg/s; m_s = 0.5 kg/s; m^* = 17.3) 183

Figure B16 Power spectral density at different locations along pipeline length (Exp.1: m_f = 0.049 kg/s; m_s = 3.47 kg/s; m^* = 70.8; 54 mm I.D. × 24 m long pipe) 184

LIST OF TABLES

Page

CHAPTER 3

Table 3.1	Physical properties of Indian fly ash	40
Table 3.2	Chemical properties of powders	41
Table 3.3	Physical properties of powders	41
Table A1	Shannon entropy at different locations along pipeline length (Flyash, University of Wollongong)	164
Table A2	Shannon entropy at different locations along pipeline length (White powder, University of Wollongong)	165
Table A3	Hurst exponent at different locations along pipeline length (Flyash, University of Wollongong)	166
Table A4	Hurst exponent at different locations along pipeline length (White powder, University of Wollongong)	167
Table A5	Shannon entropy variation along pipeline length (Indian flyash)	168

LIST OF SYMBOLS AND ABBREVIATIONS

D	Internal diameter of pipe [m]
d_s	Particle diameter [m]
d_{50}	Median particle diameter [µm]
e	Energy distribution index for IMF's
E	Total energy of the signal
E_i	Energy of i^{th} IMF
f	Frequency [Hz]
Fr	Froude number ($Fr= V/(gD)^{0.5}$)
Fr_m	Mean Froude number related to the section of pipe ($Fr_m = V_m/(gD)^{0.5}$)
Fr_{min}	Minimum Froude number at the inlet to the pipe ($Fr_{min} = V_{min}/(gD)^{0.5}$)
g	Acceleration due to gravity [m/s^2]
H	Hurst exponent
I (t)	Mutual information function
I_i (t)	i^{th} IMF component
L	Length of pipe or test section [m]
m^*	Solids loading ratio ($m^*= m_s/m_f$)
m_f	Mass flow rate of air [kg/s]
m_s	Mass flow rate of solids [kg/s]
n,N	Number of data values in the time series

P	Pressure [N/m^2]
p	Probability
p_i	Probability of i^{th} component in the time series
R	Radius of pipe [m]
Re	Reynolds number of gas ($Re = \rho VD/\mu_f$)
Re_p	Reynolds number of particle ($Re_p = \rho_s Vd/\mu_f$)
R(t)	Sample sequential range
R_{xy}	Cross-correlation function between two signals
R/S	Rescaled range
S	Shannon entropy (bits)
t	Time (seconds)
S(t)	Standard deviation of time series
V	Superficial air/gas velocity [m/s]
WT	Wavelet coefficients
X(t), x(t)	Time series
x_{max} (t)	Upper envelope of signal
x_{min} (t)	Lower envelope of signal
$\bar{X}$	Average of time series values
Y_i	Departure of time series X_i from the average value
Z_i	Cumulative departure of X_i from the average value
ΔP	Pressure drop through a straight horizontal pipe or pipe section [Pa]
ΔP_b	Pressure drop through a bend [Pa]
λ_f	Air/gas only friction factor
λ_s	Solids friction factor through straight pipe

μ_f	Dynamic viscosity for single fluid (e.g. air) [Pa.s]
ρ_f	Density of air [kg/m^3]
ρ_{bl}	Loose-poured bulk density [kg/m^3]
ρ_s	Particle density [kg/m^3]
τ	Delay time [Seconds]
ω	Frequency in radians per sample
$\psi(\xi)$	Wavelet function

Superscripts

a,b,c,d	Exponents of the power function

Subscripts

bl	Bulk
e	Equivalent
f	Fluid (air)
h	Horizontal
i	Inlet condition
min	Minimum
p	Particle
s	Solids
T	Total
t , *f*	Translational and dilation parameters

Abbreviations

BD	Bottom discharge
DEM	Discrete element model
ECT	Electrical capacitance tomography
EMD	Empirical mode decomposition
FFT	Fast Fourier transform
HHT	Hilbert-Huang Transformation
I.D.	Internal diameter of pipe
IMF	Intrinsic mode function
N.B.	Minimum transport boundary
PCC	Nominal Bore
PMC	Pressure minimum curve
PSD	Power spectral density
RMS	Root mean square

CHAPTER 1: INTRODUCTION AND OBJECTIVES

1.1 Introduction

Pneumatic conveying has been frequently used to transport solids in large number of industries, such as power, mining, chemical, agriculture, food, cement and pharmaceutical. Distinct modes of solid-gas flow (e.g. dilute and dense phase, or suspension and non-suspension flow, respectively) occur inside the pipelines depending upon the solid loading ratio (m^*), gas velocity and the characteristics of the solid being conveyed, such as particle size, bulk density, permeability and deaeration, etc. For coarser products, the favorable mode of conveying is dilute-phase or suspension flow(Marcus et al. 1997), which involves majority of the solid particles being conveyed in suspension by the carrier gas, while fine powders are able to be conveyed in fluidized dense-phase mode, where majority of solid particles travel as non-suspension dunes along the bottom of pipeline. This is known as fluidized dense-phase flow and is a typical characteristic of Geldart A type powders (Mallick, 2009), such as fly ash, cement, pulverized coal, etc, that demonstrate good air retention properties. Fluidized dense-phase mode of conveying offers a number of advantages over the conventional dilute-phase (suspension) flows, such as large solids to gas flow rate ratio, resulting in reduced gas flow requirement and power consumption, reduced conveying velocities resulting in decrease in pipeline wear rate and product damage, smaller pipe and support size and reduced filtration area requirement(Mallick and Wypych, 2009). However, in spite of these advantages, wide spread installation of such sytems is still limited as designing a reliable fluidized dense-phase pneumatic conveying system is not a trivial task. This is due to the highly turbulent nature of the dunes that involve complex solid-solid, solid-air and solid-wall interactions that are difficult to be fundamentally modelled (Mallick, 2009). Due to the difficulty of developing non-linear governing equations for such a complex flow phenomenon, existing methods of modelling solids friction proposed by Pan and Wypych (1998) to Jones and Williams (2003) to

Mallick (2009) rely heavily on empirical approaches. These existing studies and modelling approaches have been generally based on steady state analysis and little efforts have been made to explore the non-linear dynamic behaviour of gas-solid flow. Identification of flow pattern or flow mechanism (such as non-suspension to suspension flow transition) is important for better understanding of the gas-solids flows. Therefore, to extract distinct flow features from the complex flow structure, reliable quantification techniques must be developed. One method that is gaining importance in recent years (Li,2002; Jama et al., 1999; William et al., 2008; Pahk and Klinzing, 2008a and 2008b; Liang et al. 2007) to better understand the dynamic nature of flow is based on studying the pressure fluctuations caused by the gas-solids flow.

Kim and Han (1999) analysed the pressure fluctuations along the height of a riser using deterministic chaos theory to explore the effects of coarse particles and humidity of air on flow. Lee et al. (2002) studied the pressure fluctuations in a fluidized bed of polymer powders by the deterministic chaos analysis. Cho et al. (2001) investigated the highly complex and irregular behaviour of multi-phase-flow (gas-solid-liquid) in the riser of a circulating fluidized bed using phase-space portraits. Bai et al. (1999) carried out research to characterize the fluctuating pressure signals to distinguish between the flow behaviour of different classes of particles in fluidized beds. To examine the chaotic behaviour of six different types of powders and to identify flow regime transitions in reactor, Luo et al. (2012) applied Hurst analysis on pressure fluctuations of the fluidized solids-gas bed. The Hurst exponent represented persistent and anti-persistent behaviour of signal; $H>0.5$ implies persistent hydrodynamic behaviour, i.e. bubbles movement is in the way of chains with local circulation of few small bubbles, while for $H<0.5$ indicates anti-persistent hydrodynamic behaviour, i.e. random movement of medium sized bubbles along with coalescence of small sized bubbles into large bubbles. Kikuchi and Tsutsumi (2001)

plotted radial distribution of Hurst exponent in the riser for three different values of solids loading ratio and showed that Hurst exponent values increase from the centre of the riser towards the wall. Al-Masry and Ali (2008) investigated the pressure fluctuations generated in bubble columns of fluidized beds. The variation in the attractor structure was observed with change in superficial gas velocity with air-water system. Zhong et al. (2009) studied the dynamic behaviour of biomass fluidized beds using Shannon entropy. Duan and Cong (2013) used the method of Shannon entropy to compare flow behaviour in different regimes and flow pattern of different powders belonging to the class of Geldart (1973) Group B and D. Karimi et al. (2011) analysed pressure fluctuations with the help of attractor analysis to identify non-linearity in fluidized beds. The results indicated that higher energy contributions from macro-structures as compared to micro-structures demonstrate nonlinearity in the fluidized bed. The different structures correspond to different phenomena taking place inside the fluidized bed. Macro-structures of high amplitude and low frequencies (up to 3 Hz) correspond to large scale phenomena, while micro-structures of high frequencies of 20-200 Hz were believed to be caused by the motion and collision among solid particles. Geng et al. (2014) employed wavelet analysis to study the flow regime in circulating fluidized beds. With the change in radial position from the center of the bed to the wall, the scale of wavelet energy percentage peak was transformed from fine to coarse scale, indicating that more clusters are inclined to aggregate near to the wall. Luo et al. (2012) applied Hilbert-Huang transformation to study the energy-frequency-time distribution of fluctuating pressure signals in an air-lift reactor. With the increase in superficial gas velocity, energy of the pressure signals in the riser shifted to higher frequency range, while it increased sharply in the low frequency range in the down-comer. Shou and Leu (2005) studied hydrodynamics of fluidized beds by applying Power Spectral Density (PSD) and wavelet transformation on fluctuating pressure signals. Band spectrum and its magnitude were found to vary with a change in

gas velocity; wide band spectrum signified increased number of bubbles, while narrow spectrum with sharp peaks indicated single bubble or slugging bed behavior. Elperin and Klochko (2002) developed a relation between flow regimes in two phase air-water vertical flow and pressure fluctuations with the help of discrete wavelet transformation. Distribution of wavelets over different scales was shown to contain valuable information regarding flow regime characteristics, and time-series was classified as being a manifestation of bubbly, annular, churn or intermittent flow. Lu et al. (2013) performed pressure signal analysis using the technique of Hilbert-Huang transformation to understand the underlying characteristics of gas-solids flow at high pressure through a horizontal pipeline. Change in flow regime with decrease in superficial velocity was indicated by a shift in energy distribution of IMF's (Intrinsic mode function)from higher frequency band to lower frequency band. Li (2002) employed wavelet multi-resolution analysis to analyse pressure-time signals and extracted the fluctuating pressure components due to the dispersed suspension flow and dune flow from the random pressure fluctuations. Pahk and Klinzing (2008a and 2008b) analysed pressure-time series to study the flow regimes based on different signal analysis techniques, such as Power Spectral Density (PSD), phase space diagram, rescaled range analysis and wavelet analysis. Cong et al. (2011) analysed pressure fluctuations by the method of PSD and wavelet transformation to reveal flow patterns and flow characteristics of dense-phase pneumatic conveying of pulverized coal through a pipeline.

From the above review, it can be seen that a considerable amount of work has been carried out to analyse the pressure fluctuations in the case of fluidized beds. However, only limited research has been reported so far towards analysing pressure fluctuations for horizontal pneumatic transport, especially for fine powders (being conveyed from fluidized dense- to dilute-phase flow). Williams et al. (2008) attempted to find the average

pulse velocity from pressure fluctuation data using time delay analysis. Dhodapakar and Klinzing (1993) observed distinct power spectral density functions for various flow regimes in horizontal pneumatic transport. Cabrejos and Klinzing (1995) performed rescaled range analyses on pressure fluctuations to identify different flow regimes for polymer particles, glass beads and alumina. Pahk and Klinzing (2008b) determined the flow characteristics for horizontal pneumatic conveying of coarse particles by analysing pressure fluctuations using different signals analysis techniques, such as power spectral density, phase space diagram, rescaled range and wavelet analysis. Largely all the methods of pressure signal analysis reported in the literature can be divided into two categories.First one involves transformation of time series to get qualitative information, while theother set of techniques are based on feature extraction. Shannon entropy, Hurst exponent and phase space diagram fall into the first category, while the power spectral density, wavelet transformation and Hilbert Huang transformation belong to the second group. Every method of signal analysis has got certain limitations and advantagesover the others. First set of techniques are able to provide only qualitative information, e.g. degree of randomness, degree of similarity between different parts of series etc. These are more suitable while performing relative comparison between different data sets. The second set of techniques are applicable when the intent is to extract certain signal features, e.g. dominant frequency, energy of the signal etc. To be precise,the technique of Shannon entropy is well defined for a source of symbol strings; it is not a unique characteristic of continuous time series. For that purpose continuous time series data with floating point numbers need to be divided into bins. Therefore selecting the number of bins and range of data values for a particular bin is important and one must be careful while deciding these parameters for different time-series if results of different time-series are to be compared. The main limitation of phase space diagram is that the attractor is reconstructed on the assumptions that the time series object of study is without noise and infinitely sampled. It

also involves selection of optimum delay period for accurate results. While applying Hurst exponent time series,one must consider the length of the time series. The Hurst exponent is a useful statistical method for inferring the properties of a time series without making assumptions about stationarity. Power spectral density provides analysis in frequency domain and is applicable when dominant frequency of the signal is sought to know periodicity of the analysed signal. However, this technique does not provide any information in time domain.For analysing the time series both in frequency and time domain, the techniques of wavelet transformation and Hilbert Huang transformation are well suited. It is apparent that the majority of the research carried out in the area of pressure signal analysis for horizontal pneumatic conveying (Dhodapakar and Klinzing, 1993; Cabrejos and Klinzing, 1995; Pahk and Klinzing, 2008a and 2008b) is for coarse granular products, which involves a comparatively less degree of complexity as compared to the conveying of fine powders under fluidized dense phase conditions. Pressure fluctuations are produced while conveying bulk materials through a pipeline due to the combined effects of particle movement, particle collisions with pipe-wall, particle-particle interactions and solid-gas interactions. Hence the pressure fluctuation signals are considered to carry substantial information at micro-scale level regarding flow dynamics and these could be related to interpret the existing flow situation inside the pipeline. Various statistical methods have been developed to analyse static pressure fluctuations, such as probability density function (PDF), root mean square (RMS) etc.(Tsuji and Morikawa, 1982). However, these traditional statistical methods can not reveal the multi-scale features of the non-linear and non stationary time-series data.

The aim of the present work is to understand the flow mechanisms during the pneumatic transport of fine powders over a wide range of gas flow velocities by relating the nature of pressure fluctuations to the flow condition inside the pipeline. Initially, Shannon entropy,

rescaled range analysis (estimation of Hurst exponent) and attractor analysis (construction of phase space diagram) have been used in the present work to analyse the pressure signals. Subsequently, the technique of power spectral density has been applied to gain information on frequency domain, followed by using Hilbert-Huang transformation to analyse non-linear and non-stationary data (i.e. data which can not be predicted or modeled). For non-stationary data spectral density change with time. Finally, an analysis has been performed using wavelet technique to conduct multi-resolution analysis of pressure time series. Also, pressure signal fluctuations near the minimum transport boundary have been studied. The minimum transport boundary affects the design and operation of pneumatic conveying systems. Reduction in mass flow rate of carrier gas from the minimum transport boundary would cause the fluidized bulk material to de-aerate resulting in material build-up and eventually blockage inside the conveying pipe (Mallick, 2009). Therefore,the reliable design of industrial plants demands for the accurate prediction of the minimum transport (or capacity limitation boundary) for the dense-phase pneumatic conveying of powders through a given pipeline system. Additionally, the possibility of using pressure transients to determine the dune velocity from the signal-lag information (i.e. the delay between signals obtained from two successive pressure transducers installed along the pipeline) has been also investigated. Work on dune velocity estimation using pressure signal fluctuations has been carried out with the prime motive of verification of the studies carried out by other researchers such as William et al. (2007) and Liu et al. (2009), who have also attempted to find particle velocity using time delay analysis of pressure signal fluctuations.

1.2 Objectives

Particular research objectives include:

(i) To develop database of fluctuating pressure signals comprising of relevant conveying parameters (such as a wide range of air and solids flow rates, static pressures in blow tank, different powders and pipeline) using a wide range of fluidized dense-phase conveying data of fine powders.

(ii) To characterize the changes in flow condition with an increase in gas velocity along the direction of flow using appropriate signal processing techniques for the analysis of pressure signals (e.g. Shannon entropy, wavelet transformation, power spectral density, Hurst exponent, phase space diagram and Hilbert-Huang transform) for fine powder conveying systems.

(iii) To relate the results of pressure signal fluctuation analysis with the possible changes in flow mechanism along the pipeline from low to high conveying velocity.

(iv) To investigate into the characteristics of pressure signals near minimum transport boundary (i.e. the minimum conveying velocity requirement to ensure pipe blockage does not occur).

(v) To investigate into the suitability of identifying of pressure signals created by the same dune, while flowing along the pipelines, and from this, to establish time lag between signals from consecutive pressure tapping points to determine the dune velocity.

This work involved analysis of the raw data obtained from pneumatic conveying laboratory at the University of Wollongong for two products (i.e. fly ash and white powder). Various signal processing techniques have been used in this thesis to extract pertinent signal features. Conveying trials were also conducted at Thapar University test rig, equipped with pressure measurement and flow visualization arrangements located at strategic points so that flow characteristics could be studied in greater detail.

1.3 Thesis Outline

This thesis comprises of the following chapters:

Chapter 1 presents the introduction on the subject and need of the work. Also, the objectives of the work and thesis outline are defined in this chapter.

Chapter 2 presents an extensive literature review on the topic, namely flow mode identification and transition on gas-solid flows through pipeline. More emphasis is given to the pressure fluctuation studies carried on gas-solid flows in horizontal pipes.

Chapter 3 details the experimental set up and procedure to conduct pneumatic conveying trials. Specifications of various components used in the test set up are also described. Calibration procedures have been also presented.

Chapter 4 deals with the various signal processing techniques to analyse pressure fluctuation time series associated with the horizontal pneumatic conveying. Detailed mathematical model, analysis procedure and input preparation have been discussed.

Chapter 5 discusses the results of all the pressure fluctuation analysis techniques, which includes investigation into the change in flow condition along the pipeline length and to relate these results with the results of transient pressure signal analysis (using different methods). This chapter also includes discussion on pressure signal behavior near minimum transport boundary.

Chapter 6 provides the overall conclusions and future recommendations.

CHAPTER 2: LITERATURE REVIEW

The purpose of this chapter is to present a review of the various studies conducted over the years by different researchers on the subject of understanding flow mechanism involved in two phase solid-gas flow through horizontal pipeline with the aid of pressure fluctuation analysis. Pneumatic transport of particulate solids is classified into dilute (or lean) phase and dense phase flow. Dilute to dense phase transition seem to be dependent on gas Froude number (Mallick, 2009). Dilute phase mode of conveying is characterized by gas Froude number greater than 12 and the dense phase mode by gas Froude number less than 8 (Mallick, 2009), however it must be noted thatthe flow mode transition significantly depends on material properties and conveying conditions and these ranges are only approximate.

Reports on previous studies are presented in chronological order to illustrate the evaluation of the various analysis techniques. It is to be noted that literature review extends into various other areas related to solid-gas flows such as flow in fluidized beds. However, the main focus would be on fluidized dense phase conveying of fine powders through horizontal pipeline.

One of the early researchers to use pressure fluctuations for the identification and prediction of the flow pattern in horizontal pneumatic conveying was Tsuji and Morikawa (1982). This work included an investigation into the variation in flow patterns usingpressure signal fluctuations due to the two-phase gas-solid flows. Experiments were conducted in a 40 mm I.D. horizontal pipe at low air velocities (6 - 20 m/s)with 0.2 and 2.8 mm plastic spherical particles.It was studied that the solids flow rate and particle size play animportant role in the type of flow pattern involved and the transition from one flow mode to another. Generally at high gas velocity, the effect on the flow pattern of a gas-solids suspension was found to be small. However, at low gas velocities, small variations

in gas velocity resulted insignificant changes in the flow patterns. Analysis was carried out in order to determinecertain signal properties, such as mean value of pressure drop per unit length of pipe, the amplitude value of the pressure fluctuations (RMS value as a function of air velocity), power spectrum of the pressure fluctuations (frequency analysis) and statistical properties (skewness and flatness factor).

Dhodapakar and Klinzing (1993) attempted to relate the dominant frequencies and magnitude of the amplitude to the flow regime in horizontal dilute phase conveying by performing power spectral density function analysis (i.e. signal analysis in frequency domain)for the wall pressure fluctuations. Based on visual observation, eight different patterns were recognized: homogeneous flow, stratified flow; dense moving strand; strands on settled layer; blowing packets or clusters; blowing dunes; settled layer and plug or slug flow. It was also mentioned that the nature of the pressure fluctuations generated from the flow inside pipe is also affected by the feeder, the air supply and the collector, as a result characteristic fluctuations of the gas-solids flow gets altered. It was reported that generally, dilute phase flow (particles suspended in carrier phase) exhibited spectral patterns with high frequency components and low amplitude.

Cabrejos (1994) and Cabrejos and Klinzing (1995) termed the pressure fluctuations as ‘finger print’ of each flow regime for different gas-solid suspensions. Analysis techniques, such as rescaled range analysis and phase space attractor were applied to analyse the wall pressure fluctuating signals generated by the solid-gas flow during horizontal pneumatic conveying in dilute gas-solids suspension mode. A phase space reconstruction reveals the dynamic characteristics of a system in a two dimensional graph. In pneumatic conveying systems, phase space diagram with larger area indicates higher irregularity in the time-series as compared to the phase space diagram with less area.Several materials (alumina,

glass beads and polyester polymers) of varying size, density and shape were used for conveying through horizontal pipeline. Different flow regimes (homogeneous flow, stratified, pulsating flow, moving dunes and dense phase) for various bulk materials conveyed were reported according to their corresponding range of Hurst exponent. Hurst exponent is a parameter used to study self-similarities in a time series. Using the Hurst exponent, one can classify time series into types and gain some insight into their dynamics. Here are some types of time series and the Hurst exponents associated with each of them. Hurst exponent value close to 0.5 is indicative of a Brownian time series. There is no correlation between the observations and a future observation; being higher or lower than the current observation is equally likely. Series of this kind are hard to predict. A Hurst exponent value between 0 and 0.5 is indicative of anti-persistent behavior (an increase will most likely be followed by a decrease or vice-versa).A Hurst exponent value between 0.5 and 1.0 indicates persistent behavior. In a persistent time series an increase in values will most likely be followed by an increase and a decrease in values will most likely be followed by another decrease. Another aim of the reported work was to examine pressure fluctuations using chaos theory. Phase space diagrams were found to change when the gas velocity was changed. As the gas velocity was reduced below saltation and the flow destabilized, a second attractor appeared in the phase space diagrams, which indicated departure from stability.

Li (2002) analysed the pressure fluctuations for 3.5 mm polyethylene pellets in horizontal pneumatic conveying pipe using wavelet analysis. From random like pressure fluctuations, the fluctuating pressure components due to dispersed suspension flow and dune flow were extracted based on the wavelet multi-resolution analysis.

Jama et al. (1999) attempted to analyse pressure fluctuations in stable and unstable zone using Hurst exponent. It was reported that stable flow generally yielded Hurst exponents in the range of 0.1 to 0.3; while as the flow approached the instability, the value of Hurst exponent became 0.08. However, it was recognized that the above conclusion was based on a limited number of data and with single material; therefore this should not be put in practice in industrial systems without additional testing.

Liang et al. (2007)developed the Shannon entropy analysis of the pressure fluctuation time series to reveal the flow characteristics of pulverized coal with high moisture content. Shannon entropy is a measure of the uncertainty or variability associated with the random variable.In pneumatic conveying, the higher value of Shannon entropy reflect dynamic behavior, e.g., turbulent motion of carrier gas and solid particles, severe interaction between particles and gas, flow instability, and chaos.Effects of conveying differential pressure, moisture content, gas flow rate and superficial gas velocity on Shannon entropy were studied. With an increase in differential pressure, the values of Shannon entropy increased quickly at lower differential pressures and increased slowly at higher differential pressure. Shannon entropy values decreasedwith an increase in moisture content in the coal.

Pahk and Klinzing (2008b) attempted to assess flow regime for various materials (polymer pellets) conveyed in dilute phase mode through horizontal pipeline using different techniques of signal analysis named power spectral density (PSD), rescaled range, phase space diagram and wavelet analysis. Power Spectral Density (PSD) is a measure of a signal's power intensity in the frequency domain.It can be used to identify dominant frequencies present in the signal.The reported work included filtration of effect of blower and feeder from the pressure signal and the power spectrum caused due to gas-particle

interaction was obtained. Thus the power spectrum density enabled distinguishing the signals caused by flow noise, blower and feeder. The magnitude of power was related to the magnitude of the pressure fluctuation. Hurst exponent was found to increase with increase in the solid loading ratio when the dominant flow pattern was homogeneous while in the dominant pulsating flow pattern, Hurst exponent was found to decrease with an increase in the solid loading ratio. Phase space diagram changed from single attractor and low eccentricity to phase diagram with high eccentricity with two attractor points as the solids were introduced into the gas flow. The wavelet signal analysis technique was applied to decompose the original signal to detect signals due to noise, blower and feeder.The estimation of the power spectrum suffers from the formal requirement that the signal being analysed is stationary. This has led to the use of alternative analysis methods that do not require the signals to be stationary, including wavelet analysis and, more recently, the Hilbert-Huang transform.

Williams et al. (2008) analysed pressure fluctuations generated by conveying cement meal in fluidized dense phase conveying using wavelet decomposition. It was found that the amplitude of oscillations increased along the length of pipeline.

Liang et al. (2013) performed stability analysis for dense phase pneumatic conveying of coal and biomass at high pressure by conducting wavelet transform and Shannon entropy analyses. With the increase in conveying velocity, Shannon entropy of biomass was found to decrease, while for pulverized coal, it increased first with an increase in conveying velocity and then decreased.

In the following section, the studies and existing correlations for minimum transport boundary in the fluidized dense phase mode of pneumatic conveying have been presented.

The accurate and reliable design of industrial processes demands understanding of operating boundaries of a given pneumatic conveying system. An unreasonably high conveying velocity would result in high cost due to greater pressure drop, particle abrasion and pipe erosion. Alternatively, systems designed with extremely low velocities are susceptible to unsteady operation due to solids deposition and may eventually lead to pipe blockage. In general, the minimum conveying velocity can be defined as the lowest safe gas velocity for the horizontal transport of solids without the deposition of solids. To date a majority of the models for prediction of minimum transport boundary are empirical. Wypych and Yi (2003) developed a model for blockage prediction for low velocity slug flow- (applicable for granular products). Mills (2004, 2004a) indicated superficial velocity equals to 3 m/s (i.e. V_f= 3 m/s) as the criteria for minimum transport boundary. Superficial velocity of gas is the velocity considering as if gas is the only phase existing inside the pipeline and there are no solid particles inside the pipeline.

Mallick and Wypych (2009) developed a Froude number based criterion using different powders such as fly ash, ESP dust and cement through the different diameter and lengths of pipeline. It was found that $Fr_{i,min}$ = 5 criterion can be used for reliable prediction of minimum transport limits even under significant scale-up conditions for the products having “good” fluidized dense-phase characteristics. It was mentioned that the Fri=6 (with 20% safety margin) criterion can be used for design purposes. However, it was stated that the above mentioned design criteria were valid only for the range of test data obtained from the conveying of powders tested for limited range of solids loadings ratio. Therefore, extrapolating the results beyond the range was not advised. Recently, Setia (2012) developed an empirical model based on the solid loading ratio (m^*) and Froude number, Fr(based on pipe diameter)and an attempt was made to provide a unified model for a wider range of powders. The model was found to be reliable with a 30% margin; however, in

certain conditions it showed under predictions. From the above studies, it seems that work performed to date on the study of minimum transport boundary is largely empirical and moreover online prediction of blockage boundary has not been attempted so far.Therefore, there is a need to investigate into an unstable flow mode phenomenon near the blockage boundary. Pressure fluctuations in that scenario could provide a more precise picture of the flow characteristics.

Velocity of solid particles/dunes is also an important parameter to be considered in reliable design of pneumatic conveying systems. Due to the complex nature of flow in fluidized dense phase mode, estimation of particle velocity is a difficult task (Liu et al., 2007) and the same issimplified as superficial gas velocity in the most of empirical models used for pressure drop calculations. To overcome this difficulty, researchers have attempted to apply numerical simulations to determine particle velocity. Numerical models may be continuous- or discrete-based with respect to particles or the solid phase. The solid phase is treated as a discrete phase described by DEM. According to Zhou et al. (2010) the main forces involved in the particle-fluid flow modeling are: (1) the pressure gradient force, (2) the fluid drag force, (3) the gravitational force (4) the inter-particle forces between particles, which include the elastic contact force and viscous contact damping force. However, only a few numerical models based studies were made in the past to investigate the particle or solid phase velocity in pneumatic conveying, largely limited to dilute-phase flows.Flow meters for measuring particle velocity were based on the Doppler method andestimate the shift in frequency of an electromagnetic or an acoustic wave transmitted and partially reflected by the conveyed particles (Sanderson and Yeung, 2002) during the gas-solid flow through pipeline. These meters could be applicable for the measurements in dilute phase flow and allow for spatially resolving sensing when multiple transmitters are used. However, for dense phase mode, this method is not encouraged due to limited

penetration depth into dense material, and in addition to this, costly set-ups and solid-borne sound restrictions.

Correlative analysis could be another approach used to measure the solid phase velocity in gas-solid flows,which involves acquiring signals from two similar sensors located along the pipeline (separated by a certain distance). Fluctuations and disturbances caused due to material flow affect the characteristics of signals generated at two sensing locations. Using cross-correlation function, the time required for disturbances to travel from the one sensor to another sensor is obtained. Advantage of this method is that its application is not limited to a specific type of sensor and hence one can make use of the cross- correlation principle,irrespective of the type of sensors used (appropriate for a given measurement problem) (Beck and Plaskowski, 1987). The sensors in the two measurement layers may be based on ultrasonic methods (Coulthard, 1993), optical methods (Ichikura and Watanabe, 1995), radiation methods or the instantaneous measurement of material properties like permittivity (Shao et al., 2000), conductivity (Baar and Riess, 1997), charge (Ma and Yan, 2000) or temperature (Xu et al., 1996). Due to inherent robustness to noise, the correlation principles are commonly used technique for the measurement of the time delays in flow applications. However, an important disadvantage of the flow meters based on cross-correlation principle is that the signal similarity between two data sets captured at adjacent locations decreases with increasing distance between two sensing locations (Godbole et al., 2007). To put in another words, signal characteristics (frequency range and amplitude) of the time series data at second location get altered from the signal captured at first location. This dependence is caused by the change in flow characteristics and non axis-parallel particle trajectories between the upstream to the downstream sensor location.

Liu et al. (2009) studied the effect of different types of powder characteristics on particle velocity in dense phase pneumatic conveying. Particle velocity for different powders was determined from pressure signals. However, signal similarity (i.e. correlation coefficient) was not verified before calculating the time delay between signals.

Spatial filtering which is an alternative approach to correlative techniques is based on the estimation of signal amplitudes caused by moving particles through the sensing element of the transducer andthe material velocity is estimated from frequency spectra of the fluctuation data (Hrach et al., 2008). However, flow meters based on spatial filtering with multiple sensing locations along the flow direction typically require larger sensor lengths as compared to the flow meters based on cross-correlation principle.

Optical flow analysis techniques, such as Particle Tracking Velocimetry (Ostendorf and Schwedes, 2001) or Particle Image Velocimetry (Schlüter and Merzkirch, 1996) are subjected to dust development in the pipe and use of these techniques is limited to certain applications only. Few other measuring techniques, such as study of acoustic emissions generated by fine powder flow and granular material (Dhoriyani et al., 2006) or the use of venturi meter (Giddings et al., 2007) have been reported, but these are typically designed and optimized only for specific conditions. In general, application of these techniques for pneumatic conveying of bulk solids in industries is very limited.

Another category of flow meters based on the principle of attenuation of waves and radiations when directed through a conveying pipeline are also used in the industries. This particular technique is best suited forthe particles which are capable of absorbingsignificant amount of microwave energy, and thus cause the attenuation of microwave signals (Nugroho and Wu, 1999). Degree of attenuation of the signal depends

uponmaterial composition and size distribution. Material concentration in gas-solid flows is determined using radiometric concentration sensors, based on the principle of the attenuation of γ-rays or x-rays (Barratt et al., 2000). However due to strict import regulations the use of ionizing radiation for many applications is restricted and moreover due to high cost and safety constraints this particular method is not practiced for the general use in industrial applications.

To obtain particle velocity and concentration by means of Electrical Capacitance Tomography (ECT) (Dyakowski et al., 1997) is another approach which involves reconstruction of cross-sectional images during a conveying process. In this case, a tomographic image can be constructed (by solving an inverse problem) from the signals acquired based on the principle of capacitancevariation. However, this technique involves large amount of measurement data to be processed due to multi-sensor setup and required high sampling rates. Therefore, reconstruction algorithms are complex in nature and real-time image generation for flow applications would be difficult. Promising reconstruction techniques with comparatively less degree of complexity have been reported recently (Zangl et al., 2007).

Jaworski and Dyakowski (2002) investigated flow instabilities within dense phase pneumatic conveying of granular material (polyamide chips of approximate dimensions 3mm × 3mm × 1mm) by analyzing ECT signals using spectral and cross-correlation techniques. Thus the velocity distribution in the pipe-cross section was determined. Fuchs et al. (2007) also applied capacitance measurement principles to determine important flow parameters for poly pellets (3.8 mm diameter and 900 kg/m^3 particle density) conveyed in dilute phase as well as dense phase pneumatic conveying. In dilute phase flow, particle velocity and concentration were determined by means of correlation methods. In dense

phase flow, slug velocity and slug length were determined by difference algorithm and Fourier transform. Recently, Williams et al. (2007) conducted pneumatic conveying trials with cement meal (d_{50}= 11 μm, the solid loading ratio in the range of 51-70) and determined average velocity from the time delay difference of peaks and troughs of the pressure signals corresponding to two different locations of pipeline. Average velocity from pressure fluctuations was found pertaining to the specified testing conditions and product. William et al. (2007) concluded that more analysis was required for different conveying conditions, thus signifying the need for further research.

Apart from being used in assessing the flow regimes in horizontal pneumatic conveying, pressure drop fluctuations have been also used to investigate into the fluidization quality of fluidized beds. Fluidized beds find wide applications in industries to be used as reactors for combustion, gasification, agglomeration or for drying and mixing processes as these provide increased heat and mass transfer rate per unit volume. A fluidized bed may operate involving different flow regimes, depending on various parameters, such as gas velocity, solids properties and bed geometry. The fluidization quality is generally assessed by the flow mechanism involved insidethe fluidized bed during operations and degree of other processes involved (such as channeling, compaction and segregation). The analysis of pressure drop fluctuations for fluidized beds includes calculation of root-mean-square (RMS) values, correlations, probability distributions and power spectral density functions etc. Apart from these techniques, recently, fractal analysis, deterministic chaos analysis (phase attractors) of pressure drop and Shannon entropy have been used as a basis for evaluating the fluidization quality of different solid particles and to assess the transition between different regimes (Duan and Cong, 2013; Zhong et al., 2009; Zhong and Zhang, 2005).

Zhong et al. (2009) performed Shannon entropy increment analysis on pressure fluctuations of biomass fluidized bed to study flow patterns and dynamic behavior. The Shannon entropy increment of steady fluidization was found to be minimum, while it was found maximum for the turbulent fluidization. Afterwards, Duan and Cong (2013) used the method of Shannon entropy to compare the dynamic behavior of certain Geldart group B and D particles in fluidized beds. The Shannon entropy of Geldart group B particle rose steadily to the maximum (resulted from the uniform expansion of bed), while the Shannon entropy of Geldart group D exhibited only slight increase during initial fluidization (due to limited expansion of bed) and then increased rapidly to a maximum as the velocity was increased (due to increased solid-gas interaction and uncertainty).

From the above studies performed by various researchers in pneumatic conveying and fluidized beds, pressure drop fluctuations appear to be a promising technique in flow-regime identification and characterization of gas-solid flows. However, it can be seen that the researchers have focused largely on dilute phase mode of conveying (for coarse granular products) for which flow mode is relatively simpler. Little work have been reported for fluidized dense phase mode of conveying fine powders and on the analysis of the generated signals using different techniques to investigate into flow condition. Because of the strong adhesion and electrostatic attraction of fine powders (with the average particle size of less than 100 μm) to the pipe wall, it is very difficult to recognize the flow patterns in the conveying pipe by direct optical visualization. Moreover, flow mechanism is far more complex (due to multiple interactions, including particle-particle, particle-wall and particle air) in the fluidized dense phase mode as compared to dilute phase. Accurate measurement of flow patterns helps improve the understanding, safety and the reliability of practical processes (Cong et al., 2011;Rahmat and Kamaruddin, 2012). Although pneumatic conveying has been of great importance for industrial applications, however,

these applications mostly depend on empirical approaches for design of pneumatic conveying systems due to the lack of sufficient information and data for the predictability of the essential flow patterns and the estimation of parameters involved. Relating the acquired pressure fluctuations to the various flow patterns existing in pneumatic conveying systems and exploring the effects of the variations of a number of flow parameters through the analysis of pressure signals are, therefore, of major concern (Pahk and Klinzing, 2008b). Hence, further research needs to be conducted to understand the fluidized dense phase mode of conveying for fine powders by applying appropriate signal analysis techniques.As compared to fluidized dense phase mode of conveying for fine powders considerable amount of progress has been made in understanding the particle mechanics (Rao et al., 2008), non-Newtonian behavior and rheology of particulates (Chhabra and Richardson, 2011). Levy (2000) attempted to simulate the plug flow in horizontal pneumatic conveying. However, writing accurate governing equations for highly turbulent fludised dense phase mode of conveying is a challenging task and requires large number of assumptions to be made.Variation in flow mechanism with change in operating conditions, such as solid loading ratio is also an important aspect, since inter particle forces affect the fluidization behavior of fine powders (Bruni et al. 2007). Therefore, change in flow mechanism along the pipeline length as well as due to change in operating conditions would need to be examined using pressure signal fluctuations. Apart from flow mode investigation, prediction of minimum transport boundary is also important to avoid unsteady flow characteristics and pipe blockage. At present, most of the models for minimum transport boundary are empirical and very little work has been reported using pressure signal fluctuations to depict minimum transport boundary. Solid velocity, which is another important parameter for modelling flow mechanisms, is to be considered in pneumatic transport. Currently ECT (Electrical capacitance tomography) based techniques are used to estimate the particle velocity in

solid-gas flow through horizontal pipeline, however little research has been performed to attempt particle velocity estimation using pressure signal fluctuation for pneumatic conveying of fine powders. Overall, this chapter provides various signal analysis techniques having potential applications for analysing pneumatic conveying of fine powders.

CHAPTER 3: TEST FACILITY AND EXPERIMENTAL PROCEDURES

3.1 Introduction

The flow mechanism involved in solid-gas flow through the pipeline is believed to depend upon a large number of operating parameters such as diameter and length of pipeline, type of product conveyed and mass flow rates, conveying gas velocity and solid loading ratio. Due to above mentioned reasons and complex flow mechanism, especially in case of fluidized dense phase conveying, limited work has been attempted so far to analyse pressure signals for the purpose of flow condition identification. Scope of present thesis includes investigation into flow mechanism with the aid of time-series analysis. Pneumatic-conveying testing is necessary to collect pressure signal fluctuations. For this thesis, test data for different products conveyed through various pipes of different diameter and length were considered. Earlier investigation was carried out on the test data made available from the University of Wollongong for conveying of two products (fly ash and white powder). Later on, analysis was performed on the test data obtained from conveying trials conducted on the test rig developed at Thapar University, Patiala, India for the conveying of Indian fly ash. Experiments were performed for a wide range of air flows and solid flow rates through pipelines of different diameters and lengths. The intent of this chapter is to provide the details of test facility, instrumentation, calibration and operational proceduresused to perform the pneumatic conveying trials.

3.2 Experimental setup

Experimental data from University of Wollongong (Mallick, 2009) consists of signal output corresponding to different transducer locations installed along the pipeline during

pneumatic conveying of fly ash and white powder through the different experimental test rigs shown in Figure 3.1 and Figure 3.2 respectively.

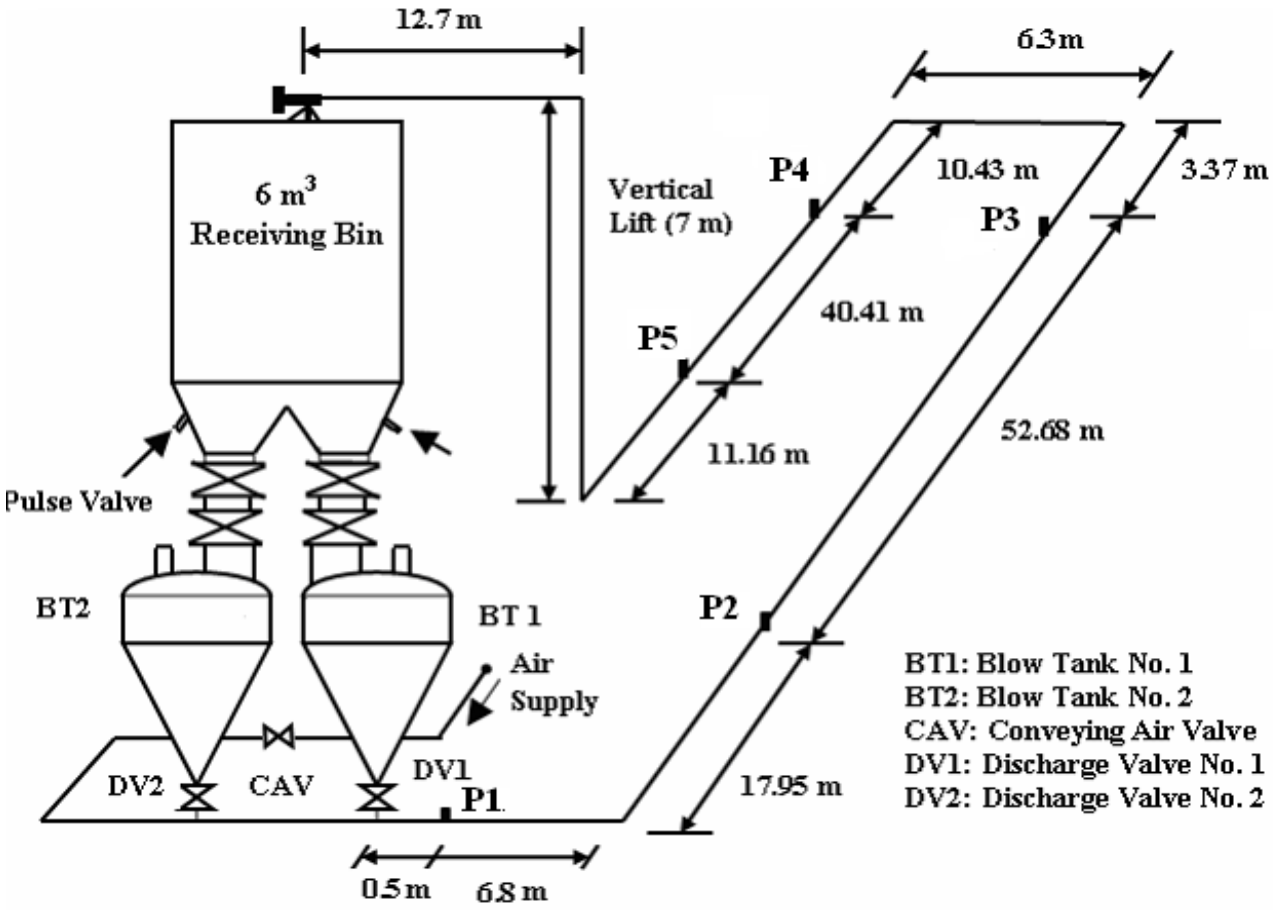

Figure 3.1: Schematic diagram for 69 mm I.D. and 168 m long test rig for fly ash indicatinglocations of pressure tapping points, blow tank, receiver bin arrangement (Mallick, 2009).

Test facility for fly ash comprised of:

a) 0.425 m^3 bottom-discharge blow tank feeding system;

b) 69 mm I.D. (internal diameter of pipe) and 168 m long mild steel pipeline, including a 7 m vertical lift;

c) Five 1 m radius 90° bends and 150 mm N.B. (nominal bore) tee-bend connecting the end of the pipeline to the feed bin;

d) 6 m^3 receiving bin;

e) Static pressure transducers (P1-P5); P1 was used to measure the total pipeline pressure drop and P2 to P5 were used to measure static pressure along the pipe length;

f) Load cells on feed bin and receiving bin;

g) Annubar with DP (Differential Pressure) meter and data acquisition unit for data recording and analysis;

Pressure signals were obtained at different locations along the pipeline with the help of static pressure transducers along the length of pipeline having specification: manufacture: Endress and Hauser, model: Cerabar PMC133, pressure range: 0-6 and 0-2 bar, maximum pressure: 40 bar (absolute), signal: 4-20 mA. A flow control/needle valve was used to control the air flow rate. To determine solid mass flow rate through the pipeline, solid mass flow rates out of the blow tank and into the receiver bin were measured using load cells. DT800 data acquisition system was used. White powder was conveyed through another test rig, Figure 3.2, as provided in the following:

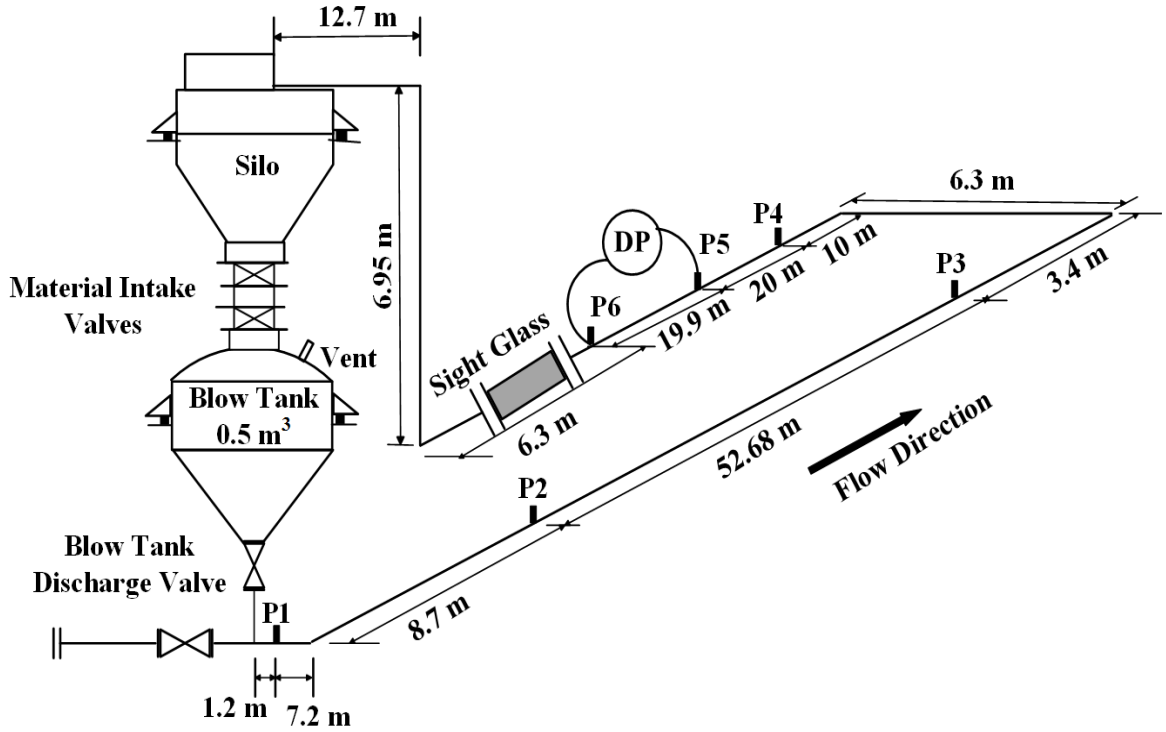

Figure 3.2: Schematic for 69 mm I.D. and 148 m long test rig for white powder, (Mallick, 2009)

This test facility comprised of:

a) 0.5 m^3 bottom-discharge blow tank feeding system;

b) 69 mm I.D.148 m long mild steel pipeline, including 6.95 m vertical lift;

c) 6 numbers of 1 m radius 90° bends;

d) Static pressure measurements via two sets of tapping locations on the straight pipe lengths: P2-P3 (52.68 m apart) and P5-P6 (19.9 m apart). The tapping locations were similar to that of the fly ash test rig (described previously), except an additional tapping point P6 was installed. The location of P6 in Figure 3.2 is the same as the location of P5 in Figure 3.1, and the new location of P5 is almost at midway between P4 and P6. The P1 tapping location was used to record total

pipeline pressure drop and P2 to P6 were used to measure static pressure along the pipeline;

e) “Sight glass” was used just after the P6 location (approximate length of 1 m) for flow visualization. The sight glass was made of toughened glass and was connected into the pipeline with struab coupling and braced with rods to protect the glass and keep it straight. Other necessary instrumentation, data acquisition unit etc. were similar to the arrangement shown in Figure 3.1.

Later on, experiments were conducted at pneumatic conveying Laboratory for Particle and Bulk Solids Technologies of Thapar University, India. Conveying of Indian fly ash was performed at the test facility shown in Figure 3.3.

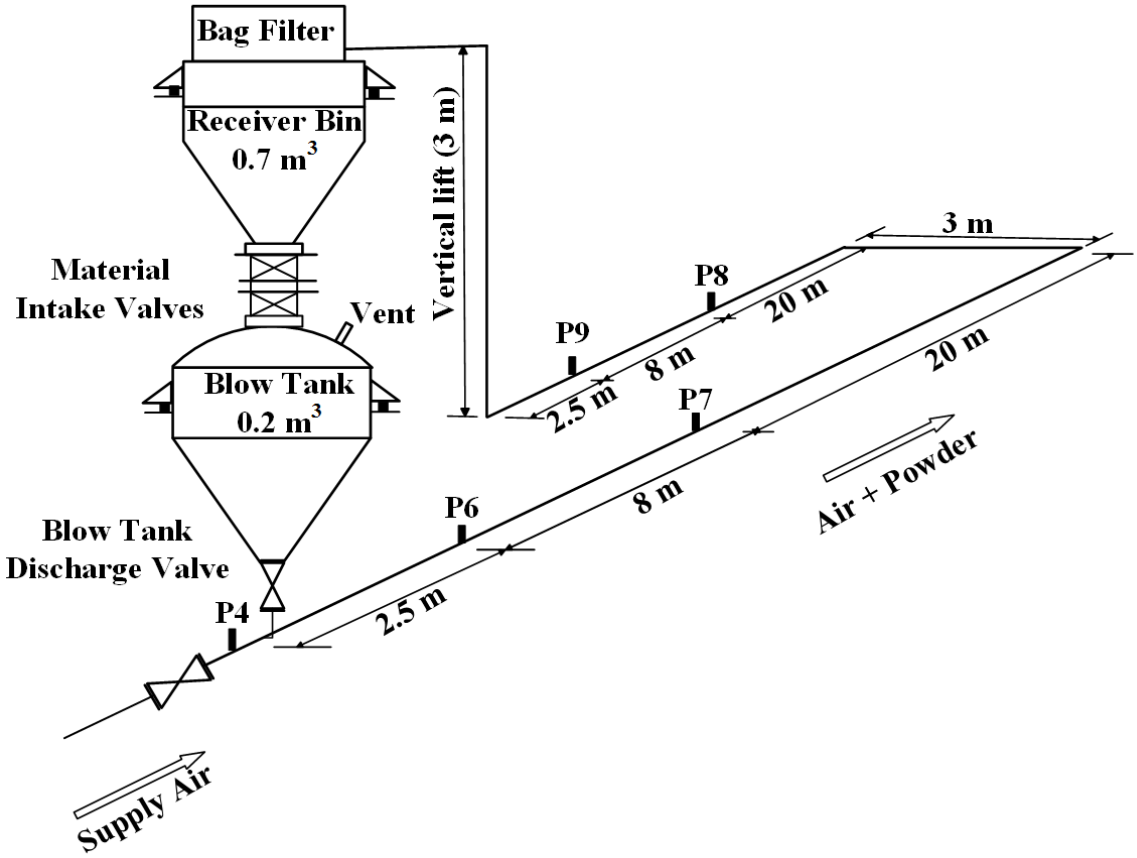

Figure 3.3: Schematic of the 51 mm I.D. x 70 m long pneumatic conveying test facility developed at Thapar University, Patiala

An electric powered rotary screw compressor (Make: Kirlosker, Model: KES 18-7.5) was used to supply compressed air having maximum delivery pressure of 750 kPa and 0.056 m^3/s of free air delivery. In order to get moisture free compressed air for conveying and instrumentation purposes, compressed air was made to pass through an air drier and subsequently was stored in an air receiver. The main compressed air stream line was divided into two streams (i.e. primary and secondary air). Primary air was used to operate and control the blow tank, while secondary air was used for instrumentation purpose. A pressure regulator and flow control valve were installed in compressed air line before the blow tank to set the maximum pressure and to vary the air flow rates over a wide range

(i.e. 0-0.6 kg/s). A vortex flow meter was installed for the measurement of air flow rates in compressed air flow line. Primary air was further divided into 3 different air streams i.e. top air, fluidization air and conveying air line with the help of a 50 mm primary air header. Figure 3.4 shows the compressed air supply and distribution.

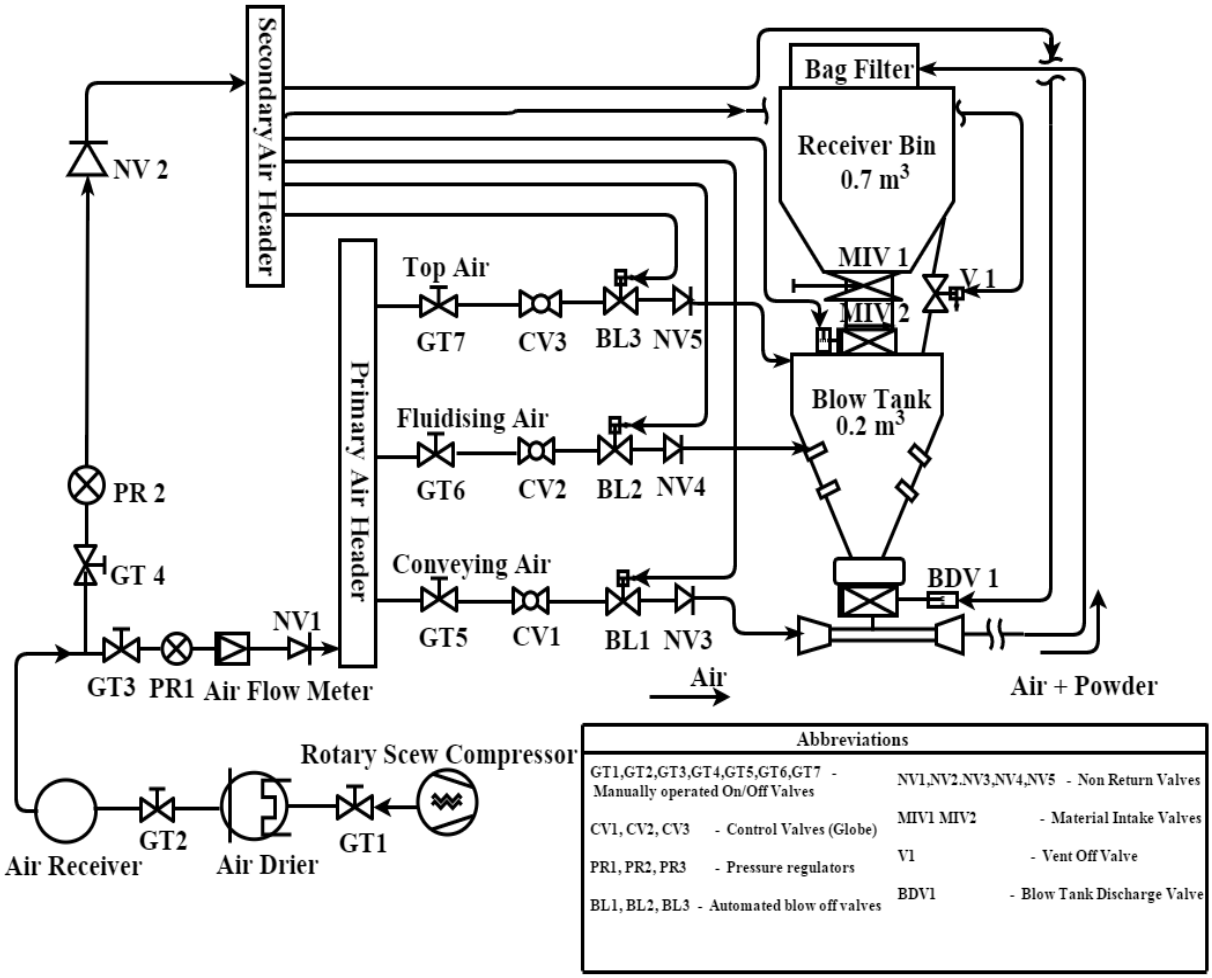

Figure 3.4: Piping and instrumentation diagram for compressed air at 51 mm I.D. x 70 m long test set of Thapar University, Patiala

Through secondary air header, compressed air was supplied to the pneumatically driven valves and mechanical bag filter installed at top of the receiving bin. The pressure of supply air to the blow tank and the pneumatically operated control panel was controlled using pressure regulators PR1 and PR2, respectively. A bank of manually operated

valveswas used to control the air supply to the different regions of the blow tank and to ensure proper distribution and fluidization of bulk material. By varying the distribution of air in the top, fluidization and conveying air, different flow conditions were achieved in the conveying pipeline.The valve opening setting was done before the start of conveying cycle and during one conveying cycle these settings were not altered. After the completion of conveying cycle, the valve openings were adjusted to achieve new mass flow rate of air for the next run of experiment.Total cycle time was about 4-6 minutes depending upon the pipeline length and material flow rate. Gate valves (GT1 to GT7) were used as on/off valves to start or cut off the supply of compressed air at various locations in the pipeline. A vent off valve, V1 (operated from the control panel) was used to release the pressure inside blow tank after completion of one conveying cycle. Valves placed in between the receiving tank and the blow tank (i.e. MIV1 and MIV2) were used to transfer the material from receiving bin to the blow tank for the successive test runs. Material intake valve, MIV1 was operated manually (used occasionally for isolation and maintenance purpose), while MIV2 was a pneumatically operated valve. Blow tank (manufactured/supplied by Mcgale Pneumatics Ltd, Nagpur) of 0.2 m^3 water filled volume (bottom discharge type) was used to feed material into the conveying pipeline. The air was supplied to the blow tank with the help of orifice plate installed at its air inlet. Blow tank was equipped with solenoid operated dome type material inlet, outlet and vent valves. Inside the blow tank, there were porous fluidizing membranes at the sloped portion of the side walls to fluidize the material inside the blow tank. On the top of the blow tank, a receiver bin of 0.70 m^3 capacity was installed. It was fitted with bag filters having reverse pulse jet type cleaning mechanism. For the measurements of solid mass flow rates, blow tank and receiver bin were supported by shear beam load-cells (Nominal load: 500 kg, sensitivity (output at nominal load): 3 mV/V, accuracy: ±0.1%, nominal range of supply voltage: 0.5-12 V). Two different mild steel pipelines (i.e. 54 mm ID and 70 m long; 54 mm ID and 24 m

long) were used to perform the conveying tests. All the pipeline configurations included a vertical lift of 3 m and 4 × 90^{o} bends of 1 m radius of curvature. Various static pressure measurement points were provided at different locations along the pipeline. P4 was used to measure the total pipeline pressure drop, while all other pressure transducers (P6 to P9) were installed to measure static pressure at their respective locations with specification: Make/Model: Endress & Hauser/Ceraber PMC 131; pressure range: 0-2 bar; maximum pressure: 3.5 bar (abs.); current signal: 4-20 mA. A standard calibration procedure was followed to calibrate all the pressure transducers, load cells and flow meter (as per Mallick, 2009). High speed data acquisition system NI-5208; with 32 different channels; 24 bitresolution; and capable of collecting samples at the rate of 200 kHz was used to capture the signals from pressure transducers. The pipelines were equipped with sight-glasses made of toughened borosilicate materials at different strategic locations for flow visualization (using high speed digital camera).

Fly ash was conveyed through the test set up for wide range of air and solid mass flow rate. Flow visualization through sight glasses confirmed the fluidized dense phase conveying ability of fly ash. Continuous dune flow was observed in conveying pipeline with gradual reduction of air flow, which in turn changed to discontinuous dune flow with further reductions in air flow rates. Even further reductions in air flow rates resulted in unstable conveying characterized by high pressure fluctuations and led to complete pipeline blockage. In the unstable conveying zone, amount of material pushed by blow tank into the conveying pipeline did not completely return to receiver bin, which led to gradual deposition of material in the conveying line. Gradual deposition of material resulted in complete blockage of pipeline in few conveying cycles. Blow tank initial pressure was varied to change the solid flow rates.

3.3 Product Characterization

Pneumatic conveying systems to transport fly ash in dry mode are extensively used in coal fired thermal power plants in India due to the high ash content of Indian coal and the increasing requirements of conveying fly ash in dry form. However, reliable design of such system demands a considerable amount of knowledge on product characterization and complex solids-gas-pipe wall interactions. An error in design and estimation of a typical fly ash pneumatic conveying system can cause significant amount of losses in terms of reduced delivery, increased energy consumption and unnecessarily larger capital investments etc. In view of investigating the flow mechanism involved in pneumatic conveying of flyash, pneumatic conveying trials have been performed at Thapar, University test setup using Indian fly ash and pressure fluctuation data were generated to be further analysed. Before conveying the fly ash through the test rig, product characterization was performed to reveal the properties, such as particle size, shape, particle density and bulk density of the material. Following procedures were used to determine these properties:

3.3.1 Particle size distribution

Particle size distribution was done using a laser diffraction analyser (Mastersizer 2000). Particles pass through a laser beam and the light scattered by them is collected over a range of angles in the forward direction. The angles of diffraction are, in the simplest case, inversely relate to the particle size. In case of volumetric analysis, the particles pass through an expanded and collimated laser beam, whose focal plane is positioned in front of a photosensitive detector consisting of a series of concentric rings. Distribution of

scattered intensity is analysed by computer to yield the particle size distribution. Figure 3.5 shows the particle size distribution of fly ash obtained by using laser diffraction analyser.

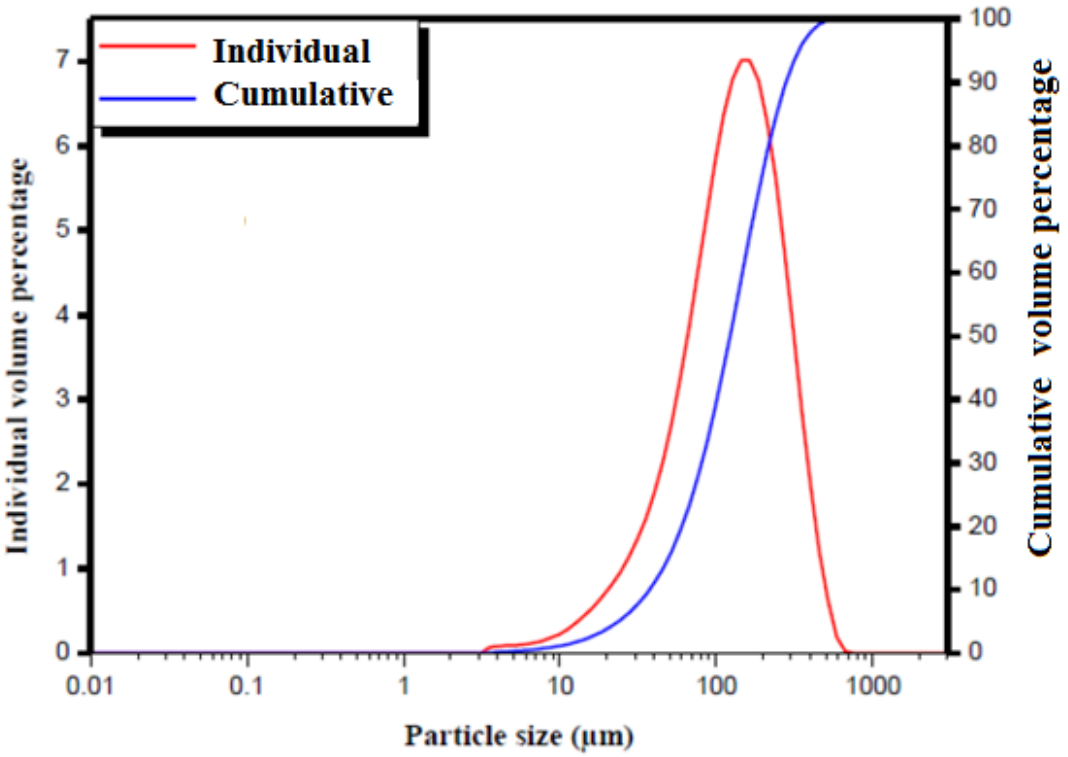

Figure 3.5: Particle size distribution of fly ash

The red line in the figure shows individual volume percentage, whereas the blue line represents the cumulative volume percentage.

3.3.2 Particle density

It is a critical parameter in pneumatic conveying because of its possible effect on pick-up velocity. It can be determined by using a specific gravity bottle or by using pycnometer.

The following table represents the particle density estimation by using containers of different capacity and measuring the volume occupied by certain amount of flyash and then by adding known volume of water so that all the air present in the empty space between particles is replaced by water and volume occupied just by solid particles is known.

3.3.3 Bulk density

The bulk density is the measure of the average density of the material. It is possible to obtain a number of densities (tapped density, loose poured density and consolidated density) depending on the amount of compaction or expansion. Bulk density is also a function of particle size distribution (Wypych et al., 2005). To determine the bulk density, same procedure was followed as described in the previous section except for using water, volume occupied by flyash and air together was considered.

3.3.4 Particle shape

To reveal the particle shape, fly ash samples were tested by scanning electron microscope (SEM), in which a high energy beam of electrons is made incident on the sample to produce the scanned image of the particles. These energetic electrons then interact with the atoms of the sample and produce different signals that are detected by the sensors. Following figure shows the image obtained using the equipment SEM-JSM-6510LV JEOL.

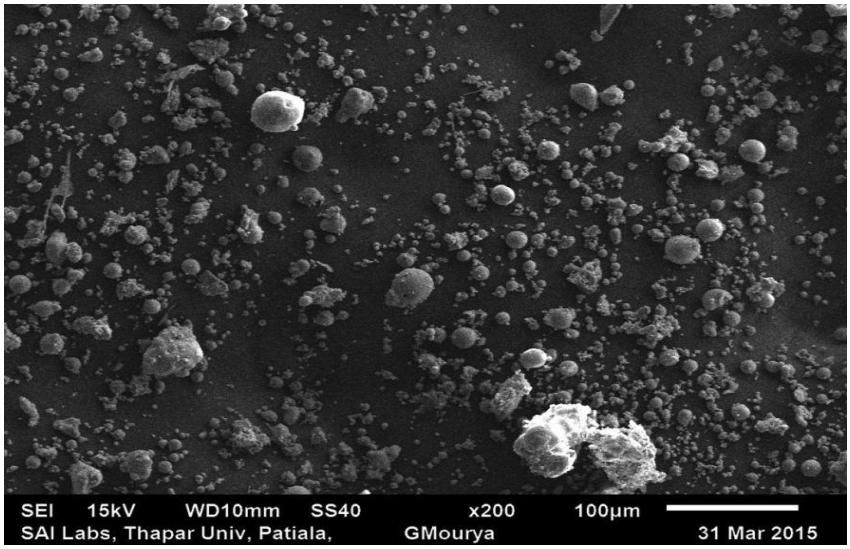

Figure 3.6: Microscope image of fly ash sample (median particle size 21 µm)

The shapes of the particles were determined with the help of microscopic images obtained from SEM. As seen in the above figure the shape of the particles is almost spherical.

Based upon characterization performed as given in the above section, physical properties fly ash conveyed through the test setup of Thapar University are listed in following Table 3.1.

Table 3.1: Physical properties of Indian fly ash

Product	ρ_s (kg/m^3)	ρ_{bl} (kg/m^3)	d_{50} (µm)
Fly ash	1790	990	19

Fly ash particles have spherical and glassy shapes with different sizes varying from less than 1µm to more than 100µm, with typical particle size measuring less than 19 µm. It is composed of silica, alumina and ferric oxides (at least 70%), a small amount of MgO, SO_3, and Na_2O. Chemical properties of Indian flyash have been presented in Table 3.2 (tested at the Sophisticated Analytical Instrument Laboratory of Thapar University).

Table 3.2: Chemical properties of Indian flyash

Element	Composition
SiO_2	56.5%
Al_2O_3	17.7%
Fe_2O_3	11.0%
$CaCO_3$	-
CaO	3.2%
MgO	5.4%
Loss of ignition	1.2%

Physical properties of powders conveyed through experimental test facility of the University of Wollongong (Mallick, 2009) are listed in Table 3.3.

Table 3.3: Physical properties of powders (Mallick, 2009)

Product	ρ_s (kg/m^3)	ρ_{bl} (kg/m^3)	d_{50*} (μm)
Fly ash	2300	700	30
White powder	1600	620	55

*median particle diameter

3.4 Calibration procedure

Calibration of load cells, pressure transducers and flow meter were performed using the standard calibration procedure as described by Mallick (2009). All the pressure

transducers were calibrated by maintaining constant static pressure in the conveying pipeline using blind flange and simultaneously recording the pressure signal from data logger. The standard calibration procedure for pressure transducers is given below:

a) Install all the pressure transducers at desired locations along the pipeline and connect these to the data logger.
b) Close the pipeline upstream of the receiver bin using blind flange.
c) Check the pipeline for air leakages, rectify if any leakage found and open the vent valve to release the air from the pipeline.
d) Adjust the pressure regulator to desired value (e.g. 50 kPa) and open the conveying pipeline valve.
e) Measure the pressure in the pipeline using a pressure gauge and record the pressure of all the transducers simultaneously from data logger.
f) Repeat the step (e) by adjusting the pressure regulator to different pressure readings.

Calibration graph thus obtained for pressure transducers P4 and P6 are shown in Fig. 3.7and 3.8.

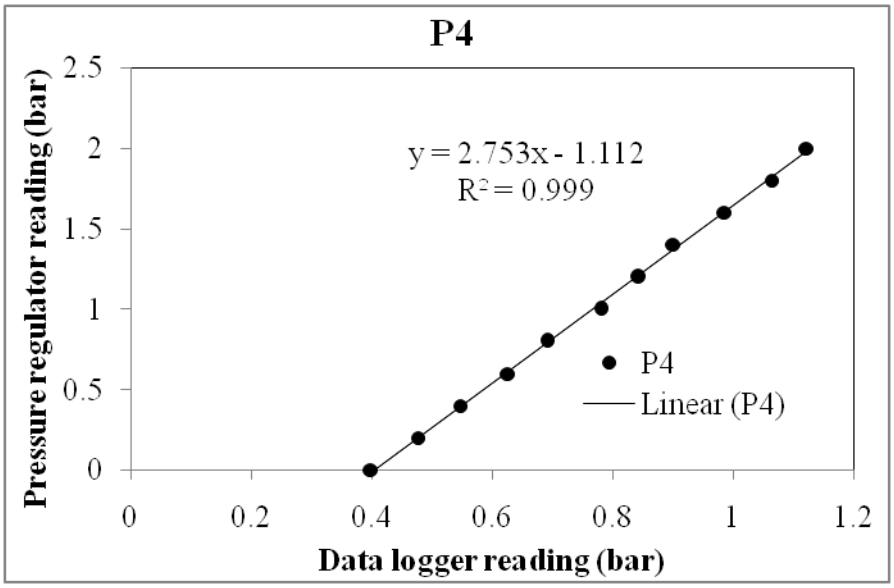

Figure 3.7: Calibration curve for pressure transducer P4

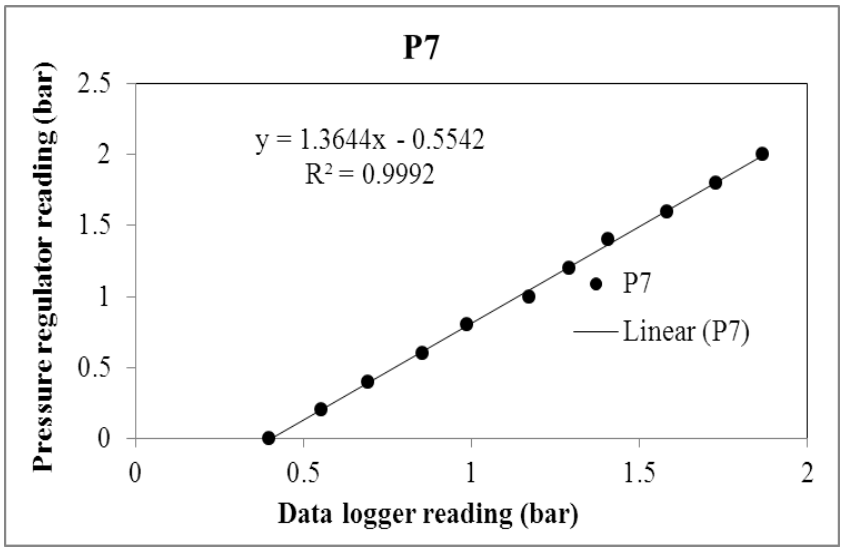

Figure 3.8: Calibration curve for pressure transducer P7

A vortex type air flow meter was used to measure the flow rate of air supplied in a conveying cycle. This flow meter has a digital display which shows the reading of volumetric flow rate of air, at the same time it also generates an analog signal, which is fed to the data logger and after further processing of signal, data logger also displays the volumetric flow rate. To calibrate the flow meter, a continuous supply of air was made in

conveying pipeline and readings of flow meter were recorded simultaneously in its digital display and at the data logger. Pressure at the inlet of flow meter is recorded with the help of pressure transducer to calculate density of inlet air to flow meter, so that its mass flow rate could be obtained.

Load cells were used to calculate the mass of material accumulated in and discharged from receiver bin and hopper. Blow tank and receiver bin were placed on shear beam type load cells. Each load cell has the maximum load bearing capacity of 500 kg. Set of such four load cells were used to carry the combined weight of blow tank and the material inside; similarly for the receiver bin and the material inside it. Output from these four load cells are combined to give a total load shared by each cell. The load cells generate a differential output voltage signal, which is fed into a data logger to calculate the corresponding weight. Two such combinations are used to measure the material discharge rate. To calibrate load cells, known weightsare put on the structure and the values are recorded in the data logger.

3.5 Pneumatic conveying testing procedure

Pneumatic conveying trials were performed by conveying fly ash through the experimental test rig set up. A series of experiments were conducted for every product conveyed at the wide range of conveying conditions (i.e. for different combinations of m_s and m_f). Static pressures were obtained from the static pressure transducers located along the pipeline length. Sufficient numbers of tests were conducted to clearly identify the blockage boundary. Some of these tests were repeated to monitor any changes to the product properties over time (product degradation due to repeated testing). High speed digital camera (with sufficient background light) was used to study the flow through sight glass

and for better understanding of the physical nature of the fluidized dense-phase flow.A standard operational procedure was used to perform the experiments over a wide range of air and solid flow rates. Air flow rates were varied by changing the openings of globe valves installed in the pipeline, whereas solid mass flow rates were varied by changing the pre-pressurization of the blow tank. There are two air lines in blow tank: one is the top air line, which supplies the air for pre-pressurization of blow tank, the other is fluidization air line, which is used to fluidize the material inside the blow tank and ensures that the materials would not stick to the walls of blow tank. Fluidization air line is also provided in receiver bin to prevent sticking of material (for flow assistance).

Between the receiver bin and blow tank, there was a manual isolation valve and product intake valve. The manual isolation valve was provided to isolate the receiver bin from a blow tank in cases of maintenance. The product intake and discharge valves were of knife-gate type. These are ON/OFF type valves (complete shut-off or full open). These are pneumatically actuated valves (with solenoid) and were operated from a control panel (having ON/OFF switches) placed next to the blow tank. The product intake valve was opened after ensuring that the discharge valve is closed and vent valve was open. After the intake of product in the blow tank, the vent valve and product intake valve were closed and the blow tank was pressurized to a sufficient pressure suitable to deliver adequate steady state conveying. After this, the discharge valve was made open for the flow of product out of the blow tank. The product discharge rates were controlled by varying flow of fluidizing air.

The standard operational procedures followed to perform the experiments are:

a) First of all, the compressor was switched on so that the air should reach the specified pressure in the air storage tank placed next to the compressor.
b) Process air and instrumentation air supply valves were opened. Pressure of process air was set to desired value using pressure regulator, whereas, the pressure of instrumentation air was set to 5 bar (g).
c) Pneumatic panel and PLC panel were switched ON. PLC was programmed according to the desired sequence of opening and closing of pneumatically actuated valves. After that computer system (connected with data logger) was made ON and the data logger connectivity was ensured.
d) Before starting of the experiments, the pressure transducers, load cells and flow meter were calibrated.
e) All the globe valves were set as per the desired flow rates and then conveying cycle was started. At the same time, data logger was also run.
f) After the complete conveying cycle, data logger was stopped and the signals from the pressure transducers, load cells were recorded in the excel file for that particular experiment.
g) The pipeline was purged to clean it for the next experiment. Globe valve settings were adjusted and the procedure was repeated to perform further experiments.
h) After performing a set of experiments pressure transducers were calibrated again so as to ensure that these were not blocked filter and cleaned if any blockage was found.

In each individual experiment, data logger recorded the load cell, flow meter and pressure transducer readings for the complete cycle. All these data points were plotted with time and steady state data was taken for further analysis work (signal/time-series analysis) for flow mode identification. The pressure fluctuation data and average values of mass flow

rates of air and solids, used as a basis for carrying out the fluctuation analysis was obtained from the part of the conveying cycle where the pressure was stable and the mass flow rates were constant. Figures from 3.9 to 3.11 show the typical plots corresponding to the air and solids flow rates and pressure variation during the complete conveying cycle.

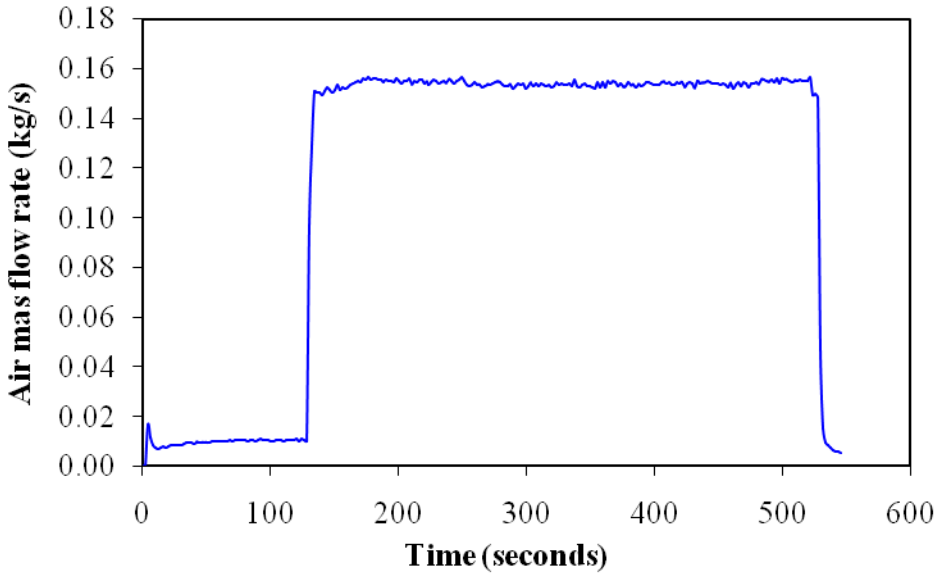

Figure 3.9: Variation of mass flow rate of air (m_f) during conveying cycle; (test setup of University of Wollongong, Figure 3.1; m_f =0.15 kg/s, m_s = 1.97 kg/s

As seen the above figure, corresponding to mass flow rate of 0.15 kg/s, steady state conveying starts and it takes approximately 110 seconds for steady state conveying to start. Figure 3.10 represents the curves for solid mass variation inside the blow tank and the receiver bin (silo) during the complete conveying cycle.

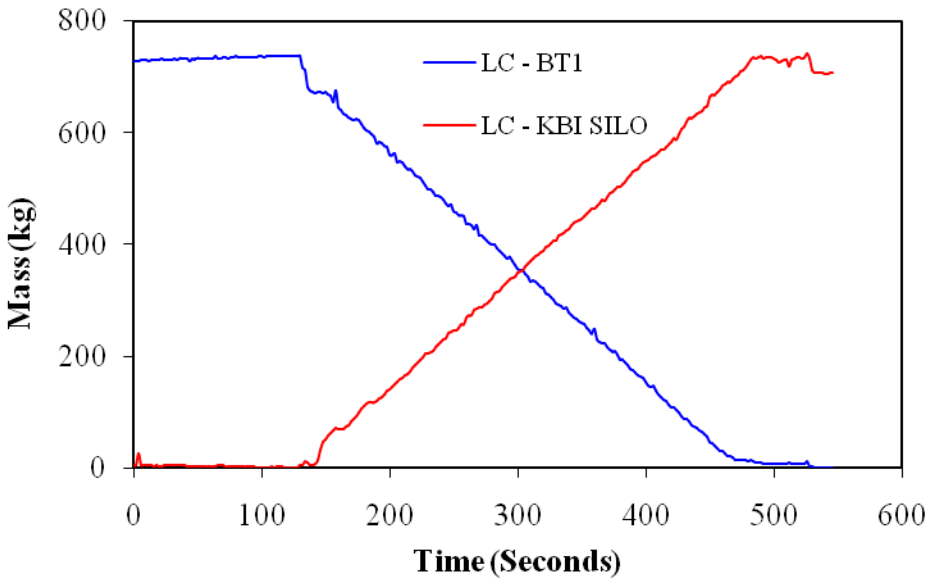

Figure 3.10: Variation of mass flow rate of solids (m_s) during conveying cycle; test setup of University of Wollongong, Figure 3.1; m_f =0.15 kg/s, m_s = 1.97 kg/s

As seen in the above figure, the blue line represents the variation of solid mass inside the blow tank, while the red line represents the solid mass variation inside the receiver bin (silo). The amount of solid mass decreases gradually inside the blow tank and it increases inside the silo and at the end of the cycle, mass in blow tank drops to zero and the entire mass is now contained in the silo. It indicates steady state conveying without any product deposition inside the pipeline. Figure 3.11 shows a typical pressure signal fluctuation obtained from one of the transducer locations installed along the pipeline length.

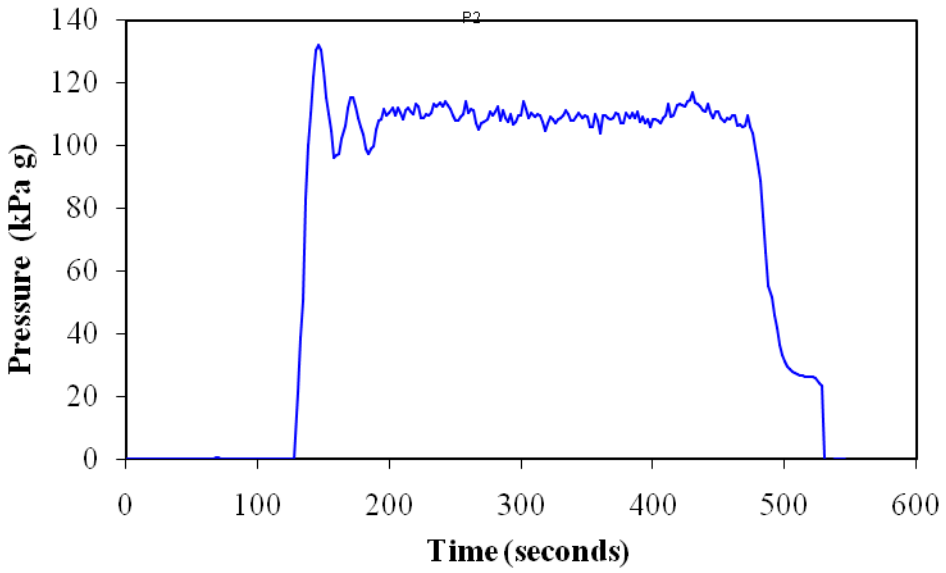

Figure 3.11: Variation of pressure during complete conveying cycle at P2 (test setup of University of Wollongong, Figure 3.1; m_f =0.15 kg/s, m_s = 1.97 kg/s

To ensure the repeatability of test data, certain tests were performed multiple times. Results from pressure transducers at different location are provided in the following figures. Figure 3.12 represents the results of an original test, while the Figure 3.13 represents the data when the experiment was repeated for a similar set of operating conditions, i.e. at about m_f =0.07 kg/s, m_s = 2.71 kg/s. As can be seen in these figures, steady state period is almost the same (i.e. between 200 to 300 seconds). At the same time, pressure ranges depicted by the transducers during first run and the repeat experiment are similar.

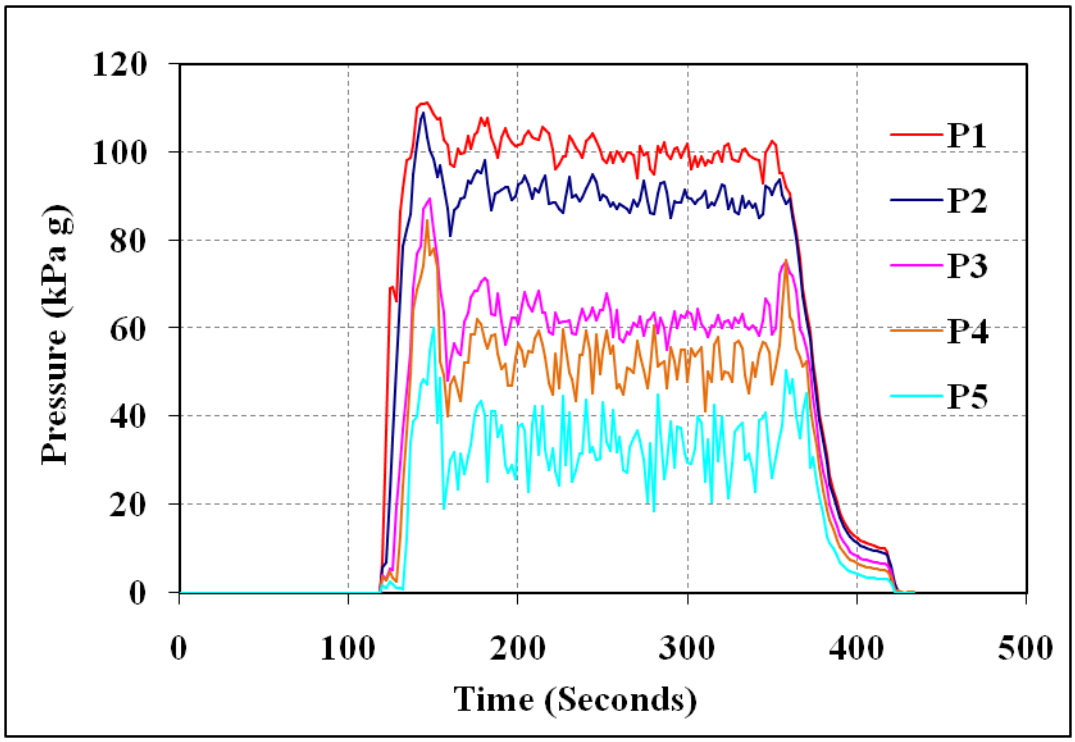

Figure 3.12: Pressure fluctuations at different transducer location during a typical pneumatic conveying trial (first run); m_f =0.07 kg/s, m_s = 2.71 kg/s

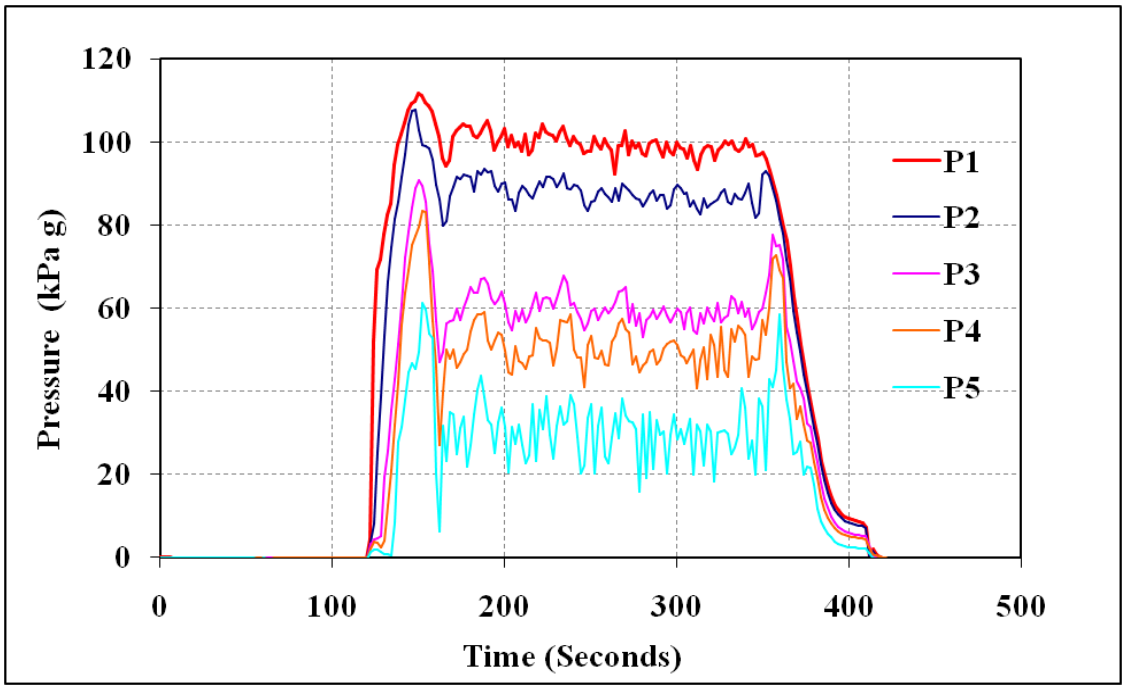

Figure 3.13: Pressure fluctuations at different transducer location during a typical pneumatic conveying trial (repeat test); m_f =0.07 kg/s, m_s = 2.71 kg/s

To further ensure the accuracy of results from pressure transducers, error analysis is performed for the mean valuescalculated from the pressure fluctuations captured at these transducers and is shown in the Figure 3.13.

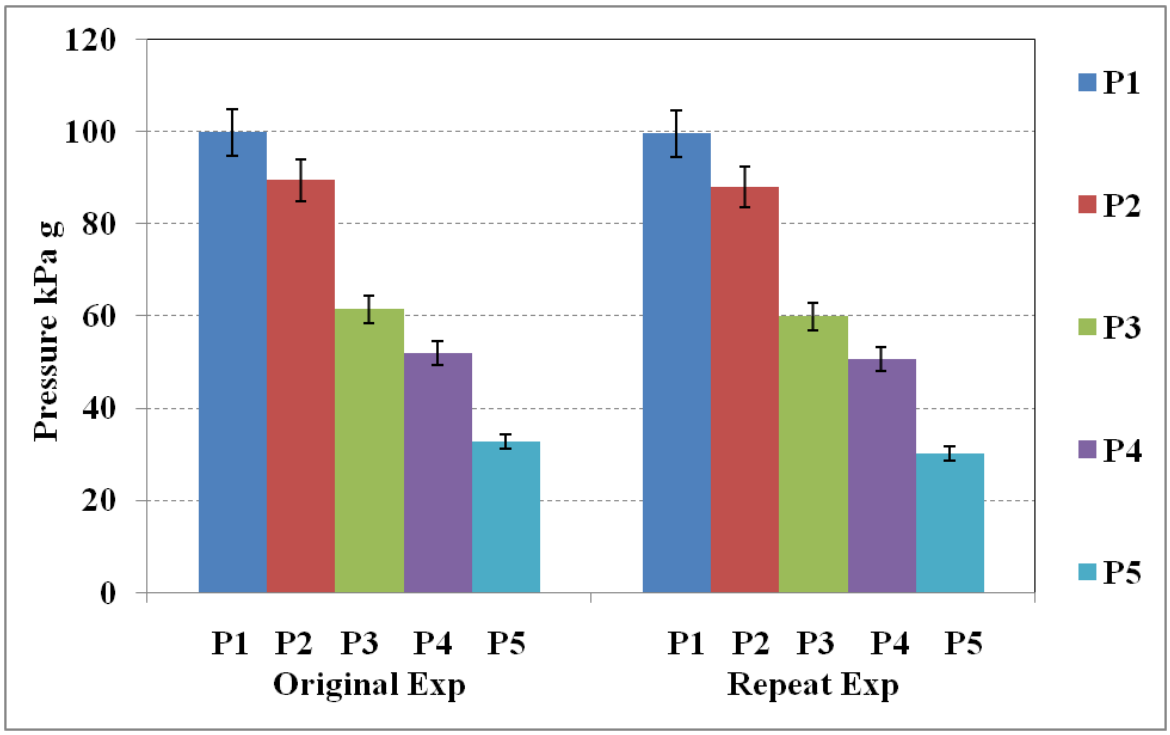

Figure 3.14: Error analysis for the data recorded by different transducers during a typical pneumatic conveying trial; m_f =0.07 kg/s, m_s = 2.71 kg/s

In the above figures, error bars with 5% error amount have been shown. Error bars for the data values at a particular location for the original and repeat test run are overlapping and are not significantly different; henceit can be concluded that thedata captured in the repeat experiment is similar to the data captured during the original experiment.

CHAPTER 4: INVESTIGATION INTO PRESSURE SIGNAL FLUCTUATIONS

4.1 Introduction

This chapter includes discussion on the pressure signal generation and various analysis methods/techniques used to perform analysis of pressure signal fluctuations. During pneumatic conveying tests, pressure at a particular location along the pipeline does not remain constant with respect to time rather it keeps on fluctuating. The data acquisition device is used to record these pressure fluctuations. The analog signal from the pressure transducers, which is in the form of current (4-20 mA), consists of components of various frequencies. For recording the accurate and complete data without missing any of the important frequency components, the selected data acquisition system should have a high sample rate (i.e. the speed at which analog to digital conversion takes place). According to the Nyquist sampling theorem (John and Dimitris, 1996),sampling rate of the signal should be more than twice the highest frequency component present in the signal. If the sampling rate happens to be less than twice the highest frequency component, some of the high frequency components will not be represented correctly in the digitized signal output. In contrast, no information is lost if a signal is sampled at the Nyquist frequency and no additional information is gained by sampling faster than this rate. The pressure signals recorded by the transducers are the "analog" signals. To process these signals in computers, there was a need to convert the signals to "digital" form. While an analog signal is continuous in both time and amplitude, a digital signal is discrete in both time and amplitude. To convert a signal from continuous time to discrete time, a process called sampling is used. The value of the signal is measured at certain intervals in time. Each measurement is referred to as a sample. When the continuous analog signal is sampled at a certain frequency (*f*), the resulting discrete signal has more frequency components

than did the analog signal. To be more precise, the frequency components of the analog signal are repeated at the sample rate. That is, in the discrete frequency response they are seen at their original position and are also seen centered around +/- *f*, and around +/- 2*f*, etc. One needs to decide upon the number of samples necessary to ensure that the information contained in the signal is preserved. If the signal contains high frequency components, signal needs to be sampled at a higher rate to avoid losing information that is contained in the signal. In general, to preserve the full information in the signal, it is necessary to sample at twice the maximum frequency of the signal. This is known as the Nyquist rate(John and Dimitris, 1996). The Sampling Theorem states that a signal can be exactly reproduced if it is sampled at a frequency *f*, where *f* is greater than twice the maximum frequency in the signal. What happens if one samples the signal at a frequency that is lower than the Nyquist (John and Dimitris, 1996) rate? When the signal is converted back into a continuous time signal, it will exhibit aphenomenon called aliasing. Aliasing is the presence of unwanted components in the reconstructed signal. These components were not present when the original signal was sampled. In addition, some of the frequencies in the original signal may be lost in the reconstructed signal. Aliasing occurs because signal frequencies can overlap if the sampling frequency is too low. The high speed data acquisition system (DT800) having 24-bit resolution had been used for acquiring the current signals from pressure transducers at the pneumatic conveying test rig of University of Wollongong, which was capable of acquiring the signals at the sampling rate of 50 samples/second. Figure 4.1.1 shows the power spectral density plots of pressure signal plots.

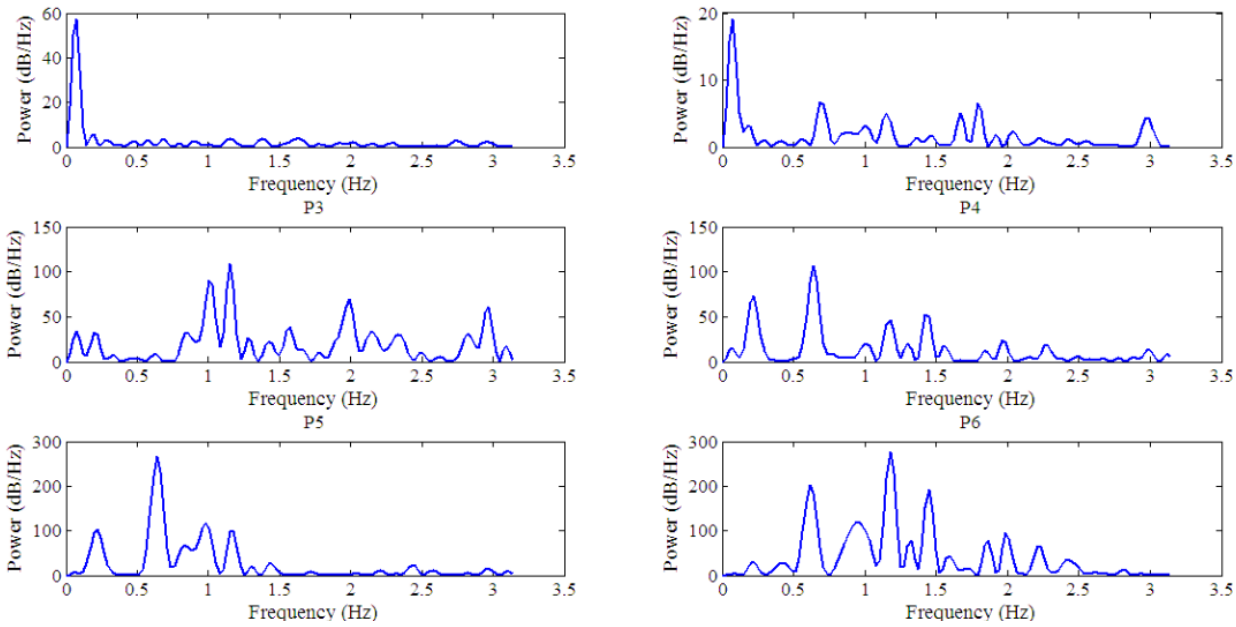

Figure 4.1.1: Power spectral density plot from pneumatic conveying of white powder at University of Wollongong

As is illustrated in Figure 4.1.1, the powers of the signals depicted by the PSD diagrams are negligible beyond 3 Hz, and dominant frequency lies between 0 – 1 Hz. Therefore the minimum sampling frequency in terms of Nyquist's criteria is 3x2 = 6 Hz. Thus, 50 Hz of sampling frequency proved more than sufficient for the analyses of the data.Variation of PSD spectrum from initial sections of the pipeline to exit of pipeline indicates signals captured near the initial locations are periodic (characterized by dominant frequency) while moving towards the end of pipeline, multiple peaks indicate random signal with no periodicity. Variation in power spectrum from one location to another and relating this variation to flow mode inside pipeline is discussed in greater details in the following chapter. Similarly, the signal output from the flow meter and load-cells have been acquired by the data acquisition system. Calibration of load cells, pressure transducers and flow meter were performed using the standard calibration procedure as described by Mallick (2009). Pressure transducers were periodically cleaned after every two sets of experiments

to ensure that these were not blocked during the course of pneumatic conveying experimentation.

At the initial stage of the work, input data were obtained from the University of Wollongong, which was in the form of raw data and was converted in the form of pressure signal plots. Before proceeding with the actual analysis, it was preferred to inspect the measured signal and the simplest method to do that was to plot a sequence of data points in the signal. Some examples of the time-pressure behavior is shown in figures from 4.1.2 to 4.1.5 for the pneumatic conveying of fly ash and white powder corresponding to different solid loading ratio.

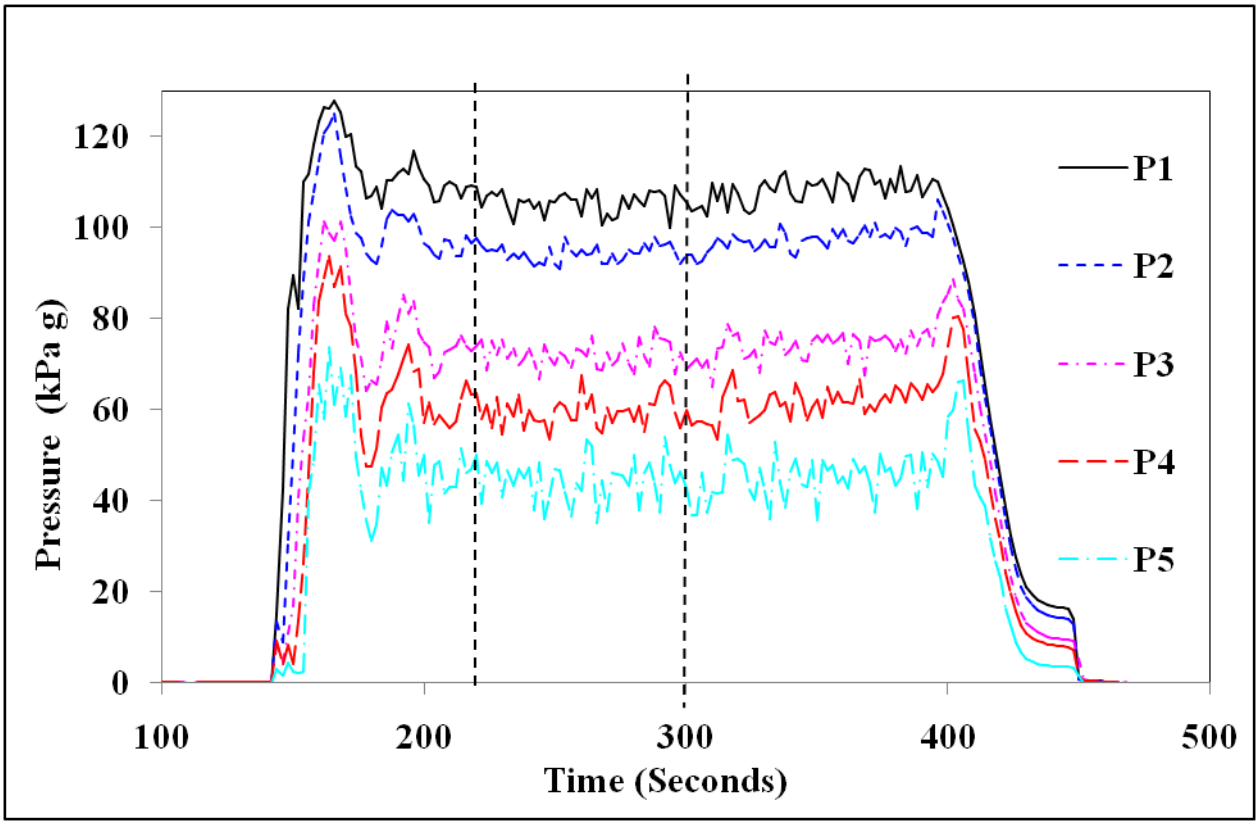

Figure 4.1.2: Pressure (gauge) versus time plot for fly ash at low solids loading ratio; (m_f = 0.107 kg/s; m_s = 2.35 kg/s; m^* = 21.96)

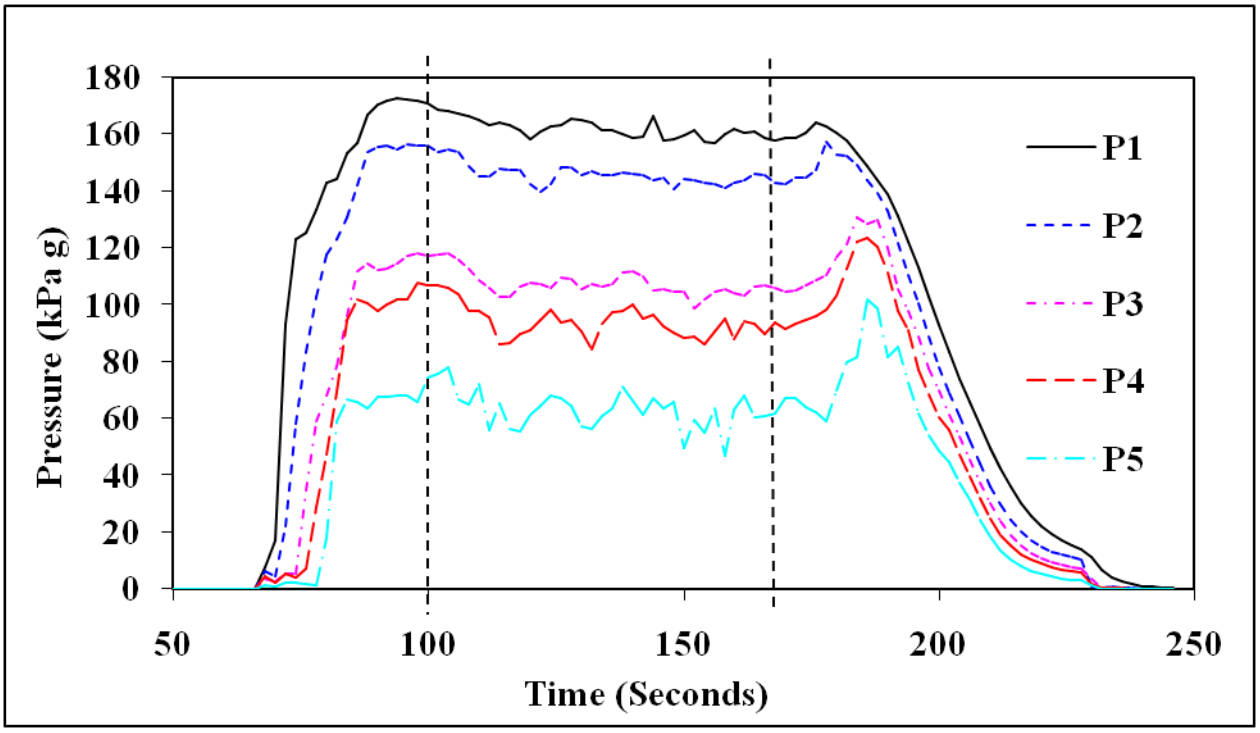

Figure 4.1.3: Pressure (gauge) versus time plot for fly ash at high solids loading ratio; (m_f = 0.07 kg/s; m_s = 4.41 kg/s; m^* = 63)

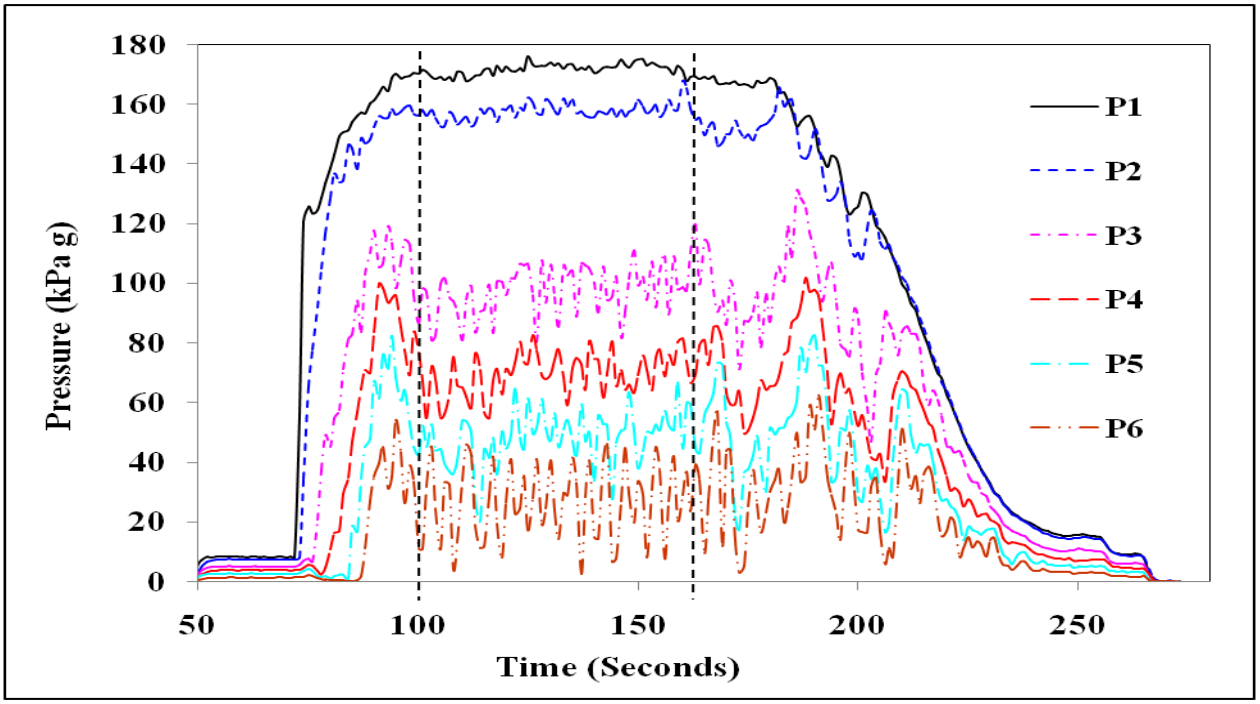

Figure 4.1.4: Pressure (gauge) versus time plot for white powder for low solids loading ratio; (m_f = 0.085 kg/s; m_s = 2.29 kg/s; m^* = 26.89)

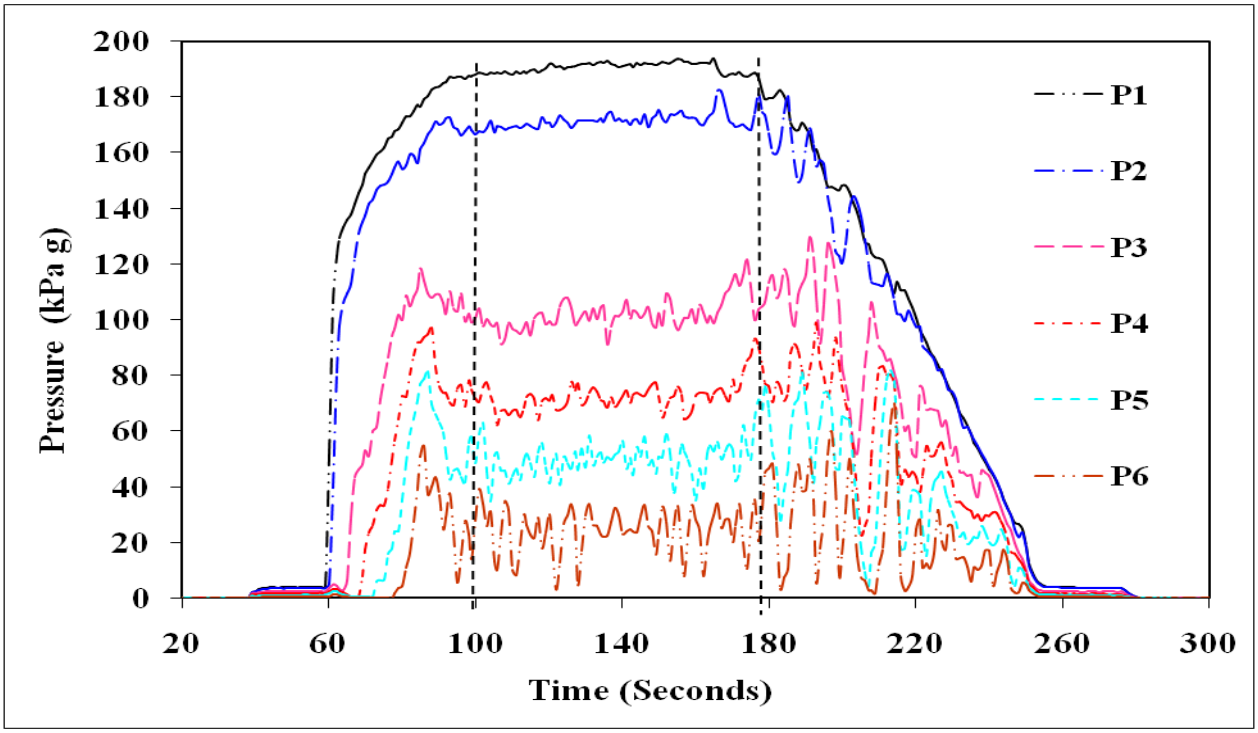

Figure 4.1.5: Pressure (gauge) versus time plot for white powder for high solids loading ratio; (m_f = 0.05 kg/s; m_s = 2.34 kg/s; m^* = 46.8)

Figure 4.1.2 illustrates the pressure fluctuations for fly ash conveyed probably in dilute phase regime (m^* = 21.96, V_f= 11.8 at P1 to 16.5 at P5 m/s). Pressure fluctuation without any obvious regularity and smaller amplitude might be associated with the oscillation of solid particles and air inside the pipeline. With the increase in the solid loading ratio and decrease in superficial velocity as seen in Figure 4.1.3 (m^* = 63, V_f = 6.5 at P1 to 10.1 at P5 m/s), the amplitude of pressure fluctuations seem to get reduced. Similarly, Figures 4.1.4 and 4.1.5, represent the pressure fluctuation behavior during the horizontal pneumatic conveying of white powder corresponding to two different solid loading ratios. Comparing these figures, i.e. corresponding to low and high solid loading ratio, it seems that, there are large differences, both in the amplitude and in the time behavior of the signals. The pressure fluctuations corresponding to a higher solid loading ratio have lower amplitude due to the smaller gas-solid interaction, than the flow corresponding to

comparatively lower solid loading ratio. Although it was possible to differentiate between the time series of pressure signals,corresponding to different flow conditions (as represented in graph form in Figures from 4.1.2 to 4.1.5). However, analysis of the pressure fluctuations, merely in the time domain is a subjective method for studying different flow mechanisms during horizontal pneumatic conveying (since amplitude and signal variation profiles are the only parameters observed).There could be a possibility of getting similar pressure profiles during pneumatic transport (Johnsson et al. 2000) corresponding to different flow regimes. Moreover, characterizing the signals solely by amplitude provides no information on the frequency scale. Therefore, the intent is to apply more objective technologies (such as spectral analysis, deterministic chaos and wavelet analysis etc) to extract the accurate and reliable information from the signals. Comparison of the pressure signal fluctuations obtained at tapping points P1 to P5 (fly ash) and P1 to P6 (for white powder) of Figures 4.1.2 to 4.1.5, show that pressure signals obtained at a given location are different to those obtained from another with respect to change in amplitude of peaks. Increased amplitude of signal peaks could be attributed to expansion of carrier gas due to pressure drop occurring in the flow direction. Thus, signal characteristics seem to be changing depending on the location of tapping points along the pipeline. However, no information on frequency of pressure peaks could be obtained just by visual inspection of the signal. Also, comparisons between Figures 4.1.2 and 4.1.3 for fly ash and Figures 4.1.4 and 4.1.5 for white powder indicate that fluctuation pattern in the signal vary with changes in the mass flow rates of air and solids. Thus, the fluctuating pressure signals seem to carry important information about the mechanisms of flow of gas-solids systems. However, these characteristics need to be evaluated and represented quantitatively. In view of this, various techniques of signal analysis, such as Shannon entropy, rescaled range analysis, phase space diagram, estimation of power spectral density, Hilbert-Huang transform and wavelet transformation, have been applied in the

present work to better understand the solids-gas flow behavior. The steady state range of pressure time series, as indicated in each figure, has been considered for analysis.

Later on experiments were also conducted on the test setup of Thapar University, Patiala (as shown in Figure 3.1). The electrical signals (i.e. current in 4-20 mA and voltage 3-12 mV) captured by the data acquisition system were converted to pressure (in kPa) versus time and load (in kg) versus time, plots by applying suitable calibration factors. The high speed data acquisition system (NI-9208) having 24-bit resolution has been used for acquiring the current signals from pressure transducers at the pneumatic conveying test rig of Thapar University, Patiala, which is capable of acquiring the pressure signals at the sampling rate of 50 samples/second. As is illustrated in Figure 4.1.6, dominant frequency depicted by the PSD diagrams lies between 0 to 1 Hz and the power of the signal is negligible beyond 3 Hz. Therefore the minimum sampling frequency in terms of Nyquist's criteria (John and Dimitris, 1996) is 3 x 2 = 6 Hz. Thus, 50 Hz of sampling frequency proved more than sufficient for the analyses of the data.

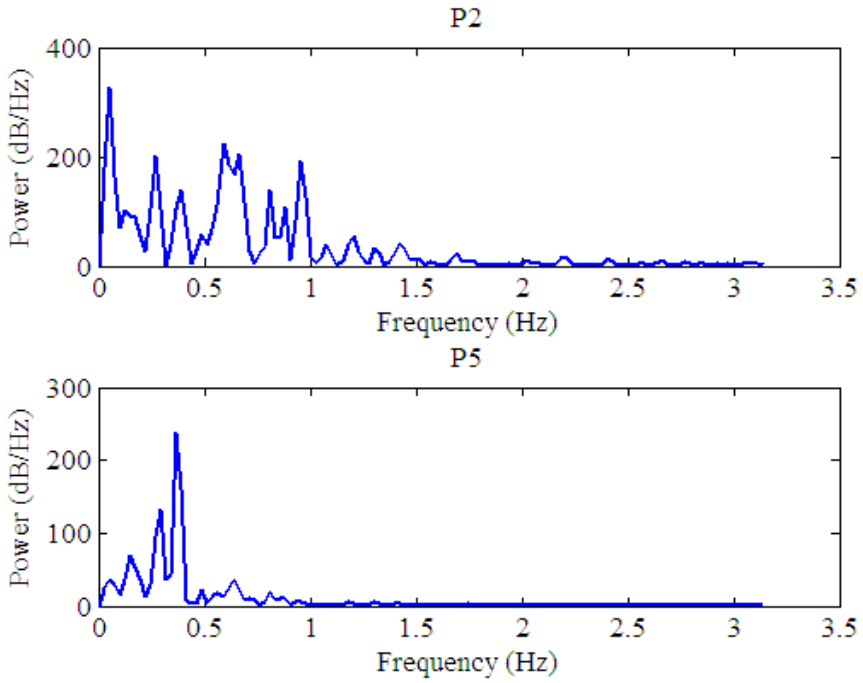

Figure 4.1.6: Power spectral density plot from pneumatic conveying of Fly ash (Thapar University, Patiala)

It is evident that are differences (expectedly) in the pressure fluctuation data due to the differences in product and pipeline properties between University of Wollongong and Thapar University. It was observed from the pressure signal plots corresponding to Thapar University, Patiala test setup that the range of steady state period was quite short (30 to 40 seconds) as compared to the steady state period obtained in the experimental data of University of Wollongong. Hence the major focus for carrying out the signal analysis work has been the experimental data obtained from the University of Wollongong.The following section would cover the brief introduction to the various signal processing techniques adopted for the analysis work.

4.2 Hurst Exponent

Hurst (1951) proposed rescaled range analysis to examine the nature of chaotic motion. This method of characterization distinguishes between different possible types of the time-series depending upon the different values of Hurst exponent associated with the series. Hurst exponent is referred to as the "index of long-range dependence". It quantifies the relative tendency of a time series either to regress strongly to the mean or to cluster in a direction. When a positive correlation exists at the time-series data (which means that a high data value in the series will probably be followed by another high value), the values of Hurst exponent lies between 0.5 and 1; in addition to this, high values of Hurst exponent indicate more persistent data (i.e. trend in the series remains the same throughout the series or increase in the data are likely to be followed by increase and decrease in values by the further decrease), exhibiting some trends in the data analysed. A value in the range of 0 to 0.5, indicates a time series with tendency to vary between high and low values which means that a high value in the time series will probably be followed by a low value and that the value after that will tend to be high.For random and completely unrelated data, there is no correlation between the current and the future observations (i.e. the chances of future observation being higher or lower than the current observation is equally likely). Series of this kind are hard to predict. For such kind of series, value of Hurst exponent, H equals to 0.5. To estimate the Hurst exponent, one must regress the rescaled range on the time span of observations first. For a given time series of recorded pressure fluctuations, X (t), with n number of values, i.e. X_1, X_2,… X_n, which are spaced in time from t=1 to t=τ, the mean of the series is defined as:

$$\bar{X} = \frac{1}{n}\sum_{i=1}^{n} X(i) \tag{4.1}$$

The departure of time series X (t) from the average of recorded signals is:

$$Y_i = X_i - \bar{X}(i = 1, 2, \ldots . n) \quad (4.2)$$

Z_i denotes the cumulative departure of X_i from the average as:

$$Z_i = Y_i + Y_{i+1}(i = 1, 2, \ldots n - 1) \quad (4.3)$$

The sample sequential range is defined as:

$$R(t) = MaxZ(t) - MinZ(t) 0 \leq t \leq \tau \quad (4.4)$$

S (t) is the standard deviation of the time series sub-record from t = 1 to t = τ, defined as:

$$S(t) = \sqrt{\frac{\sum_{i=1}^{n}(X - \bar{X})^2}{n - 1}} \quad (4.5)$$

The ratio of R (t) and S (t) is defined as the rescaled range.

Total numbers of data points for the Hurst Exponent calculation were taken in the form of 2^N. The time-series (pressure versus time) was divided into two sub-intervals of equal length. The entire procedure for calculating the rescaled range was repeated for each sub-interval, which provided two different values of rescaled range. An average was taken for each of the values of rescaled range. Each sub-interval was further divided and the

rescaled range was calculated for each interval and then average values of R/S were estimated from all the sub-intervals. The procedure of subdivision was continued until interval sizes became adequately small (i.e. number of data points in the sub-interval got reduced to 8) as shown in the Figure 4.2.1. Thus, a series of values of R/S from different steps were obtained (in each step, time series had different numbers of intervals). These values were plotted against number of data points in the corresponding sub-section. Finally, the Hurst exponent values were calculated by plotting a linear regression line through these points on logarithmic scale, where the slope of the line was an estimate of the Hurst exponent.

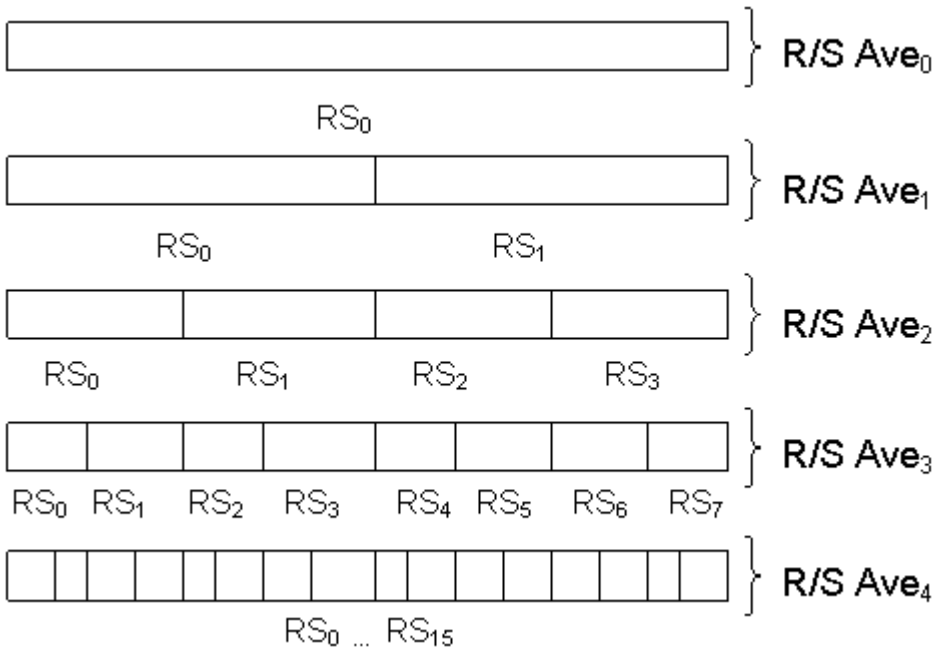

Figure 4.2.1: Illustration of the procedure used for calculation of Hurst exponent

4.3 Phase space diagrams

A phase space (Nolte, 2010) represents a space in all possible states of a system, with each point in the system corresponding to each possible state of the system. In other words, the phase space representation provides all that the system can be and its shape can easily explain qualities of the system that might not be obvious otherwise. In more simple words, phase space is simply an X-Y or X-Y-Z graph, on which the history of the system through time is seen with respect to the changing coordinates prescribed by the variables of the system. Phase space diagrams are useful to represent chaotic/complex systems or non-linear dynamic systems that are extremely sensitive to disturbance in its initial conditions. Chaos/complex systems have behaviors that may superficially appear random, but have recognizable larger scale patterns. It is possible to construct the d-dimensional state space plot by means of only one characteristic variable by using the method of delay coordinates (Lin et al., 2001). The values of the variable at different time delays {0, Δt, 2Δt,…, (d-1) Δt} are used as coordinate values in the embedding space. In the present case, 2-dimensional phase space diagrams have been constructed using the method of delays (Takens, 1981), which involves plotting original time series X (t) versus its delayed versions, i.e. X (t+τ), where $\tau$is the delay time to collect one data point. Selection of optimum value of delay time is important for phase space construction. If the selected time lag is too short, then there are chances that it would be influenced by noise, on the other hand, if too long delay time is chosen, then the phase space attractor would not reveal the local flow characteristics. The optimum value of delay time is selected as the first minimum of a mutual information function (Takens, 1981).The mutual information is low where the auto-correlation is low. However, in contrast to the auto-correlation, it also measures non-linear dependencies. As delay we use the first minimum of the mutual information or, if such a minimum is not apparent, we use the first delay, where a steep

decay of the mutual information changes to a slow decay. The estimation of an appropriate embedding dimension is using the amount of false nearest neighbors. This approach checks whether the neighborhoods of all points in the phase space change by increasing the embedding dimension. If the embedding is too low, many neighbors are only projections. Thus, such an embedding dimension would be optimal, where the amount of false nearest neighbors almost vanishes.Variation in size of the attractor and shape of trajectory provides qualitative information on the nature of time-series; periodic or chaotic systems have characteristic phase space portraits. Phase space diagram with larger area (i.e. an attractor is more scattered on the phase-space diagram) indicates higher irregularity in the time-series as compared to the phase space diagram with less area.

4.4 Shannon entropy

The concept of thermodynamic entropy (according to the second law of thermodynamics)indicates degree of randomness in a thermodynamic process. Then, Boltzmann (2012) explored the entropy in molecular movement theory and indicated that entropy is the measurement of the chaos in degree of molecular motion (De Araujo et al., 2003). Shannon (1948), known as the founder of information theory, first introduced the concept of entropy in information theory, and suggested thatentropy is a measurement of the content of information in a certain information source and the degree of indeterminacy involved in the system (Shannon, 1948). The entropy related to information content is known as Shannon entropy. The main reason which leads to Shannon entropy as a choice of pressure signal analysis is that it is not influenced by the information carrier and data value so as to be used in extensive fields. Shannon entropy can be utilized to express the degree of uncertainty involved in predicting the output of a probabilistic event (Camesasca

et al., 2006). It means that if one is able to predict the outcomes of an event, exactly before it happens, the probability will be a maximum value and, as a result, the Shannon entropy will be a minimum value. In addition to this, if one is absolutely able to predict about the outcomes of an event, theShannon entropy will be zero. In other words, Shannon entropy calculates the degree of complexity of the distribution of the samples of a signal. The largest entropy is obtained when the distribution is flat (all the samples are identically distributed and the series carries a maximum amount of information). On the contrary, if some values are more likely, while other data samples are missing or infrequent (e.g., the sample distribution is Gaussian), the entropy decreases. For a pressure time series with n number of data points denoted by X_1, X_2……. X_n, there could be n number of possible outcomes with probabilities of p_1, p_2…. p_n. Shannon entropy can be obtained by:

$$S = -\sum_{i=1}^{n} p_i \log_b(p_i) \quad (4.6)$$

Where, n is the length of the signal; when b = 2, e and 10, the unit of S are bit, nat and hart, respectively. p_i is the probability of i^{th} component in the signal, which satisfies the following constraint.

$$\sum_{i=1}^{n} p_i = 1 \quad (4.7)$$

p_i can be estimated by the joint probability density formula. Shannon entropy calculations have been carried out with base b =2 in the present work. Detailed procedure for calculating the Shannon entropy is given below.

1. Normalize the time series with respect to the mean.
2. Find out the maximum and minimum values of data points in the series.
3. Repeat the step-1 and step-2 for the entire experimental data to determine the overall minimum and maximum data values among the entire data. Overall range selected should be the same for comparing the results of Shannon entropy from different time-series and it was found to be -50 to + 50.
4. Divide the entire range into a number of intervals (bins).
5. Count the number of data points within each interval.
6. Calculate probability of a data value to occur inside a particular bin.
7. Calculate Shannon entropy for the time series using equation 4.6.

A larger value of Shannon entropy in general implies more disorder and chaotic nature of the time series.

4.5 Power spectral density (PSD)

Power spectral density also referred to as frequency domain analysis or spectral density estimation, involves decomposing a complex signal into simpler parts. In other words, a process that quantifies the various amounts (e.g. amplitudes, powers, intensities, or phases), versus frequency is called spectrum analysis. Spectrum analysis can be performed on the entire signal or a signal can be broken into short segments and spectrum analysis may be applied to these individual segments. For dividing the signals into segments, periodic functions (such as, *sin (t)*) are particularly well-suited. For analyzing non-periodic functions,general mathematical techniques based on Fourier analysis are used. The Fourier transform of a function produces a frequency spectrum, which contains entireinformation

content of the original signal, but in a different form. This means that the original function can be fully reconstructed by an inverse Fourier transform. In order to achieveideal reconstruction, both the amplitude and phase of each frequency component must be preserved. The amplitude and phase can be represented using a 2-dimensional vector and as a complex number. In signal processing it is common practice to consider the squared amplitude (or power),therefore the resulting plot is referred to as a power spectrum. In practice, almost all software and electronic devices used for generating frequency spectra are based on fast Fourier transform (FFT) which computes the discrete Fourier transform of a sampled signal. Due to reversibility, the Fourier transform is termed as a functionrepersenting frequency instead of time; thus, it is a frequency domain representation. Linear operations that could be performed in the time domain have counterparts that can often be performed more easily in the frequency domain. Frequency analysis also simplifies the understanding and interpretation of the effects of various time-domain operations, both linear and non-linear. The Fourier transform of a stochastic (random) waveform (noise) is also random. Some kind of averaging is required in order to create a clear picture of the underlying frequency content (frequency distribution). Typically, the data are divided into time-segments of a chosen duration and then transforms are performed on each one. Then the magnitude or (usually) squared-magnitude components of the transforms are summed into an average transform. This is a very common operation performed on digitally sampled time-domain data using the discrete Fourier transform. This type of processing is called Welch's method(Welch, 1967).

Power spectral density (Stoica and Moses, 1997) is a method to understand how the strength of a signal is distributed over different frequencies present in the signal, i.e. it is a method to distinguish different frequencies present in the signal corresponding to the

strong and weak fluctuations. Thus, power spectral density helps to analyse the signal in frequency domain and is used to identify the dominant frequency in the signal. The measured signal contains the various frequency components in it, since the power contained in each signal with different frequency will be different, so the PSD is the graph of power versus frequency. In other words, it shows at which frequencies, the variations are strong and at which frequencies, variations are weak. Power spectral density can also be used to distinguish between periodic and chaotic nature of the signal. Broad band of frequencies in the power spectrum indicate the chaotic behavior of the signal, while periodic nature is reflected by power density spectrum having clear dominant peaks. Power spectral density of real valued input signal, x (t), is estimated using the method of periodogram. The power spectral density is calculated in units of power per radians per sample. The corresponding vector of frequencies is computed in radians per sample which has the same length as PSD. The periodogram given by Welch (1967) (a windowed version of Bartlett's method, Bartlett 1948, that uses overlapping segments) is an estimate of the PSD of the signal defined by the sequence [x_1, ... , x_N]. Periodogram is defined as the modulus squared of the discrete Fourier transform and is given as below:

$$S\left(e^{jw}\right) = \frac{1}{2\pi N}\left|\sum_{n=1}^{N} x_n e^{-jwn}\right|^2 \quad (4.8)$$

Where, ω is frequency in radians per sample.PSD is basically trying to decompose input data into a series of sinusoidal waves of different frequencies. It requires high frequency sinusoidal waves to reproduce input data properly when the input data have signals that have shapes quite different from a sinusoidal wave, especially when they have sharp

corners. A situation like this may cause a problem called aliasing and it is affected by a sampling rate.

4.6 Wavelet Transformation

Spectral analysis was developed for the analysis of invariant (stationary) time series. A stationary time series has a constant mean and a constant variance over time. However, the turbulent solid-gas flow inside the pipeline during fluidized dense phase pneumatic conveying give rise to non-stationary time series. Interactions among such oscillatory systems often lead to nonlinear outcomes, including synchronization, amplitude and frequency modulation. To cope with the non-stationarity and inhomogeneity of pressure time series, time frequency analysis using wavelet transforms offers a more suitable investigation approach. A spectral graph merely provides information about the periodicities in a time series by summarizing the distribution and density of a particular frequency range in a signal, whereas wavelet analysis describes how the frequency of a signal changes over time and allows studying the dynamics of the signal components.

Wavelet method is used to analyse the transient time series, having fluctuations, which vary in amplitude as well as in frequency. This method is used when one would like to separate the shorter period oscillations from the longer. A wavelet is a wavelike oscillation with amplitude that starts at zero, increases and then decreases back to zero. Wavelets are functions created to have specific properties that make them useful for signal processing. Wavelets can be combined, using a technique called convolution (reverse, shift, multiply and sum), with portions of an unknown signal to extract information from it. In this technique, the time series is decomposed into time and frequency space simultaneously.

One gets information on both amplitude of the peaks in the signal and how this amplitude varies with time.

Grossmann and Morlet (1984) introduced the Wavelet theory by working on seismic signals, which was further refined by Daubechies (1990) and Meyer (1993). According to Boashash (2015), wavelet is a mathematical function used to divide a continuous time signal into different scale components. Each scale corresponds to a definite frequency range. Application of wavelets is quite useful while dealing with signals having various frequency characteristics. As compared to Fourier transform (in which signal is represented as the sum of sinusoids), wavelets are more suited to represent irregularities and sharp peaks in a random signal. The Fourier basis function is localized only in frequency, but not in time. Wavelets are a new family of localized functions of different frequencies, which are generated by the dilation and translation of a single prototype function known as mother wavelet (Mallat, 1999). Mother wavelet is denoted by ψ (ξ), on which scaling and translation operations are performed to generate scaled and translated versions of the mother wavelet functions (Tong, 2011). Wavelet transformation is capable of providing information both in time and frequency domain. In the present work, analysis has been performed using one-dimensional continuous wavelet transform. For a signal x(t), wavelet transform is defined as the integral transform of family of function given by:

$$\psi_{t,f} \equiv f\psi^{*}(f(b-t)) \tag{4.9}$$

Where,'t' and 'f' are translational and dilation parameters. Scaling operation of the mother wavelet can be used to sort the different frequency information present in the signal, while translational operation (i.e. shifting of the mother wavelet along the time axis) is used to

extract the time based information from the signal to be analysed. Thus, family of scaled and translated wavelets is created from mother wavelet ψ (ξ) depending upon different scaling and translational parameters. In the present analysis, Daubechies of order four has been chosen as the mother wavelet. Wavelet transformation involves computation of wavelet coefficients, given by:

$$WT(t, f) = \int_{-\infty}^{\infty} x(b)\psi_{t,f}(b)\,db = f\int_{-\infty}^{\infty} x(b)\psi^{*}\left(f(b-t)\right)db \qquad (4.10)$$

Low scale wavelet coefficients compress the wavelet and provide information on high frequency characteristics of the signal, while high scale coefficients stretch the wavelet and correlate better with the low frequency content of the input signal. Wavelet scalograms are plotted to represent the percentage energy for each wavelet coefficient. In this plot x-axis represents time, the y-axis represents scale and color of each x-y point represents the percentage of the energy of each wavelet coefficient. Since frequency is inversely proportional to the scale, frequency at which wavelet coefficients carry maximum energy can be detected using scalogram.

4.7 Hilbert Huang Transform (HHT)

Most of the established data-analysis methods are based on assumptions of linearity and stationary. For analyzing linear, but non-stationary data, methods such as wavelet analysis were designed. In addition, various nonlinear time-series-analysis methods (Tong 1990; Kantz and Schreiber 1997; Diks 1999) were designed for nonlinear, but stationary and deterministic systems. However, analyzing the data from real systems, which are most

likely to be both non-linear and non-stationary, is a tedious task. Conventionally used mathematical models for data expansion in terms of an a priori established basis cannot be relied for representing nonlinear and non-stationary data. It is essential to have an adaptive basis for analyzing non-linear and non-stationary data. A few adaptive methods, available for signal analysis, as summarized by Widrow and Stearns (1985), are all designed for stationary processes. In non stationary and nonlinear data, where adaptation is absolutely necessary, no available methods can be found. Being adaptive means that the definition of the basis function has to be data-dependent, i.e. a posteriori-defined basis. Therefore, new methods to examine data from the real world are certainly needed. A recently developed method, the Hilbert–Huang transform (HHT), provided by Huang et al. (1998) seems to be able to meet some of the above mentioned challenges.

Huang et. al (1998) provided a signal processing technique to analyse non-linear and non-stationary signals. While applying HHT, the original signal is decomposed into a number of IMF's (Intrinsic Mode Functions) based upon Empirical Mode Decomposition (EMD). An IMF must satisfy two conditions: the number of extrema and number of zero crossings must either be equal or differ at most by one and the mean value of envelope defined by the local minima and local maxima is zero. The empirical mode decomposition of the time series data x (t) has been achieved in following steps (Huang et al., 1998). Local minima and local maxima of the original signal x (t) were identified. Then, by using cubic spline interpolation, upper envelope x_{max} (t) and the lower envelope x_{min} (t) of the signal were defined. The mean of upper and lower envelopes was calculated using:

$$m_1(t) = \frac{x_{max}(t) + x_{min}(t)}{2} \quad (4.11)$$

Subtracting m_1 from the original signal x (t) provided:

$$h_1(t) = x(t) - m_1(t) \quad (4.12)$$

Constraints for a function to be IMF were verified and the above procedure was iterated k times until both the constraints were satisfied.

$$h_{1k}(t) = h_{1(k-1)}(t) - m_{1k}(t) \quad (4.13)$$

$$I_1(t) = h_{1k}(t) \quad (4.14)$$

I_1 (t) is the first IMF component and contains the highest frequency component of the signal. IMF thus obtained was separated from the original signal and the residue obtained r_1 (t) was considered as the new data series. To further extract the IMF from r_1 (t), it was subjected to the sifting process. The process of extracting IMF's from the subsequent residues was continued until the residue became an isomonotonic function (i.e. no more IMF's could be extracted) or it contained lowest frequency components. Hilbert transform was applied to all the IMF components extracted using the following expressions:

$$L_i(t) = \frac{1}{\pi} P \int_{-\infty}^{\infty} \frac{I_i(\tau)}{t-\tau} d\tau \quad (4.15)$$

Where, P is the Cauchy principal value. An analytical signal can be constructed as:

$$Z_i(t) = I_i(t) + jL_i(t) = a_i(t)e^{j\theta_j(t)} \quad (4.16)$$

Amplitude and phase angle are determined as:

$$a_i(t) = \sqrt{I_i^2(t) + L_i^2(t)}$$

(4.17)

$$\theta_i(t) = \arctan\left(\frac{L_i(t)}{I_i(t)}\right) \quad (4.18)$$

Instantaneous frequency was obtained from the first derivative of the phase angle as:

$$\omega_i(t) = \frac{1}{2\pi}\frac{d\theta_i(t)}{dt} \quad (4.19)$$

Time-frequency distribution of amplitude was referred to as Hilbert spectrum and was given as:

$$H(\omega, t) = Re\sum_{i=1}^{n} a_i(t)e^{j\int \omega_i(t)dt} \quad (4.20)$$

Where n is the number of IMF's.

The energy distribution index was calculated for each IMF as the ratio of local energy of the each IMF and total energy of the pressure signal, given as:

$$e = \frac{E_i}{E} \quad (4.21)$$

$$E_i = \int_{-\infty}^{+\infty} |I_i(t)|^2 \quad (4.22)$$

4.8 Cross-correlation

Cross-correlation analysis technique was used to estimate the dune velocity in fluidized dense phase pneumatic conveying. In this method, cross-correlation function was used to determine the time taken (τ) by the dune to travel through two neighboring points located along the pipeline. If the distance between two neighboring points is known then dune velocity can be estimated as (V_d = L/τ). However, accuracy of velocity determination using this method depends on selection of correlated signals, sampling rate of data acquisition system and the distance between neighboring points. The cross correlation of two different signals, x(t) and y(t), is defined as follows (Jung et. al, 2009).

$$R_{xy}(\tau) = \lim_{T\to\infty} \frac{1}{T} \int_0^T x(t)y(t+\tau) \qquad (4.23)$$

$R_{xy}(\tau)$ specifies how much signal x (t) correlates to y (t + τ). In other word, it specifies how much x(t) is similar to y(t) while y(t) is shifted in time by τ . If these two signals are more similar when the y is shifted in time by τ_{max}, then, $R_{xy}(\tau)$ will have a peak (maximum) when $\tau = \tau_{max}$. x(t) can be considered the signal from the first transducer and y (t) as the signal from the second transducer. However, In all practical circumstances, the engineering signals are sampled at regularintervals of certain time duration. In that case, cross-correlation function defined by equation (4.23) will not be applicable and for that purpose, the crosscorrelation for discrete signals need to be calculated, which is given as the following(Seraj et al., 2013):

$$R_{xy}(m) = \lim_{T\to\infty} \frac{1}{L} \int_{n=0}^{L} x(n)y(n+\tau) \quad (4.24)$$

In this modified cross correlation (equation 4.24), instead of having infinite numbers of sampled signals, cross correlation is calculated by selecting a window of L samples from signal x(n) and by multiplying it with the same number of samples from y(n), when the signal y(n) is shifted in time by m. Peak in the value of R_{xy} versus n plot, corresponds to the instant when signals are best aligned and would provide the shift in signals (m). For performing the cross correlation method defined above, a software code has been developed using MATLAB version 7.10 software.

Various signal analysis techniques described in this chapter can be grouped into two broad categories. The first set of techniques aim to provide qualitative information and are well suited to make comparison of different time-series while another set of techniques are based on specific signal feature extraction.These involve Shannon entropy, Hurst exponent and phase space diagram, while the other group includes power spectral density, wavelet transformation and Hilbert Huang transformation. When the intent is to compare different time-series, first set of techniques are generally used to provide qualitative information (e.g. degree of randomness, degree of similarity between different parts of series etc.). However when the purpose is to extract certain signal features (e.g. dominant frequency, energy of the signal etc), the second sets of techniques would be more appropriate.The technique of Shannon entropy is well defined for a source of symbol strings; it is difficult to apply it for the continuous time series with floating point data. To perform Shannon entropy analysis for a continuous time series data with floating point numbers,binning has to be carried out. Therefore selection of number of bins and range of data points falling in a particular bin need to be performed. Construction of the phase space diagram is based on certain assumptions that the time series is without noise and infinitely sampled. It also involves selection of optimum delay period for accurate results. The Hurst exponent is a

useful statistical method for inferring the properties of a time series without making assumptions about stationarity of signal. Power spectral density helps to identify whether the time-series is periodic based on existence of dominant frequency in the signal. However, this technique does not provide any information in time domain. For this purpose, i.e. to obtain information both in frequency and time domain, the techniques of wavelet transformation and Hilbert Huang transformation are well suited.

CHAPTER 5: RESULTS AND DISCUSSION

Various techniques of signal analysis were applied to the time-series (pressure drop versus time) data generated from conveying trials performed for different powders (fly ash, white powder etc.) through different pipelines. Two main objectives of the present study of the time-sampling pressure measurements during pneumatic conveying are identification and monitoring of different flow regimes and the demarcation of transition points between

regimes. In the first case, the aim was to identify a pattern in the pressure fluctuation behavior for each flow regime and to distinguish between different patterns with the aid of quantitative methods of time-series analysis. The second aim was to verify the behavior of the parameters obtained from analyzing techniques with the change in operating parameters. This chapter presents the results from various signal processing techniques (as described in Chapter 4) applied to pressure fluctuations obtained from conveying of different powders (fly ash and white powder). For the same powder, results obtained corresponding to different operating parameters, such as the mass flow rate of air and solids, solid loading ratio and superficial air velocity etc have been shown. This chapter also includes an investigation into pressure fluctuations near minimum transport boundary. At the end of the chapter,results of an investigation intoestimation of the dune velocity from pressure fluctuation data have been shown.

5.1 Hurst Exponent

Results of calculation of Hurst exponent, also called rescaled range analysis, are presented in this section to analyse the pressure fluctuation signals generated by the horizontal solid-gas flow through a pneumatic conveying system. The first calculation of the ratio R/S is made for the whole set of data values in the time series. Initially, for the time series with a total number of 64 data points, time lag would be, $\tau = 64$. Then, the time lag is reduced by a factor of 2 ($\tau = 32$) and two independent values of R/S are obtained, one for each half of the original set. Next, it was attempted to reduce τ again by a factor of 2, until τ became equal to 8. The results (R/S values) corresponding to the same value of τ in each step were averaged and plotted in a log-log plot as a function of τ. In the present case, total four

points were obtained as shown in Figure 5.1.1 (Figure shows the results of Hurst exponent calculation for a typical experimental data set).

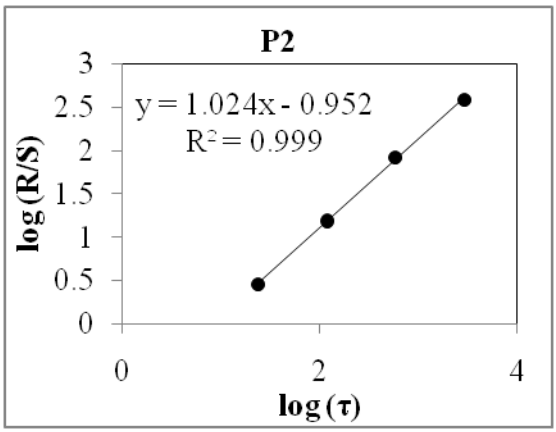

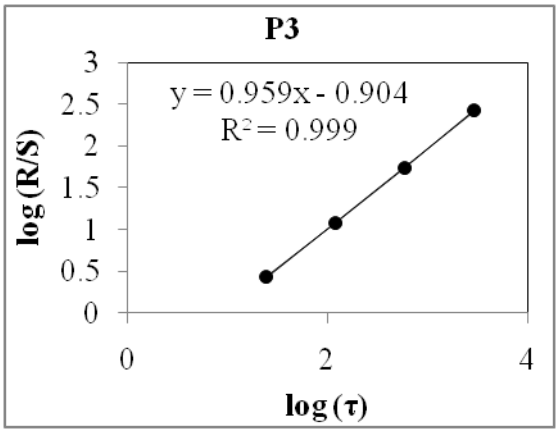

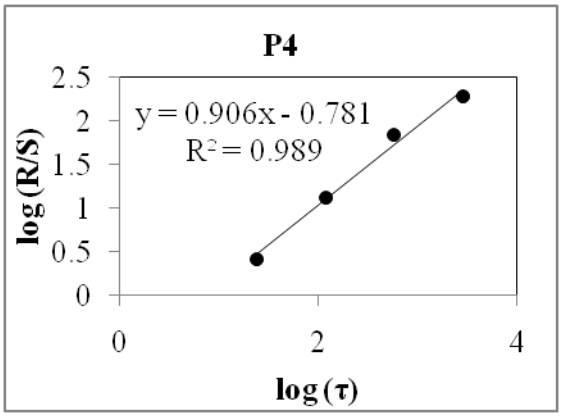

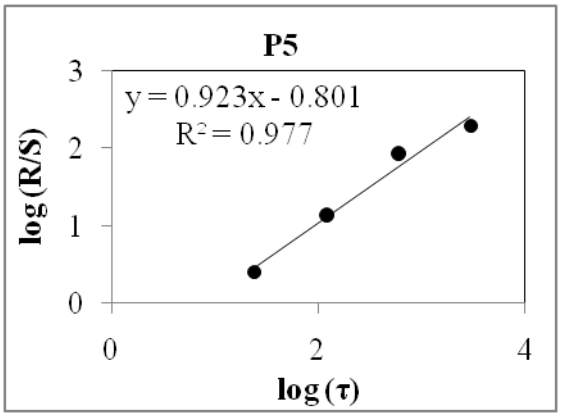

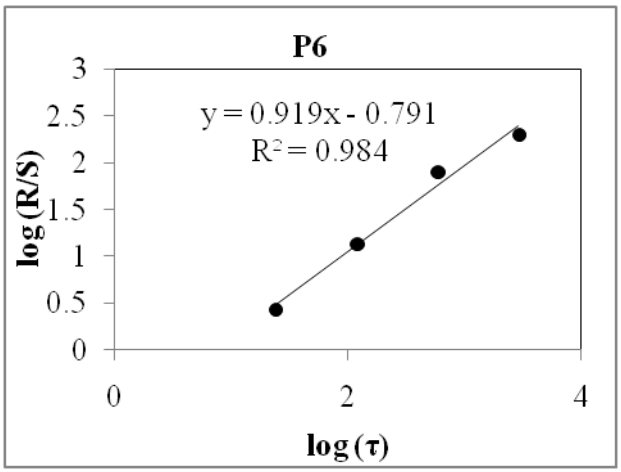

Figure 5.1.1: Hurst Exponent calculation; Exp-37

(Flyash; m_f = 0.03 kg/s; m_s = 5.83 kg/s; m^* = 182.37)

As can be seen in the above figure, the resultant rescaled range correlates linearly with the time lag, τ. The individual value of the Hurst exponent (H) has been obtained from the slope of the linear regression line with a correlation coefficient (R^2) greater than 0.95 for all the data recorded. Five subplots in the figure represent five transducer locations (P1 to P5) along the pipeline. Program in Matlab version 7.10 has been developed to perform the calculations and to determine the Hurst's exponent, using a least square technique. The same numbers of data points were used for each experiment to facilitate accurate comparison.Figure 5.1.2 and 5.1.3 show the variation of Hurst exponent, along the length of pipelines for fly ash and white powder, respectively. Each figure shows a set of plots corresponding to different conveying trials.

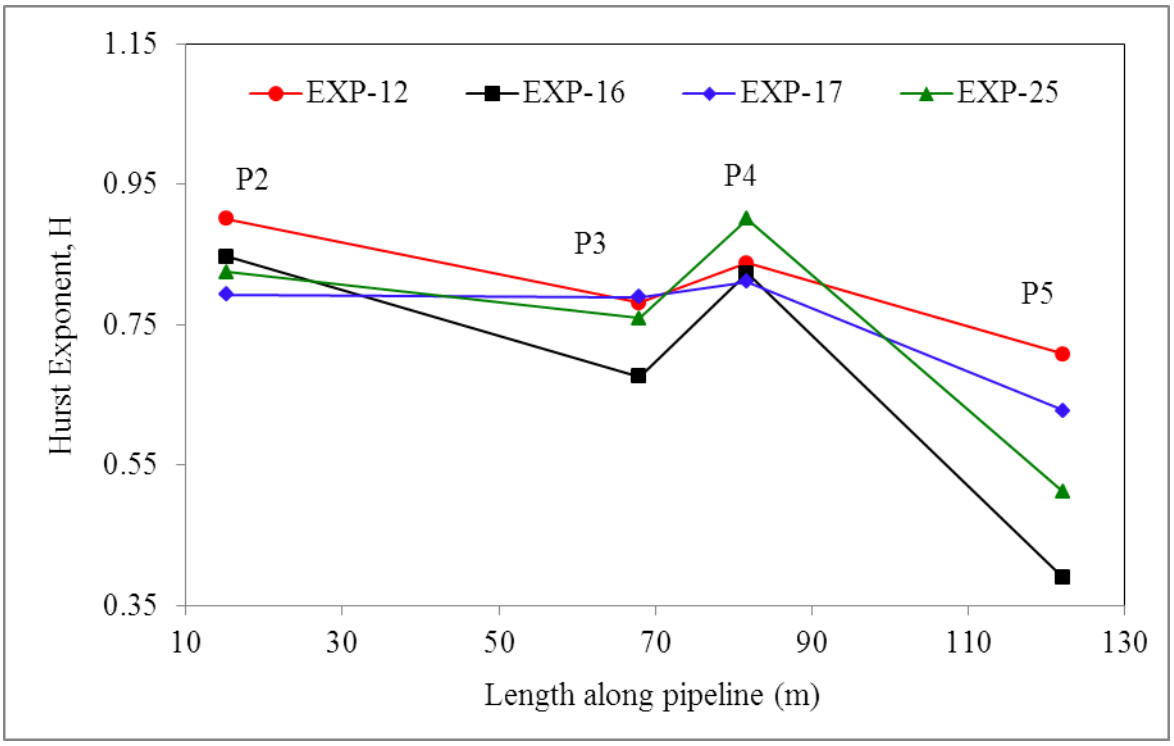

Figure 5.1.2: Variation of Hurst Exponent along the length of pipeline for fly ash

In Figure 5.1.2, the mass flow rate of air (m_f) and mass flow rate of solids (m_s) are given as:

Exp.12: m_f = 0.089 kg/s; m_s = 2.62 kg/s; m^* = 29.7; V_f = 10.13 m/s (at P2) - 14.08 m/s (at P5)

Exp.16: m_f = 0.04 kg/s; m_s = 2.79 kg/s; m^* = 69.10; V_f = 4.84m/s (at P2) - 7.06 m/s (at P5)

Exp.17: m_f = 0.027 kg/s; m_s = 2.41 kg/s; m^* = 89.25; V_f = 3.5 m/s (at P2) - 6.08 m/s (at P5)

Exp.25: m_f = 0.065 kg/s; m_s = 4.19 kg/s; m^* = 64.4; V_f = 6.76m/s (at P2) - 10.10 m/s (at P5)

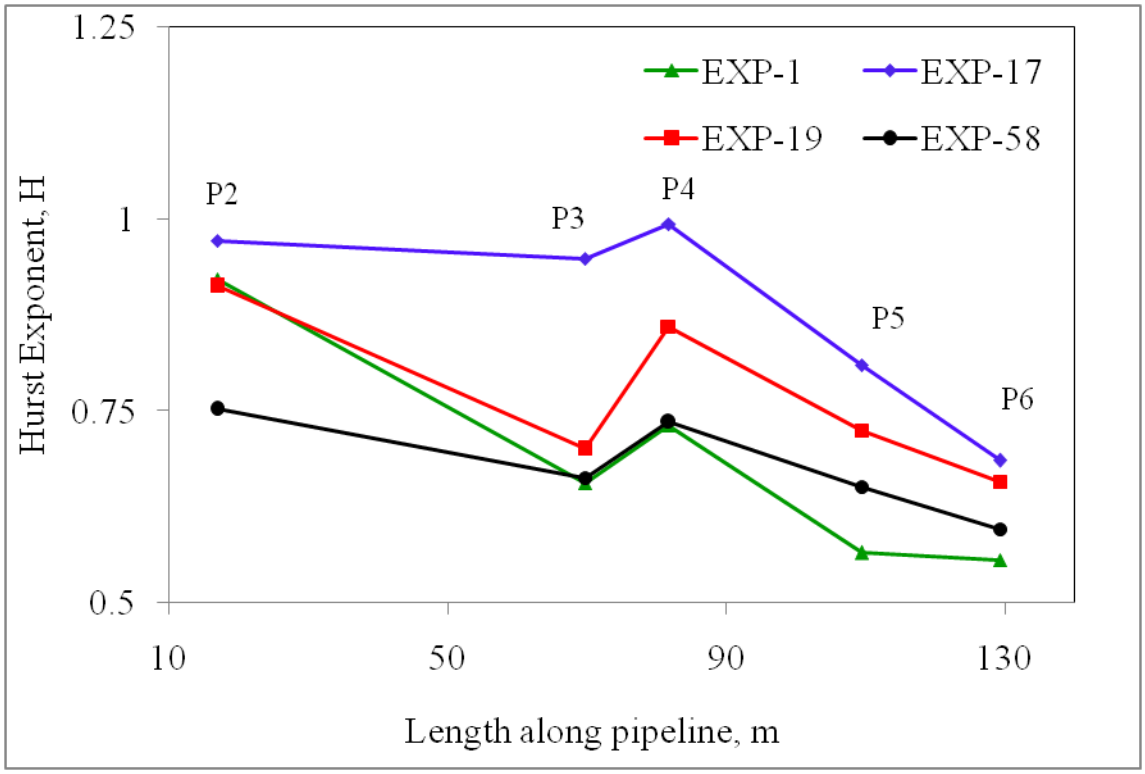

Figure 5.1.3: Variation of Hurst Exponent along length of pipeline for white powder

In Figure 5.1.3, the mass flow rate of air (m_f) and mass flow rate of solids (m_s) are given as:

Exp.1: m_f = 0.09 kg/s; m_s = 2.07 kg/s; m^*= 23; V_f = 7.65m/s (at P2) - 15.13 m/s (at P6)

Exp.17: m_f = 0.06 kg/s; m_s = 2.53 kg/s; m^* = 42.16; V_f = 4.37 m/s (at P2) - 9.73 m/s (at P6)

Exp.19: m_f = 0.11 kg/s; m_s = 2.9 kg/s; m^* = 26.36; V_f = 8.72m/s (at P2) - 17.45 m/s (at P6)Exp.58: m_f = 0.15 kg/s; m_s = 2.73 kg/s; m^* = 18.2; V_f = 13.27m/s (at P2) - 23.31 m/s (atP6)

Figure 5.1.2 shows that for fly ash, with an increase in the length of travel along the pipeline (i.e. with the increase in conveying velocity due to the expansion of gas), the calculated values of Hurst exponent first decrease in the straight pipe section P2 to P3; then increase in the section P3 to P4 (the section having two closely coupled bends) and then decrease in the straight pipe section P4 to P5. Similarly, Hurst exponent values decrease for white powder in the straight pipe section P2 to P3 (Figure 5.1.3), then increase in the section P3 to P4 (where the two bends are located) and then decrease in the straight pipe section P4 to P5 and P6. If the estimated value of Hurst exponent are $0.5<H<1$, then the time-series should exhibit long term correlation, whereas it should have an anti-persistence behavior if $0<H<0.5$; time series data represents random noise and generally do not show any trend when H=0. 5, as given by Darhos et al. (1992). A decrease in the value of Hurst exponent in the straight pipe sections indicates increased disorder in the time series and enhanced pulsations in the flow. Probable explanation for the same could be increased superficial conveying velocity along the straight pipe section and increased gas pulsations, which in turn causes increased particle momentum and particle turbulence. Increased value of Hurst exponent in the section P3 to P4 (while flowing through the closely coupled bends) indicates decreased turbulence and pressure fluctuations, which could be due to the decrease in the particle momentum caused by the roping phenomenon (Chu and Yu, 2008) of particles around and after the bends. As solid-gas flow approaches a bend in the pipe layout, an accentuated double vortex type of flow coupled with a series of impacts occurs, which reduces the particle velocity. Bends cause secondary and centrifugal flows and may even cause significant phase separation by virtue of their geometry. Particle velocity decreases at the exit to the bend due to friction of the outer bend wall (caused by the change in direction of particles, i.e. loss of momentum and centrifugal force acting on the particles). In addition, sliding can occur even in the most commonly used bend types. Bends in close proximity (less than 60.6 m (20 ft) from each

other) could potentially cause severe deceleration effects, where the conveying velocity can be drastically reduced.

It can be clearly observed in Figure 5.1.2 and Figure 5.1.3 that the slope of variation in H is steeper in straight pipe section P4 to P5 (for fly ash) and P4 to P6 (for white powder) as compared to the section P2 to P3, suggesting that a greater change in flow mechanism takes place in the latter sections of pipeline as compared to the initial section. Therefore, a probability of flow regime transition is higher in the section P4 to P5. A comparison of Figure 5.1.2 and 5.1.3 shows a similar trend of Hurst exponent variation for both powders (i.e. fly ash and white powder). In Figure 5.1.2 for fly ash, the variation of Hurst exponent for Exp. 17 (m^* = 89.26) is found to be negligible in the straight pipe section P2-P3 as compared to other experiments. Similarly for white powder, as seen in Figure 5.1.3, the overall range of Hurst exponent value calculated for Exp. 17 (m^* = 42.16) is found to be higher as compared to other experiments (m^* = 21 to 26). Higher values of Hurst exponent corresponding to the high particle loading ratio could be due to the fact that small size particles tend to attenuate the carrier phase turbulence and rate of attenuation is further increased with increase in the solid loading ratio (Paris, 2001); in other words, at high solids loading ratio, fine particles influence the carrier phase turbulence to greater extent as compared to flows with fewer amounts of solids. Thus, reductions in the air turbulence by fine particles negate the increase caused due to superficial velocity. Gore and Crowe (1989) reasoned that the fine particles would travel with the most energetic gas eddies, resulting in diminished gas turbulent kinetic energy, resulting from the fluctuating drag force used to transport the particles. Therefore, the overall magnitude of turbulence is less corresponding to the higher solid loading ratio as compared to the lower values of solids loading ratio, which is reflected with higher value of Hurst exponent when solid loading ratio is high. Thus, the analysis has yielded the Hurst's exponent, a statistical parameter,

which is able to characterize the wall pressure signals and indicative of the flow condition inside the pipeline. Higher values of Hurst exponent (generally more than 0.5) have indicated towards stable flow condition inside pipeline without much turbulence, while comparatively low values have indicated towards multiple interactions between different phases inside pipeline.

5.2 Phase space diagram

In this section, an attempt has been made to study the chaotic nature of the pressure fluctuation signals by the method of constructing a phase space diagram or attractor analysis. Although reconstructing the phase space of an attractor requires several variables to be measured, Lin et al. (2001) showed that a single one dimensional signal can be used to recover the topological properties of an attractor. Area covered by the attractor on the phase space diagram provides the qualitative nature of the time series. As explained previously in the Chapter 4, the time lag (τ) and the embedded dimension (m) are two important parameters necessary to compute the correlation dimension. These were determined by the aid of experience gained from literature (Williams, 1997). Lag length (τ) is conventionally chosen as the first minimum of the mutual information function (Lin et al., 2001).

$$I(t) = \sum_{n=1}^{N} p\big(x(t), x(t+\tau)\big) \log_2 \left[\frac{p\big(x(t), x(t+\tau)\big)}{p(t)p(t+\tau)}\right] \qquad (5.1)$$

Where p (•) and p (•,•) are the individual and joint probability densities, respectively. In this case, the optimal time lag is taken to be the time at which the mutual function has the first minimum. Applying the above method to the pressure time signal, the results have been obtained and are shown in Figure 5.2.1 (i.e. the plot of mutual information versus time lag for a typical time series data). Mutual information has been calculated using Matlab version 7.10 with different values of time lag.

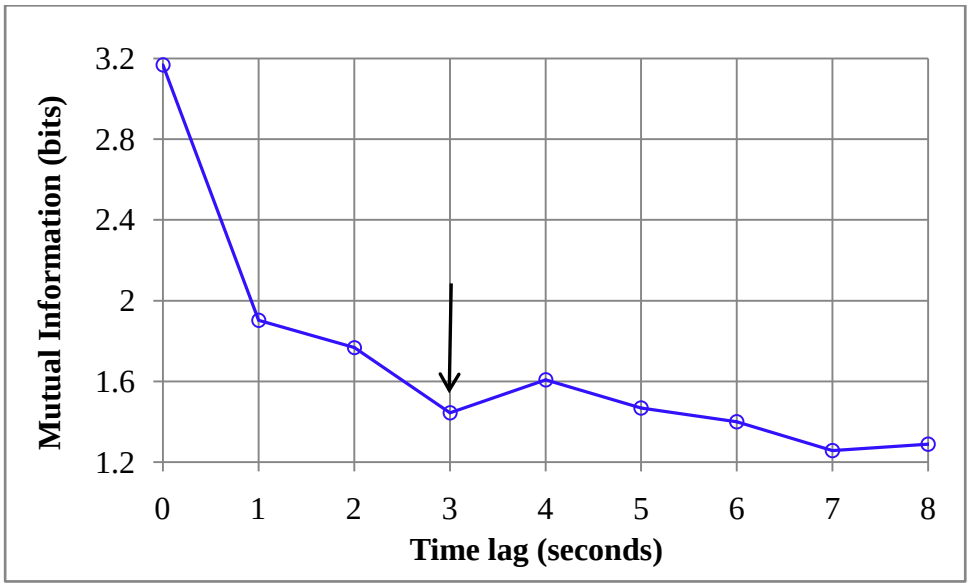

Figure 5.2.1: Variation of mutual information versus time lag Exp-24; White powder; (at P2)

It can be seen in the above figure that the first minimum of mutual information exists at time lag of 3 (i.e. τ=3 seconds). Hence, phase space diagram would be constructed using time lag (τ=3 seconds) for this particular case. The embedding dimension m is usually chosen using the 'false nearest neighbors' method. This method measures the percentage of close neighboring points in a given dimension that remain so in the next highest dimension. The minimum embedding dimension capable of containing the reconstructed attractor is that for which the percentage of false nearest neighbors drops to zero for a

given tolerance level. Figure 5.2.2 shows the plot of percentage of false nearest neighbors versus embedding dimension for a typical time series data.

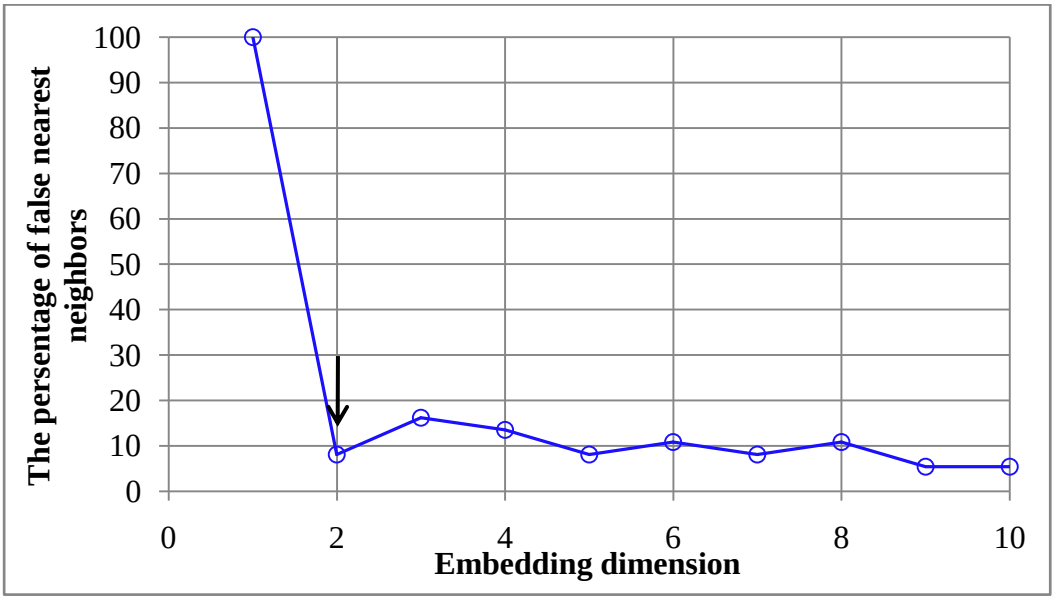

Figure 5.2.2: Variation of false nearest neighbors percentage embedding dimension Exp-24; White powder; (at P2)

It can be seen in the above figure that percentage of false nearest neighbors falls to minimum for embedding dimension (m=2). Hence, for the construction of phase space diagrams, minimum embedding dimension (m=2) has been chosen. Figures 5.2.3 to 5.2.6 show the two-dimensional phase space constructed from the plot of the signal versus the same signal delayed by three sampling units (τ = 3 from first minimum of mutual information). These figures show the variations of phase-space diagram with the change in length along the pipeline for fly ash and white powder, in the high velocity (Figures 5.2.3 and 5.2.5, respectively) and at low velocity regime (Figures 5.2.4 and 5.2.6, respectively).

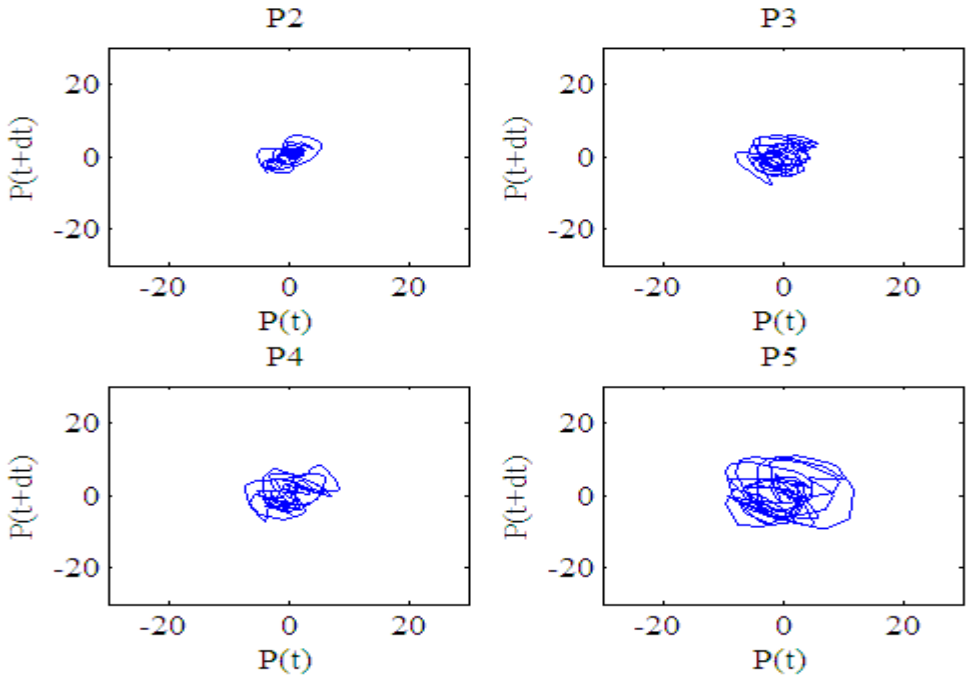

Figure 5.2.3: Variation of phase space attractor along length of pipeline for fly ash:

m_f= 0.11 kg/s ; m_s=2.36 kg/s; m^*= 21.45; V_f = 12.28 m/s (at P2) - 16.6 m/s (at P5)

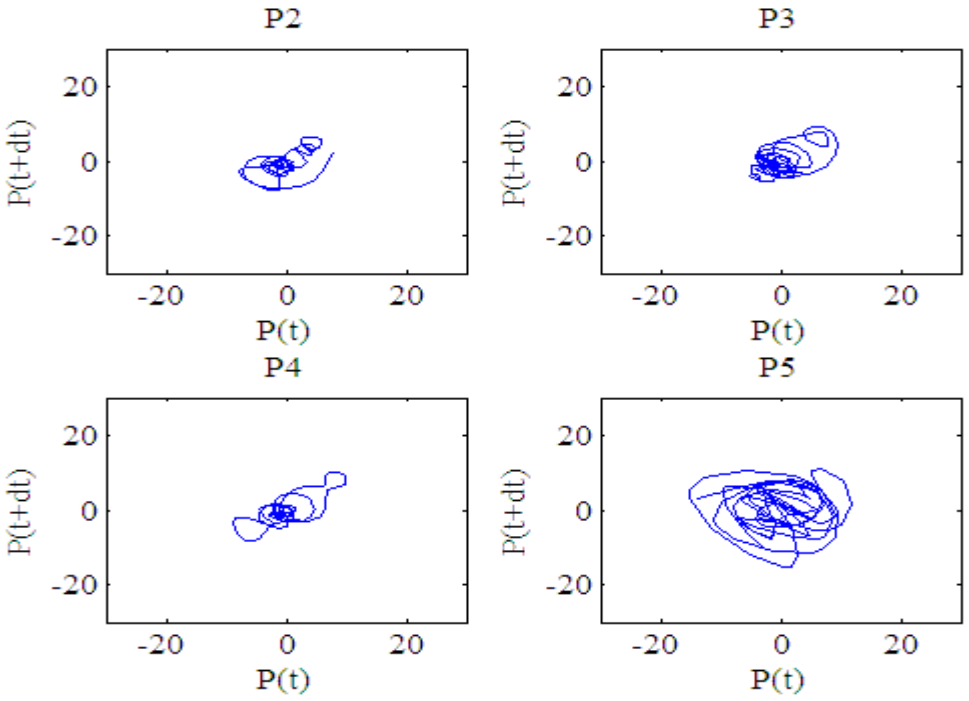

Figure 5.2.4: Variation of Phase space attractor along length of pipeline for fly ash:

m_f=0.07 kg/s; m_s=3.98 kg/s; m^* = 56.85; V_f = 7.11 m/s (at P2) - 10.6 m/s (at P5)

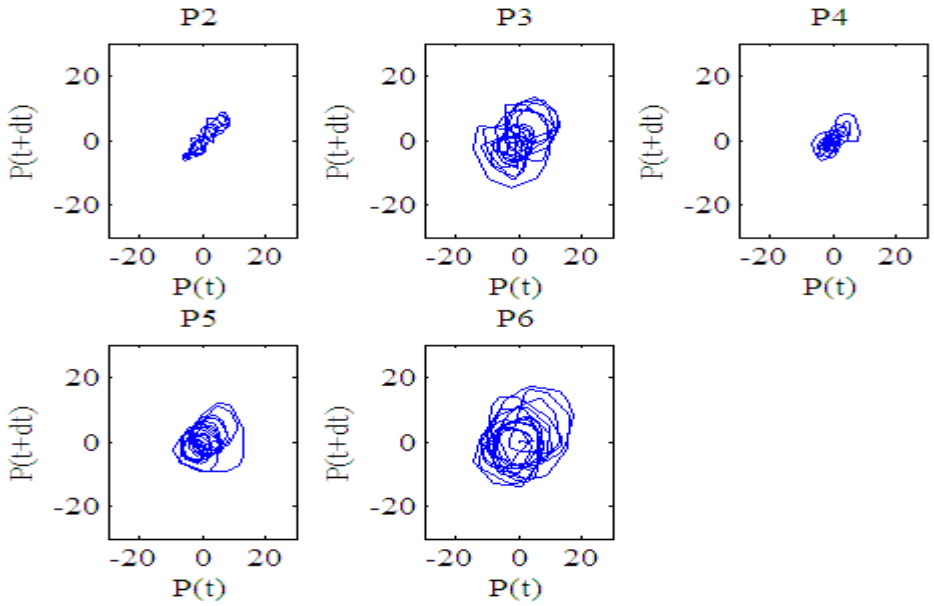

Figure 5.2.5: Variation of phase space attractor along length of pipeline for white powder:

m_f=0.20 kg/s; m_s=1.83 kg/s; m^* = 9.15; V_f = 20.86 m/s (at P2) - 31.28 m/s (at P5)

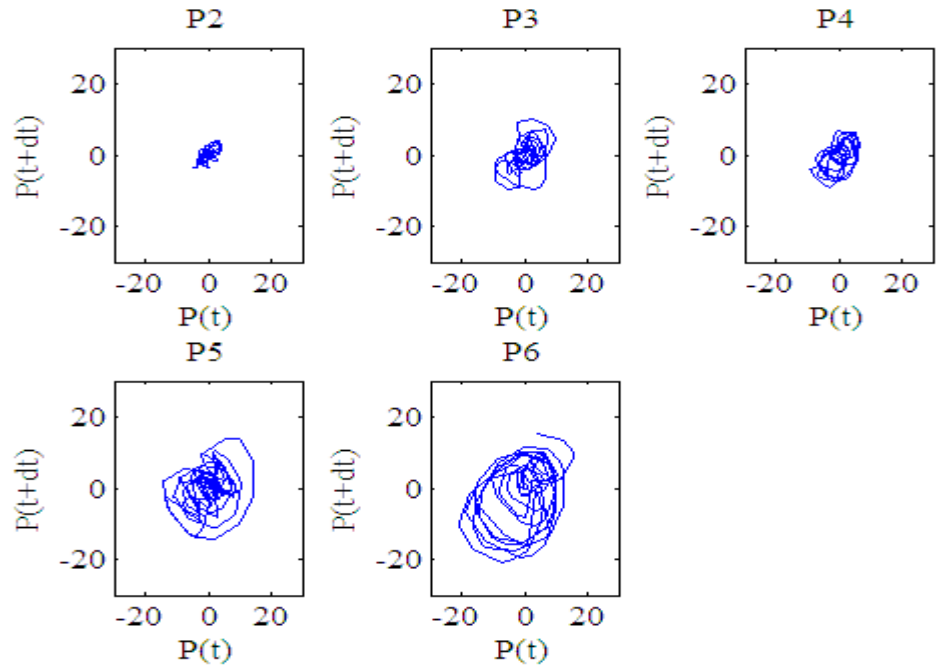

Figure 5.2.6: Variation of phase space attractor along length of pipeline for white powder:

m_f = 0.05 kg/s; m_s= 2.19 kg/s; m^*= 43.8; V_f = 4.18 m/s (at P2) - 9.09 m/s (at P5)

It can be seen in Figures 5.2.3 and 5.2.4 that for fly ash, the size of the phase space attractor increases from transducer location P2 to P3 and then it slightly decreases to P4 or remain the same as P3. Then the size of the phase space attractor increases to P5. Overall, the size increases significantly from P2 to P5. Similarly, for the case of white powder, the phase space attractor size increases from P2 to P3, then decreases at P4 and then increases again quite significantly to P5 and further to P6. Once again, the phase space attractor size increases along the flow direction. The larger area of phase space attractor is an indication of more uncertainty in the pressure time series and greater degree of disorder in the flow mechanism. An increase in the size of attractor along the length of pipeline indicates that the flow mechanism is becoming more complex and unpredictable towards the end of the pipeline. Just at the exit of the closely coupled bends, the non-increment of size of the phase-space attractor indicates reduced pressure fluctuations, which may be caused by the roping phenomenon at the outlet of the bends. Comparison of Figures 5.2.3 and 5.2.4 for fly ash provides information on the impact of the solid loading ratio on the attractor size and hence on the solids-gas flow mechanism. As seen in Figure 5.2.3 (m^* = 21.45) attractors are symmetrical about the center point, as compared to those obtained in Figure 5.2.4 (m^* = 56.85), having a higher degree of eccentricity (which indicates a higher degree of randomness and complexity in the flow). Due to the higher mass concentration at high solid loading ratio, particle-particle collisions as well as particle-wall collisions play a dominant role in addition to turbulence attenuation of carrier phase (4-way coupling phenomenon (Gray, (2012)). However, for white powder, the attractors obtained are more eccentric and scattered corresponding to low solid loading ratio (m^* = 9.15) as seen in Figure 5.2.5 as compared to high solid loading ratio (m^* = 43.8) shown in Figure 5.2.6. Eccentricity in the phase space diagrams indicates that time series data is random (i.e. with multiple events) without converging towards certain set of values. One probable reason for the reduction in size of attractors corresponding to higher loading ratio could be the

enhanced rate of turbulence attenuation of carrier phase by small particles with higher particle concentration (Hwang and Eaton, 2006). Thus phase space diagrams could be used for comparing different time-series signals and area covered on the phase space diagram could be related to time series characteristics in terms of degree of randomness. However this particular method involves selection of certain parameters, such as time lag and embedding dimension which makes the process somewhat complex in terms of computation.

5.3 Shannon entropy

In this section, the entropy method is proposed, which consists of computing the Shannon entropy derived from the pressure fluctuation time-series. It is known that entropy increment represents an event that transits from ordered to disorder in thermodynamics. Similar to the thermodynamic entropy increment, Shannon entropy increment also represents an event that transits from order to disorder. Therefore, the transient behavior, such as dynamic flow patterns and transitions could be described wellusing Shannon entropy increment. The present work attempts to study Shannon entropy variationsfor investigating thenature of gas-solid flow and different flow patterns involved. It focuses on studying the fluctuating and random behavior of gas-solid flow in the aspect of Shannon entropy increment. Shannon entropy has been calculated for the pressure signals obtained at each location on the pipeline for a series of experiments conducted corresponding to different flow rates of air and mass. The first step towards the calculation of the entropy was to determine the overall range of variation in the entire time series data in hand. For that purpose, pressure versus time series was normalized with respect to the mean of individual series (i.e. $P\text{-}P_m$ was calculated for each pressure signal corresponding to

different transducer locations (i.e. P1 to P5) in different conveying trials. This activity was performed for the complete time series data (including fly ash and white powder) and range of variation in data values (from minimum to maximum) for every signal was calculated to know the maximum range of variation, which was found (-18 to 18). The overall range of pressure deviation was divided into total eight numbers of bins (i.e. Intervals) and then for individual time series, numbers of data points falling into each bin (interval limit) were counted to obtain the probability. Finally to calculate the Shannon entropy, the equation 4.6 was used (given in Chapter 4). A program was written in MATLAB version 7.10 to calculate the value of the Shannon entropy. The estimated values of Shannon entropies along the length of pipelines for fly ash and white powder have been plotted in Figures 5.3.1 and 5.3.2, respectively, for different solids and air flow rates.

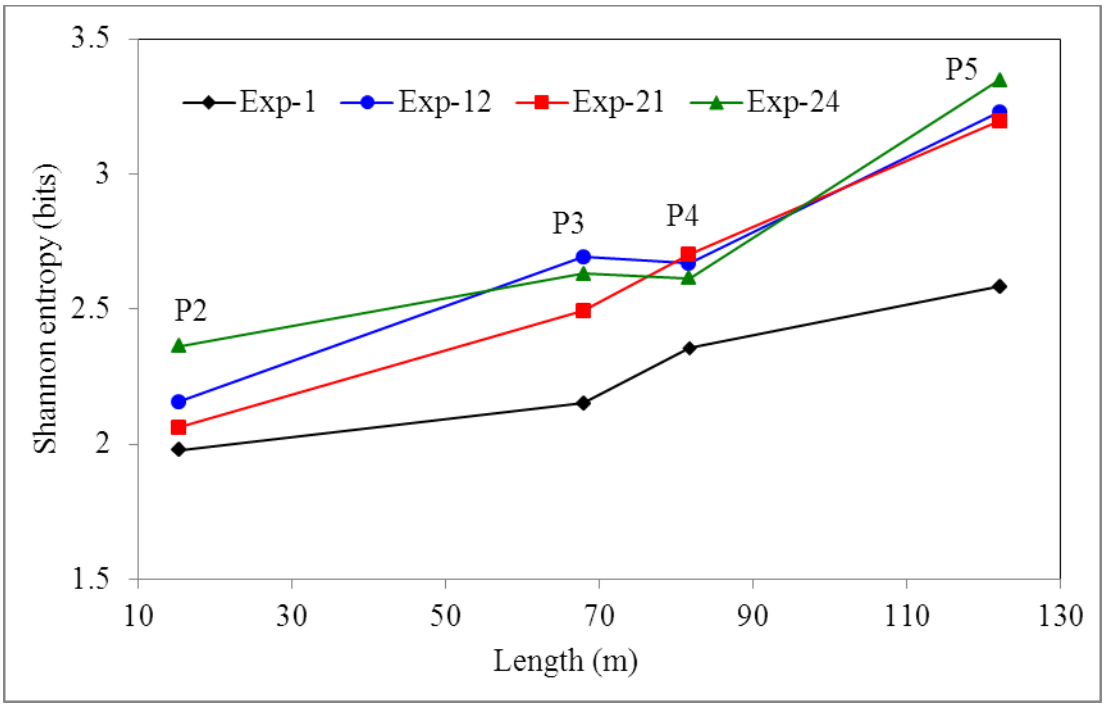

Figure 5.3.1: Variation of Shannon entropy along length of pipeline for fly ash

In Figure 5.3.1, the mass flow rate of air (m_f) and mass flow rate of solids (m_s) are given as:

Exp.1: m_f = 0.15 kg/s; m_s = 1.96 kg/s; m^* = 13.06;V_f = 16.4 m/s (at P2) - 21.7 m/s (at P5)Exp.12: m_f = 0.089 kg/s; m_s = 2.62 kg/s; m^* = 29.43;V_f = 10.13m/s (at P2) - 14.08 m/s (at P5)Exp.21: m_f = 0.1 kg/s; m_s = 3.84kg/s; m^* = 38.4; V_f = 10.21m/s (at P2) - 14.45 m/s (at P5)Exp.24: m_f = 0.07 kg/s; m_s = 3.98 kg/s; m^* = 56.85; V_f = 7.11m/s (at P2) - 10.57 m/s (at P5)

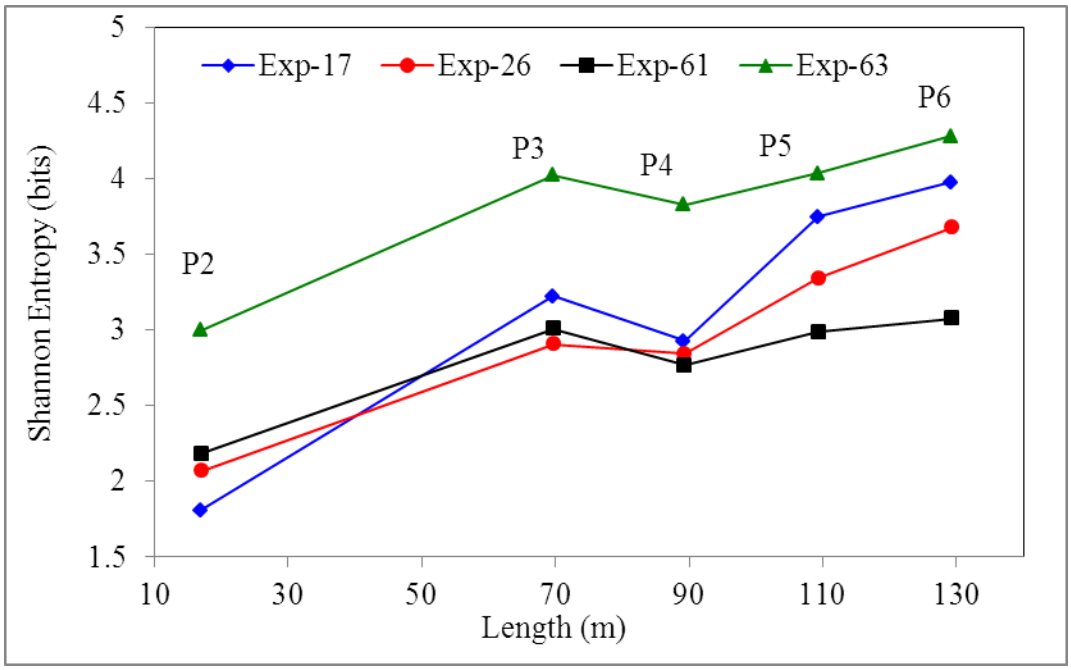

Figure 5.3.2: Variation of Shannon entropy along length of pipeline for white powder

In Figure 5.3.2, the mass flow rate of air (m_f) and mass flow rate of solids (m_s) are given as:

Exp.17: m_f = 0.06 kg/s; m_s = 2.53 kg/s; m^* = 42.16; V_f = 4.37m/s (at P2) - 9.73 m/s (at P5)

Exp.26: m_f = 0.05 kg/s; m_s = 2.19 kg/s; m^* = 43.8; V_f = 4.18m/s (at P2) - 9.09 m/s (at P5)

Exp.61: m_f = 0.1 kg/s; m_s = 2.19 kg/s; m^* = 21.9; V_f = 16.7m/s (at P2) - 27.01 m/s (at P5)Exp.63: m_f = 0.14 kg/s; m_s = 3.20 kg/s; m^* = 22.85; V_f = 12.67 m/s (at P2) - 21.53 m/s (at P5)

Figure 5.3.1 shows that for fly ash, there is an increase in the values of Shannon entropy from P2 to P5, except that there is a drop in the value of entropy between P3 and P4 for most of the experiments. Similarly for white powder (Figure 5.3.2), Shannon entropy increases from P2 to P6, except between P3 and P4.The increase in the value of Shannon entropy is indicative of the increase in randomness in the pressure signal. Thus flow mechanism tends to become more turbulent and complex towards the end of the pipeline. The low values of Shannon entropy near the entry of the pipeline could be caused by the low velocity of air, which is not sufficient to overcome the inertia of solid particles and therefore the majority of flow is caused due to solid particles moving along the bottom of the pipeline. The drop in the value of Shannon entropy in the section P3 to P4 might be caused by the roping phenomenon (due to centrifugal action, solid particles tend to get dragged along the outer wall of the bend) and the associated momentumloss of particles around the bend (Mohanarangam et al., 2009). Thus, it is possible to understand the dynamic behaviors of multiphase flows by information theory based Shannon entropy analysis. Comparison of time-series with different values of Shannon entropy could be easily made and related to flow mode inside pipeline.

Of all the three techniques applied, Hurst exponent by rescaled range was found to be dependent on the length of the time-series and results were highly affected by change in number of data points. The Hurst exponent calculation is more accurate for series with large number of data points as compared to a short series (Katsev and L'Heureux, 2003). As seen in the results from the phase space diagram, the attractor does not provide enough

information near the bend location as compared to the results of Shannon entropy and Hurst exponent. Moreover, in the process of selecting optimum delay time, there are chances of introducing error in the construction of phase space attractor (Wang et al., 2007). Moreover, the process of quantifying the characteristics of phase space attractor is far more complicated due to the huge computational efforts required. Hence, of the three methods discussed, the method of Shannon entropy could be considered as most reliable for the given application as the calculation accuracy is not affected by the information carrier and data value.

Above mentioned three techniques, provided information on the qualitative nature of entire time-series as a whole, i.e. content of information (Shannon entropy) in the signal, degree of co-correlation between different parts of the signal (Hurst exponent) and the amount of chaos (attractor analysis).These techniques mainly focus on searching for the hidden information in the time series signal and using these techniques, emphasis is made on the extraction and selection of key features that distinguish different pressure time signals, representing different flow mechanisms. The extracted features include chaotic invariants and information theory features. The results obtained are promising and clear differences were seen in the extracted features from the various pressure fluctuations, corresponding to different flow conditions. However, by using these techniques, one cannot obtain information on multiple features in terms of different frequencies and amplitude of multi scale components of the signal, which are present due to multiple interactions and complexity of the flow phenomenon. For that purpose, analysis based on frequency domain or both frequency and time domain need to be performed so as to obtain information on the frequency content of pressure signals. In the following sections, results from frequency based signal analysis techniques have been discussed.

5.4 Power spectral density

Spectral analysis of pressure fluctuation time-series has been performed using Fast Fourier Transform (FFT), which expresses the behavior of time-series in the frequency domain. Power spectral density analysis, estimated by FFT (Bendat and Piersol, 1980) has been used as a quantitative analysis to identify different flow regimes. The power spectrum illustrates the behavior of the pressure signals in the frequency domain. It characterizes the pressure signals based upon the presence of dominant frequency and bandwidth of spectra. Changes in power spectra, as a result of changes in flow dynamics have been discussed in terms of broadening and sharpening of spectra, and the shift of dominant frequencies. Figures 5.4.1 to 5.4.2 show the variation in the power spectral density obtained at different transducer locations located along the pipeline for fly ash and white powder. Results of two typical experiments have been shown for each of fly ash and white powder.

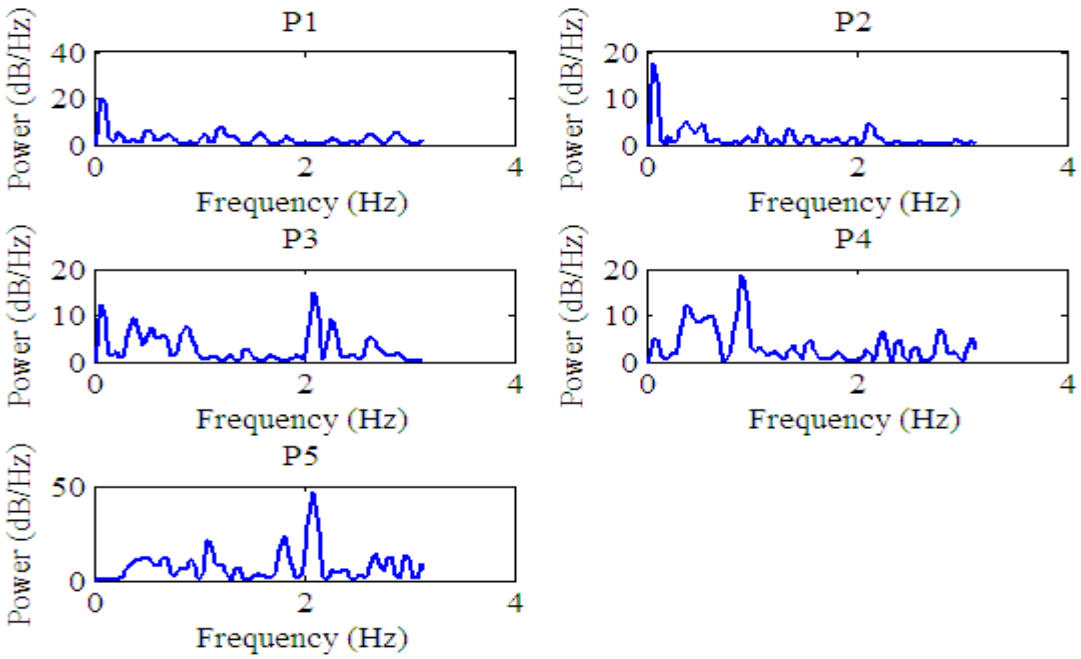

Figure 5.4.1: Variation of power spectral density along pipeline length for fly ash;

(m_f = 0.107 kg/s; m_s = 2.35 kg/s; m^* = 21.96)

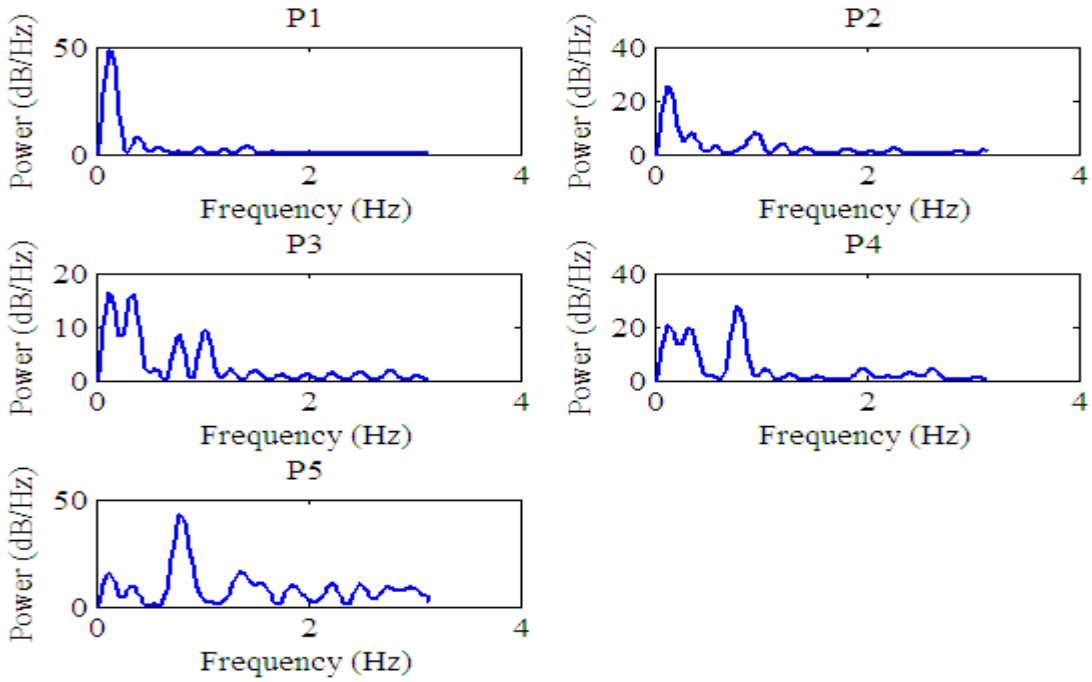

Figure 5.4.2: Variation of power spectral density along pipeline length for fly ash;

(m_f = 0.07 kg/s; m_s = 4.41 kg/s; m^* = 63)

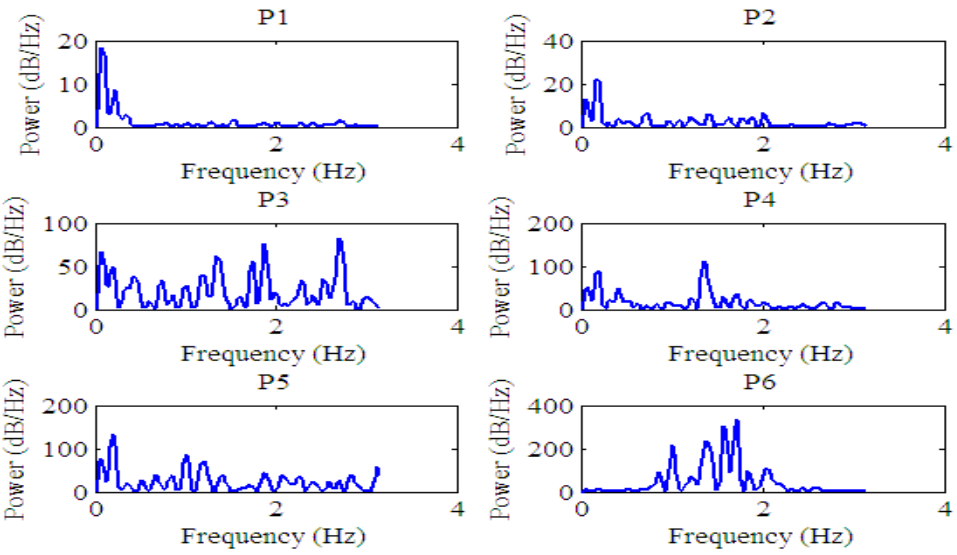

Figure 5.4.3: Variation of power spectral density along pipeline length for white powder;

(m_f = 0.085 kg/s; m_s =2.29 kg/s; m^* = 26.89)

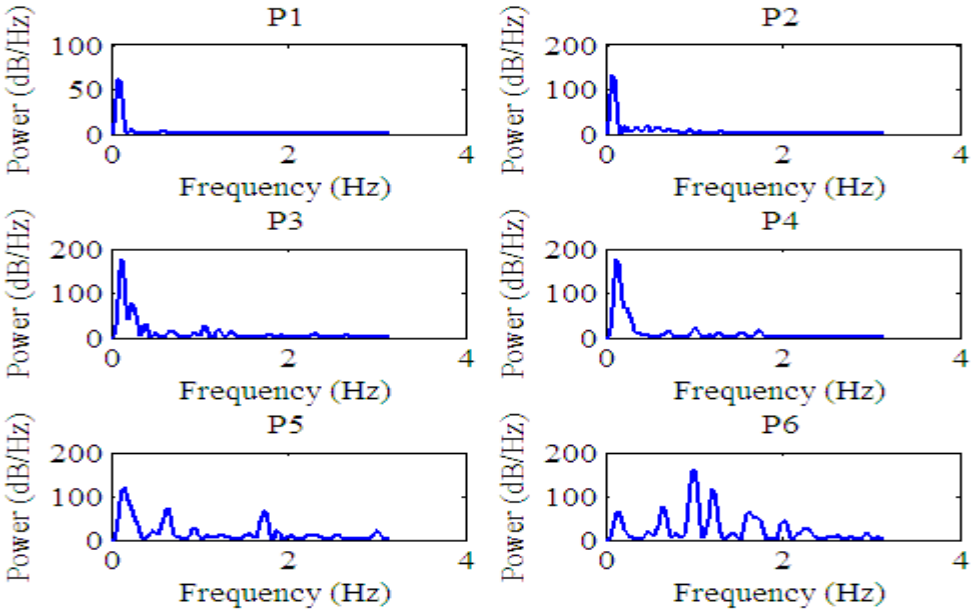

Figure 5.4.4: Variation of power spectral density along pipeline length for white powder;

(m_f = 0.05 kg/s; m_s = 2.34 kg/s; m^* = 46.8)

It can be seen in the above figures that both the band spectrum and magnitude of spectral densities vary with the change in transducer location along the pipeline length. At initial locations (i.e. P1 and P2 as shown in Figure 5.4.1), power spectrum obtained is quite

narrow and single dominant peak can be clearly observed in the spectrum. Presence of a single frequency component at 0.1 Hz indicates the periodic nature of the pressure signal, which might have occurred due to the periodic rising of dunes at a frequency of 0.1 Hz near the pipeline entrance (product feeding zone). Along the pipeline and in the direction of flow (i.e. from P2 to P3), the spectrum gets wider and in addition to the single dominant frequency, other frequency components also appear in the spectrum. Therefore, it appears that from a dominant non-suspension dune flow at the blow tank location (where most of the product is fed into the pipeline as a non-suspension dune), more randomized interactions between the solid particles, air and pipe wall are initiated along the flow direction due to the increase in gas velocity. These interactions consequently become stronger while travelling further downstream in the pipeline and is reflected by multiple peaks with significant power observed in the power spectrum instead of a single dominant frequency peak. Another important characteristic of the power spectra profile, observed for each flow condition, was the increase in power density of the signal from inlet towards the end of the pipeline and was found to be maximum at P5 for fly ash and at P6 for white powder, which indicate increased amplitude of pressure fluctuations along the pipeline length. Thus, both frequency and amplitude of the pressure fluctuations increase in the straight pipe section of the pipeline, which might have resulted from the turbulence enhancement and multiple flow interactions taking place at different scales. While at the locations near bends, (i.e. from P3 to P4), change in magnitude of PSD is comparatively less significant as reflected in the Figures 5.4.2, 5.4.3 and 5.4.4, which indicates the slow movement of solid particles (i.e. reduced product turbulence) in the bends due to the loss in momentum caused by pipe wall friction when the solid particles are directed towards the outer wall of bend due to the centrifugal force acting on the particles (Mohanarangam et al., 2009). It can also be observed that for white powder, increase in power density (while moving from P1 to P6) in Figure 5.4.3 ($m^* = 26.89$) is much higher when compared

to the increase found in Figure 5.4.4 (m^* = 46.8). This could be due to the fact that with the increase in the solid loading ratio (m^*), rate of carrier phase turbulence attenuation by adding fine particles (50-90 μm) is increased (Kulick et al., 1994; Paris, 2001; Hwang and Eaton, 2006; Benavides and Wachem, 2008), which causes decreased amplitude of fluctuations, resulting in lower power density. Hetsroni (1989) also investigated various experimental data for horizontal and vertical two-phase pipe flows and concluded that particles with Re_phigher than 400 tend to increase the turbulence intensity due to vortex shedding of particles, while particles with Re_p(based on superficial gas velocity and particle diameter)less than 400 tend to suppress the turbulence intensity. When fine particles are introduced into the clean air stream, the drag force is brought about by relative motion between the stream of gas and the solids flowing in it. The solid particles lose kinetic energy as a result of impact and friction and further energy is required to keep them suspended in the gas stream. All this lost energy is replenished from the kinetic energy in the gas stream resulting in reduced carrier gas turbulence.From the above discussion, it can be concluded that significant differences between the spectra obtained from pressure measurements at different transducer locations could be used to study different characteristics of changing flow conditions along the pipeline length. Presence of dominant frequency, width of PSD spectra could be used to distinguish between periodic and non-periodic signals. Further, degree of periodicity in the signal could be related to nature of flow inside pipeline. Typical periodic signal indicated dense-phase mode of transport, while non-periodic signal with wider spectrum indicates suspension mode of flow (due to presence of random interactions between gas and particles.)

5.5 Hilbert-Huang Transformation

Since the pressure fluctuation signal obtained from gas–solid flow contains ample multi-scale information regarding particle movement, collisions between particles and pipe wall, particles and air, which is closely associated with the flow pattern, therefore Hilbert–Huang transform was applied to perform a multi-resolution on the acquired pressure fluctuations, identifying the information on flow patterns carried in the pressure signals collected from the gas–solid flow. Hilbert–Huang transform (HHT) is a local and adaptive non-linear and non-stationary signal processing approach, which is completely different from the Fourier spectral analysis. Hilbert–Huang transform decomposes the pressure signal into IMFs with different scales and multi-resolution levels. Figure 5.5.1 and 5.5.2 show results of the first two steps applied to a typical pressure signal for extracting intrinsic mode functions. Figure 5.5.3 shows the EMD decomposition, in which the extracted IMFs are listed in the different rows, from high-frequency (IMF1) to low-frequency (IMF5).

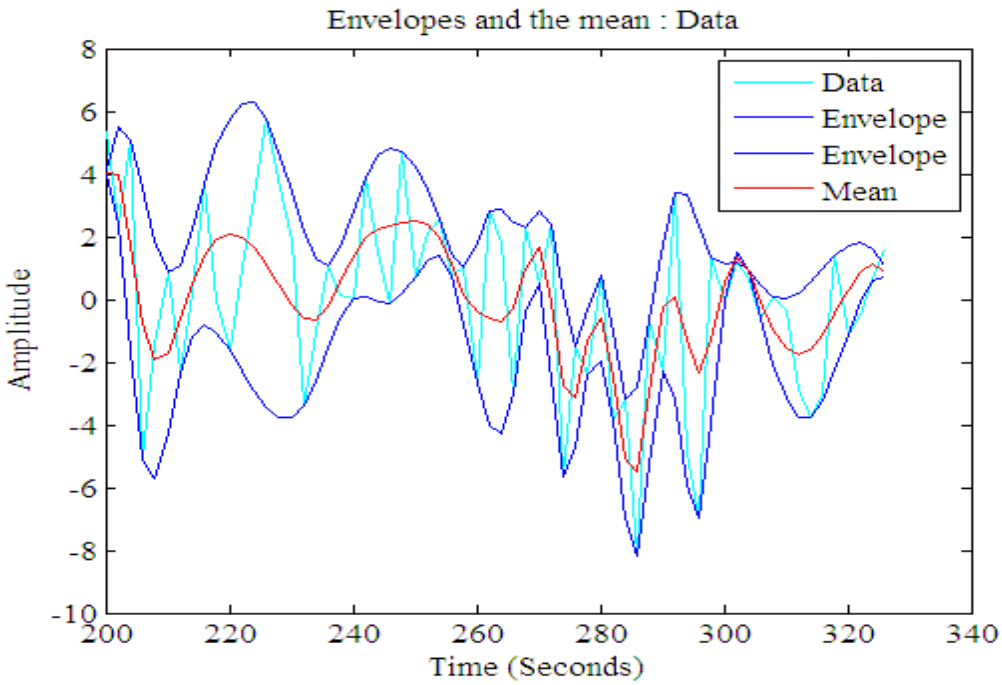

Figure 5.5.1: Upper and lower envelopes of mean adjusted series at 1st step (applied to typical pressure signal)

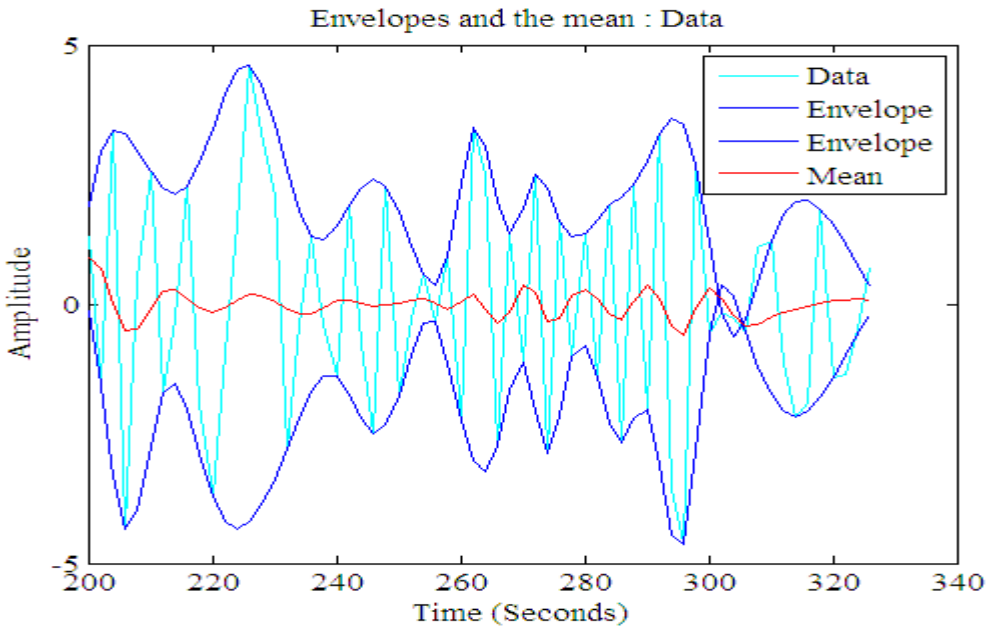

Figure 5.5.2: Upper and lower envelopes of mean adjusted series at 2nd step (applied to typical pressure signal)

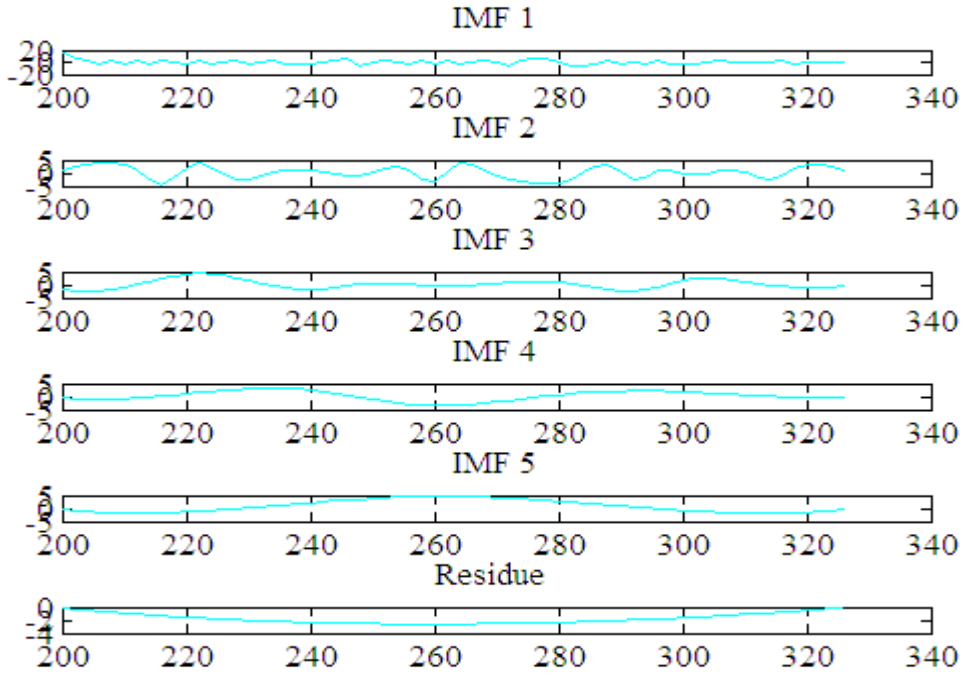

Figure 5.5.3: Intrinsic mode function extracted from a signal

In order to find out the quantitative relation between the energy transmission of IMFs of the pressure fluctuations and the flow patterns of pressurized gas–solid flow, the energy distribution index e (ratio of energy corresponding to the particular IMF to the total signal energy) is calculated as the characteristic of pressure fluctuations corresponding to different flow patterns.Figures 5.5.4 to 5.5.7 show the variation of energy distribution index of IMF's along the length of the pipeline (i.e. from P2 to P5 for fly ash and from P2 to P6 for white powder).

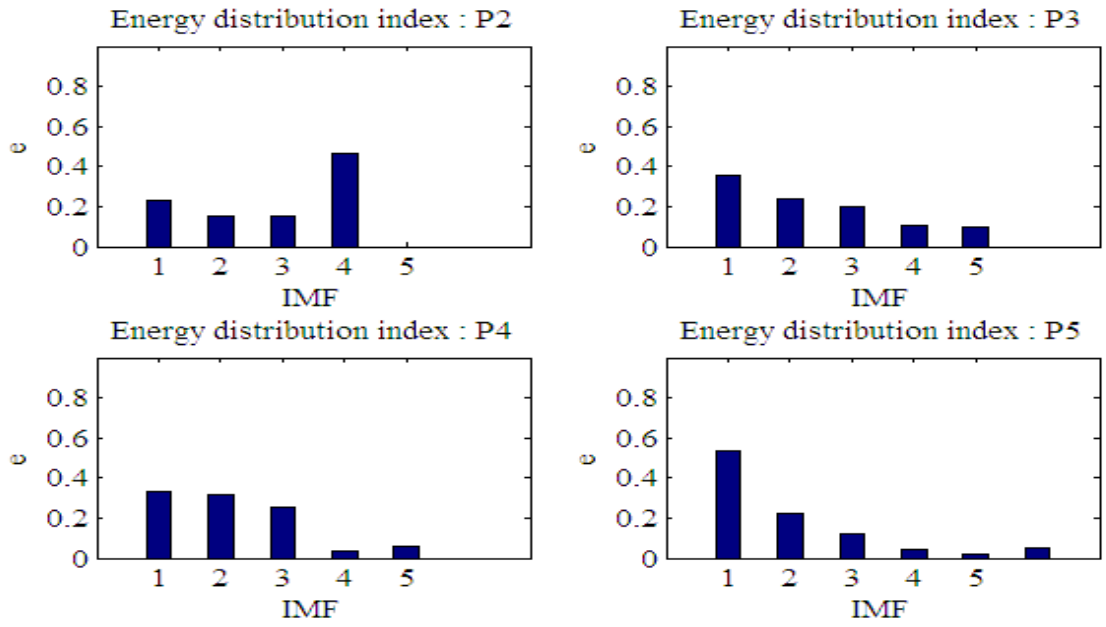

Figure 5.5.4: Variation of energy distribution index (by Hilbert Transformation) along pipeline length: fly ash (m_f = 0.107 kg/s; m_s = 2.35 kg/s; m^* = 21.96)

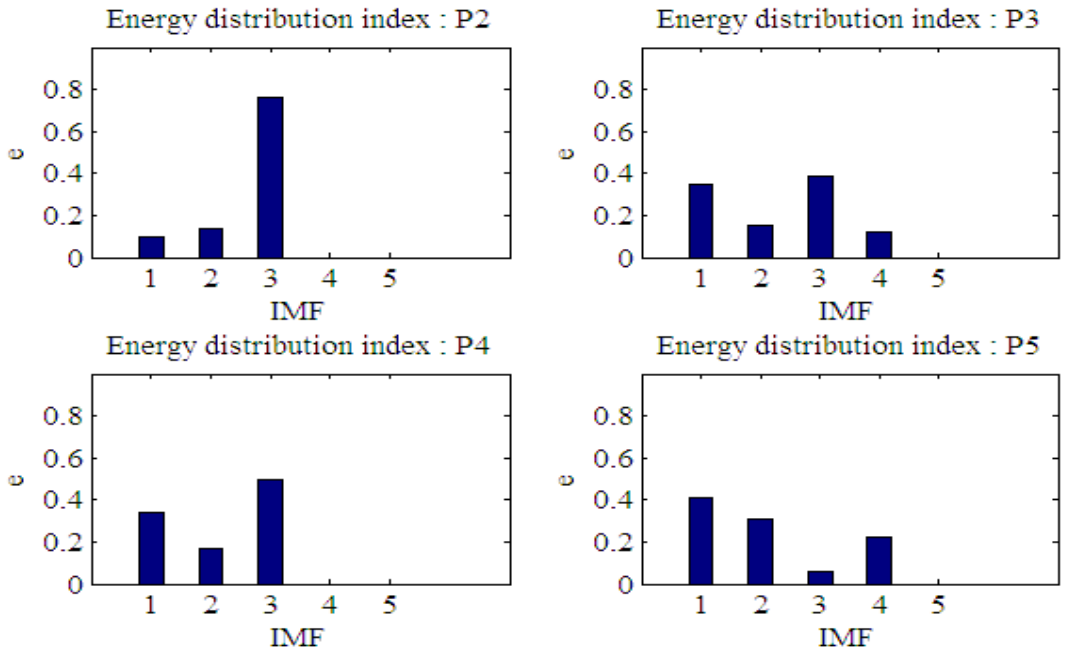

Figure 5.5.5: Variation of energy distribution index (Hilbert Transformation) along pipeline length: fly ash (m_f = 0.07 kg/s; m_s = 4.41 kg/s; m^* = 63)

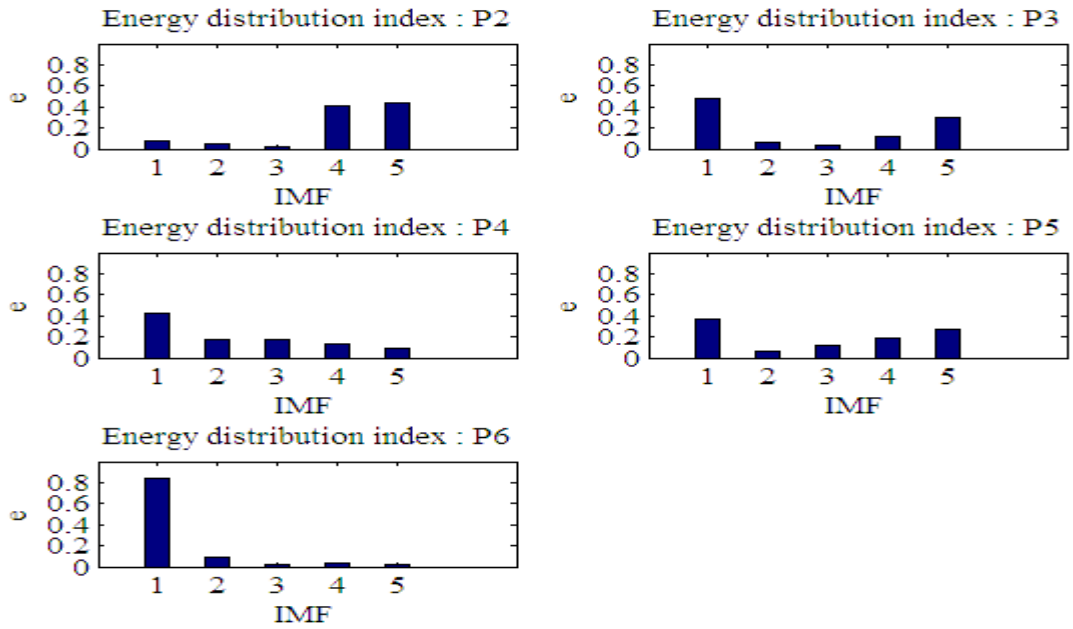

Figure 5.5.6: Variation of energy distribution index (Hilbert Transformation) along the pipeline length: white powder (m_f = 0.085 kg/s; m_s =2.29 kg/s; m^* = 26.89)

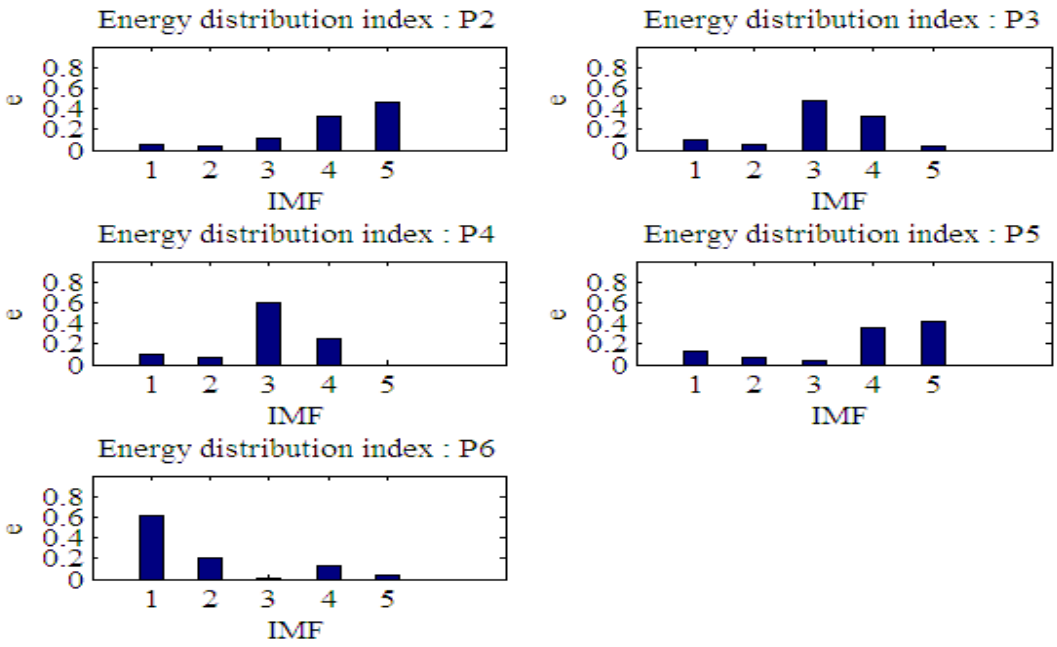

Figure 5.5.7: Variation of energy distribution index (Hilbert Transformation) along pipeline length: white powder (m_f = 0.05 kg/s; m_s = 2.34 kg/s; m^* = 46.8)

It can be seen from the above figures (Figures 5.5.4 to 5.5.7) that the total energy of the signal is distributed among various IMF's extracted from empirical mode decomposition of the original signal. At the first transducer location (i.e. P2), which is near to the entry of pipeline, IMF4 (which is extracted at the end of the EMD process) has the highest value of the energy distribution index and the other IMF's have smaller values as compared to IMF4, therefore it contributes maximum to the total signal energy. While at P3, IMF1 component shows increased contribution to the total energy and energy contribution by IMF4 is reduced (as compared to that found at location P2). Moving further along the pipeline, i.e. from P3 to P4, there is not much change in the energy distribution of different IMF's. For the transducer location P5, which is located near to the exit of the pipeline (test rig used for fly ash, University of Wollongong, Australia), major energy contribution shifts to IMF1 (i.e. first IMF component). Similarly for white powder, maximum energy shifts from IMF5 to IMF1 while moving from P2 to P6. IMF1 is the highest frequency

component extracted and subsequently low frequency IMF components are extracted; IMF extracted in the last point is the lowest frequency component. It can be concluded from the results that while moving from the entry to the exit of pipeline, energy distribution shifts from coarse scale (low frequency) to fine scale (high frequency) band. The probable reason for the same could be the change in flow mechanism from non-suspension dune flow (low frequency) to suspension flow (high frequency) along the length of the pipeline. As an increase in the gas superficial velocity along the length of the pipe results in higher gas pulsation intensity, which further intensifies the pulsation of the particles dispersed in the carrier phase and hence the particles are increasingly exchanged between the different layers across the pipe cross-section as the particle sedimentation tendency weakens. The final results of increasing gas superficial velocity are that the sedimentation layer in the bottom of the pipeline becomes thin, the solid concentrations near the bottom of pipe gets reduced and particle velocity increases. Consequently, the dominant scales of the pressure fluctuations shift toward fine scales. Therefore Hilbert–Huang transform for the pressure fluctuations and energy distribution over IMFs with the different scales are helpful for the understanding of the particle behavior and flow pattern transition of dense phase gas–solid two phase flow. The Hilbert–Huang transform shows variation of the instantaneous frequencies and amplitudes of the pressure fluctuation signal with time, while the Fourier transform cannot provide the variation with time. Thus, this method enables us to obtain the frequency and amplitude content of local complex flow behaviors (i.e. at a specific time instant or within certain time period), which are associated with the gas–solid flow. As compared to wavelet transform, this method need not select primary function beforehand; the decomposition procedure of the original signal is self-adapting.

5.6 Wavelet Transformation

All the above-mentioned methods for flow pattern recognition rely on various statistical properties of the measured signal in the time, frequency or pseudo-phase domain. Hence, in order to obtain reliable results, the analysed signal must have sufficient length (i.e. number of data points in the signal) to yield accurate estimates of the characteristic parameters. This requires longer periods of steady state conveying, which makes these methods more appropriate for laboratory tests, however to provide information about the instantaneous state of the flow in the on-line mode would be a difficult task using these techniques. In addition to this, the flow structure is highly unstable in the vicinity of the transition between flow regimes, and patterns characteristic of different regimes tend tovary along the pipeline, which makes the objective of flow regime identification even more difficult to achieve. Therefore, it is desirable to identify the flow regime using a short-length signal.

In the present section, a promising approach for flow pattern classification based on the wavelet transform has been investigated. This method has been widely used in signal processing and analysis and have shown to be a superior tool for the analysis of non-stationary and transient signals due to its localization properties in the time domain. Moreover, the localization of the wavelets in the frequency domain means that the wavelet transform coefficients incorporate features of the PSD and, consequently can be used for flow regime identification. These anticipations were validated by Kirpalani et al. (2001), who applied the continuous wavelet transform to the analysis of time series of wall pressure fluctuations in various two phase flow regimes. They found that the wavelet spectrum of the measured signal possesses features that are similar to the PSD of the wall pressure time series reported by Hubbard and Dukler (1966).

It was shown in the earlier section that the power spectral density can be used as an objective flow regime indicator. However, the accurate estimation of the power spectra requires the analysed signal to be sufficiently long. The Fourier basis function is localized only in the frequency, but not in time. Even though the spectral density function indicates that the major frequency is generated by slow moving dunes, however, it cannot reveal the movement of those dunes in the pipeline over time. This is a disadvantage of the Fourier transform, which is unable to permit time localization.In that case, the wavelet transform, provides signal decomposition, which is intermediate between the time- and frequency-domain representations. Moreover, the wavelet spectrum can be well estimated even for a moderate length samples (Percival, 1995). The measured pressure signals were processed using MATLAB software (version 7.10).

Figures 5.6.1 to 5.6.4 show the continuous wavelet scalogram for fly ash and white powder.

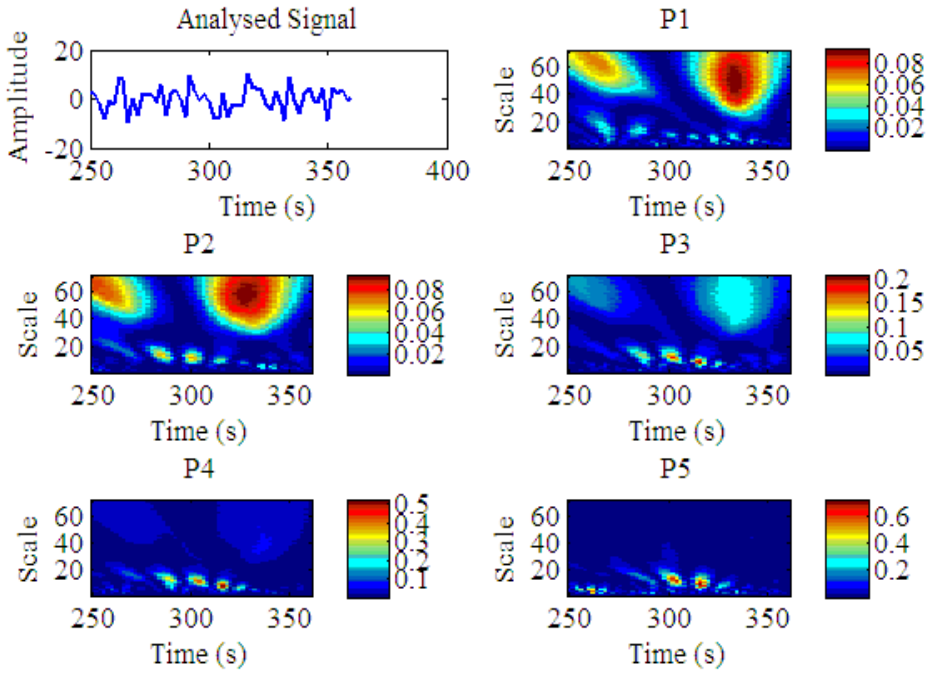

Figure 5.6.1: Variation of wavelet scalogram along the length of pipeline:

fly ash (m_f = 0.107 kg/s; m_s = 2.35 kg/s; m^* = 21.96)

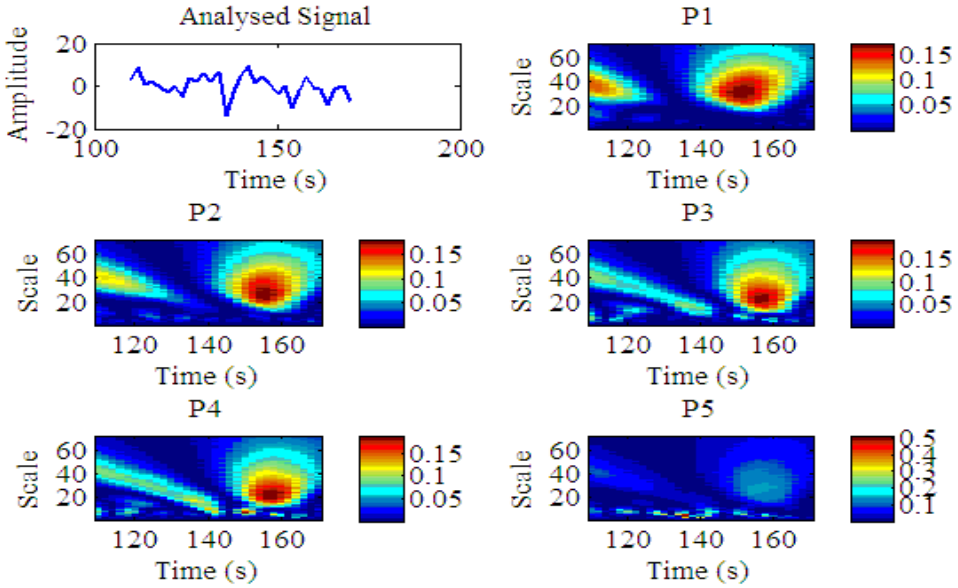

Figure 5.6.2: Variation of wavelet scalogram along the length of pipeline:

fly ash (m_f = 0.07 kg/s; m_s = 4.41 kg/s; m^* = 63)

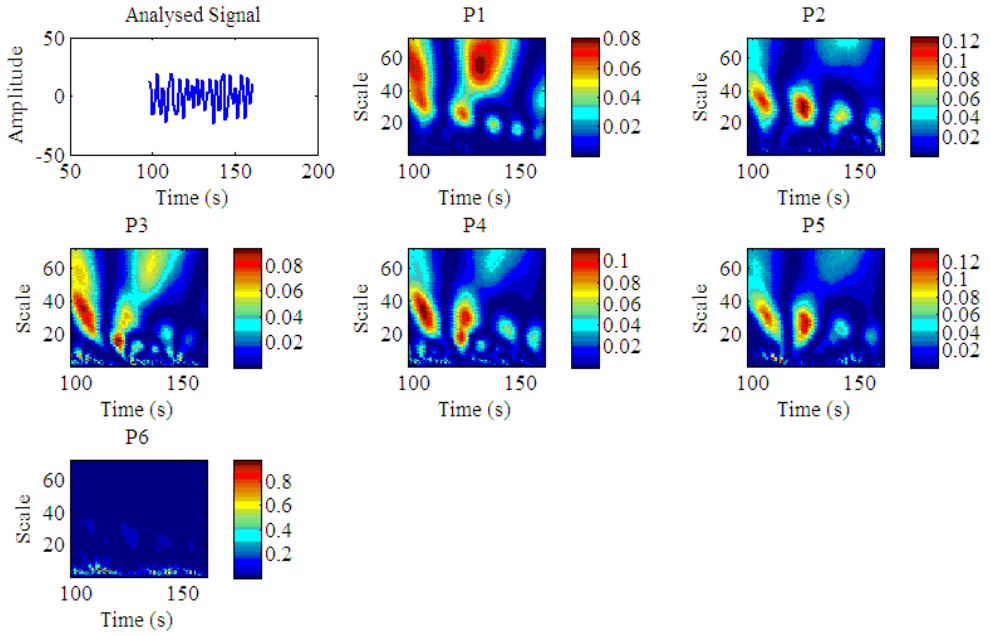

Figure 5.6.3: Variation of wavelet scalogram along the length of pipeline: white powder

(m_f = 0.085 kg/s; m_s =2.29 kg/s; m^* = 26.89)

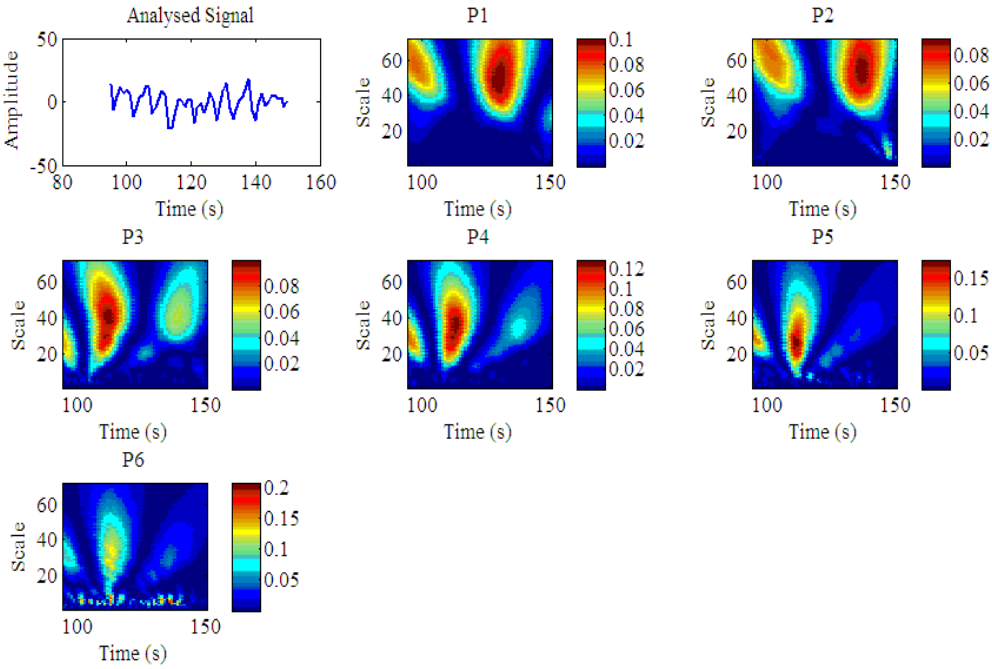

Figure 5.6.4: Variation of wavelet scalogram along the length of pipeline:

White powder (m_f = 0.05 kg/s; m_s = 2.34 kg/s; m^* = 46.8)

As seen in the above figures, color spectrum of the wavelet scalogram varies from P1 to P5/P6. Color intensity reflects the energy of the wavelet coefficients and the color bar in each plot provides energy values corresponding to different colors. Dark red color indicates the maximum energy, while dark blue color represents the minimum energy. At initial locations (i.e. at P1 and P2 as shown in Figure 5.6.1), maximum energy is concentrated in the upper region of the plot and corresponds to high scale coefficients (i.e. scale 50). Since higher scale coefficients describe the low frequency components of the signal, therefore it indicates that signal is composed of large number of low frequency components, which might be due to the reduced turbulence at the starting of the pipe location and in turn indicates dune flow mechanism. While going from P2 to P3, color intensity is reduced corresponding to higher scales (i.e. changes from dark red to light blue) and higher intensity shifts to lower scales (i.e. scale 20). Thus, parent signals contain comparatively higher frequency features as compared to the signal obtained at location P1.With further movement along the pipeline (i.e. from P3 to P5), color intensity almost diminishes at higher scales and multiple numbers of highly concentrated points are seen at lower scales (scale 10), which indicate the presence of large number of pressure fluctuations at different time instants in the signal. Similarly, for white powder, maximum color intensity shifts from higher scale (scale 55) to lower scale (scale 5), while moving from P1 to P6 (as seen in Figure 5.6.3 and 5.6.4). It can also be observed that magnitude of the maximum energy increases while moving from P1 to P5/P6, which indicates increase in amplitude of pressure fluctuations. Thus, it can be concluded that signal composition varies from pipeline inlet towards exit in terms of different frequency components and magnitude of amplitude as well. These variations in the signal characteristics provide indication on change in flow mechanism along the pipeline, from slow moving dunes near pipeline entry to the highly turbulent flow with multiple interactions at exit of pipeline.

Therefore it can be written that a wavelet scalogram of typical pressure signal with energy concentration corresponding to high scale coefficients indicates dense phase mode of flow while the scalogram having most of the energy corresponding to low scale coefficients indicates towards dilute mode of transport.It can be noted here that for computing the wavelet coefficients transform fast algorithm exists as compared to the Fourier transform. Moreover, the estimation of the wavelet coefficients do not demand for a large sample size, which makesthis method appropriate to be applied for flow conditions in the vicinity of transition boundaries between the flow regimes. Thus, the proposed method can be better used for the on-line identification of flow regimes in solid-gas systems.

The purpose of attempting large number of techniques for pressure signal analysis was to speculate the potential of pressure fluctuations to be used as an important input for studying the flow behavior.As seen in the above sections, results of all the signal processing techniques (each having distinctive numerical basis) are consistent in terms of predicting the variation in flow mechanism along the pipeline length during dense phase conveying of fine powders. Thus, pressure signals carry vital information related to the flow behavior inside pipeline and the same could be extracted using any of the techniques mentioned in the above sections, however degree of accuracy and completeness of information obtained would vary from one technique to another.

5.7 Minimum Transport Boundary

Apart from investigating change in flow mechanism along the pipeline length, all the techniques of pressure signal analysis were applied to fluctuation data obtained from the conveying trials conducted near minimum transport boundary. In case of fluidized dense

phase pneumatic conveying of fine powders, reduction in mass flow rate of air beyond steady state conveying causes formation of unsteady dunes, which are characterized by enhanced pressure fluctuations. Further decrease in air flow rate would cause build-up of product along the bottom of pipeline in the form of deposits. Therefore, system would deviate from steady state conveying operationand during this period, the generated pressure signal pressure would continue to grow with time. This limit is called the minimum transport boundary (Mallick, 2009). Reduction in gas flow rate beyond this limit would cause the flow blockage (indicated by rapid rise in pressure). Figure 5.7.1 shows the pressure signal fluctuations obtained from dense phase conveying of flyash with solid loading ratio (m^* = 150) and superficial gas velocity in the range of 4-7 m/s.

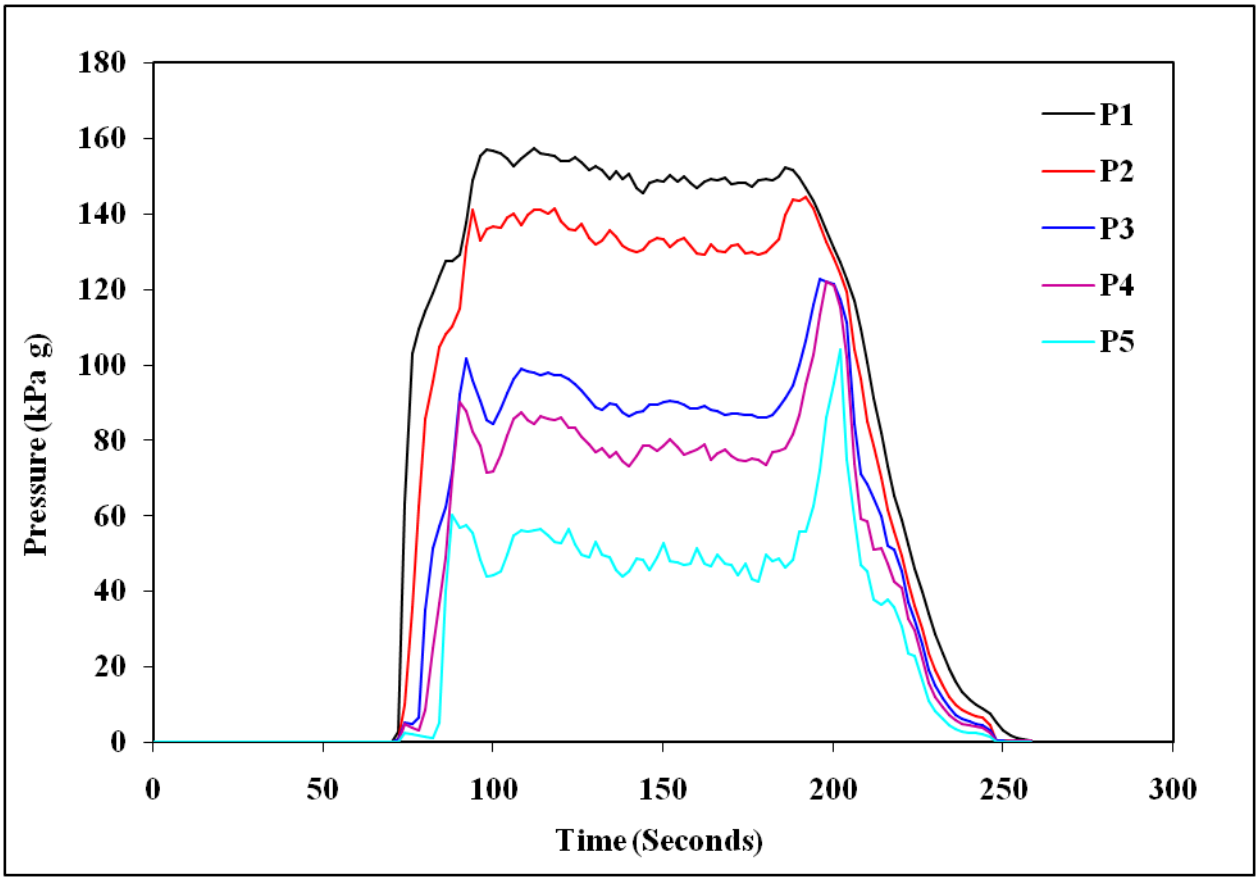

Figure 5.7.1: Pressure signals for Flyash; Exp-35; m_f = 0.04 m/s; m_s = 5.98 m/s; m^* = 150.6; V_f = 4 m/s (at P1) - 7 m/s (at P5)

As can be seen in the above figure, while operating near minimum conveying velocity, duration of steady state conveying is quite less (only about 50 seconds). Further reduction in superficial gas velocity would cause unsteady state flow and system would cease to operate under steady state conveying, as seen in Figure 5.7.2.

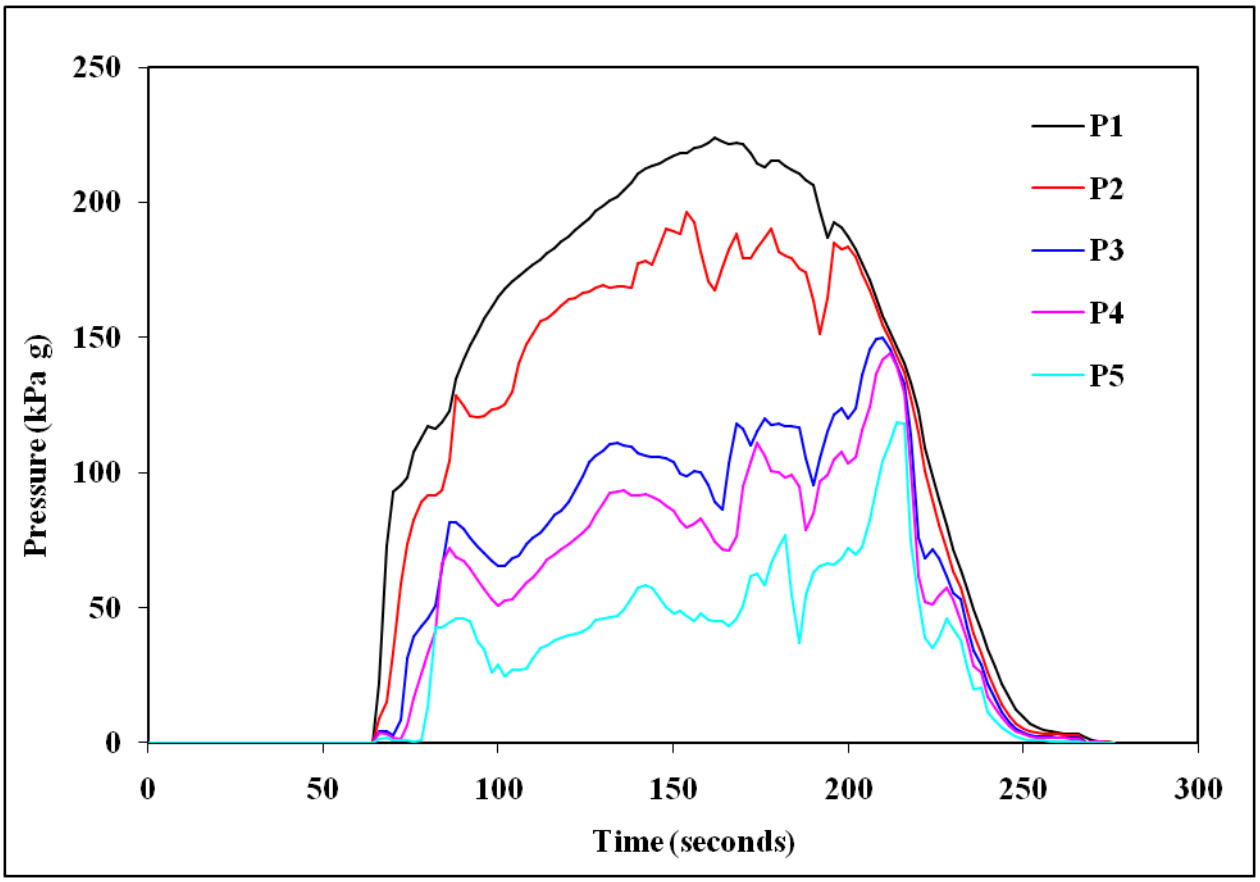

Figure 5.7.2: Pressure signals for Flyash; Exp-37; m_f = 0.03 m/s; m_s = 5.84 m/s; m^* = 182.3; V_f = 2 m/s (at P1) - 5 m/s (at P5)

As seen in the above figure, for solid loading ratio, m^* = 182.3 and superficial velocity in the range of 2-5 m/s, product is no more conveyed in steady state, as there is a continuous rise in pressure drop values with time.

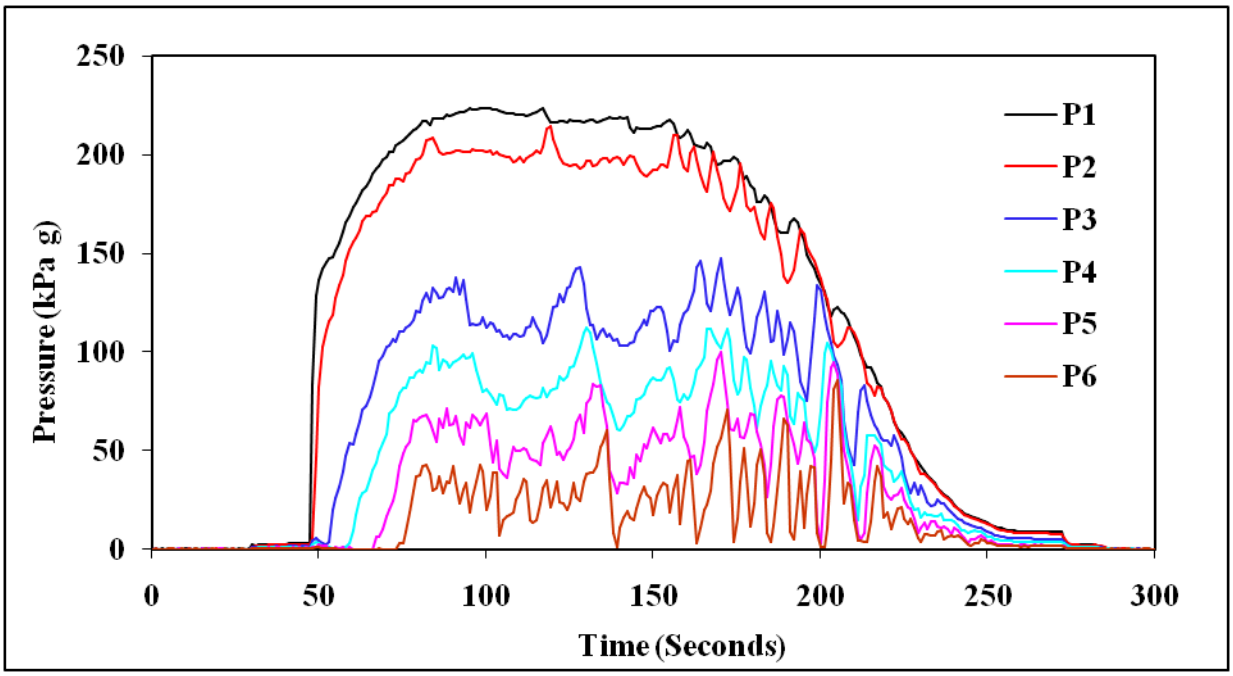

Figure 5.7.3: Pressure signals for White powder; Exp-23; m_f = 0.04 m/s; m_s = 2.05 m/s; m^* = 50.8; V_f = 3 m/s (at P1) - 7 m/s (at P6)

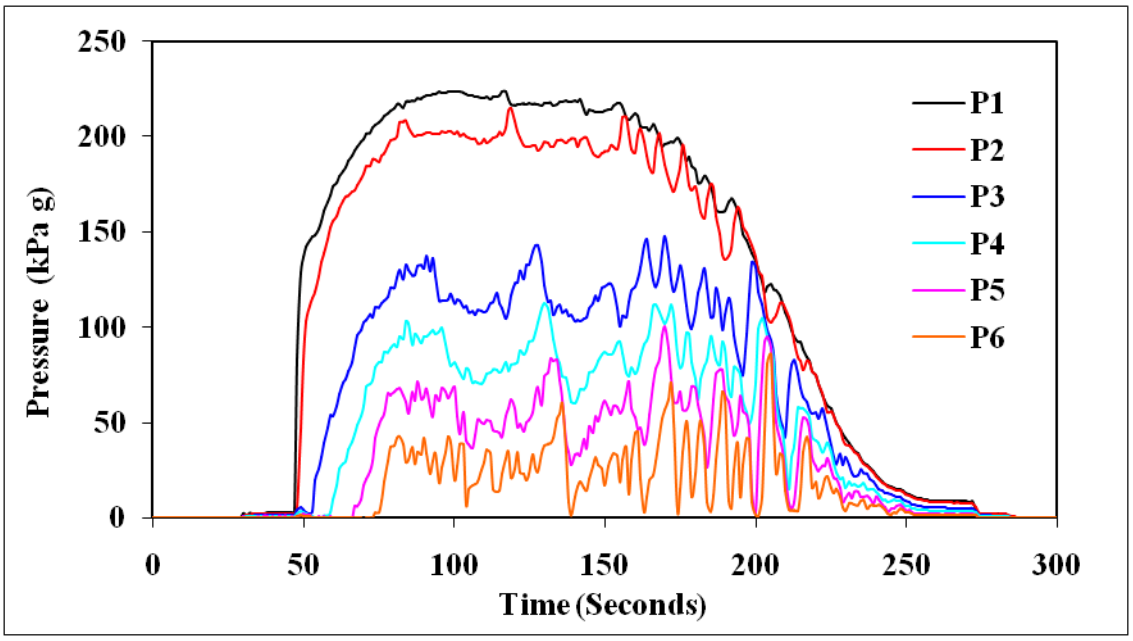

Figure 5.7.4: Pressure signals for White powder; Exp-20; m_f = 0.01 m/s; m_s = 2.53 m/s; m^* = 253; V_f = 1 m/s (at P1) - 2 m/s (at P6)

The minimum transport boundary or capacity limitation boundary affects the design and operation of pneumatic conveying systems. While operating at minimum transport boundary, further reduction in mass flow rate of fluid/air would cause the fluidized bulk material to de-aerate sufficiently for a blockage to occur. Therefore,proper sizing and design of the dense phase pneumatic conveying systems for industrial plants, demands for the accurate prediction of the minimum transport (or capacity limitation) boundary. Some fundamental models for minimum transport boundary (based on powder mechanics) have been developed for the low-velocity slug-flow of granular products (Wypych and Yi, 2003). However, the flow mechanism involved in the dense-phase conveying of powders is far more complex due to multi scale interactions between the particles, carrier gas and pipe/bend wall, and most of the existing models have been empirical (Mills et al.,1982; Mills, 2004; Mills, 2004a). Preliminary investigation by Mallick (2009) has shown that such models have been based on certain products and pipeline conditions and have not been tested properly under important criteria, such as scale up accuracy. With this background, an attempt has been made is to predict the minimum conveying velocity based on analysis of pressure fluctuations. To define the safe minimum transport boundary, a Froude number based criteria at the pipe inlet was used (Fr_i = 6), which was developed by Mallick and Wypych (2009) using different powders such as flyash, ESP dust and cement data conveyed through pipelines of various diameter and length. Froude number is a dimensionless parameter which represents ratio of the inertia force on an element of the fluid to the weight of the fluid element (i.e. inertia force divided by the gravitational force).

$$Fr = \frac{V_f}{\sqrt{gD}} \quad (5.2)$$

Where $V_f$is the superficial gas velocity, g is the acceleration due to gravity and D is the pipe inner diameter. Dimensionless Froude number has been used in open channel flow, particularly in wave and surface behavior calculations. For the purpose of estimation of minimum conveying velocity, the Fr for a given powder can be used as basis to represent the inertial forces required to overcome a certain gravitational force (i.e. to push the "mixture" weight though the pipeline). Other pneumatic conveying researchers also have found Fr a useful parameter to represent minimum transport, such as Roski (1987).

The Froude number based criterion was aimed to address the requirement of different conveying velocities for different pipe diameters. However, Mallick et al. (2011) indicated that constant Froude number criteria to predict the blockage boundary provides limited accuracy when used under scale up conditions and further studies were recommended towards developing more accurate criteria for minimum transport boundary. Therefore with the aim of predicting blockage boundary using pressure signal fluctuations, time-series data corresponding to certain number of the conveying trials, which were conducted with high value of solid loading ratio (m^* more than 70, close to the blockage boundary) were chosen and signal analysis techniques were applied to the pressure fluctuations data. The following figures show the results of PSD analysis, Wavelet scalogram, attractor construction, Hilbert transformation, Hurst exponent and Shannon entropy applied on the experimental data obtained from conveying trials conducted with high value of solid loading ratio (m^*).

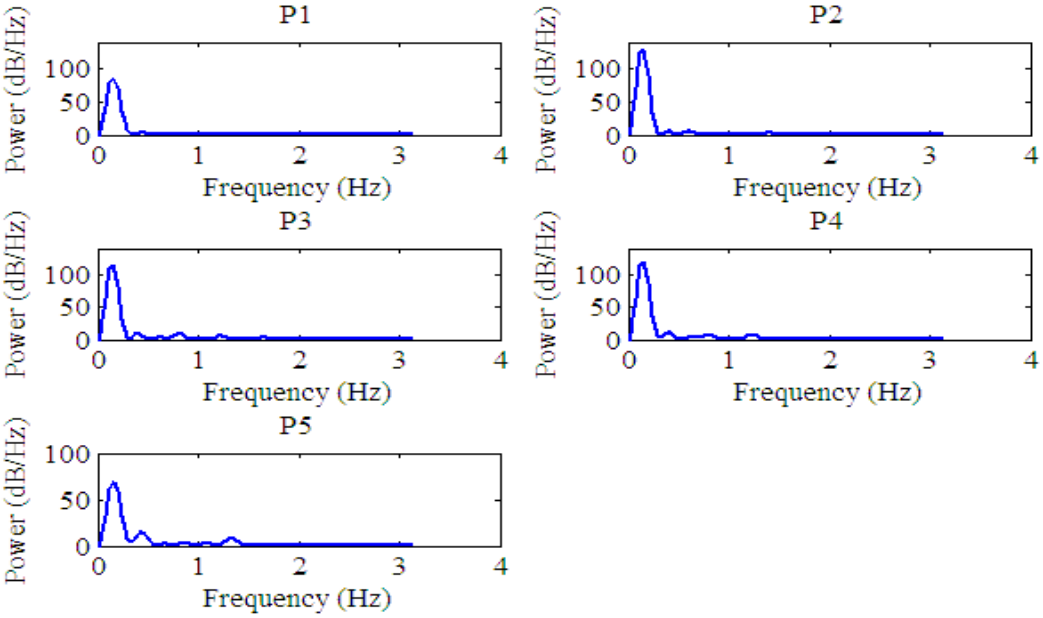

Figure 5.7.5: Variation of power spectral density along the length of pipeline:

Flyash; Exp-36 (m_f = 0.03kg/s; m_s = 4.38 kg/s; m^* = 136; V_f = 4-6 m/s)

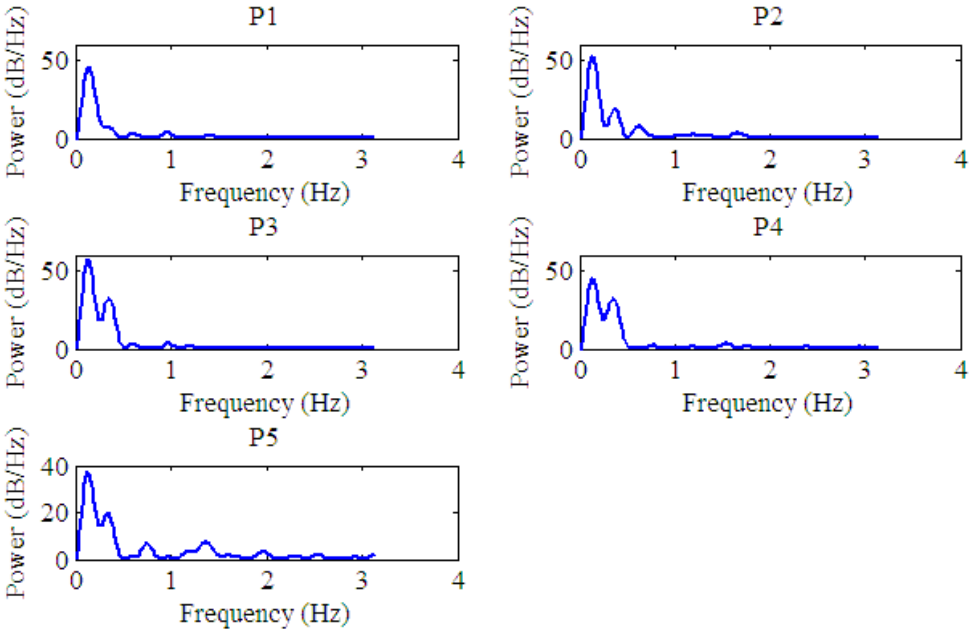

Figure 5.7.6: Variation of power spectral density along the length of pipeline:

Flyash; Exp-35 (m_f = 0.04 kg/s; m_s = 5.98 kg/s; m^* = 150; V_f = 4.5-7.5 m/s)

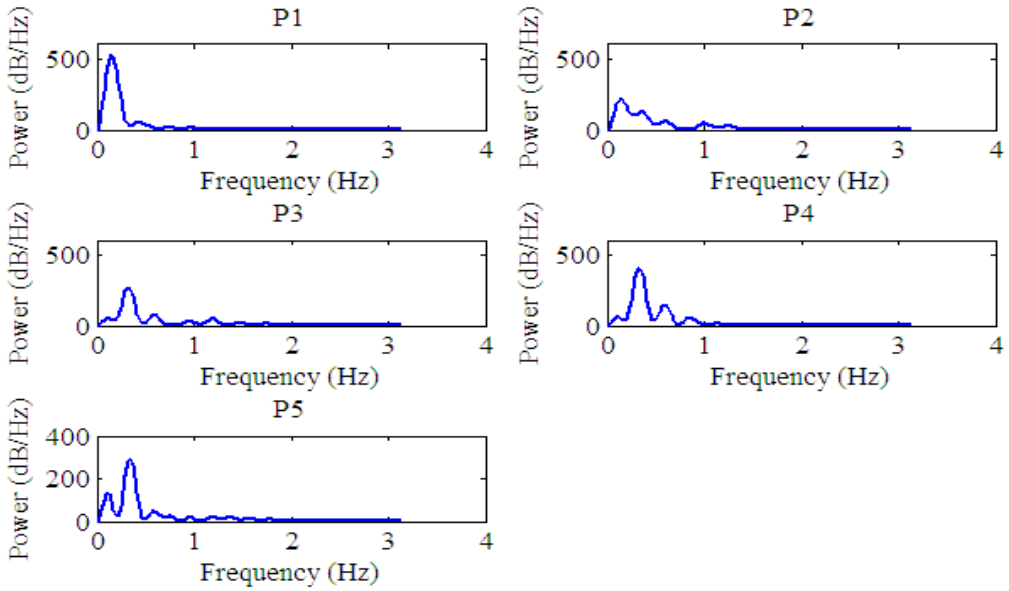

Figure 5.7.7: Variation of power spectral density along the length of pipeline: Flyash; Exp-37 (m_f = 0.032 kg/s; m_s = 5.84 kg/s; m^* = 182.5; V_f = 2 - 5 m/s)

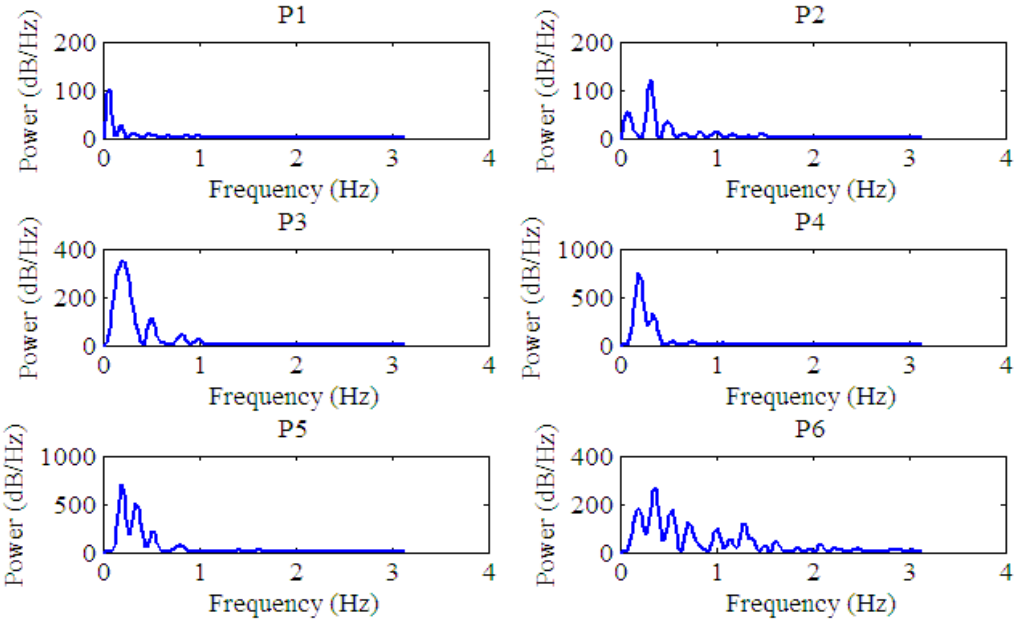

Figure 5.7.8: Variation of power spectral density along the length of pipeline: White powder; Exp-20 (m_f = 0.01kg/s; m_s = 2.53kg/s; m^* = 253; V_f = 1-2 m/s)

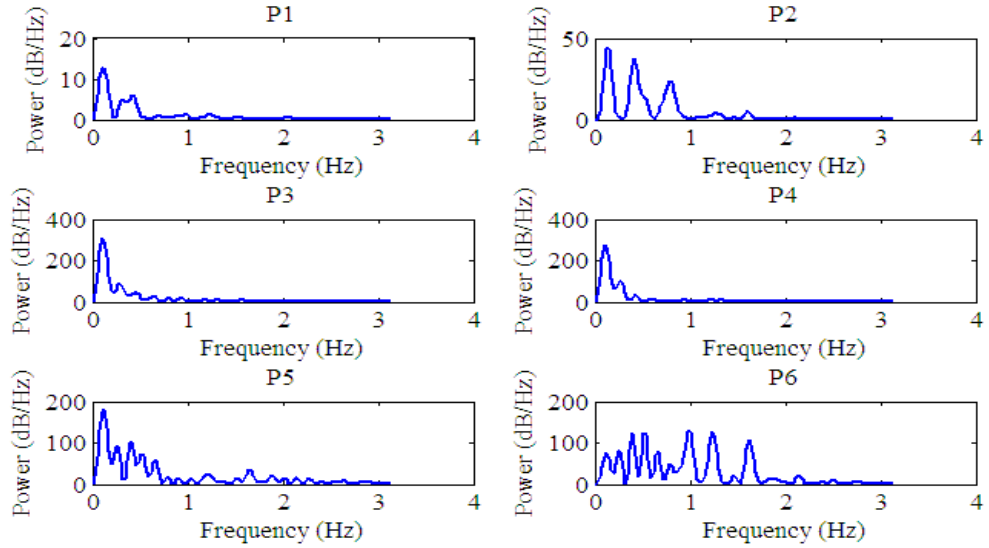

Figure 5.7.9: Variation of power spectral density along the length of pipeline: White powder; Exp-21 (m_f = 0.01kg/s; m_s = 2.64kg/s; m^* = 264; V_f = 1-2 m/s)

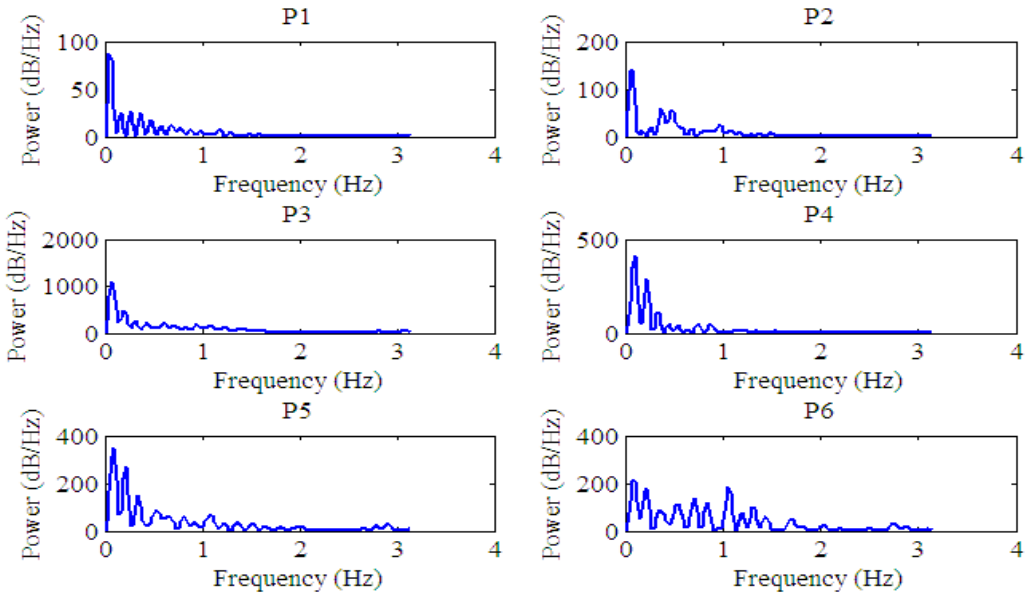

Figure 5.7.10: Variation of power spectral density along the length of pipeline: White powder; Exp-24 (m_f = 0.04kg/s; m_s = 1.93 kg/s; m^* = 47.28; V_f = 3-7 m/s)

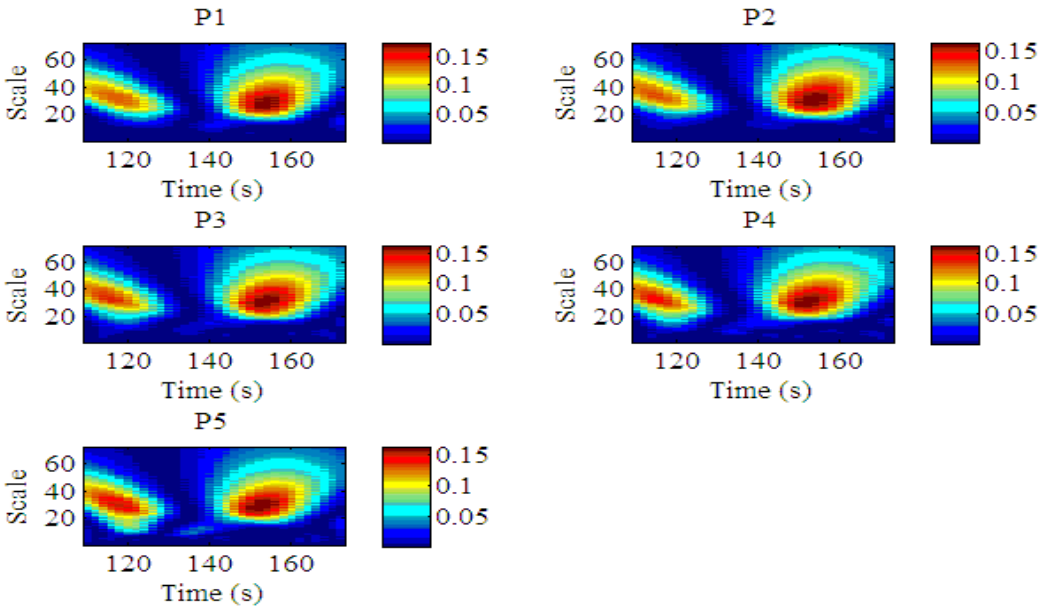

Figure 5.7.11: Variation of wavelet scalogram along the length of pipeline: Flyash; Exp-36 (m_f = 0.03kg/s; m_s = 4.38 kg/s; m^* = 136; V_f = 4-6 m/s)

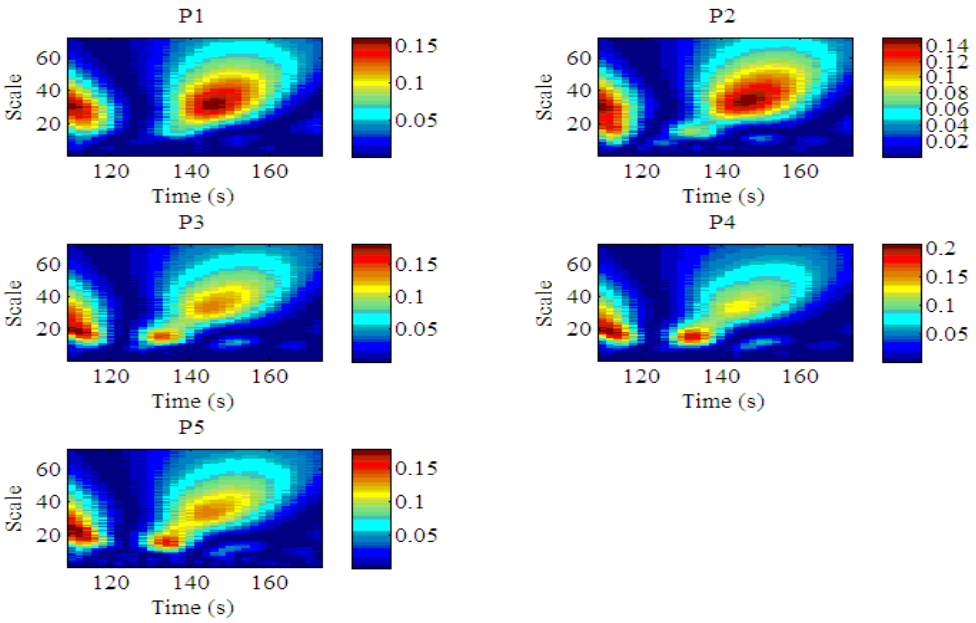

Figure 5.7.12: Variation of wavelet scalogram along the length of pipeline: Flyash; Exp-35 (m_f = 0.04 kg/s; m_s = 5.98 kg/s; m^* = 150; V_f = 4.5-7.5 m/s)

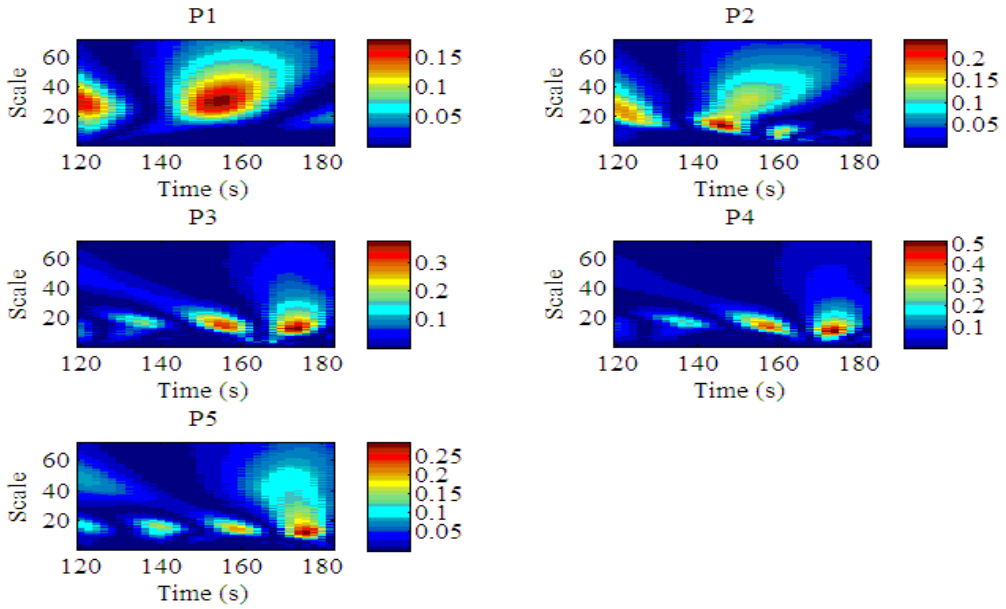

Figure 5.7.13: Variation of wavelet scalogram along the length of pipeline:

Flyash; Exp-37 (m_f = 0.032 kg/s; m_s = 5.84 kg/s; m^* = 182.5; V_f = 2 - 5 m/s)

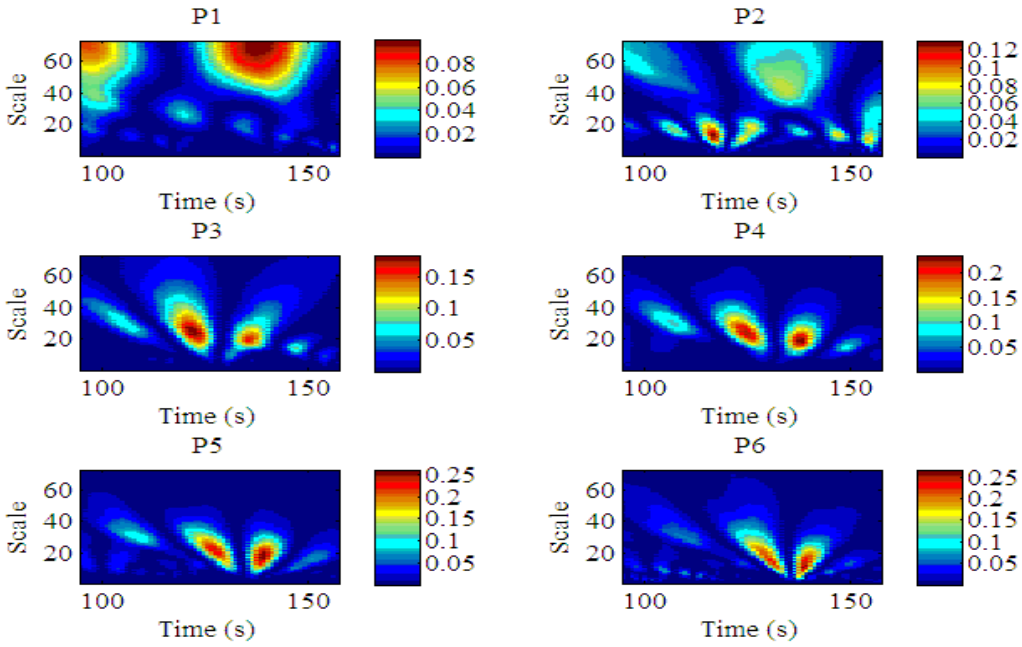

Figure 5.7.14: Variation of wavelet scalogram along the length of pipeline:

White powder; Exp-20 (m_f = 0.01kg/s; m_s = 2.53kg/s; m^* = 253; V_f = 1-2 m/s)

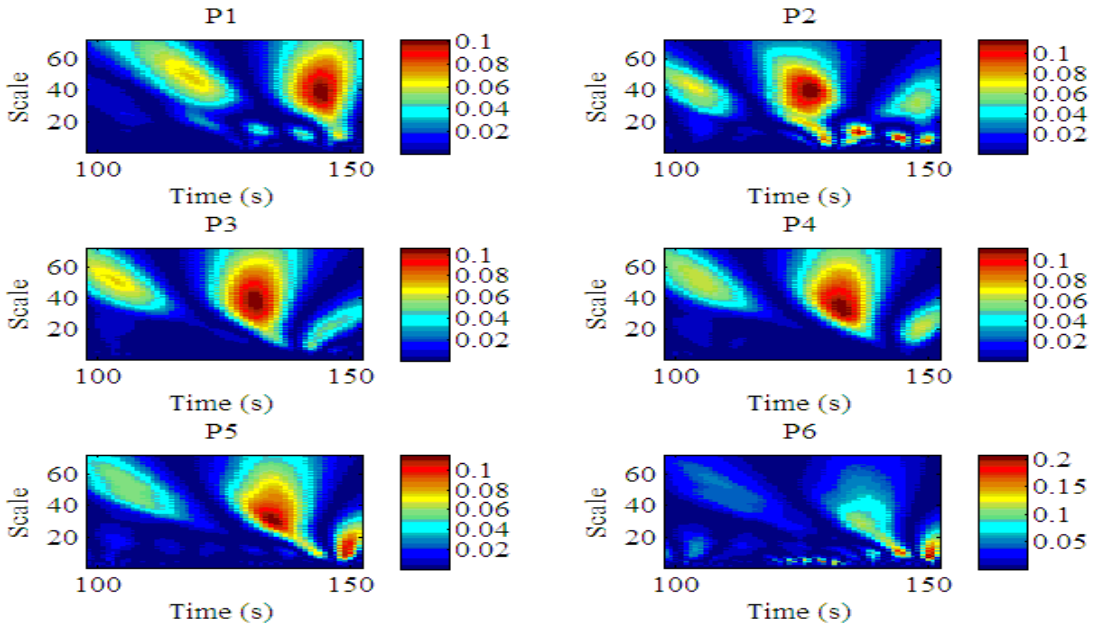

Figure 5.7.15: Variation of wavelet scalogram along the length of pipeline:

White powder; Exp-21 (m_f = 0.01kg/s; m_s = 2.64kg/s; m^* = 264; V_f = 1-2 m/s)

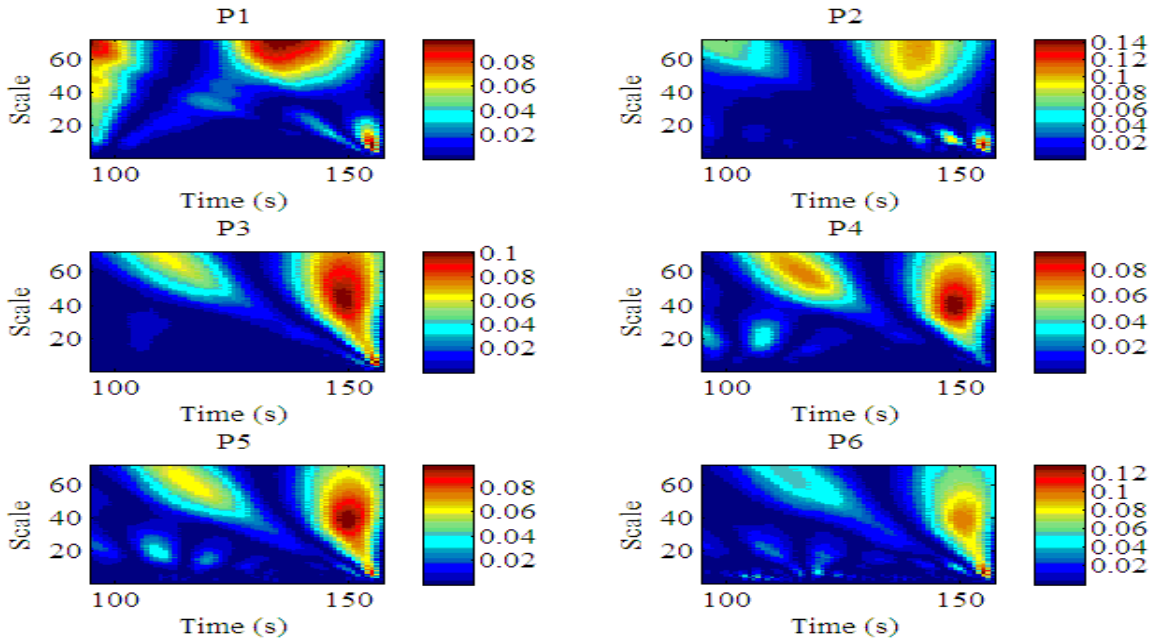

Figure 5.7.16: Variation of wavelet scalogram along the length of pipeline:

White powder; Exp-24 (m_f = 0.04kg/s; m_s = 1.93 kg/s; m^* = 47.28; V_f = 3-7 m/s)

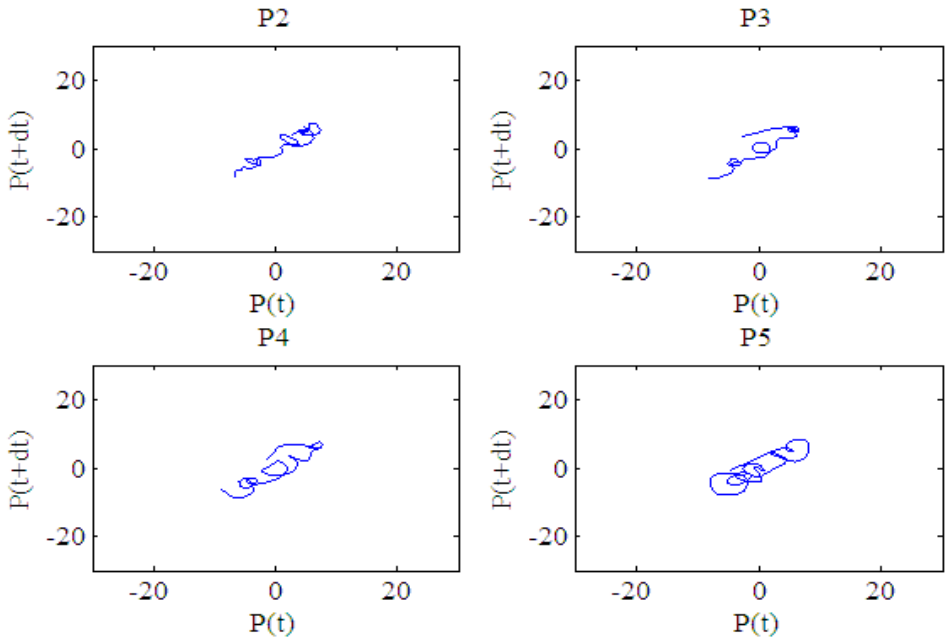

Figure 5.7.17: Attractor variation along the length of pipeline:

Flyash; Exp-36 (m_f = 0.03kg/s; m_s = 4.38 kg/s; m^* = 136; V_f = 4-6 m/s)

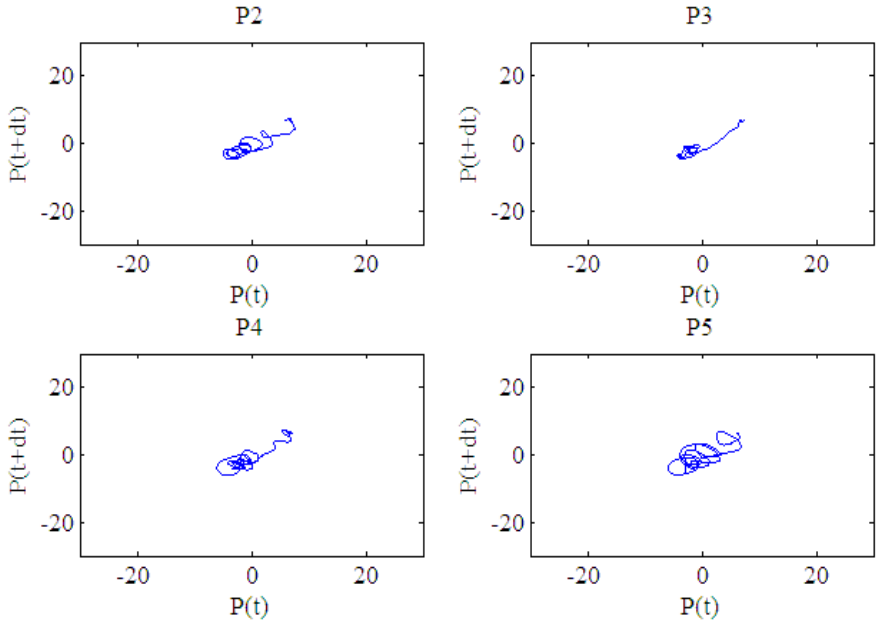

Figure 5.7.18: Attractor variation along the length of pipeline:

Flyash; Exp-35 (m_f = 0.04 kg/s; m_s = 5.98 kg/s; m^* = 150; V_f = 4.5-7.5 m/s)

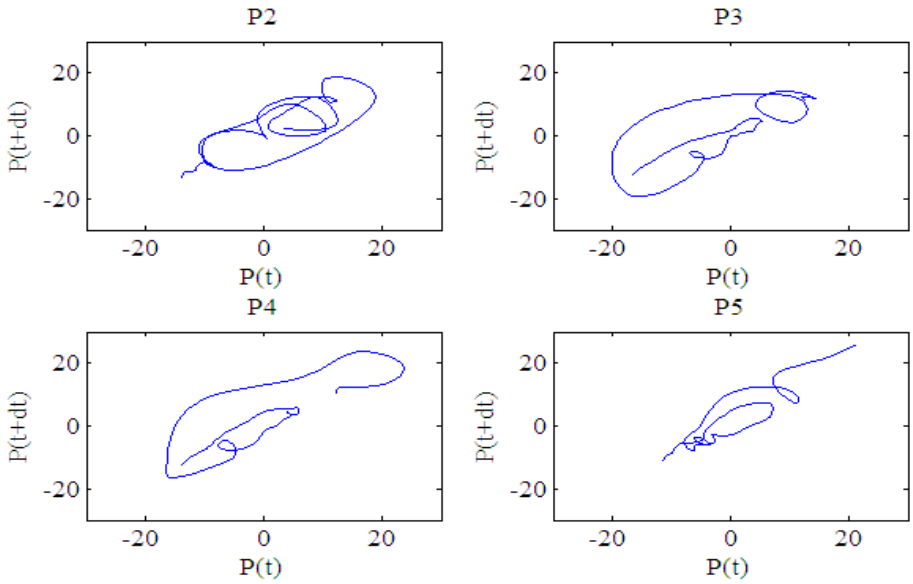

Figure 5.7.19: Attractor variation along the length of pipeline:

Flyash; Exp-37 (m_f = 0.032 kg/s; m_s = 5.84 kg/s; m^* = 182.5; V_f = 2 - 5 m/s)

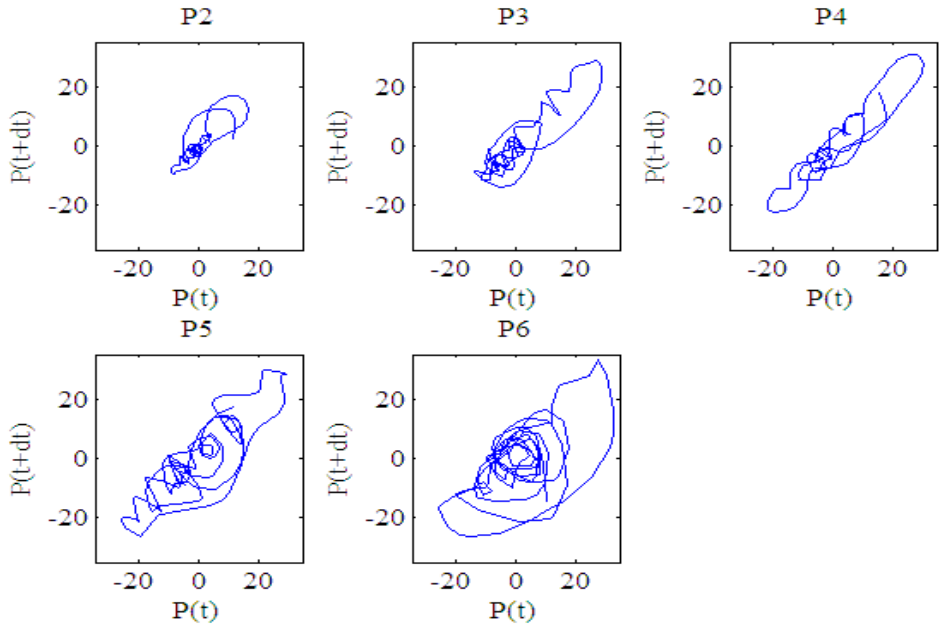

Figure 5.7.20: Attractor variation along the length of pipeline:

White powder; Exp-20 (m_f = 0.01kg/s; m_s = 2.53kg/s; m^* = 253; V_f = 1-2 m/s)

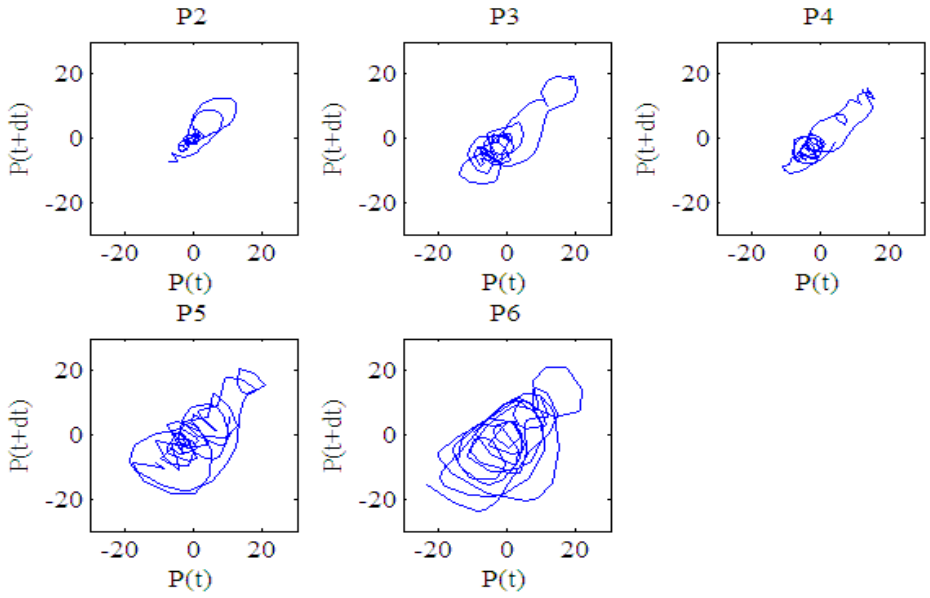

Figure 5.7.21: Attractor variation along the length of pipeline:

White powder; Exp-21 (m_f = 0.01kg/s; m_s = 2.64kg/s; m^* = 264; V_f = 1-2 m/s)

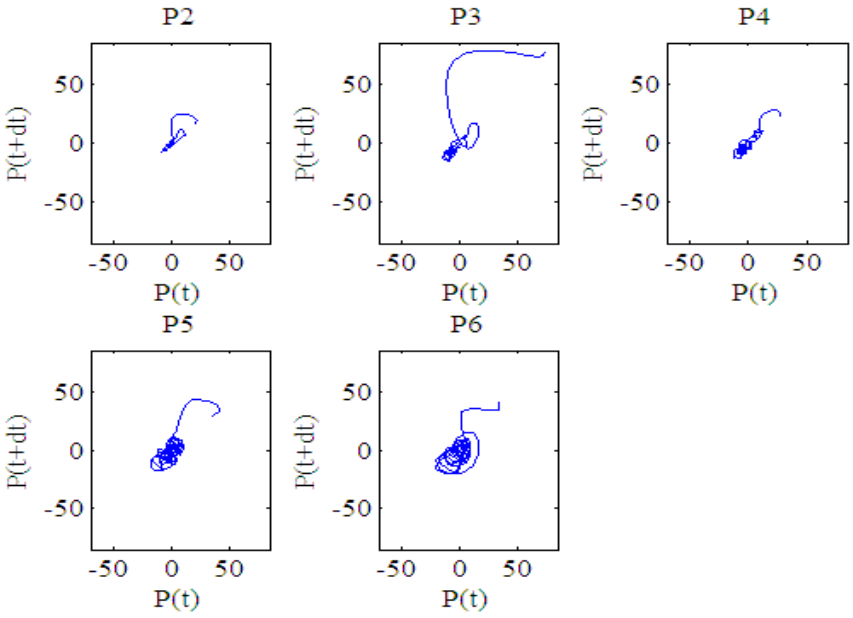

Figure 5.7.22: Attractor variation along the length of pipeline:

White powder; Exp-24 (m_f = 0.04kg/s; m_s = 1.93 kg/s; m^* = 47.28; V_f = 3-7 m/s)

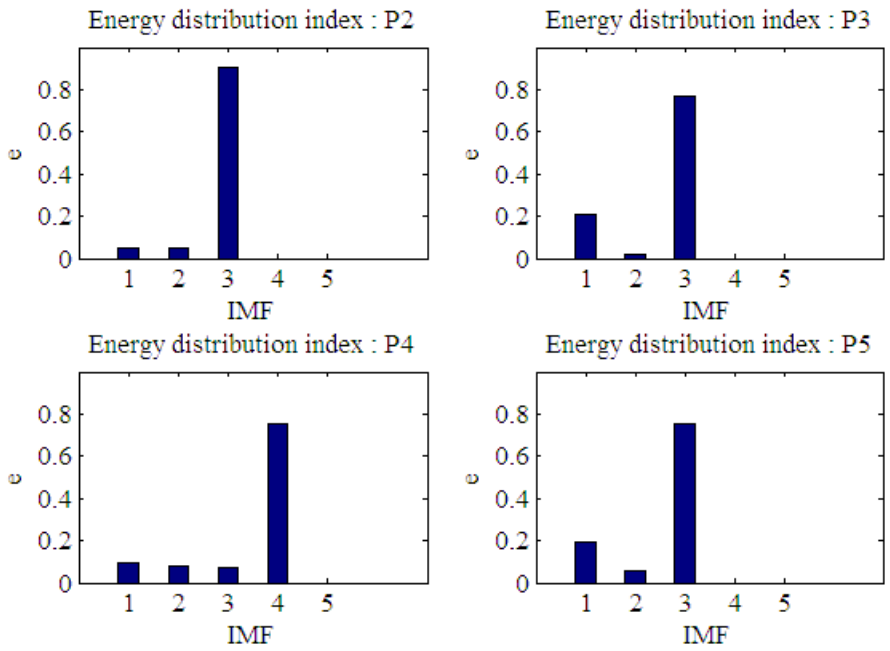

Figure 5.7.23: Variation of energy distribution among various IMF's along the length of pipeline: Flyash; Exp-36 (m_f = 0.03kg/s ; m_s = 4.38 kg/s ; m^* = 146; V_f = 4-6 m/s)

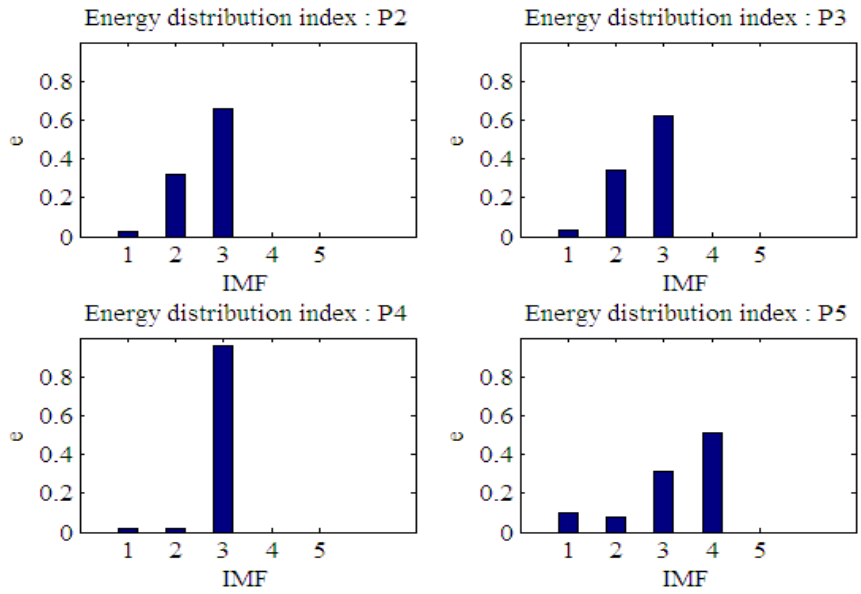

Figure 5.7.24: Variation of energy distribution among various IMF's along the length of pipeline: Flyash; Exp-35 (m_f = 0.04 kg/s; m_s = 5.98 kg/s; m^* = 150; V_f = 4.5-7.5 m/s)

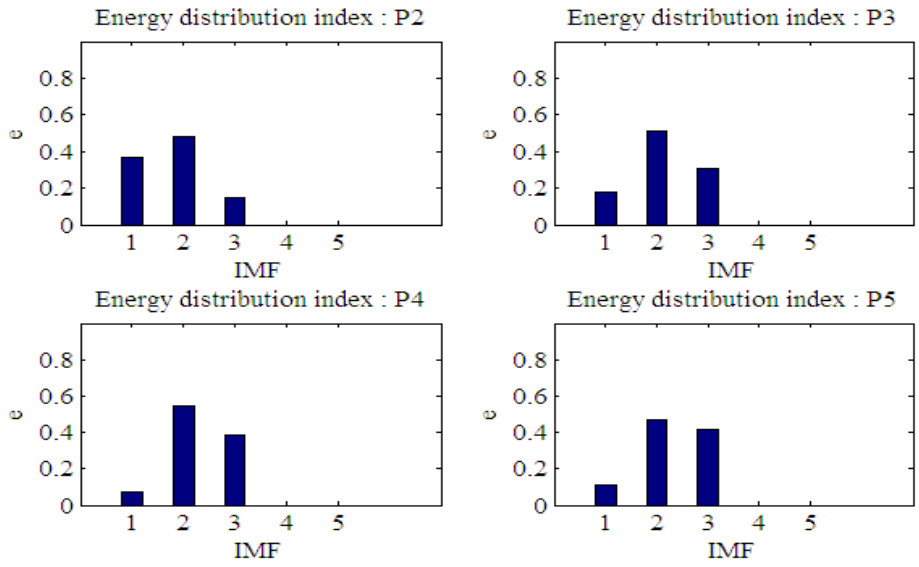

Figure 5.7.25: Variation of energy distribution among various IMF's along the length of pipeline: Flyash; Exp-37 (m_f = 0.032 kg/s; m_s = 5.84 kg/s; m^* = 182.5; V_f = 2 - 5 m/s)

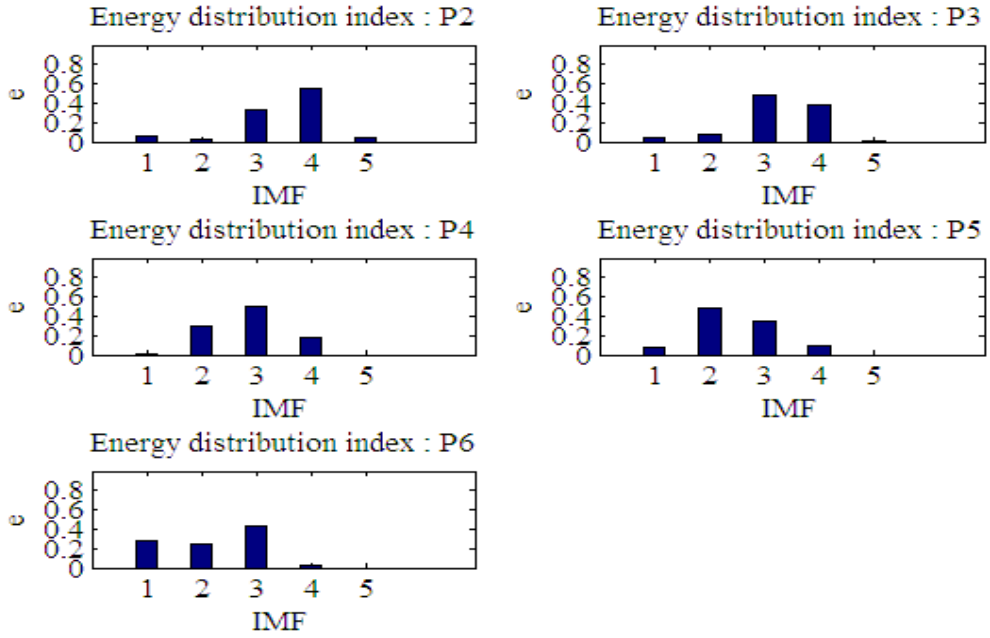

Figure 5.7.26: Variation of energy distribution among various IMF's along the length of pipeline: White powder; Exp-20 (m_f = 0.01kg/s; m_s = 2.53kg/s; m^* = 253; V_f = 1-2 m/s)

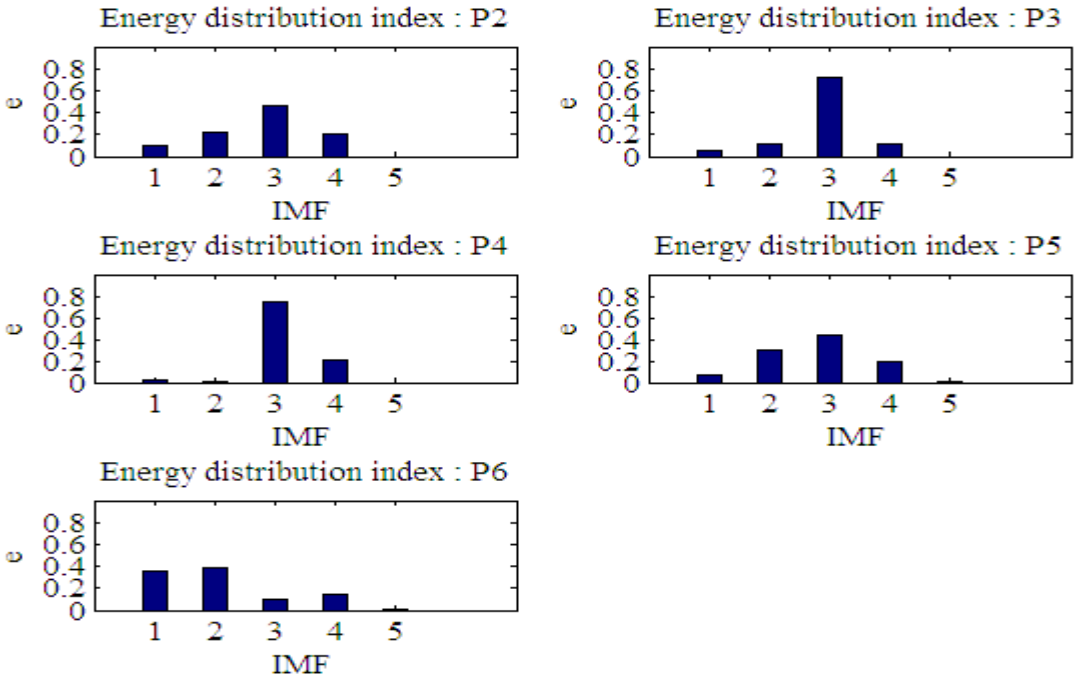

Figure 5.7.27: Variation of energy distribution among various IMF's along the length of pipeline: White powder; Exp-21 (m_f = 0.01kg/s; m_s = 2.64kg/s; m^* = 264; V_f = 1-2 m/s)

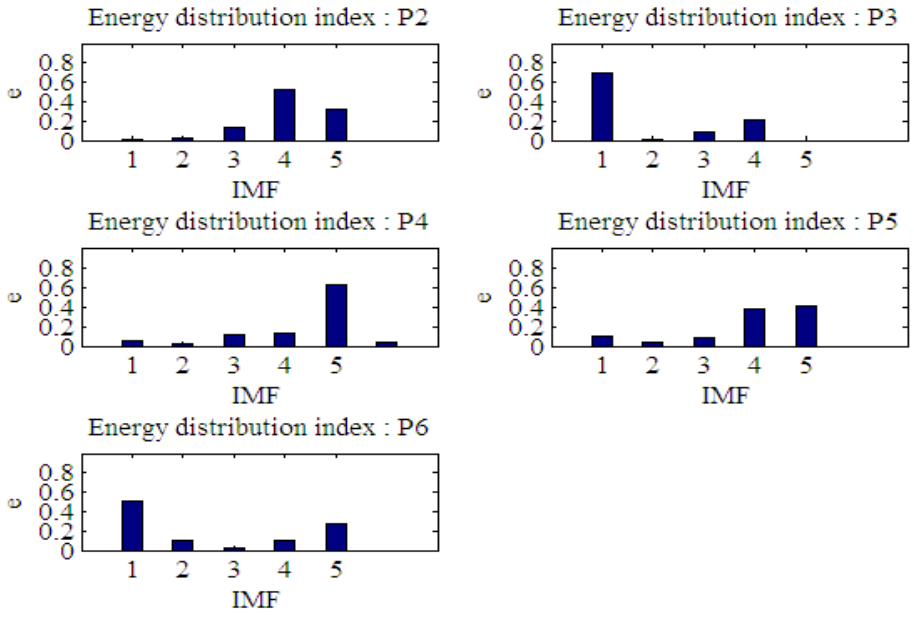

Figure 5.7.28: Variation of energy distribution among various IMF's along the length of pipeline: White powder; Exp-24 (m_f = 0.04kg/s; m_s = 1.93 kg/s; m^* = 47.28; V_f = 3-7 m/s)

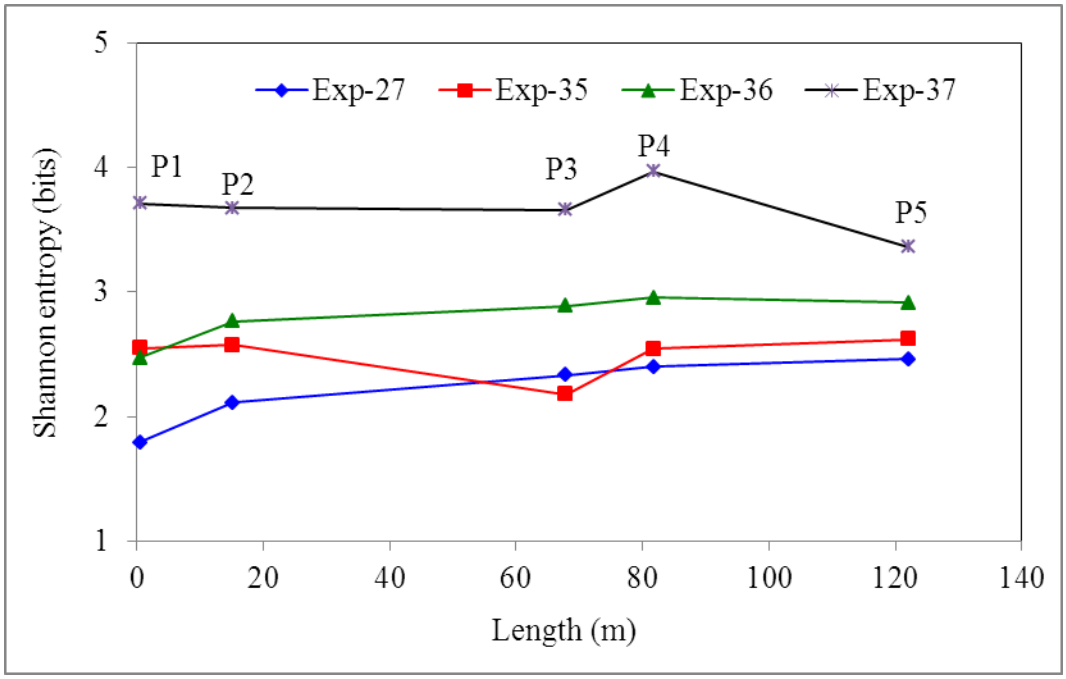

Figure 5.7.29: Variation of Shannon entropy along pipeline length; Flyash

Exp.27: m_f = 0.038 kg/s; m_s = 4.16 kg/s; m^* = 110; V_f= 3.7 m/s (at P2) - 6.1 m/s (at P5)

Exp.35: m_f = 0.04 kg/s; m_s = 5.98 kg/s; m^* = 150; V_f = 4.5m/s (at P2) - 7.5 m/s (at P5)

Exp.36: m_f = 0.03 kg/s; m_s = 4.38 kg/s; m^* = 146; V_f= 4 m/s (at P2) - 6 m/s (at P5)

Exp.37: m_f = 0.032 kg/s; m_s = 5.84 kg/s; m^* = 182.5; V_f= 2 m/s (at P2) - 5 m/s (at P5)

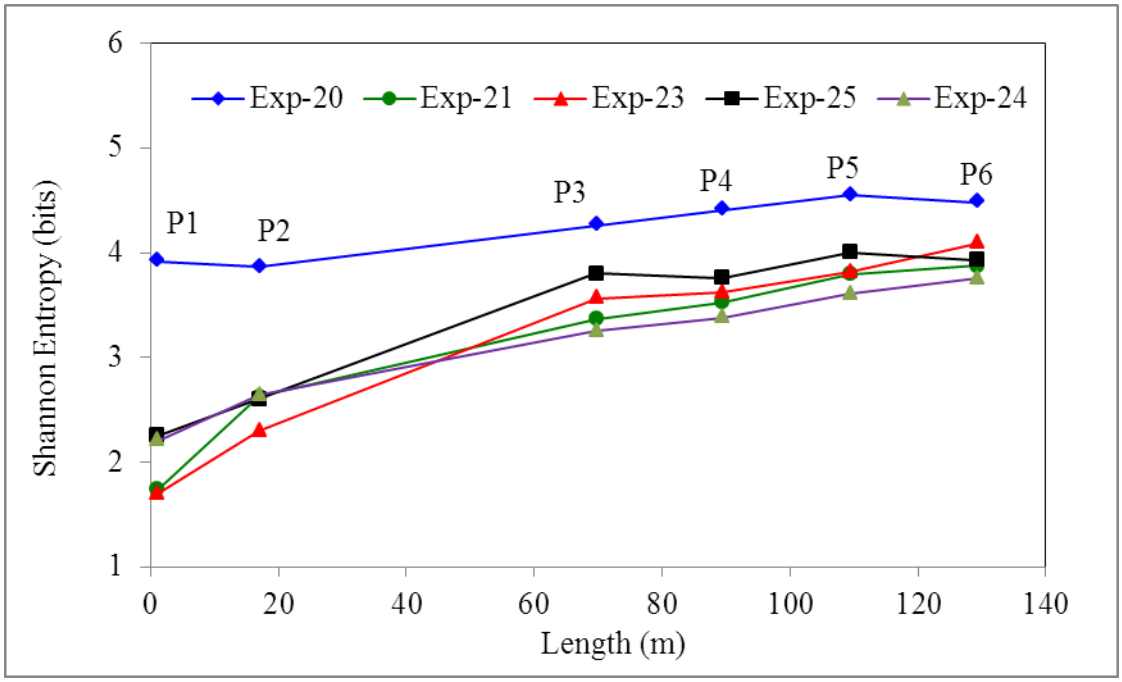

Figure 5.7.30: Variation of Shannon entropy along pipeline length; White powder

Exp.20: m_f = 0.01 kg/s; m_s = 2.53 kg/s; m^* = 253; V_f = 1 m/s (at P2) - 2 m/s (at P6)

Exp.21: m_f = 0.01 kg/s; m_s = 2.64 kg/s; m^* = 264; V_f = 1 m/s (at P2) - 2 m/s (at P6)

Exp.23: m_f = 0.04 kg/s; m_s = 2.05 kg/s; m^* = 51.25; V_f = 3 m/s (at P2) - 7 m/s (at P6)

Exp.24: m_f = 0.04 kg/s; m_s = 1.93 kg/s; m^* = 48.25; V_f = 3 m/s (at P2) - 7 m/s (at P6)

Exp.25: m_f = 0.04 kg/s; m_s = 2.15 kg/s; m^* = 53.7; V_f = 3 m/s (at P2) - 7 m/s (at P6)

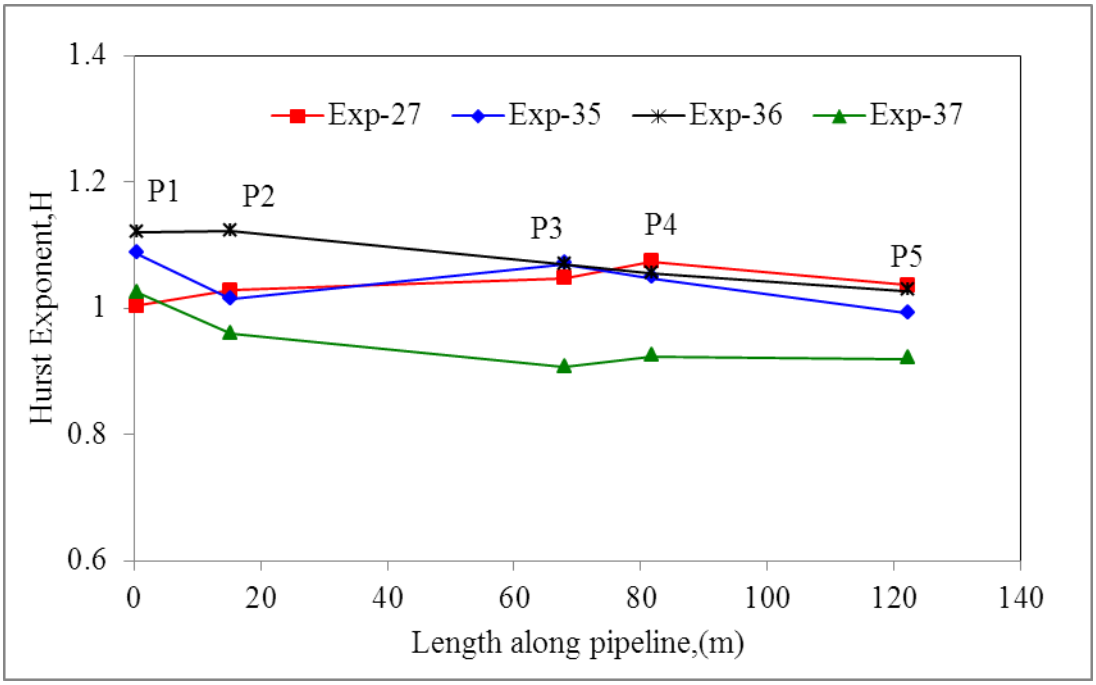

Figure 5.7.31: Variation of Hurst exponent along pipeline length; Flyash

Exp.27: m_f = 0.038 kg/s; m_s = 4.16 kg/s; m^* = 110; V_f = 3.7 m/s (at P2) - 6.1 m/s (at P5)

Exp.35: m_f = 0.04 kg/s; m_s = 5.98 kg/s; m^* = 150; V_f = 4.5m/s (at P2) -7.5 m/s (at P5)

Exp.36: m_f = 0.03 kg/s; m_s = 4.38 kg/s; m^* = 146; V_f = 4 m/s (at P2) - 6 m/s (at P5)

Exp.37: m_f = 0.032 kg/s; m_s = 5.84 kg/s; m^* = 182.5; V_f = 2 m/s (at P2) - 5 m/s (at P5)

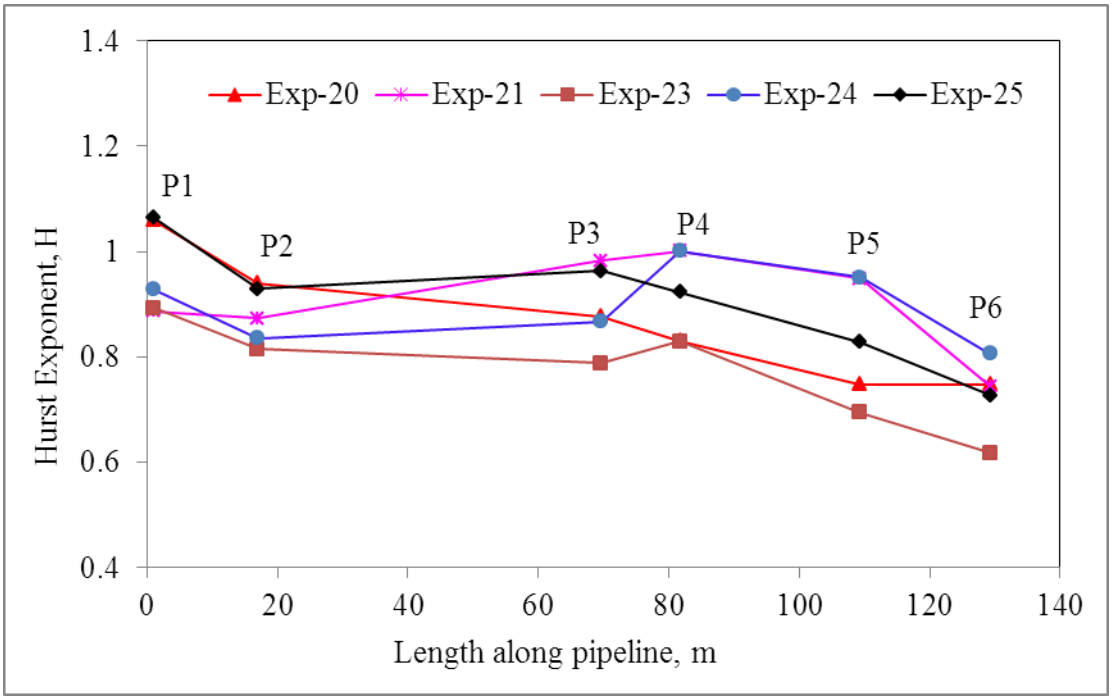

Figure 5.7.32: Variation of Hurst exponent along pipeline length; White powder

Exp.20: m_f = 0.01 kg/s; m_s = 2.53 kg/s; m^* = 253; V_f = 1 m/s (at P2) - 2 m/s (at P6)

Exp.21: m_f = 0.01 kg/s; m_s = 2.64 kg/s; m^* = 264; V_f = 1 m/s (at P2) - 2 m/s (at P6)

Exp.23: m_f = 0.04 kg/s; m_s = 2.05 kg/s; m^* = 51.25; V_f= 3 m/s (at P2) - 7 m/s (at P6)

Exp.24: m_f = 0.04 kg/s; m_s = 1.93 kg/s; m^* = 48.25; V_f= 3 m/s (at P2) - 7 m/s (at P6)

Exp.25: m_f = 0.04 kg/s; m_s = 2.15 kg/s; m^* = 53.7; V_f= 3 m/s (at P2) - 7 m/s (at P6)

As seen in the figures from 5.7.5 to 5.7.10, power spectrum obtained is different from what was observed in the previous section (section 5.4) for dilute and dense phase conveying (i.e. conveying well above the minimum transport boundary, with adequate air velocity to sustain stable conveying), where it was found that power spectrum changes with change in transducer location along pipeline length. However in the present case (while operating near minimum transport boundary) there is no significant change observed in the PSD spectrum from P1 towards P5, dominant frequency peak could be

seen in all the spectrums obtained at different locations. Similarly for the wavelet scalogram as seen the figures (from Figure 5.7.11 to 5.7.16), there is no significant change observed in the color intensity and in the pattern of scalogram while moving from inlet towards outlet of the pipeline. Size of the attractor does also remain nearly the same from P2 to P5 as seen in figures from Figure 5.7.17 to 5.7.22. Similarly there is no change observed in the energy distribution index (e) among different IMF from inlet towards exit of the pipeline as seen in figures from Figure 5.7.23 to 5.7.28. Variation in Shannon entropy and Hurst exponent is almost flat as seen in figures from Figure 5.7.29 to 5.7.32. Therefore, it can be concluded from the above results that while operating near transport boundary (i.e. capacity limitation boundary); minimal change is observed in the calculated parameters from signal analysis techniques while moving from inlet towards outlet of the pipeline. Probable explanation for the same could be that near minimum transport boundary, flow mechanisms involve highly dense phase dunes of material moving inside the pipeline and effect of gas expansion along the pipeline is negligible on the flow mechanism (due to limited mass flow rate of air) and it remains nearly the same while operating near minimum transport boundary. Hence, one or all of these signal parameters could be used for on-line prediction of flow mechanism near minimum transport boundary, i.e. if no change is observed in the different parameters such as PSD spectrum, wavelet scalogram etc obtained at different locations along pipeline length, then it could be said that system is operating near minimum transport boundary and further reduction in the superficial velocity might lead to unstable flow and subsequently blockage inside the pipeline. Such an analysis would help the designer to effectively design a good dense phase conveying system equipped with online prediction of minimum transport boundary (blockage boundary) – benefited by high solid loading ratio (m^*), yet preventing the blockage to occur in the pipeline.

5.8 Dune velocity estimation

While a number of parameters influence the performance of a pneumatic conveying system such as air flow rate, solids flow rate, pressure drop, equivalent length of the pipeline, solids concentration and others, it is the gas velocity in the pipeline that is the key parameter for dense phase conveying. Velocity is probably the most important parameter in pneumatic conveying and insufficient velocity could lead to a poorly performing system or a system that will not convey at all. In pneumatic conveying systems, velocity of both the phases i.e. conveying air and solid particles play important roles. Superficial air velocity term is used to represent conveying air velocity while particle velocity term is used to represent the motion of particulate medium in pneumatic conveying. Superficial air velocity can be calculated using the ideal gas law at the average pressure drop values determined for the pipe section considered. However, calculation of individual particle motion and velocity is much more complex. In fluidized dense phase mode of conveying, material moves in the form of fluid like dunes inside the pipeline, hence in the present work, the term dune velocity has been used to characterize motion of particulate material in case of fluidized dense phase conveying. The behavior of solids in fluidized dense phase is much more complex as compared to dilute phase. Formation, size and subsequent separation of dunes are affected significantly by the gas velocity. Moreover, solid velocity is believed to vary locally from one location to another as particles are accelerated and decelerated while moving from one dune to another. It is important to know dune velocity for accurate determination of pressure drop inside pipeline. Existing empirical models such as provided by Mallick et al. (2013) for pressure drop estimation in fluidized dense phase conveying pipelines are based on superficial air velocity instead of dune velocity, which could be one of the reasons causing inaccuracy of

these models under scale up conditions. Replacing superficial air velocity term with dune velocity could improve the solid friction factor modeling, which is used to estimate total pipeline pressure drop. Therefore dune velocity is an important parameter to be considered for the accurate design and modeling of pneumatic conveying systems. William et al. (2007) attempted to find the average particle velocity from time delay analysis of pressure fluctuations (obtained from locations 2 m apart along the pipeline) for the cement meal (median particle diameter: 11 μm and m^* in the range of 51-70). Later on, Liu et al. (2009) also estimated the particle average velocity for different products (such as flyash, cement and gypsum etc.) based on time interval of signal emergence of every pressure transmitter in different places along pipeline length. However, signals at different locations were not investigated for degree of similarity. Therefore, in the following section, an attempt has been made to estimate the dune velocity using pressure signal fluctuations and cross-correlation technique using independent test data in view of verifying the studies carried out by other researchers such as William et al. (2007) and Liu et al. (2009), who have also attempted to find particle velocity using time delay analysis of pressure signal fluctuations.

In the present work, cross-correlation function is used to match the two signals obtained from adjacent pressure tapping points on the pipeline separated by certain distance. Bo Mi (1994) also used the wall pressure signals and cross-correlation function to find the slug velocity in low-velocity pneumatic conveying. For applying the cross correlation method, the outputs of two transducers (P5 and P6) are compared. Each of the two pressure transducers chosen for applying the cross correlation method are placed within a certain distance (19.9 m) between them along the conveying pipeline. The passing of solid particles causes a peak in the output of both transducers. Since the second transducer is placed at a certain distance away from the first transducer along the pipeline, when a solid particle passes through the pipeline, first it reaches the first transducer and then, with a

time delay, it reaches the second transducer. Therefore, similar peaks are expected to be generated in the output of these sensors with a time delay between the peaks. This time delay is equal to the time required for a solid particle to reach from the first to the second transducer. Accuracy of this technique is dependent on the selection of correlated signals, sampling rate of data acquisition system and the distance between two neighboring test points. In Figure 5.8.1, the output signals of two sensors obtained from the test rig have been shown. As can be seen, there are similar spikes in outputs from these sensors. The signal from the second sensor is similar to the signal from the first sensor (as seen in the enlarged view of two signals; Figure 5.8.2), which is delayed in time. This time delay is equal to the distance between the sensors divided by the velocity of the solid particles. The cross correlation of the signals obtained from two sensors was calculated (as described in the Chapter 4, Equation 4.24) and plotted as a function of τ, the time when maximum cross correlation occurs (τ_{max}), was taken as equal to the time delay between the two signals. After calculating τ_{max} and by knowing the distance between two sensors, the speed of the dune can be calculated as described in the previous chapter (Chapter4). τ_{max} is the time when the maximum cross-correlation occurs. The maximum of cross-correlation function indicates the point where two signals are best aligned. In other words it can be said that the same dune has travelled from one location to another in certain duration of time. Thus the peak in the cross-correlation vector corresponds to the time-delay between two signals. The shorter time lag corresponds to a faster flow, while the longer one to the slower flow.

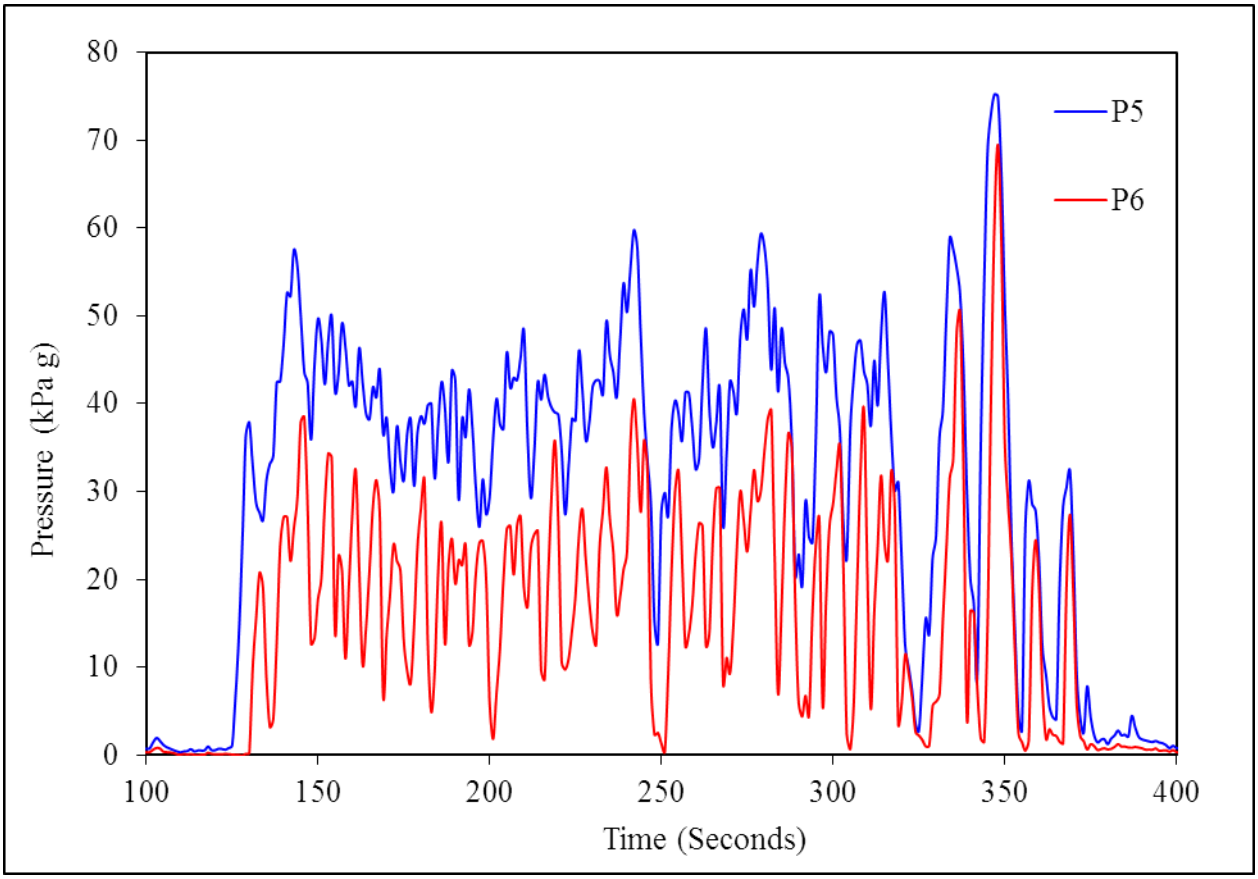

Figure 5.8.1: Output signals from two pressure transducers when distance between them in 19.9 m (Exp-14; White powder; m_f = 0.15 m/s; m_s = 1.38 m/s; m^* = 9.49 m/s; V_f = 23.5 m/s at P5 to 27.2 m/s at P6)

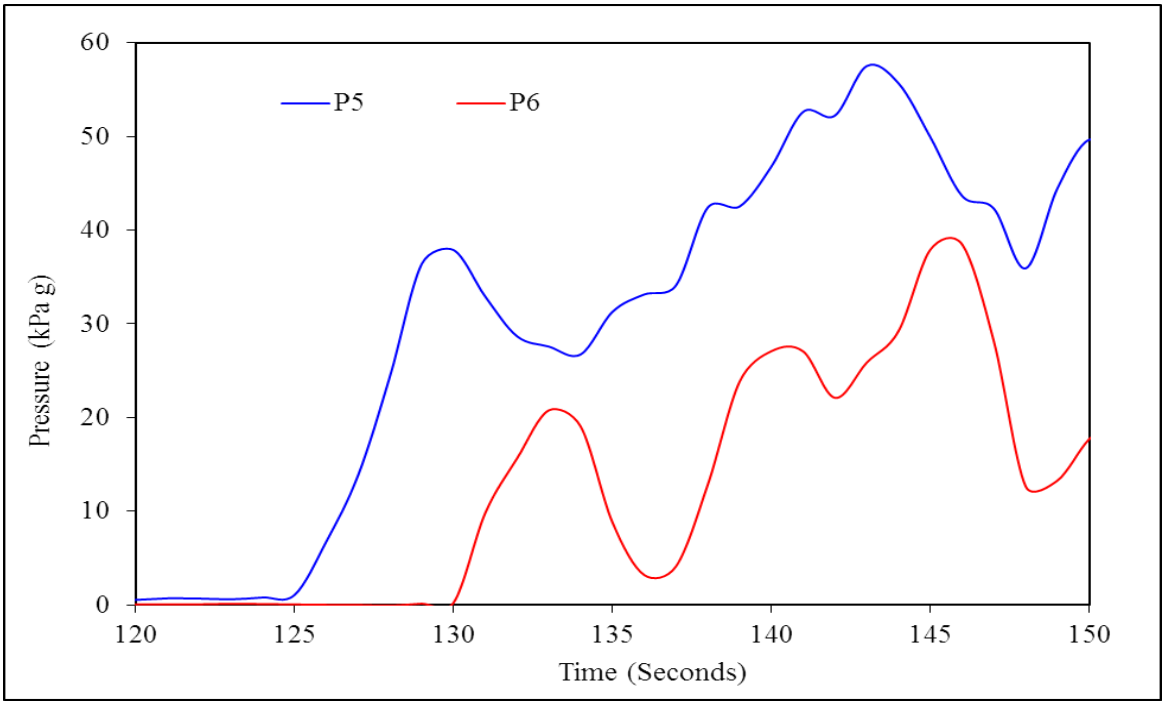

Figure 5.8.2: Detailed examination of pressure signals (at the beginning of cycle) at transducer locations P5 and P6 (19.9 m apart) (Exp-14; White powder; m_f = 0.15 m/s; m_s = 1.38 m/s; m^* = 9.49 m/s; V_f = 23.5 m/s at P5 to 27.2 m/s at P6)

Closer investigation into the structure of pressure fluctuations (as shown in Figure 5.8.2) from two adjacent transducer locations P5 and P6, which are 19.9 m apart, shows that there was time delay of the pressure pulse minima and maxima between each subsequent pressure transducer locations. Figure 5.8.3 and 5.8.4 show the cross-correlation curve obtained from different pressure fluctuation time series, which show maximum value of cross-correlation coefficient as 0.5 corresponding to time delay of 4 seconds.

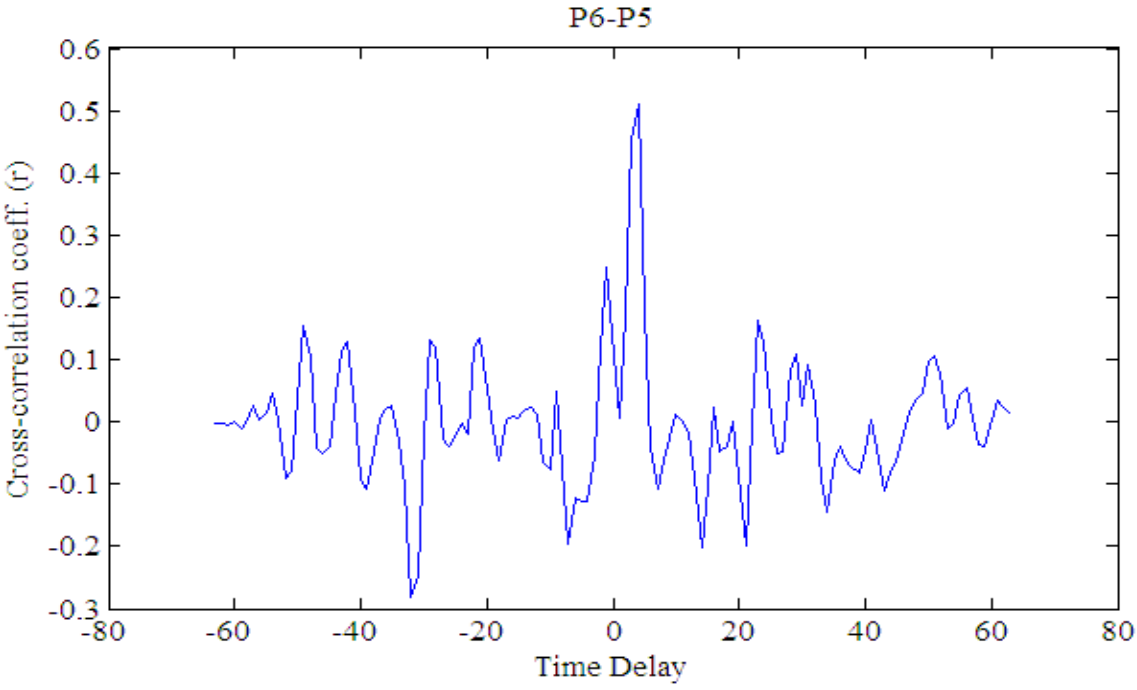

Figure 5.8.3: Typical cross-correlation between two signals when distance between transducers is 19.9 m (Exp-14; white powder)

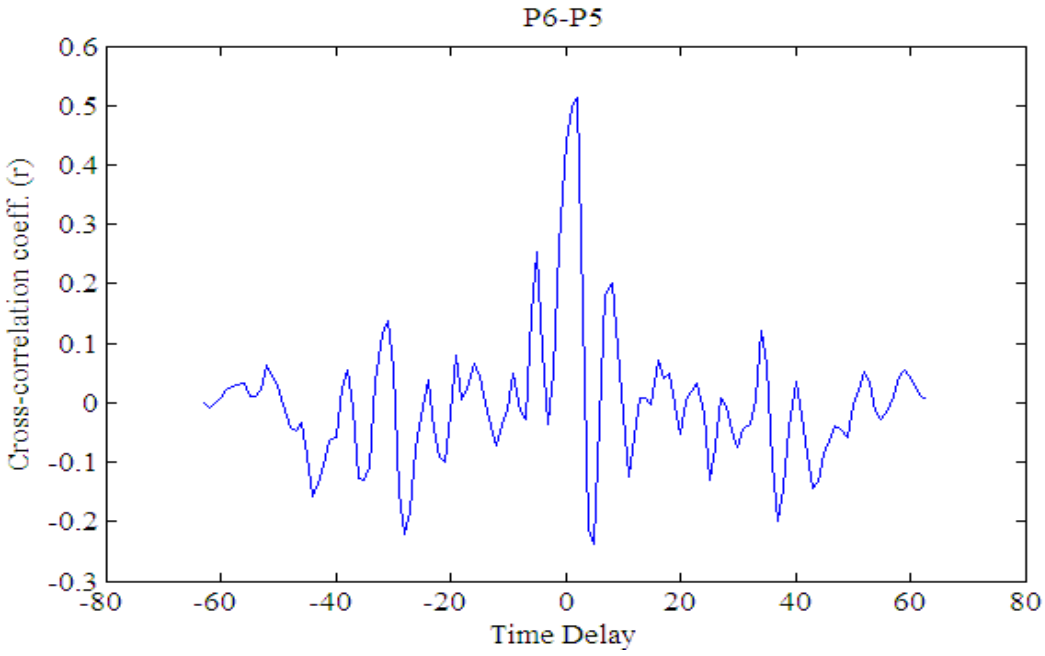

Figure 5.8.4: Typical cross-correlation between two signals when distance between transducers is 19.9 m (Exp-71; white powder)

However, two important comments should be made. Firstly, the time lag cannot be established with sufficient accuracy, due to insufficient numerical value of the cross-correlation coefficient, which indicates that while moving from one point to another inside pipeline, signal features have been changed significantly (due to the possible change in dune characteristics). It was found that values of cross-correlation coefficient calculated for certain number of pressure transient plots were quite less (less than 0.5), which indicates that the two signals from the adjacent locations are not properly matched. At the same time, for certain number of pressure transient plots, cross-correlation function provided zero value of time delay (which indicates that these set of pressure fluctuation data corresponds to high dune velocity) and determination of accurate time delay using pressure fluctuations would actually require test rig with longer straight pipe section. Due to above mentioned reasons, it can be concluded that accurate estimation of the dune velocity by cross-correlation between pressure signals is not possible with the present practice of experimental procedure and requires further analysis.

CHAPTER 6: CONCLUSION AND FUTURE SCOPE OF WORK

6.1 Conclusions

Based on analysis of pressure signal fluctuations using different methods of signal processing (i.e. Shannon entropy, Hurst exponent, phase space diagram, power spectral density, Hilbert-Huang transform and wavelet analysis) it can be concluded that pressure signals can be used to reveal information on the change in flow dynamics during pneumatic transport of fine powders. While moving along the length of the pipeline, decrease in the value of Hurst exponent, an increase in the area covered by the phase-space diagram and an increase in Shannon entropy values along the direction of flow indicated that there was an increase in degree of complexity of flow mechanism (or turbulence) along the length of pipeline.

Power spectral density (PSD) spectrum was found to change from spectrum with single dominant peak at the pipe inlet to spectrum having multiple peaks at the exit of pipeline. Energy distribution among various IMF components also changed from maximum energy corresponding to low frequency IMF's near pipeline inlet to high frequency IMF's at the pipeline exit. Similarly, energy distribution among different wavelet coefficients changed from high scale (low frequency) near pipeline entry to low scale (high frequency) at the exit of pipeline.

Results from these techniques of pressure fluctuation analysis in frequency domain show that in the region near to the pipeline entry, low frequency components are present (probably due to the presence of slow moving dunes) as compared to high frequency components near to the exit of the pipeline. This could be due to increased level of turbulence (as observed during experimentation also). While in the vicinity of closely coupled bends, all the techniques show that the change in the computed variable is

generally goes in the opposite directions compared to that found in long straight pipe runs. This provides indication towards probable momentum loss of particles in the bend.

Results from all the different techniques (based on distinctive numerical basis) were found to be consistent in terms of flow mode identification and transition inside the pipeline. Therefore, it could be concluded that pressure signals could be considered as potential input for the flow mechanism investigations during pneumatic conveying, using any of the techniques mentioned in the present analysis.

Apart from flow mode identification, signal fluctuations could also be used for online prediction of minimum transport/blockage boundary and to avoid potential blockage of pipeline. Online prediction of flow mechanism has not been attempted so far because the flow visualization using sight glass is extremely difficult as most of the times fine powders tend to coat the glass after certain duration of conveying and the method is subjective to the observer's judgment. Compared to this, visualization of pressure fluctuations (and related signal parameters) obtained from strategic locations along the pipeline during conveying would be more objective method of flow monitoring.

In an attempt to investigate into applicability of pressure signal fluctuations for dune velocity estimation, it was found that degree of cross-correlation between two signals from adjacent transducers was not sufficient (as the signal characteristics were modified while moving from one location to the other).

6.2 Future scope of work

Certain areas of investigation require further efforts and are listed in the following:

(i) While applying the signal processing methods on pressure signal fluctuations, the results using different techniques may differ in terms of accuracy and content of information delivered. Therefore careful choice of the signal processing technique, appropriate for the time-series data in hand is important to extract useful information from the signal, which is not addressed in the present scope of work. Therefore further studies should be carried out to compare different signal processing techniques on the basis of degree of accuracy achieved in results and amount of computational efforts required.

(ii) The accurate measurement of particle velocity would actually require further studies on deciding on the optimum distance between two pressure transducers so that signal characteristics do not alter significantly while moving from one location to the other and at the same time one is able to capture the delay between signals in case of high dune velocity. Alternatively, other reliable techniques to measure dune velocity for fine aerated powders need to be developed.

(iii) Apart from online prediction of blockage boundary in the pipeline, further improvements in the operation of the pneumatic conveying system could be made by connecting material outlet valve (at the blow tank outlet) to the fluctuating pressure signal data from the data acquisition system and accordingly it should be able to decrease the product flow rate to a requisite quantity till steady state is regained (to avoid complete blockage of pipeline).

REFERENCES

Al-Masry, W.A. and Ali, E.M., 2008. Hydrodynamic Characteristic of Bubble Columns using Hurst and Chaos Analysis of Acoustic Sound Signals.*Journal of Saudi Chemical Society*, *12*, pp.443-456.

Baar, R. and Riess, W., 1997. Two phase flow velocimetry measurements by conductive-correlative method. *Flow Measurement and Instrumentation*, *8*(1), pp.1-6.

Bai, D., Grace, J.R. and Zhu, J.X., 1999. Characterization of gas fluidized beds of group C, A and B particles based on pressure fluctuations. *The Canadian Journal of Chemical Engineering*, 77(2), pp.319-324.

Barratt, I.R., Yan, Y., Byrne, B. and Bradley, M.S.A., 2000. Mass flow measurement of pneumatically conveyed solids using radiometric sensors. *Flow Measurement and Instrumentation*, *11*(3), pp.223-235.

Bartlett, M.S., 1948. Smoothing periodograms from time series with continuous spectra. *Nature*, *161*(4096), pp.686-687.

Bartlett, M.S., 1950. Periodogram analysis and continuous spectra. *Biometrika*, *37*(1/2), pp.1-16.

Beck, M.S. and Pląskowski, A., 1987. *Cross correlation flowmeters, their design and application*. CRC Press.

Benavides, A. and van Wachem, B., 2008. Numerical simulation and validation of dilute turbulent gas–particle flow with inelastic collisions and turbulence modulation. *Powder Technology*, *182*(2), pp.294-306.

Bendat, J.S. and Piersol, A.G., 1980. Engineering applications of correlation and spectral analysis. *New York, Wiley-Interscience, 1980. 315 p., 1*.

Boashash, B., 2015. *Time-frequency signal analysis and processing: a comprehensive reference*. Academic Press.

Boltzmann, L., 2012. *Lectures on gas theory*. Courier Corporation.1995 - 490 pagina's

Bruni, G., Lettieri, P., Newton, D. and Barletta, D., 2007. An investigation of the effect of the interparticle forces on the fluidization behaviour of fine powders linked with rheological studies. *Chemical Engineering Science*,*62*(1), pp.387-396.

Cabrejos, F. J. 1994. PhD Dissertation: Experimental investigation on the fully developed pipe flow of dilute gas-solids suspensions, School of Engineering, University of Pittsburgh.

Cabrejos, F.J. and Klinzing, G.E., 1995. Characterization of dilute gas-solids flows using the rescaled range analysis. *Powder Technology*, *84*(2), pp.139-156.

Camesasca, M., Kaufman, M. and Manas-Zloczower, I., 2006. Quantifying fluid mixing with the Shannon entropy. *Macromolecular theory and simulations*, *15*(8), pp.595-607.

Chhabra, R.P. and Richardson, J.F., 2011. *Non-Newtonian flow and applied rheology: engineering applications*. Butterworth-Heinemann.

Cho, Y.J., Song, P.S., Kim, S.H., Kang, Y. and Kim, S.D., 2001. Stochastic Analysis of Gas-Liquid-Solid Flow in Three-Phase Circulating Fluidized Beds. *Journal of chemical engineering of Japan,* 34(2), pp.254-261.

Chu, K.W. and Yu, A.B., 2008. Numerical simulation of the gas− solid flow in three-dimensional pneumatic conveying bends. *Industrial & Engineering Chemistry Research*, *47*(18), pp.7058-7071.

Cong, X., Guo, X., Gong, X., Lu, H. and Dong, W., 2011. Experimental research of flow patterns and pressure signals in horizontal dense phase pneumatic conveying of pulverized coal. *Powder Technology*, *208*(3), pp.600-609.

Coulthard, J. 1993. Ultrasonic cross-correlation flow meters. *Proc. of the IEE Colloquium on Ultrasound in the Process Industry,* 7(1-3).

Daubechies, I. 1990. The Wavelet transform, time-frequency localization and signal processing, *IEEE Trans. Inform. Theory,* 36(5), pp.961- 1005.

De Araujo, D.B., Tedeschi, W., Santos, A.C., Elias, J., Neves, U.P.C. and Baffa, O., 2003. Shannon entropy applied to the analysis of event-related fMRI time series. *NeuroImage, 20*(1), pp.311-317.

Dhodapkar, S.V. and Klinzing, G.E., 1993. Pressure fluctuations in pneumatic conveying systems. *Powder Technology, 74*(2), pp.179-195.

Dhoriyani, M.L., Jonnalagadda, K.K., Kandikatla, R.K. and Rao, K.K., 2006. Silo music: sound emission during the flow of granular materials through tubes. *Powder Technology, 167*(2), pp.55-71.

Diks, C. 1999. *Nonlinear time series analysis: Methods and applications.* Singapore: World Scientific Press, 180 pp.

Drahoš, J., Bradka, F. and Punčochář, M., 1992. Fractal behaviour of pressure fluctuations in a bubble column. *Chemical engineering science,47*(15), pp.4069-4075.

Duan, F. and Cong, S., 2013. Shannon entropy analysis of dynamic behavior of Geldart group B and Geldart group D particles in a fluidized bed. *Chemical Engineering Communications, 200*(4), pp.575-586.

Dyakowski, T., Edwards, R.B., Xie, C.G. and Williams, R.A., 1997. Application of capacitance tomography to gas-solid flows. *Chemical Engineering Science, 52*(13), pp.2099-2110.

Elperin, T. and Klochko, M., 2002. Flow regime identification in a two-phase flow using wavelet transform. *Experiments in Fluids,* 32(6), pp.674-682.

Fuchs, A., Zangl, H. and Wypych, P., 2007. Signal modelling and algorithms for parameter estimation in pneumatic conveying. *Powder Technology,173*(2), pp.126-139.

Geldart, D., 1973. Types of gas fluidization. *Powder technology*, 7(5), pp.285-292.

Geng, Q., Zhu, X., Yang, J., You, X., Liu, Y. and Li, C., 2014. Flow regime identification in a novel circulating-turbulent fluidized bed. *Chemical Engineering Journal*, *244*, pp.493-504.

Giddings, D., Azzopardi, B.J., Aroussi, A. and Pickering, S.J., 2007. Absolute measurement of pneumatically conveyed powder using a single long throat venturi. *Powder technology*, *172*(3), pp.149-156.

Gibbs, J. W. 2012. Physics History. American Physical Society.

Godbole, A., Kosasih, B. and Fuchs, A., 2007. Particle trajectories in dilute phase pneumatic conveying. *Particulate Science and Technology*, *25*(4), pp.381-385.

Gore, R.A. and Crowe, C.T., 1989. Effect of particle size on modulating turbulent intensity. *International Journal of Multiphase Flow*, *15*(2), pp.279-285.

Gray, S. L. 2012. Master Dissertation: Turbulence modulation of poly disperse particles in a square particle-laden jet, Numerical Investigation, Virginia Polytechnic Institute and State University.

Grossmann, A. and Morlet, J., 1984. Decomposition of Hardy functions into square integrable wavelets of constant shape. *SIAM journal on mathematical analysis*, *15*(4), pp.723-736.

Hetsroni, G., 1989. Particles-turbulence interaction. *International Journal of Multiphase Flow*, *15*(5), pp.735-746.

Hrach, D., Fuchs, A. and Zangl, H., 2008, February. Capacitive flowmeter for gas-solids flow applications exploiting spatial frequency. In *Sensors Applications Symposium, 2008. SAS 2008. IEEE* (pp. 26-30). IET.

Huang, N.E., Shen, Z., Long, S.R., Wu, M.C., Shih, H.H., Zheng, Q., Yen, N.C., Tung, C.C. and Liu, H.H., 1998, March. The empirical mode decomposition and the Hilbert spectrum for nonlinear and non-stationary time series analysis.

In *Proceedings of the Royal Society of London A: Mathematical, Physical and Engineering Sciences* (Vol. 454, No. 1971, pp. 903-995). The Royal Society.

Hubbard, M.G. and Dukler, A.E., 1966. The characterization of flow regimes for horizontal two-phase flow. *Proceedings of the 1996 Heat Transfer and Fluid, pp.100-121.*

Hurst, H.E., 1951. {Long-term storage capacity of reservoirs}. *Trans. Amer. Soc. Civil Eng.*, *116*, pp.770-808.

Hwang, W. and Eaton, J. K. 2006. Homogeneous and isotropic turbulence modulation by small heavy (St∼50) particles. *J. Fluid Mech.,564,* pp.361–393.

Ichikura, Y. and Watanabe, K. 1995. Measurement of particle flow by optical systems. *Proc. of the 21th International Conference on Industrial Electronics, Control and Instrumentation,Orlando, FL, USA.2,* pp.1173-1178.

Jama, G.A., Klinzing, G.E. and Rizk, F., 1999. Analysis of unstable behavior of pneumatic conveying systems. *Particulate science and technology*, 17(1-2), pp.43-68.

Jaworski, A.J. and Dyakowski, T., 2002. Investigations of flow instabilities within the dense pneumatic conveying system. *Powder Technology*, *125*(2), pp.279-291.

Johnsson, F., Zijerveld, R.C., Schouten, J.C., Van den Bleek, C.M. and Leckner, B., 2000. Characterization of fluidization regimes by time-series analysis of pressure fluctuations. *International journal of multiphase flow*,*26*(4), pp.663-715.

Jones, M.G. and Williams, K.C., 2003. Solids friction factors for fluidized dense-phase conveying. *Particulate Science and Technology*, *21*(1), pp.45-56.

Jung, S.H., Kim, J.S., Kim, J.B. and Kwon, T.Y., 2009. Flow-rate measurements of a dual-phase pipe flow by cross-correlation technique of transmitted radiation signals. *Applied Radiation and Isotopes*, *67*(7), pp.1254-1258.

Kantz, H. and Schreiber, T., 1997. *Nonlinear time series analysis* (Vol. 7). Cambridge university press.

Karimi, M., Mostoufi, N., Zarghami, R. and Sotudeh-Gharebagh, R., 2011. Nonlinear dynamics of a gas–solid fluidized bed by the state space analysis.*Chemical engineering science*, *66*(20), pp.4645-4653.

Katsev, S. and L'Heureux, I., 2003. Are Hurst exponents estimated from short or irregular time series meaningful?. *Computers & Geosciences*, *29*(9), pp.1085-1089.

Kikuchi, R. and Tsutsumi, A., 2001. Characterization of nonlinear dynamics in a circulating fluidized bed by rescaled range analysis and short-term predictability analysis. *Chemical engineering science*, *56*(23), pp.6545-6552.

Kim, S.H. and Han, G.Y., 1999. An analysis of pressure drop fluctuation in a circulating fluidized bed. *Korean Journal of Chemical Engineering*, *16*(5), pp.677-683.

Kirpalani, D.M., Sparks, B.D. and McCracken, T.W., 2001. A wavelet based approach for determining two-phase flow patterns. *In Proceedings of the 4th International Conference on Multiphase Flow, New Orleans. Tulane University, New Orleans.*

Kulick, J.D., Fessler, J.R. and Eaton, J.K., 1994. Particle response and turbulence modification in fully developed channel flow. *Journal of Fluid Mechanics*, *277*, pp.109-134.

Lee, S.H., Kim, S.D. and Park, S.H., 2002. Statistical and deterministic chaos analysis of pressure fluctuations in a fluidized bed of polymer powders. *Korean Journal of Chemical Engineering*, *19*(6), pp.1020-1025.

Levy, A., 2000. Two-fluid approach for plug flow simulations in horizontal pneumatic conveying. Powder Technology, 112(3), pp.263-272.

Li, H., 2002. Application of wavelet multi-resolution analysis to pressure fluctuations of gas–solid two-phase flow in a horizontal pipe. *Powder Technology*, *125*(1), pp.61-73.

Liang, C., Zhao, C., Chen, X., Pu, W., Lu, P. and Fan, C. 2007. Flow Characteristics and Shannon Entropy analysis of dense phase pneumatic of pulverized coal with variable moisture content at high pressure. *Chemical Engineering & Technology*, 30 (7), pp.926-931.

Lin, T.J., Juang, R.C., Chen, Y.C. and Chen, C.C., 2001. Predictions of flow transitions in a bubble column by chaotic time series analysis of pressure fluctuation signals. *Chemical engineering science*, *56*(3), pp.1057-1065.

Liu, Z.M., Yi, H., Duan, G. and Fu, Z. 2007. Particle velocity and pressure drop in long-di***stance*** dense-phase pneumatic conveying of fly ash. *AIP Conference Proceedings,Macau, China*, 914, pp.107-112.

Liu, Z., Du, B., Zhao, W., Li, X., Li, J., Bu, C. and Yi, H., 2009. Effect of characterization of powder on particle velocity in dense-phase pneumatic conveying. In *Journal of Physics: Conference Series* (Vol. 147, No. 1, p. 012068). IOP Publishing.

Lu, P., Han, D., Jiang, R., Chen, X., Zhao, C. and Zhang, G., 2013. Experimental study on flow patterns of high-pressure gas–solid flow and Hilbert–Huang transform based analysis. *Experimental Thermal and Fluid Science*, *51*, pp.174-182.

Luo, L., Yan, Y., Xie, P., Sun, J., Xu, Y. and Yuan, J., 2012. Hilbert–Huang transform, Hurst and chaotic analysis based flow regime identification methods for an airlift reactor. *Chemical Engineering Journal*, *181*, pp.570-580.

Ma, J. and Yan, Y., 2000. Design and evaluation of electrostatic sensors for the measurement of velocity of pneumatically conveyed solids. *Flow Measurement and Instrumentation*, *11*(3), pp.195-204.

Mallat, S., 1999. *A wavelet tour of signal processing*. Academic press.

Mallick, S.S., 2009. PhD Dissertation: Modelling of fluidised dense-phase pneumatic conveying of powders, University of Wollongong.

Mallick, S.S. and Wypych, P.W., 2009. Minimum transport boundaries for pneumatic conveying of powders. *Powder Technology*, *194*(3), pp.181-186.

Mallick, S.S. and Wypych, P.W., 2010. An investigation into modeling of solids friction for dense-phase pneumatic conveying of powders. *Particulate Science and Technology*, *28*(1), pp.51-66.

Mallick, S.S., Wypych, P.W. and Pan, R., 2011. Minimum transport boundaries for dense-phase pneumatic conveying of powders. In *The proceedings of Bulk Solids India*.

Mallick, S.S., Wypych, P.W. and Pan, R., 2013. Modeling dense-phase pneumatic conveying of powders using suspension density. *Particulate Science and Technology*, *31*(4), pp.340-347.

Meyer, Y., Wavelets: Algorithms and Applications, SIAM, Philadelphia, 1993. *MR 95f, 94005*.

Mi, B., 1994. Low-velocity pneumatic transportation of bulk solids. *University of Wollongong Thesis Collection*, p.830.

Mills, D., Mason, J.S. and Stacey, R.B. 1982. A design study for pneumatic conveying of fine particular material. *In the proceedings of Solidex 82:The solids handling conference, Harrogate, England,* pp. C1-C75.

Mills, D., 2004. Pneumatic Conveying Design Guide, Sec. Ed.

Mills, D., 2004. An investigation of the unstable region for dense phase conveying in sliding bed flow. *Granular Matter, 6*(2-3), pp.173-177.

Mittal, A., Mallick, S.S. and Wypych, P.W., 2014. An investigation into flow mode transition and pressure fluctuations for fluidized dense-phase pneumatic conveying of fine powders. *Particuology, 16*, pp.187-195.

Mohanarangam, K., Yang, W., Zhang, H.J. and Tu, J.Y., 2009, December. Effect of particles in a turbulent gas-particle flow within a 90^{o} bend. In *Seventh International Conference on CFD in the Minerals and Process Industries, CSIRO, Melbourne, Australia*.

Nolte, D.D., 2010. The tangled tale of phase space. *Physics today. American Institute of Physics.* S-0031-9228-1004-010-X

Nugroho, A.T. and Wu, Z., 1999. Microwave Imaging of 3D Lossy Dielectric Objects Using Algebraic Reconstruction Techniques. In *Proc. of 1 st World Congress of Industrial Process Tomography* (pp. 201-205).

Ostendorf, M. and Schwedes, J., 2001. Measurement of the dynamic behavior of bulk solids using optical flow analysis. *Handbook of Powder Technology*, *10*, pp.851-860.

Pahk, J.B. and Klinzing, G.E., 2008a. Comparison of flow characteristics for dilute phase pneumatic conveying for two different plastic pellets. *Journal of the Chinese Institute of Chemical Engineers*, *39*(2), pp.143-150.

Pahk, J.B. and Klinzing, G.E., 2008b. Assessing flow regimes from pressure fluctuations in pneumatic conveying of polymer pellets. *Particulate Science and Technology*, *26*(3), pp.247-256.

Pan, R. and Wypych, P.W., 1998, September. Dilute and dense phase pneumatic conveying of fly ash. In *Proceedings of the 6th International Conference on Bulk Materials Storage and Transportation, Wollongong, NSW, Australia* (pp. 183-189).

Paris, A.D., 2001. PhD Dissertation: Turbulence attenuation in a particle-laden channel flow. Stanford University

Percival, D.P., 1995. On estimation of the wavelet variance. *Biometrika*,*82*(3), pp.619-631.

John, G.P. and Dimitris, G.M., 1996. Digital Signal Processing: Principles, Algorithms and Applications. *Prentice Hall.*

Rahmat, M.F. and Kamaruddin, N.S., 2012. Application of fuzzy logic and electrodynamic sensors as flow pattern identifier. *Sensor Review*, *32*(2), pp.123-133.

Rao, K.K., Nott, P.R. and Sundaresan, S., 2008. *An introduction to granular flow*. New York: Cambridge University Press.

Roski, H.J., 1987. The influence of stepped-pipelines in pneumatic long-distance transport of building materials. *the proceedings of Pneumatech*, *3*, p.3rd.

Sanderson, M.L. and Yeung, H., 2002. Guidelines for the use of ultrasonic non-invasive metering techniques. *Flow measurement and Instrumentation*,*13*(4), pp.125-142.

Schlüter, T. and Merzkirch, W., 1996. PIV measurements of the time-averaged flow velocity downstream of flow conditioners in a pipeline. *Flow Measurement and Instrumentation*, *7*(3), pp.173-179.

Seraj, H., Rahmat, M.F. and Khalid, M., 2013. Measurement of velocity of solid/air two phase fluid using electrostatic sensors and cross correlation technique. *Scientia Iranica*, *20*(3), pp.786-792.

Setia, G. 2012. ME Dissertation: Modelling minimum transport boundary for dense phase pneumatic conveying of fine powders. Thapar University, Patiala.

Shao, F., Lu, Z., Wu, E. and Wang, S., 2000. Study and industrial evaluation of mass flow measurement of pulverized coal for iron-making production.*Flow Measurement and Instrumentation*, *11*(3), pp.159-163.

Shou, M.C. and Leu, L.P., 2005. Energy of power spectral density function and wavelet analysis of absolute pressure fluctuation measurements in fluidized beds. *Chemical Engineering Research and Design*, *83*(5), pp.478-491.

Shannon, C.E., 1948. A mathematical theory of communication, bell System technical Journal 27: 379-423 and 623–656. *Mathematical Reviews (MathSciNet): MR10, 133e.*

Stoica, P. and Moses, R.L., 1997. *Introduction to spectral analysis* (Vol. 1, pp. 3-4). Upper Saddle River: Prentice hall.

Takens, F. 1981. Detecting strange attractors in turbulence in Dynamical Systems and Turbulence, In D. A. Rand and L.-S. Young.Lecture Notes in Mathematics, vol. 898. Springer-Verlag. pp. 366–381.

Tsuji, Y. and Morikawa, Y., 1982. Flow pattern and pressure fluctuation in air-solid two-phase flow in a pipe at low air velocities. *International Journal of Multiphase Flow*, *8*(4), pp.329-341.

Tsuji, Y. and Morikawa, Y., 1982. LDV measurements of an air–-solid two-phase flow in a horizontal pipe. *Journal of Fluid Mechanics*, 120, pp.385-409.

Tong, H. 1990. *Nonlinear time series analysis:A Dynamical System Approach.* Oxford University Press, ISBN 0-19-852224-X.

Tong, R., 2011, July. Wavelet analysis of pressure fluctuation in gas-solid two-phase flow in a horizontal pipe. In *Mechanic Automation and Control Engineering (MACE), 2011 Second International Conference on* (pp. 932-935). IEEE.

Welch, P.D., 1967. The use of fast Fourier transform for the estimation of power spectra: A method based on time averaging over short, modified periodograms. *IEEE Transactions on audio and electroacoustics*, *15*(2), pp.70-73.

Weber, M., 1981. Principles of hydraulic and pneumatic conveying in pipes.*Bulk Solids Handling*, *1*(1), pp.57-63.

Wang, X., He, R., Suda, T. and Sato, J., 2007. Phase-plane invariant analysis of pressure fluctuations in fluidized beds. *Tsinghua Science & Technology*, *12*(3), pp.284-289.

Williams, G.P., 1997. *Chaos theory tamed*. Washington DC: Joseph Henry Press.

Williams, K.C., Jones, M.G. and Yadav, Y., 2007. Pressure fluctuations in dense phase pneumatic conveying of powders. *Proceedings for PARTEC-07*.

Williams, K.C., Jones, M.G. and Cenna, A.A., 2008. Characterization of the gas pulse frequency, amplitude and velocity in non-steady dense phase pneumatic conveying of powders. *Particuology*, *6*(5), pp.301-306.

Widrow, B. and Stearns, S.D., 1985. Adaptive signal processing. *Englewood Cliffs, NJ, Prentice-Hall, Inc., 1985, 491 p., 1*.

Wypych, P.W. and Yi, J., 2003. Minimum transport boundary for horizontal dense-phase pneumatic conveying of granular materials. *Powder Technology*, *129*(1), pp.111-121.

Wypych, P.W., Hastie, D.B. and Yi, J., 2005. *Prediction of optimal operating conditions for dense-phase pneumatic conveying systems*. Final research report for the International Fine Particle Research Institute, Inc, USA.

Wang, X., He, R., Suda, T. and Sato, J., 2007. Phase-plane invariant analysis of pressure fluctuations in fluidized beds. *Tsinghua Science & Technology*, *12*(3), pp.284-289.

Xu, Y., De Graaf, G. and Wolffenbuttel, R.F., 1996. DSP cross-correlator for use in a thermal flow meter. In *Instrumentation and Measurement Technology Conference, 1996. IMTC-96. Conference Proceedings. Quality Measurements: The Indispensable Bridge between Theory and Reality., IEEE* (Vol. 1, pp. 519-522). IEEE.

Zangl, H., Watzenig, D., Steiner, G., Fuchs, A. and Wegleiter, H., 2007. Non-iterative reconstruction for electrical tomography using optimal first and second order approximations. In *World Congress on Industrial Process Tomography WCIPT5*.

Zhong, W. and Zhang, M., 2005. Characterization of dynamic behavior of a spout-fluid bed with Shannon entropy analysis. *Powder Technology*, *159*(3), pp.121-126.

Zhong, W.Q., Jin, B.S., Zhang, Y., Wang, X.F., Zhang, M.Y. and Xiao, R., 2009. Shannon entropy increment analysis on dynamic behavior of a biomass fluidized bed. In *Journal of Physics: Conference Series* (Vol. 147, No. 1, p. 012071). IOP Publishing.

Zhou, Z.Y., Kuang, S.B., Chu, K.W. and Yu, A.B., 2010. Discrete particle simulation of particle–fluid flow: model formulations and their applicability. *Journal of Fluid Mechanics*, *661*, pp. 482-510.

APPENDIX A

Table A1: Shannon entropy at different locations along pipeline length (Flyash, University of Wollongong)

	Shannon entropy				
	P1	**P2**	**P3**	**P4**	**P5**
Exp-1	1.151	1.978	2.152	2.355	2.582
Exp-3	0.965	1.576	2.194	2.772	2.915
Exp-11	2.653	2.217	2.527	2.637	2.764
Exp-12	2.363	2.157	2.692	2.668	3.23
Exp-13	1.916	2.469	2.629	3.086	3.645
Exp-14	2.542	2.308	2.616	3.101	3.516
Exp-15	2.252	2.172	2.632	3.003	3.256
Exp-16	1.52	1.647	2.091	2.172	2.607
Exp-17	1.5363	1.7449	1.8586	2.0962	2.1536
Exp-20	2.843	2.464	2.683	2.959	3.283
Exp-21	2.44	2.061	2.493	2.7024	3.196
Exp-23	2.549	2.328	2.616	2.8527	3.097
Exp-24	2.397	2.363	2.63	2.614	3.348
Exp-25	1.892	1.898	1.794	2.109	2.99
Exp-26	2.251	2.35	2.625	2.858	2.904
Exp-27	1.796	2.1137	2.336	2.403	2.461
Exp-29	2.7481	2.058	2.296	2.563	2.629
Exp-32	2.756	2.666	2.814	3.2716	3.3707
Exp-35	2.55	2.577	2.182	2.546	2.62
Exp-36	2.475	2.764	2.888	2.954	2.916
Exp-37	3.712	3.673	3.661	3.965	3.362
Exp-39	2.649	2.333	2.532	2.851	2.891

Table A2: Shannon entropy at different locations along pipeline length (White powder, University of Wollongong)

	Shannon Entropy					
	P1	**P2**	**P3**	**P4**	**P5**	**P6**
Exp-1	3.2811	3.1821	3.5523	3.3538	3.4422	4.1251
Exp-2	1.9893	2.2517	3.797	3.6971	3.8646	3.8841
Exp-3	2.2078	2.7573	3.5095	3.229	3.604	3.9319
Exp-4	1.773	2.2752	2.8893	2.5816	3.4369	3.6642
Exp-5	2.2482	2.38	3.0605	3.1269	3.2446	3.3852
Exp-6	1.9783	2.6523	3.8034	3.3598	4.1091	4.2465
Exp-8	2.3713	2.6898	2.9815	2.9624	3.1401	3.4236
Exp-9	1.9612	2.3905	3.0306	2.4621	2.8918	2.9414
Exp-11	2.5926	2.808	3.8807	3.6165	3.8194	4.0631
Exp-14	1.4409	1.9341	2.8953	2.9764	3.3116	3.7374
Exp-15	2.3057	2.7183	3.6882	3.6403	3.697	3.9616
Exp-16	1.1014	1.8125	3.2254	2.9266	3.7486	3.9763
Exp-17	1.878	2.0597	2.6609	2.8867	3.2704	3.5519
Exp-19	1.9228	2.38	3.478	3.1099	3.6779	3.9331
Exp-20	3.9181	3.8678	4.2639	4.4117	4.5503	4.483
Exp-21	1.7424	2.6284	3.3711	3.5258	3.7981	3.8755
Exp-23	1.6976	2.2977	3.5672	3.6217	3.8129	4.0921
Exp-24	2.21	2.6403	3.2561	3.3795	3.6054	3.7539
Exp-25	2.2553	2.6039	3.8051	3.7612	4.0062	3.9314
Exp-26	1.6747	2.0698	2.9072	2.8437	3.3429	3.6767
Exp-52	2.8254	2.6707	3.5618	2.8574	3.5562	3.7156
Exp-53	1.9371	1.8821	2.9599	2.1472	2.8957	3.3789
Exp-54	2.0857	2.2103	2.9944	3.1945	3.2932	3.3546
Exp-55	2.4293	2.2171	3.767	3.5317	3.7089	4.0207
Exp-56	2.6904	2.6257	3.2895	2.5088	2.9097	3.6035
Exp-57	2.5359	2.8019	3.0432	2.8109	3.0212	3.5321
Exp-58	2.7742	2.7161	3.4396	3.5912	3.6763	3.7181
Exp-59	2.865	2.9829	3.5712	3.563	3.6726	3.9144
Exp-60	2.6703	2.9842	3.8492	3.8462	3.9914	4.0019
Exp-61	2.3908	2.1819	3.0058	2.7665	2.9847	3.0743
Exp-62	3.1221	3.1612	3.7916	3.9047	4.2516	4.1459
Exp-63	3.1691	3.0008	4.0246	3.8299	4.0347	4.281
Exp-64	2.7333	2.897	3.8295	3.4605	3.8214	4.0835
Exp-65	3.3183	3.4339	4.1967	3.976	4.2922	4.13

Table A3: Hurst exponent at different locations along pipeline length (Flyash, University of Wollongong)

	Hurst Exponent				
	P1	**P2**	**P3**	**P4**	**P5**
Exp-1	0.935472	0.664125	0.737695	0.577915	0.551408
Exp-3	1.0079	0.608928	0.716797	0.578778	0.603896
Exp-11	0.517806	0.84158	0.655509	0.630407	0.59127
Exp-12	0.871894	0.901293	0.781362	0.838198	0.707766
Exp-13	1.06713	0.737151	0.592214	0.589828	0.56263
Exp-14	0.878437	0.742682	0.750271	0.591051	0.424176
Exp-15	0.916597	0.871487	0.952251	0.7596	0.725897
Exp-16	0.916324	0.846774	0.675809	0.823615	0.389846
Exp-17	0.933754	0.79327	0.789703	0.81167	0.627592
Exp-20	0.64302	0.783694	0.739583	0.543631	0.319642
Exp-21	0.74798	0.808761	0.823616	0.71523	0.491575
Exp-23	0.733671	0.849795	0.776873	0.71935	0.576982
Exp-24	1.06046	0.942893	0.816804	0.847368	0.621245
Exp-25	0.730146	0.825143	0.759244	0.901087	0.511414
Exp-26	0.954938	1.05036	1.00742	0.995446	0.938815
Exp-27	1.00464	1.02799	1.04815	1.07374	1.03687
Exp-29	1.061	0.7975	0.6207	0.8318	0.7646
Exp-32	0.941437	0.904181	0.89051	0.925189	0.84221
Exp-35	1.08683	1.0138	1.07043	1.04774	0.99232
Exp-36	1.1202	1.12205	1.06951	1.05463	1.02765
Exp-37	1.02399	0.959474	0.906302	0.923821	0.919618
Exp-39	0.79996	0.812437	0.65753	0.482199	0.513519

Table A4: Hurst exponent at different locations along pipeline length (White powder, University of Wollongong)

	Hurst exponent					
	P1	**P2**	**P3**	**P4**	**P5**	**P6**
Exp-1	1.03239	1.01164	0.700493	0.735439	0.580212	0.519285
Exp-2	1.03205	0.847295	0.830163	0.882561	0.839956	0.379136
Exp-3	1.11618	1.11588	1.00485	0.991387	0.704486	0.635603
Exp-4	0.89943	0.867878	0.904219	0.84696	0.554804	0.458752
Exp-5	1.05453	0.968964	1.01416	0.960835	0.983576	0.817758
Exp-6	1.02336	0.910062	0.525708	0.621364	0.547145	0.598865
Exp-8	1.08448	0.921502	0.656141	0.731323	0.565114	0.556117
Exp-9	1.13378	1.08276	1.00235	0.97385	0.926356	0.891517
Exp-11	1.18537	1.08252	0.78582	0.850098	0.824378	0.532759
Exp-14	1.01296	0.990636	0.864359	0.831296	0.950711	0.539943
Exp-15	1.07119	1.118	0.810415	0.749312	0.548448	0.373113
Exp-16	0.944989	0.920803	0.921201	0.891187	0.809654	0.645215
Exp-17	1.00216	0.97193	0.94796	0.993403	0.809606	0.685311
Exp-19	0.952374	0.91218	0.700291	0.859952	0.724801	0.658135
Exp-20	1.05917	0.940195	0.876689	0.830973	0.747452	0.747154
Exp-21	0.886406	0.872473	0.982809	1.0008	0.948665	0.744419
Exp-23	0.891979	0.815	0.788234	0.829684	0.694318	0.617363
Exp-24	0.92807	0.835834	0.866676	1.00014	0.950819	0.806401
Exp-25	1.06385	0.929409	0.962567	0.923434	0.82846	0.727547
Exp-26	1.10068	1.04868	0.797156	0.766596	0.687133	0.56683
Exp-52	1.09039	1.04424	0.65117	0.81559	0.707362	0.59625
Exp-53	1.10774	1.02449	0.695133	0.66234	0.510992	0.422228
Exp-54	0.852042	0.714018	0.748242	0.797887	0.699747	0.542189
Exp-55	0.973949	0.933662	0.671557	0.718698	0.690712	0.454258
Exp-56	1.24259	1.17455	0.869571	0.99036	0.764218	0.622084
Exp-57	0.86319	0.905931	0.817861	0.792944	0.825445	0.7901
Exp-58	0.870601	0.752158	0.663085	0.735477	0.650869	0.596313
Exp-59	1.00577	0.986011	0.80575	0.697281	0.619478	0.715107
Exp-60	0.978596	0.966251	0.629061	0.603031	0.609409	0.614125
Exp-61	1.05261	0.682058	0.89611	0.739406	0.622632	0.517872
Exp-62	0.962349	0.774791	0.840892	0.734526	0.510755	0.641032
Exp-63	0.899513	0.952627	0.857324	0.842691	0.763479	0.582461
Exp-64	1.10064	1.03978	0.94824	0.990631	0.887341	0.729786
Exp-65	1.0357	0.885509	0.870454	0.941723	0.895015	0.767139

Table A5: Shannon entropy variation along pipeline length (Indian flyash)

	Shannon entropy	
	P2	**P5**
Exp-24-1	4.5393	1.8031
Exp-24-2	4.4298	1.5375
Exp-24-3	4.3328	1.7357
Exp-24-4	4.5136	1.9366
Exp-24-5	2.1011	1.1441
Exp-24-6	4.9959	2.1559
Exp-24-7	2.1011	1.1441
Exp-24-8	2.6256	2.1655
Exp-24-9	2.6256	2.1655
Exp-24-10	4.3697	2.1932
Exp-70-1	4.232	2.8365
Exp-70-2	4.1938	2.8179
Exp-70-3	4.4612	2.8483
Exp-70-4	4.1364	2.7088
Exp-70-5	4.0754	2.8365
Exp-70-6	3.9402	2.3645
Exp-70-7	4.2069	3.2891
Exp-70-8	4.3842	3.2861
Exp-70-9	4.3223	3.5938
Exp-70-10	4.5106	2.2553
Exp-70-11	3.767	2.8549
Exp-70-12	4.0865	2.8624

APPENDIX B

Additional results using the test data of Thapar University

In the following section, results from analysis of pressure signals obtained from Thapar University test rig have been provided. The entire signal analysis work performed on the test data of University of Wollongong has also been performed on the Thapar University test rig data for the reason of comprehensiveness. In the following figures, values of various signal processing parameters have been presented. Results have been shown for the Indian fly ash conveyed through two different test rigs (50 mm ID, 70 m long and 50 mm ID, 24 m long). Time series data in the form of pressure fluctuations were obtained from different conveying trials conducted corresponding to different mass flow rates of air and solids. In the present case, results have been shown only at two locations along pipeline length (i.e. start and end locations). Reason being the variation observed in the signal parameters at intermediate locations was of lesser amount due to shorter length of pipeline. Towards the end of this section comparison has been made between results obtained from different test rigs.

Shannon Entropy

The following figures show the value of Shannon entropy at two different locations along pipeline length (i.e. entry and end location).

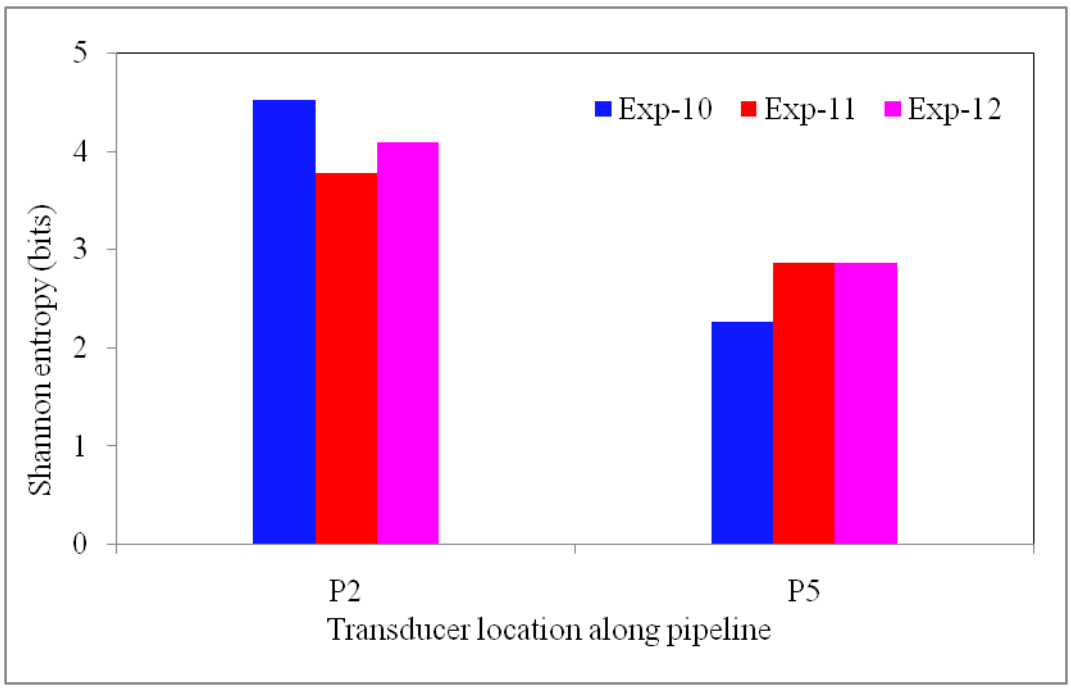

Figure B1: Shannon entropy variation along pipeline length (54 mm I.D. × 70 m long pipe)

Exp.10: m_f = 0.039 kg/s; m_s = 0.7968 kg/s; m^* = 20.43; V_f = 12.0 m/s (at P2) - 15.6 m/s (at P5)

Exp.11: m_f = 0.035 kg/s; m_s = 0.5588 kg/s; m^* = 15.96; V_f = 11.4 m/s (at P2) - 14.2 m/s (at P5)

Exp.12: m_f = 0.0324 kg/s; m_s = 0.629 kg/s; m^* = 19.41; V_f = 10.12 m/s (at P2) - 12.9 m/s (at P5)

As seen in the above figure, value of Shannon entropy at P5 (located towards the end of test rig) is less as compared to value at P2 (located near the pipeline entry). There were two straight pipe sections and one closely coupled bend located between transducer locations P2 and P5 along the pipeline length (as shown in Figure 3.3). It was observed that change in the entropy in the straight pipe sections was quite small, however the value dropped considerably in the closed couple bend, giving rise to overall decrease in the Shannon entropy. The following figure shows the results for 54 m I.D. and 24 m long pipeline test rig.

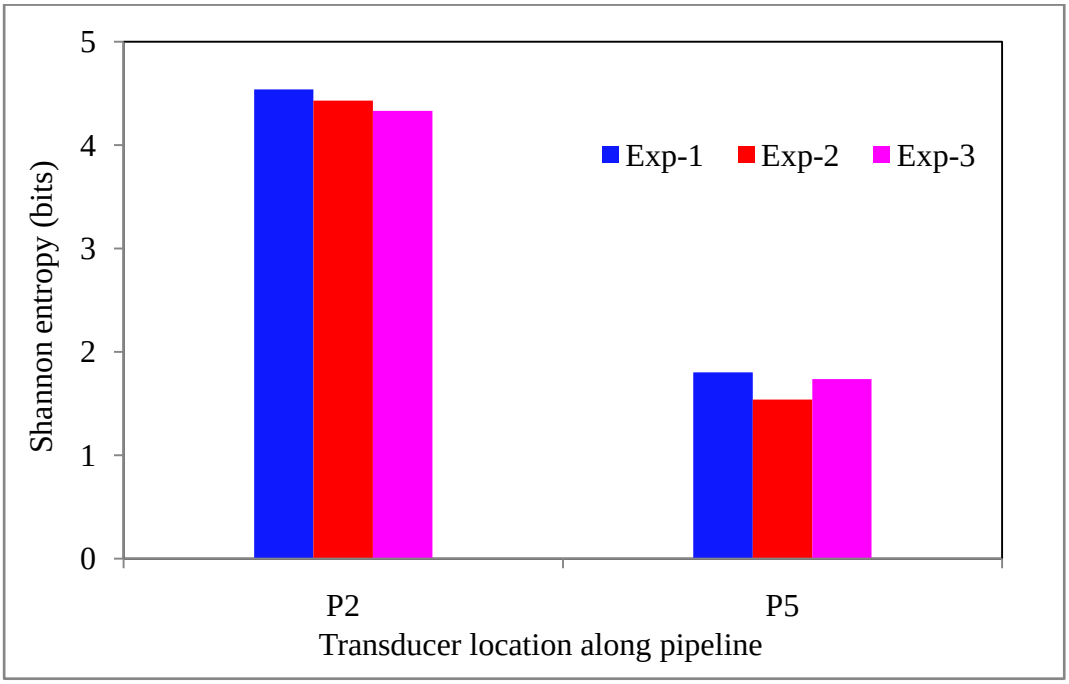

Figure B2: Shannon entropy variation along pipeline length

(54 mm I.D. × 24 m long pipe)

Exp.1: m_f = 0.049 kg/s; m_s = 3.47 kg/s; m^* = 70.8; V_f = 16.0 m/s (at P2) - 20.7 m/s (at P5)

Exp.2: m_f = 0.048kg/s; m_s 3.49kg/s; m^* = 72.7; V_f = 14.1 m/s (at P2) - 18.8 m/s (at P5)

Exp.3: m_f = 0.046kg/s; m_s = 3.61kg/s; m^* = 78.4; V_f= 15.6 m/s (at P2) - 19.6 m/s (at P5)

As seen in the above figure, Shannon entropy drops as in the previous case of 70 m long pipeline, however the amount of drop in the Shannon entropy value is higher as compared to 70 m long pipeline. This may be due to reduction in straight pipe section length, which causes negligible expansion of the carrier phase, instead provides hindrance to the flow due to early changes in direction of flow as compared to 70 m long pipeline test rig. Hence the carrier phase as well as solid phase turbulence gets reduced.

Power Spectral Density (PSD)

Power spectral density spectrum results obtained from the pressure versus time series data of the flyash conveyed through pipeline of 54 mm I.D. × 70 m long corresponding to different flow conditions have been shown in the following figures.

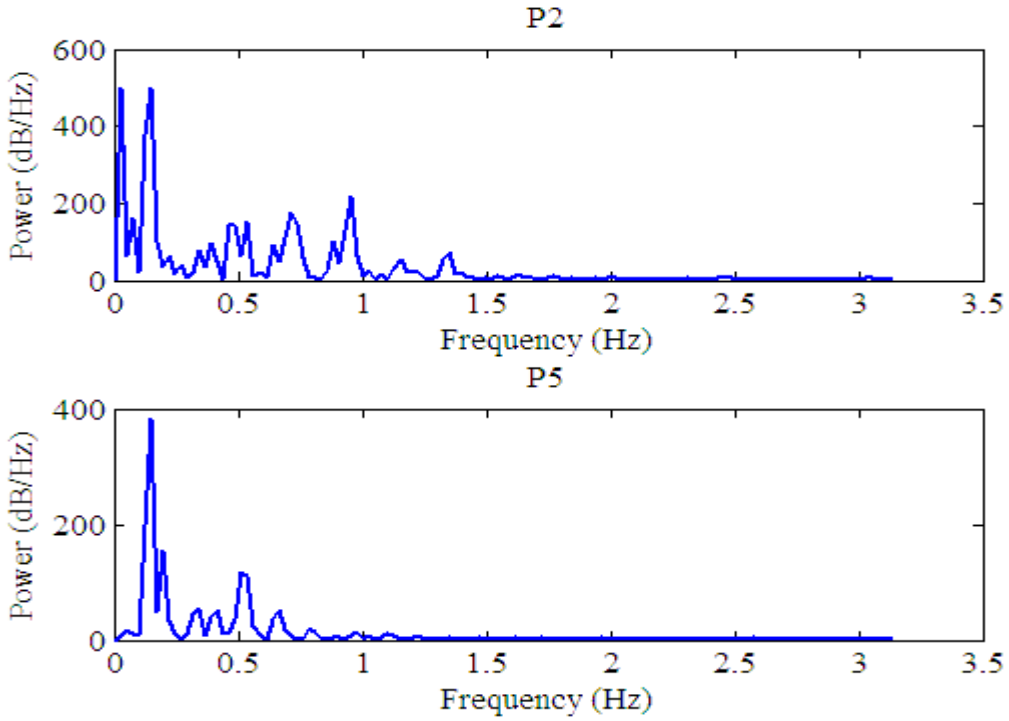

Figure B3: Power spectral density at different locations along pipeline length (54 mm I.D. × 70 m long pipe; m_f = 0.031 kg/s; m_s = 1.21 kg/s; m^* = 39.03)

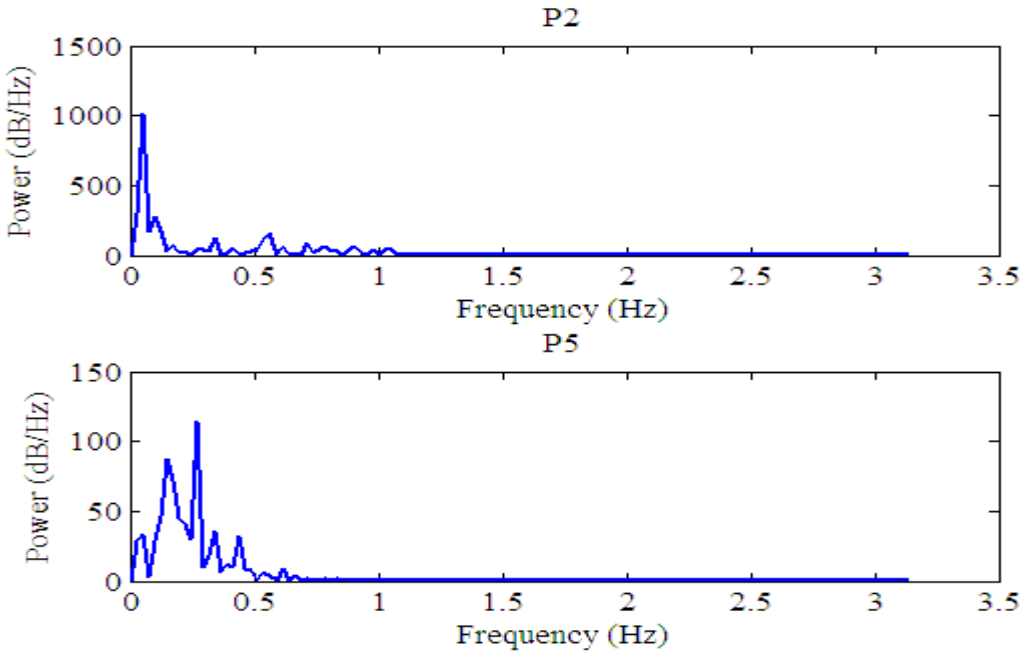

Figure B4: Power spectral density at different locations along pipeline length (54 mm I.D. × 70 m long pipe; m_f = 0.029 kg/s; m_s = 0.5 kg/s; m^* = 17.3)

As seen in the above figures, there is no significant change observed in the power spectral density spectrum obtained at locations P2 and P5. Power of the signal has been reduced from P2 to P5, which indicates lesser amplitude of pressure fluctuations.

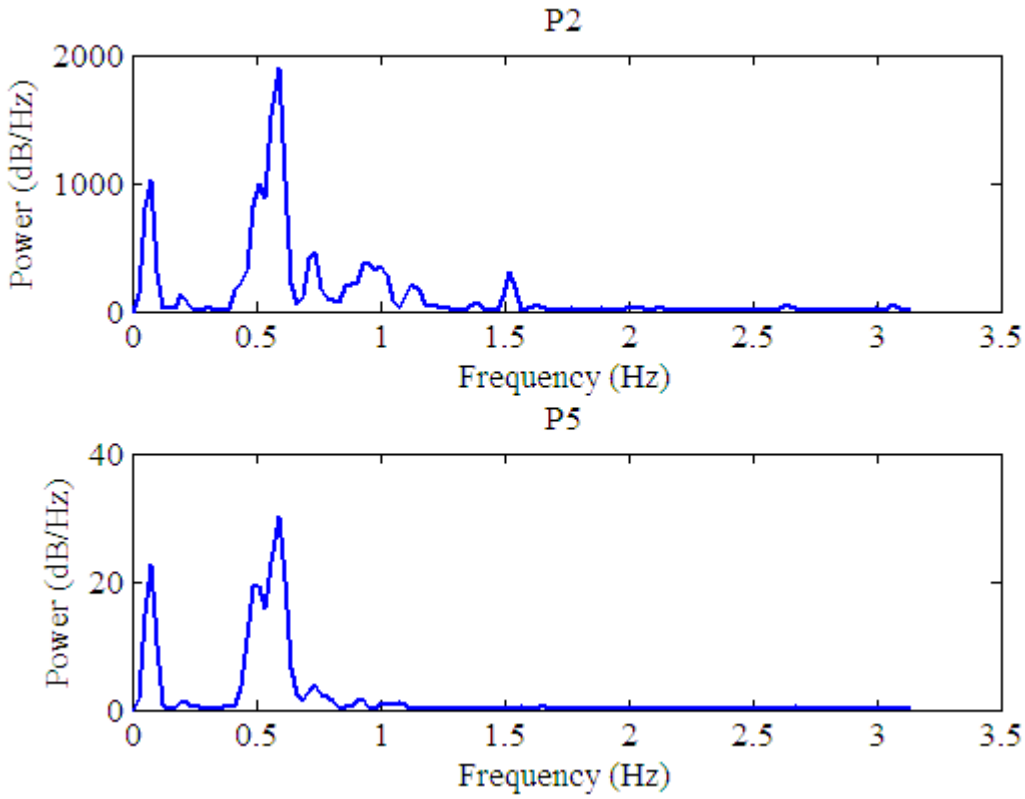

Figure B5: Power spectral density at different locations along pipeline length (Exp.1: m_f = 0.049 kg/s; m_s = 3.47 kg/s; m^* = 70.8; 54 mm I.D. × 24 m long pipe)

It can be observed in the above figure that power spectral density spectrums obtained at locations P2 and P5 are similar without any obvious change. There is no shift in the position of dominant frequency. However drop in signal power is much higher than the drop occurred for 70 m long pipeline. Probable reason for the same could be influence of bends dominant to that of straight pipe sections due to shorter length of test setup.

Phase space diagram

Before constructing the phase space diagram, calculations were made for the selection of optimum delay time and embedding dimension. Following figure shows the mutual information versus time lag.

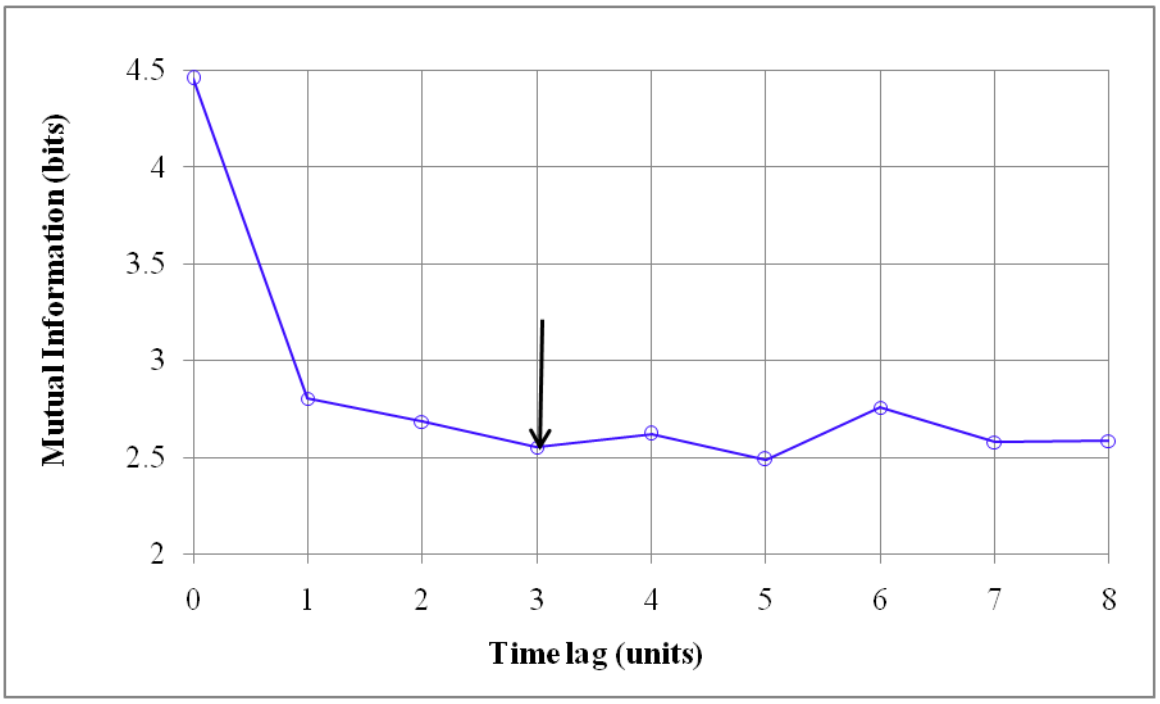

Figure B6: Variation of mutual information versus time lag Exp-1; Fly ash; (at P2)

As can be seen in the above figure that first minimum of mutual information lies at time lag of 3. Hence phase space diagram would be constructed using $\tau = 3$. Following figure represents percentage of false nearest neighbors versus different embedding dimensions.

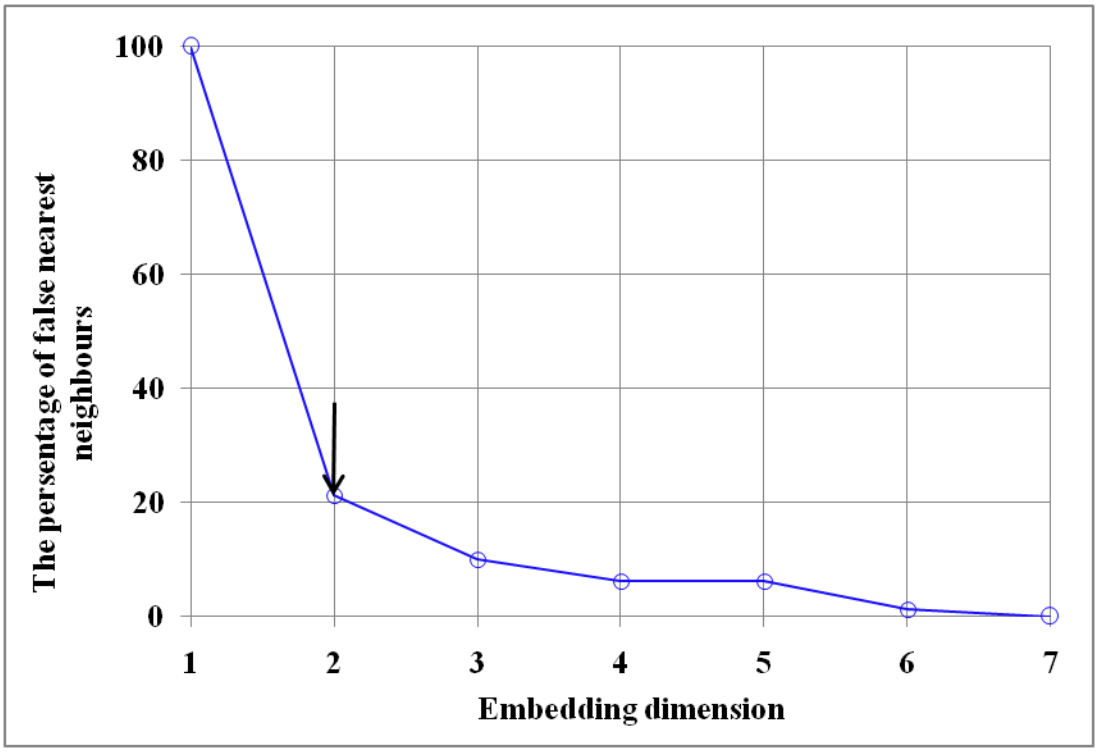

Figure B7: Variation of false nearest neighbors percentage embedding dimension Exp-1; Fly ash; (at P2)

As can be seen in the above figure that percentage of false nearest neighbors falls to the minimum corresponding to embedding dimension of 2 (m = 2). Hence the same has been chosen for the attractor construction.Phase space diagram results obtained from the pressure versus time series data of the flyash conveyed through pipeline of 54 mm I.D. × 70 m length corresponding to different flow conditions have been shown in the following figures.

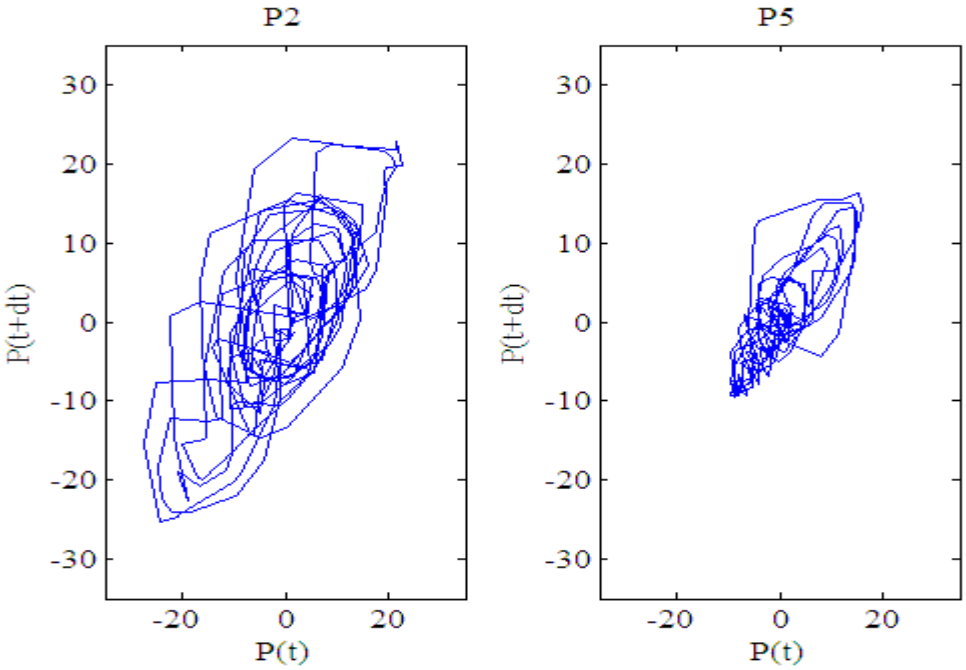

Figure B8: Phase space diagram at different locations along pipeline length (54 mm I.D. × 70 m long pipe; m_f = 0.031 kg/s; m_s = 1.21 kg/s; m^* = 39.03)

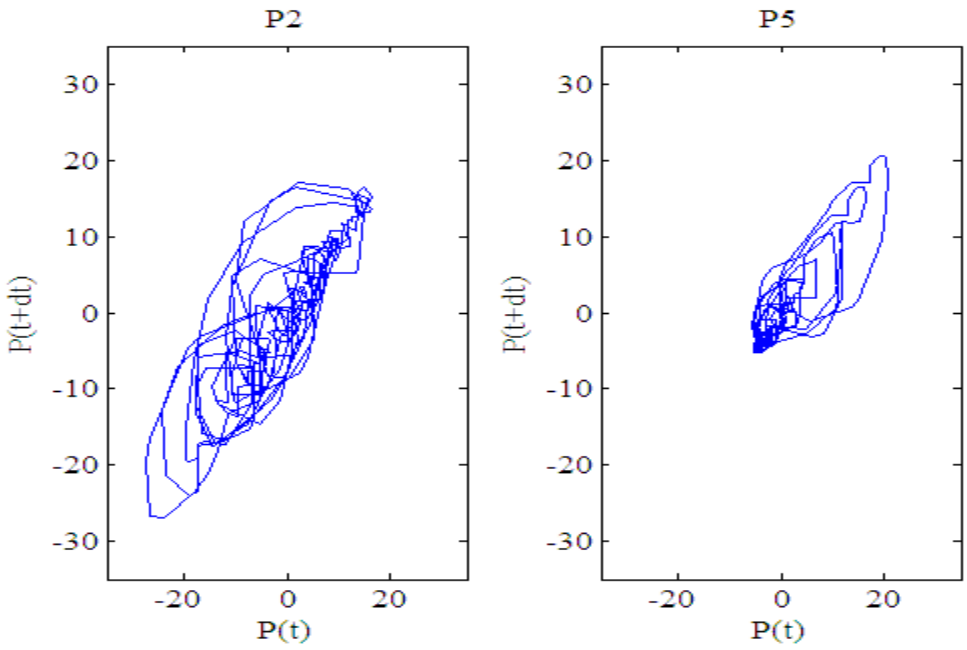

Figure B9: Phase space diagram at different locations along pipeline length (54 mm I.D. × 70 m long pipe; m_f = 0.029 kg/s; m_s = 0.5 kg/s; m^* = 17.3)

As seen in the above figures the area of the phase space diagram has been decreased while moving from P2 to P5, which indicates fewer amounts of fluctuations in the signal, which in turn indicates less turbulence in the flow.

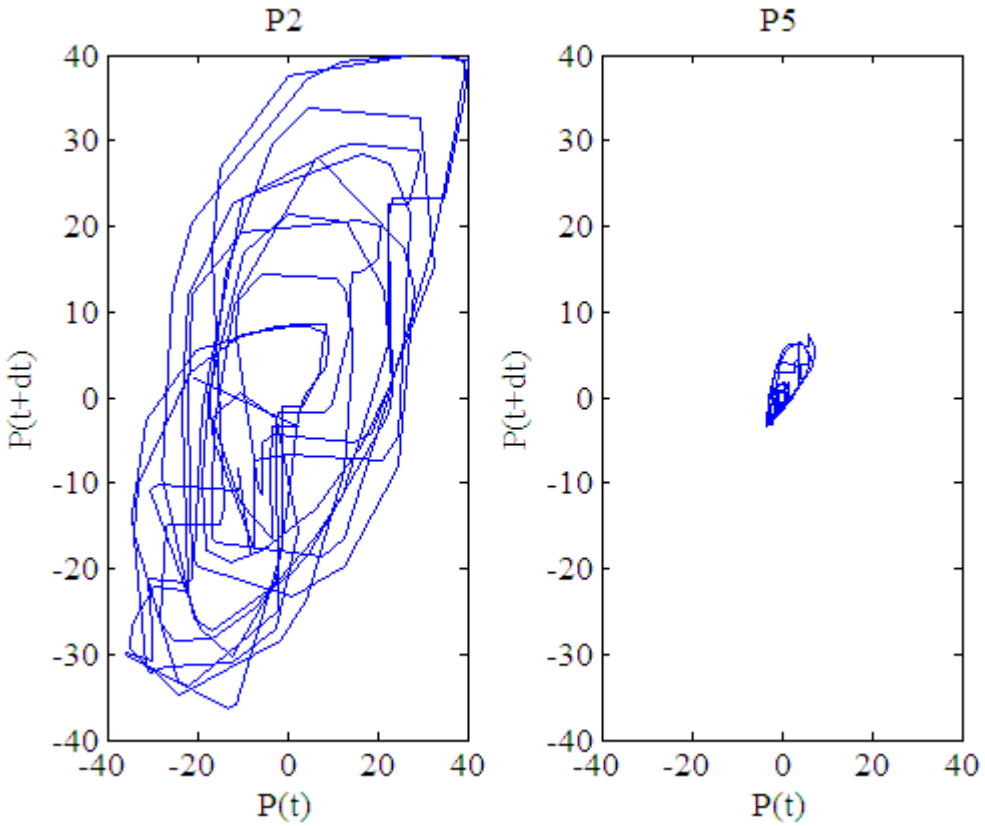

Figure B10: Phase space diagram at different locations along pipeline length (Exp.1: m_f = 0.049 kg/s; m_s = 3.47 kg/s; m^* = 70.8; 54 mm I.D. × 24 m long pipe)

Similar to the results found in the previous techniques, reduction in the area of phase space diagram for the 24 m long pipeline is fairly large as compared to the change found for 70 m long pipeline.

Wavelet scalogram

Figures 5.9.11 and 5.9.12 show the wavelet scalogram corresponding to two different flow conditions (i.e. mass flow rates of carrier phase and of solids).

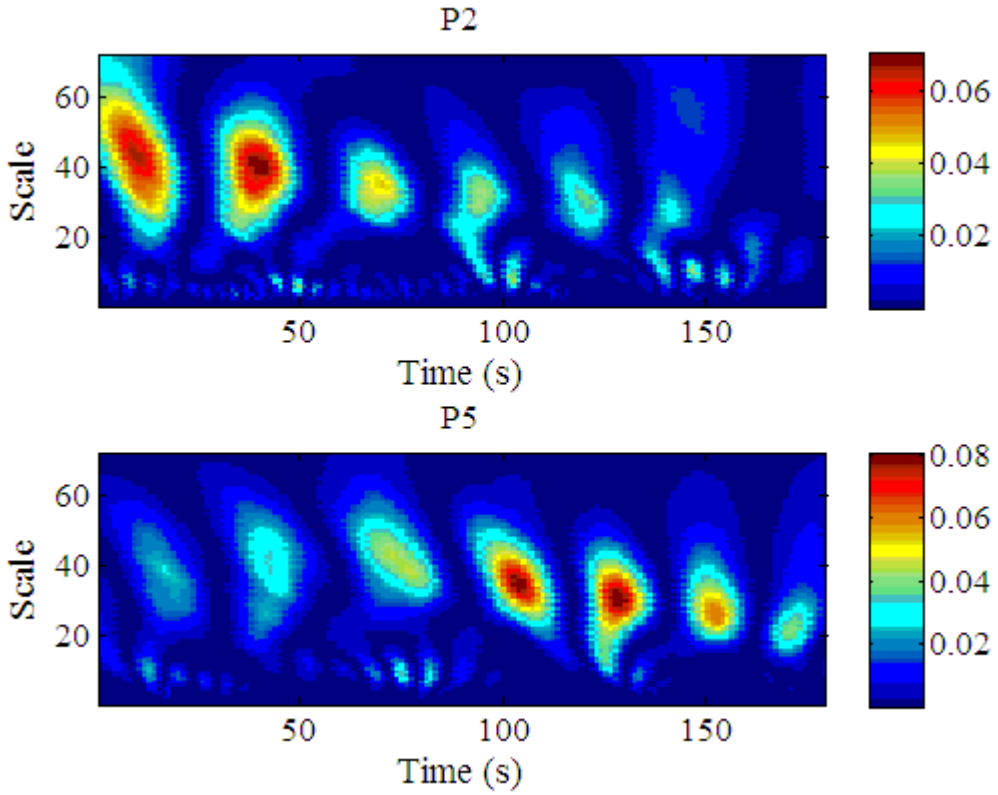

Figure B11: Wavelet scalogram at different locations along pipeline length (54 mm I.D. × 70 m long pipe; m_f = 0.031 kg/s; m_s = 1.21 kg/s; m^* = 39.03)

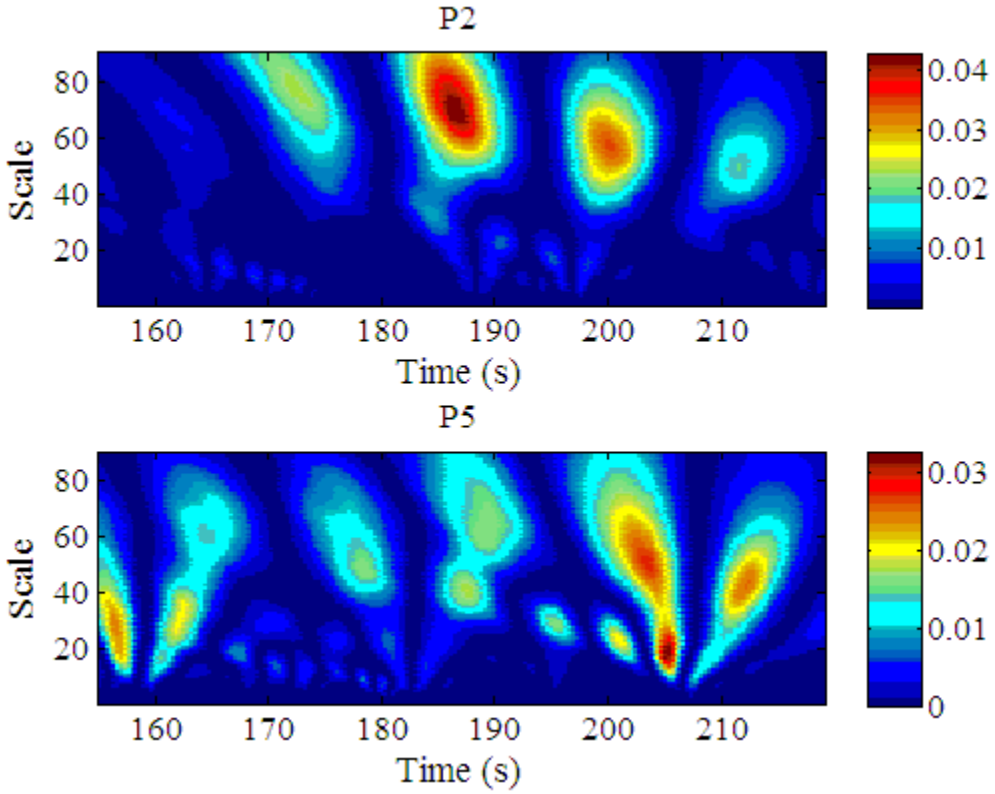

Figure B12: Wavelet scalogram at different locations along pipeline length (54 mm I.D. × 70 m long pipe; m_f = 0.029 kg/s; m_s = 0.5 kg/s; m^* = 17.3)

As seen in the above figures, energy concentration in the scalogram is shifted from higher scales (low frequency) to lower scales (higher frequency) while moving from P2 towards P5. However, the total amount of energy in the signal has decreased, which indicates less amplitude of fluctuations (i.e. less turbulence).

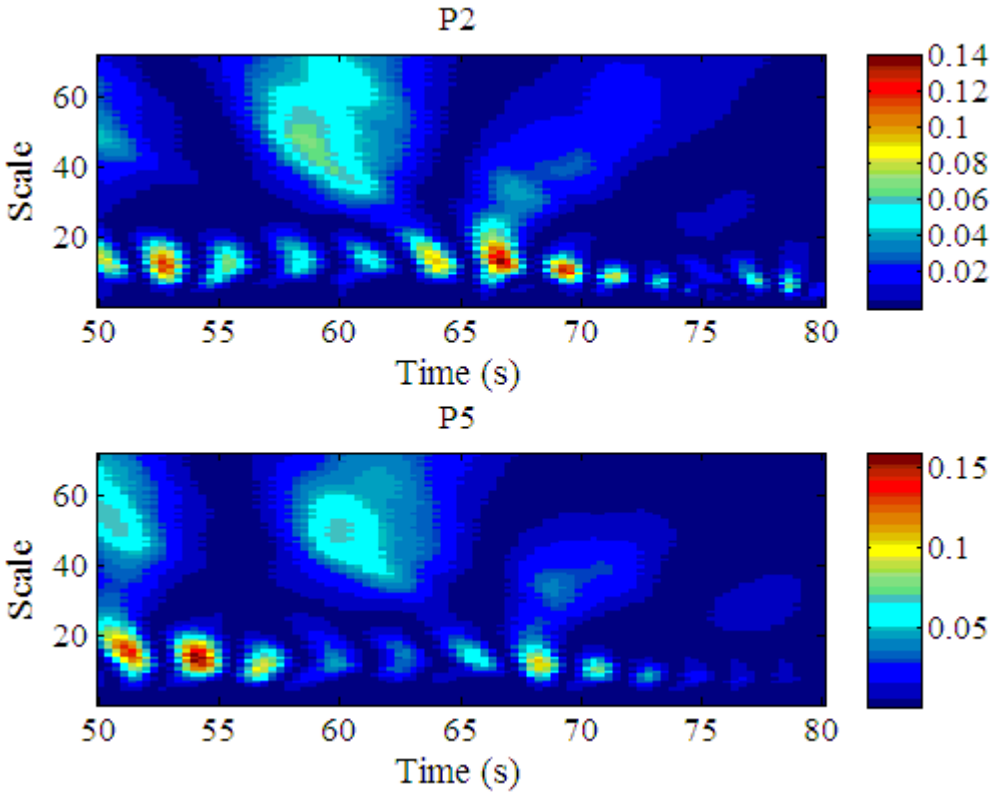

Figure B13: Wavelet scalogram at different locations along pipeline length (Exp.1: m_f = 0.049 kg/s; m_s = 3.47 kg/s; m^* = 70.8; 54 mm I.D. × 24 m long pipe)

It can be observed that the change observed in the wavelet scalogram is not significant. No definite conclusion could be drawn from the observation made in above figure.

Hilbert Transformation:

Following figures show the plots of energy distributions index of IMF's (Intrinsic Mode Functions) calculated from Hilbert transformation.

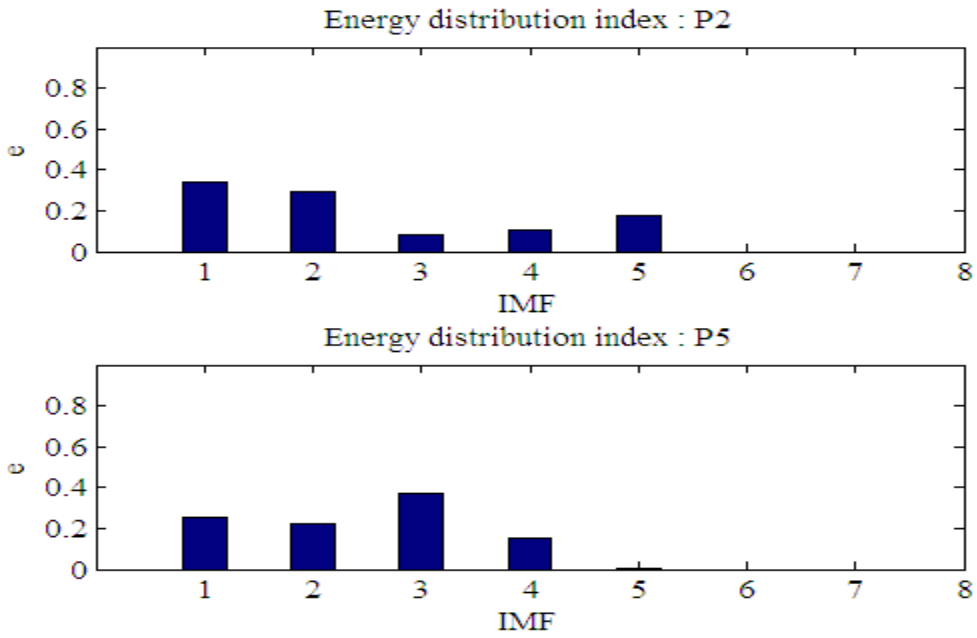

Figure B14: Power spectral density at different locations along pipeline length (54 mm I.D. × 70 m long pipe; m_f = 0.031 kg/s; m_s = 1.21 kg/s; m^* = 39.03)

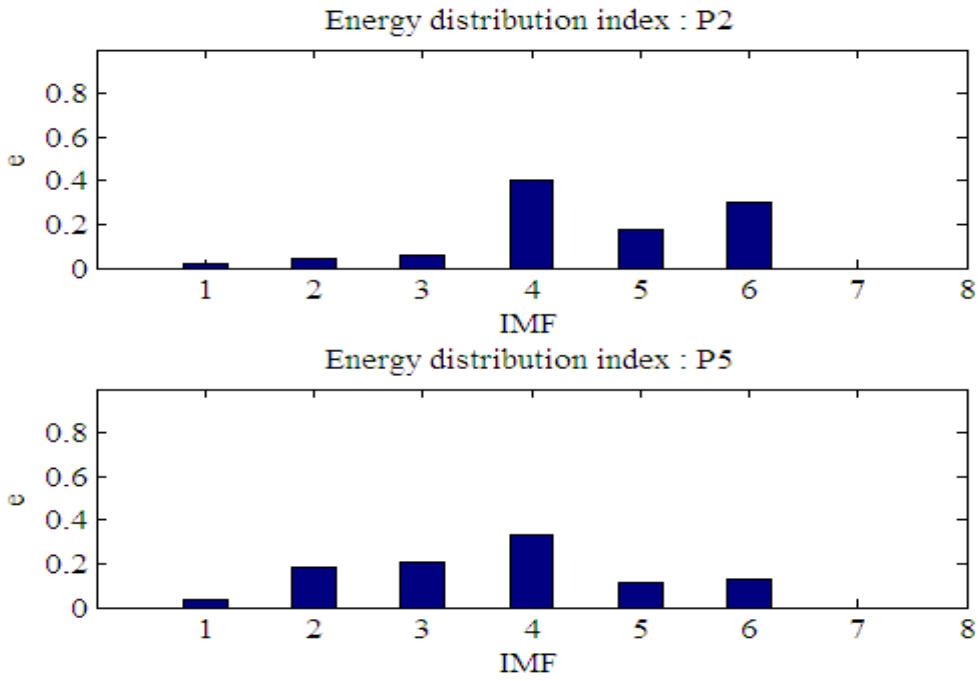

Figure B15: Power spectral density at different locations along pipeline length (54 mm I.D. × 70 m long pipe; m_f = 0.029 kg/s; m_s = 0.5 kg/s; m^* = 17.3)

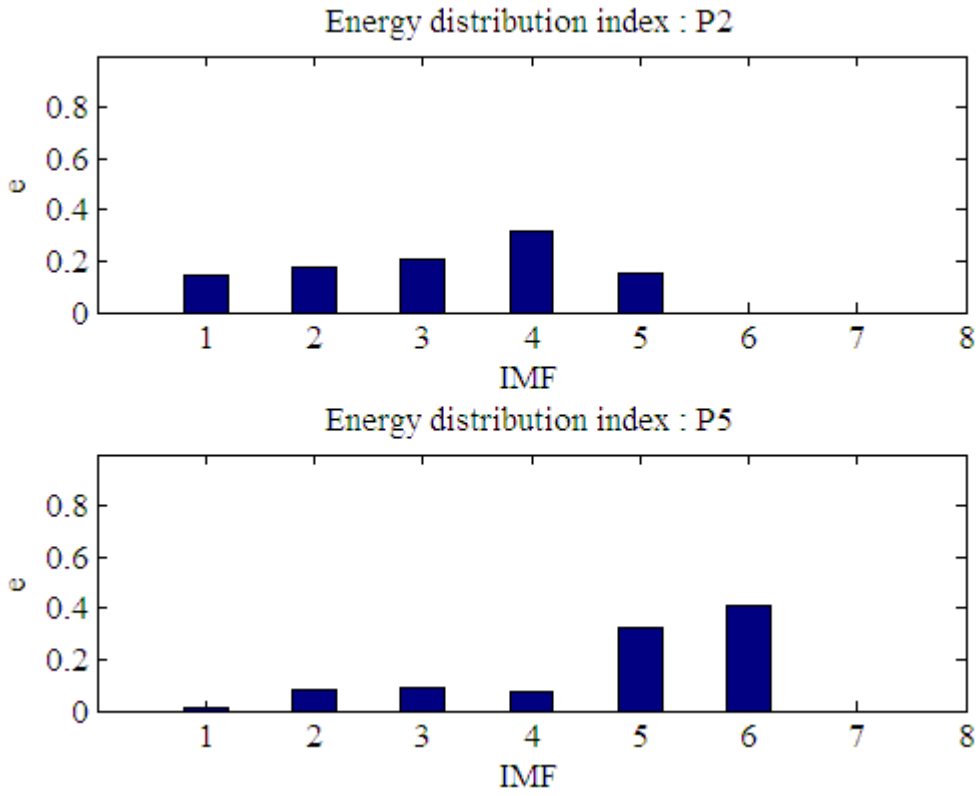

Figure B16: Power spectral density at different locations along pipeline length (Exp.1: m_f = 0.049 kg/s; m_s = 3.47 kg/s; m^* = 70.8; 54 mm I.D. × 24 m long pipe)

As seen in the above figures, the change observed in the energy distribution index is not significant. Signal parameters indicate fewer fluctuations at the end location of pipeline as compared to the location at start. The probable explanation for the same could be shorter length of Thapar University test rig, due to which change in the signal characteristics in the straight pipe sections is lesser as compared to the bends (straight pipe length being comparatively shorter).

LIST OF PUBLICATIONS DURING THE COURSE OF PhD

Referred SCI journal papers (published/accepted) – 4 Nos.

Sr. No.	Title of paper	Authors' Names	Journal	Volume, Year, Page no.	Impact Factor
1.	An Investigation into Pressure Fluctuations for Fluidized Dense-Phase Pneumatic Conveying of Fine Powders	**A. Mittal,** S.S.Mallick and P.W.Wypych	Powder Technology (Elsevier)	Volume 277, June 2015, Pages 163–170	2.499
2.	An Investigation into Flow Mode Transition and Pressure Fluctuations for Fluidized Dense-Phase Pneumatic Conveying of Fine Powders	**A. Mittal,** S.S.Mallick and P.W.Wypych	Particuology (Elsevier)	Volume 16, October 2014, Pages 187–195	2.058
3.	Study of pressure fluctuations during and improved modeling methods for dense phase pneumatic conveying of powders	**A. Mittal,** G.Setia, S.S.Mallick and P.W.Wypych	Particulate Science & Technology	Volume 33, 2015, Pages 67-75	0.59
4.	An Investigation into the Transition of Flow Mechanism during Fluidized Dense-Phase Pneumatic Conveying of Fine Powders	**A. Mittal,** S.S.Mallick and P.W.Wypych	ParticulateScience & Technology	Volume 34, 2016, Pages 23-32	0.59

Referred conferences (published/accepted) – 3 nos.

Sr. No.	Title of paper	Authors' Names	Conference-year	Country
1.	Study of pressure fluctuations during and improved modeling methods for dense phase pneumatic conveying of powders	**A. Mittal,** G. Setia, S.S. Mallick, P.W. Wypych	**PGBSIA-2013** (*First International Conference on* Powder, Granule and Bulk Solids: Innovations and Applications, 2013)	Thapar University, Patiala, **India**
2.	An Investigation into Flow Mechanism during Horizontal Pneumatic Conveying of Fine Powders by Analysing Pressure Fluctuations	**A. Mittal,** G.Setia and S.S.Mallick	**Chops-2015** **(***8th International Conference for* Conveying and Handling of Particulate Solids, 3-7 May 2015	Tel-Aviv, **Israel**
3.	Investigation into Pressure Signal Fluctuations during Fluidised Dense-Phase Pneumatic conveying of Powders	**A. Mittal**	**PGBSIA-2016** (*2nd International Conference on* Powder, Granule and Bulk Solids: Innovations and Applications, 2013)	Jaipur, India